The Role of the Deubiquitylase MYSM1 During Alphavirus Infection

Amer Nubgan

Thesis submitted in accordance with the requirements of the University of Liverpool for the degree of Doctor of Philosophy

September 2017

Declaration

I Amer Nubgan, confirm that the work presented in this thesis is the result of my own work and effort. The material contained in the thesis has not been presented, nor is currently being presented, either wholly or in part, for any other degree or other qualification.

Research in this thesis was carried out at the Institute of Infection and Global Health (University of Liverpool, UK).

Abstract

The Role of the Deubiquitylase MYSM1 During Alphavirus Infection
Amer Nubgan

The members of the genus *Alphavirus* are positive-sense RNA viruses and it is one of two within the family *Togaviridae.* Most alphaviruses are predominantly transmitted to susceptible vertebrates by a mosquito vector. Alphavirus disease in humans can be severely debilitating, and depending on the particular viral species, infection may result in encephalitis and possibly life threatening symptoms. Chikungunya virus (CHIKV) is the aetiological agent represents a substantial health burden to affected populations, with clinical symptoms that include severe joint and muscle pain, rashes, and fever, as well as prolonged periods of disability in some patients. In recent years, CHIKV has received significant attention from public health authorities as a consequence of the dramatic emergence infections in the Indian Ocean islands and the Caribbean as well as the recent emergence of CHIKV in the Americas. Infections have also been reported around Europe such as in Italy, France and Greece. Currently, no safe, approved or effective vaccine or treatment exists for CHIKV infection.

The ubiquitin-proteasome system (UPS), the major intracellular proteolytic pathway, mediates different kinds of cellular processes, which may be targeted by viruses to aid their replication within cells. In recent years it has been well established that both the forward reaction of ubiquitination, and the reverse reaction of deubiquitination are targeted during virus infection to enhance their replication, either by targeting of cellular proteins or encoding viral homologues of key pathway proteins. The reverse reaction is undertaken by a large family of enzymes termed deubiquitylases or DUBs, and many of these have been shown to play a crucial role, not only in virus replication but also in the regulation of the immune system and vesicle trafficking. The DUBs are attractive drug targets and have increasingly been implicated in cellular processes germane to malignancy which makes the continued characterisation of the role of DUBs during virus infection a worthwhile objective.

In on-going experiments in the research group a DUB siRNA pools library screen identified 12 DUBs (USP1, USP4, USP5, USP34, USP45, USP46, OTUD6A, UCHL1, JOSD2, BRCC3 and MYSM1). Depletion of these hits in HeLa cells lead to an increase in cell viability following Semiliki Forest Virus (SFV) infection (and predicted to be pro-viral) and thus could potential be candidate antiviral targets. Inroads into understanding the role of the DUB hits during the alphavirus infection, focusing initial on the BSL2 model virus SFV, and extending this to CHIKV (at BSL3). In the present study, further screening focused on the deconvolution siRNA pools for the DUB hits. Investigation of the subsequent follow up experiments with one strong candidate DUB from this list, MYSM1.

Two different approaches were taken. Firstly, the effect of depletion of MYSM1 by siRNA treatment was further investigated in HeLa cells. Secondly, the analysis was extended to investigate the role of MYSM1 in fibroblasts utilising MYSM1 genetic knockout murine embryo fibroblasts.

Results from this study indicate that depletion of MYSM1 in HeLa cells by siRNAs resulted in a reduction in both SFV and CHIKV replication, as assayed by measuring RNA levels and plaque formation. It was also found that MYSM1 genetic knockout in MEF cells lead to increase in both SFV and CHIKV replication. In addition, depletion of MYSM1 by siRNAs in MRC-5 cells lead to increase in SFV replication. In conclusion, MYSM1 generated interesting data, implying a role during virus infection that appeared to depend on the cell type being infected. Up to now it is unclear what the effector mechanisms are that contribute to these observations, subject to further mechanistic and functional studies, may increase the options available for targeting this vital DUB during Alphavirus infections.

Abbreviations and Symbol	
aa	Amino acid
Ae.	Aedes mosquito species
BCA	Bicinchoninic acid
BFV	Barmah Forest virus
BFV	Barmah Forest virus
BHK-21	Baby hamster kidney cells
BHK-21	Baby hamster kidney-21
bp	Base-pairs
BSA	Bovine serum albumin
C	Capsid
CDC	Centers for Diseases Control and Prevention
CEF	Chicken embryo fibroblast
CHIKV	Chikungunya virus
CPE	Cytopathic effect
CYLD	Cylindromatosis protein
DC	Dendritic cells
DMEM	Dulbecco's Modified Eagle Medium
DMSO	Dimethyl sulphoxide
DNA	Deoxyribonucleic Acid
dNTP	2'-deoxynucleotide 5'-triphosphate
DPBS	Dubecco's phosphate buffered saline
dsDNA	Double-stranded deoxyribonucleic acid
DTT	Dithiothreitol
DUB	Deubiquitylase enzyme
EBOV	Ebola virus
ECSA	East/Central/South African (chikungunya virus)
EDTA	Ethylenediaminetetraacetic acid
EEEV	Eastern Equine Encephalitis Virus
ELISA	Enzyme-linked immunosorbent assay
ER	Endoplasmic reticulum
FBS	Foetal Bovine Serum
FCS	Foetal Calf Serum
H_2O	Water
HCV	Hepatitis C virus
HECT	Homologous to E6AP C-Terminus
HEK-239T	Human embryonic kidney cells-293T
HIV-1	Human immunodeficiency virus-1
HPV	Human papillomaviruses
hr	Hour(s)
HSV	Herpes simplex virus
ICP0	Infected cell protein 0
IFN	Interferon
IKK	Inhibitor of kappa B kinase
lKKγ	I-kappa-B kinase subunit gamma
IRAK	Interleukin-receptor associated kinase
IRF	IFN regulatory factor
ISGF	Interferon-stimulated gene factor

ISREs	IFN-stimulated response elements
IκB	Inhibitor of kappa B
JAK	Janus family tyrosine kinase
JAMMs/MPN+	JAB1/MPN/MOV34 metallo-enzymes
JEV	Japanese encephalitis virus
kb	Kilobases
KDa	*KiloDalton*
KSHV	Kaposi's sarcoma-associated herpesvirus
LGP2	Laboratory of genetics and physiology 2
LMP	Low melting point
LPS	Lipopolysaccharide
m	Mili
M	Molar
MAVS	Mitochondrial adaptor protein
MDA5	Melanoma differentiation-associated gene 5
MDV	Marek's disease virus
MERS-CoV	Middle East Respiratory Syndrome Coronavirus
MHC	Major histocompatibility complex (types I or II)
min	Minute(s)
MINDY	Motif interacting with Ub- containing novel DUB family
MJD	Josephins
MOI	Multiplicity of infection
MPN	Domain JAB/Mov34
MRC-5	Medical research council cell strain 5
mRNA	Messenger RNA
MV	Measle virus
MyD88	Myeloid differentiation-88
MYSM1	Myb-like, SWIRM, and MPN domains-containing protein 1
n	Sample size
NCBI	National centre for biotechnology information
NDV	Newcastle disease virus
NEMO	NF-κB essential modulator
NF-κB	Nuclear factor kappa-light-chain-enhancer
NK	Natural killer cells
NLRs	NOD-like receptors
nsP	Non-structural protein
ONNV	O'Nyong nyong virus
ORF	Open reading frame
OTU	Ovarian tumour proteases
PAMP	Pathogen associated molecular pattern
PBS	Phosphate buffered saline
PCR	Polymerase chain reaction
PFU	Plaque forming unit
PKR	Protein kinase R
PLpro	Papain-like protease
PML	Promyelocytic Leukemia
Poly (I:C)	Polyinosinic-polycytidylic acid
Poly (I:C)/LV	Poly (I:C)-LMW/LyoVec

poly-A	Polyadenylate
PRR	Pathogen recognition receptor
PTM	Post-translational modification
PVDF	Polyvinylidene
QPCR	Quantitative RT-PCR
RBR	RING between RING
RC	Replication complex
RIG-I	Retinoic acid-inducible gene-I
RING	Really interesting new gene
RIP1	Receptor interacting protein 1
RISC	RNA-induced silencing complex
RNA	Ribonucleic acid
RNAi	RNA interference
rpm	Revolutions per minute
RRV	Ross River virus
RSV	Respiratory syncytial virus
RT	Reverse transcription
RV	Rabies virus
SANT	Swi3, Ada2, N-Cor and TFIIIB
SARS-CoV	Respiratory syndrome coronavirus
SDS-PAGE	SDS polyacrylamide gel electrophoresis
sec	Seconds
SeV	Sendai virus
SFV	Semliki Forest virus
shRNA	Short hairpin RNA
SINV	Sindbis virus
siRNA	Small interfering RNAs
ssRNA	Single-stranded ribonucleic acid
STAMBPL1	STAM binding protein-like 1
STAT	Signal transducers and activators of transduction
SWIRM	SW13, RSC8 and MOIRA
TC	Tissue culture
TIM	T-cell immunoglobulin and mucin domain
TIR	Toll/IL-1 receptor
TLR	Toll-like receptor
TNFAIP3	Tumor necrosis factor alpha-induced protein 3
TRAF	TNF receptor-associated factor
TRIF	TIR domain-containing adaptor-inducing interferon-β
U2OS	Human umbilical vein endothelial
UCHs	Ubiquitin C-terminal hydrolases
USPs	Ubiquitin specific proteases
UTR	Untranslated region
VACV	Vaccinia virus
VEEV	Venezuelan Equine Encephalitis virus
VSV	Vesicular stomatitis virus
WEEV	Western Equine Encephalitis virus
WNV	West Nile Virus
+ssRNA	Single-stranded positive-sense RNA

Acknowledgments

I would firstly like to thank my supervisors, Neil Blake and Judy Coulson, who enabled this PhD to happen. From helping me design a project to suit both my interests as a nascent scientist, to putting up with my interminable delays during the write up, they have helped shape my understanding of science and inspired me. In this vein, I would especially like to thank Professor Ana Nijnik (McGill University, Toronto, Canada), to provide MEFs obtained from Wild Type (WT) and *Mysm1*$^{-/-}$ (KO). General thank you to all of The Institute of Infection and Global Health/ Clinical Infection/Immunology and Microbiology department past and present technicians team and students, and including but not limited to, Stacey King, Naomi Coombs, Murad Wali and Saeed Aldossari. It has been a privilege working with you. I would especially like to thank The Iraqi Minster of Higher Education and Scientific Research/ University of Baghdad for funding me. Thank you also to many of my colleagues and friends and in particular Sylwia Klich and Suzanna Gore, for their support.

And so to my family. Dedicated to the memory of my father, Saeed, who always believed in my ability to be successful in the academic arena. You are gone but your belief in me has made this journey possible. My mother, for instilling in me and endless curiosity and interest in the natural world, for your dedication to making the world a better place and for your faith in my abilities. My brothers and sisters, for providing sibling rivalry, and for being my best friends.

Chapter 1

Introduction

1.1 Alphaviruses

1.1.1 Overview

Alphaviruses represent a large group of RNA viruses with a broad host range, which are primarily spread by arthropod vectors. They include a number of viruses that cause significant human disease, which are spreading globally. Outbreaks of human and livestock infections regularly occur, and are thus of economic and public health concern (Gebhart *et al*., 2015). Alphaviruses include Eastern Equine Encephalitis virus (EEEV), Venezuelan Equine Encephalitis virus (VEEV), Semliki Forest virus (SFV), Chikungunya virus (CHIKV), Ross River virus (RRV), Western Equine Encephalitis virus (WEEV), and Sindbis Virus (SINV) (Forrester *et al*., 2012; Nasar *et al*., 2012). Human symptoms of alphaviral infections range from fever, rash, nausea and polyarthritis to fatal encephalitis. Although mortality is low for many alphaviruses, combined disease can be debilitating, with clinical sequelae lasting from months to years in some patients (Weaver & Lecuit, 2015). CHIKV is causing most recent concern due to spread to across Asia, Africa, Americas and Europe (Appendix A) (Weaver, 2014). At present, there is no effective vaccine or treatment to prevent CHIKV infection (Burt *et al*., 2017). Thus, further understanding of the interaction of CHIKV with the host cell is essential for the development of treatments and vaccines.

1.1.2 Taxonomy

The *Alphavirus* genus is one of two genus within the *Togaviridae* family. The other being the *Rubivirus* genus, of which there is only one member, the Rubella virus (Strauss & Strauss 1994). The *Alphavirus* genus currently consists of 7 phylogenetic groupings (Figure 1.1), consisting of 31 different species with multiple serotypes (Forrester *et al*., 2012; Nasar *et al*., 2012).

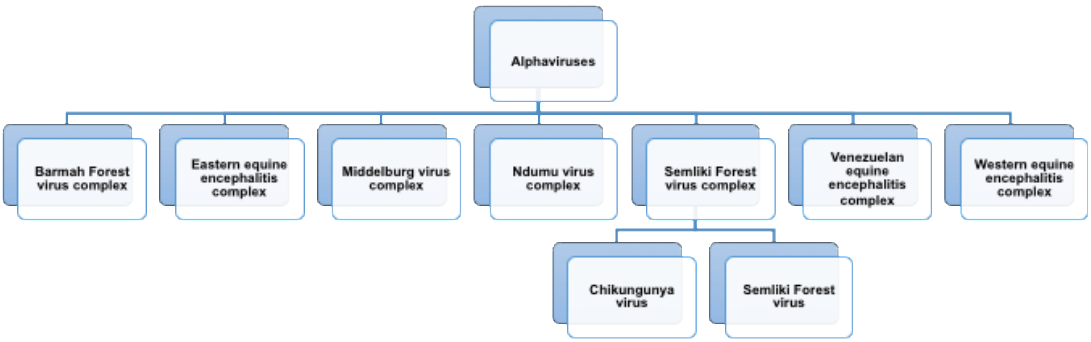

Figure 1.1 Flowchart representation of the phylogenetic groupings of the Alphavirus genus. The seven phylogenetic complexes based on full genome alignment (excluding portions of nsP3 and capsid) are shown, with the Semliki Forest virus complex expanded to highlight Chikungunya virus and Semliki forest virus**.** Figure adapted from Forrester *et al*., (2012).

Alphaviruses are found across the globe, with individual species confined to specific regions by environmental barriers for example vertebrate hosts and mosquito vectors (Forrester *et al*., 2012). They are often classified as either Old World (Africa, Europe and Asia), or New World (Americas) alphaviruses (Weaver, 2014). Old World alphaviruses include Barmah Forest virus (BFV), CHIKV, SINV, Mayaro virus, O' Nyong-Nyong virus (ONNV), RRV and SFV (Suhrbier *et al*., 2012). Whereas, New World viruses include VEEV, EEEV and WEEV (Rupp *et al*., 2015). The division of alphaviruses on the basis of geographical location i.e. Old or New World, is mostly supported by genomic and amino acid sequence alignments (Lavergne *et al*., 2006; Powers *et al*., 2006). Alphaviruses considered to be medically important are detailed in the Table 1.1.

Table 1.1 Medically Important Mosquito-Borne Alphaviruses

Virus	Human Disease Syndrome	Reservoir Hosts	Main Vectors	Secondary Amplification Vectors	Regions Found
Eastern equine encephalitis virus	Febrile illness, encephalitis	Passerine, birds	*Culiseta melanura, Culex spp.*	None	North, Central and South America and the Caribbean
Venezuelan equine encephalitis virus	Febrile illness, encephalitis	Rodents	*Culex spp.*	Equines	Central and South America
Western equine encephalitis virus	Febrile illness, encephalitis	Birds	*Culex tarsalis, Culex quinquefasciats*	-	North, Central and South America
Chikungunya virus	Arthralgia/ rash	Primates	*Aedes spp.*	Humans	Africa, Asia, Americas and Europe
O'nyong-nyong virus	Arthralgia/ rash	Unknown	Unknown	Humans	Africa
Ross River virus	Arthralgia/ rash	Marsupials	*Culex annulirostris, Oculerotatis vigilax*	Humans?	Australia

**Table adapted from Weaver & Barrett, (2004)*

1.1.3 Alphavirus Transmission

Most members of the *Alphavirus* genus are arboviruses, viruses transmitted to vertebrate hosts by arthropod vectors. The Eilat virus and salmon pancreas disease virus are exceptions to this. Eilat virus is a virus of mosquitoes, but is thought to be incapable of infecting vertebrate cells (Nasar *et al*., 2014), whereas salmon pancreas disease viruses is a fish virus that can be transmitted directly from fish to fish (Weston *et al.,* 1999). Alphavirus vectors include mosquitoes, ticks and lice, in which alphaviruses produce persistent infections, lifelong and asymptomatic (Gebhart *et al*., 2015). After consumption of blood from an infected host, the virus is able to replicate in the salivary glands of the vector. Subsequently, other animals fed on by the vector can then become infected by virus transmitted through the saliva (Weaver & Reisen, 2010). Vertebrate hosts include birds, rodents, equids, primates (including humans) and small mammals (Mayer *et al*., 2017; Weaver & Reisen, 2010).

1.1.4 Alphavirus Structure

Alphavirus virions are small, approximately 700 ˚A in diameter and with a molecular mass of approximately 5.2 x 10^3 KDa (Paredes *et al*., 1993). The viral genome packaged in the virions is a single-stranded positive-sense RNA (+ssRNA) genome, with a 7-methylguanosine cap located at its 5' terminal and a polyadenylate (poly-A) tail located at its 3' terminal (Strauss *et al*. 1984; Hefti *et al*., 1975). It is linear and has a length of approximately 11.8 kb (Strauss & Strauss 1994). The virions, shown schematically in Figure 1.2, contain a lipid bilayer derived from the host cell membrane. This envelope is studded with glycoprotein spikes consisting of glycoproteins E1 and E2 arranged in a T=4 lattice structure formed from 80 trimers (Cheng *et al*., 1995; Zhang *et al*., 2002). Inside the lipid bilayer envelope there is a 400 ˚A icosahedral nucleocapsid constructed from 240 monomers, as with the glycoprotein spikes, they are also arranged in a T=4 lattice (Cheng *et al*., 1995; Zhang *et al*., 2002). Electron cryomicroscopy has shown evidence that there is contact between the nucleocapsid and the glycoproteins across the lipid bilayer (Paredes *et al*., 1993).

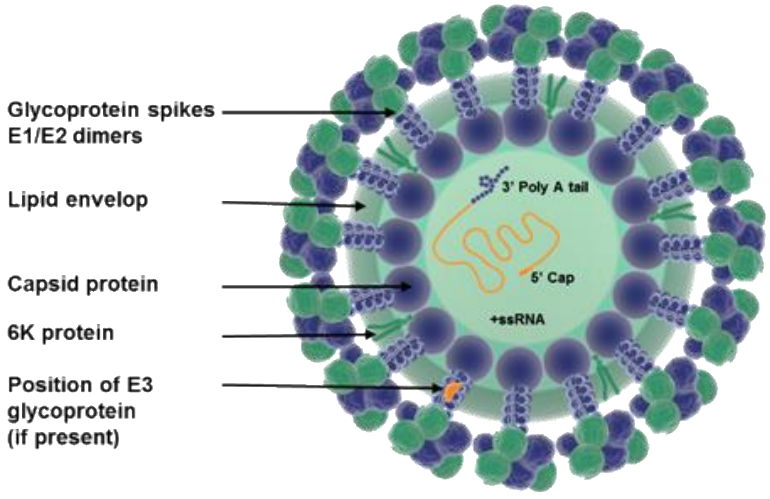

Figure 1.2 Schematic representation of an alphavirus virion. A +ssRNA molecule with a 5' cap and a 3'poly-A tail is encased by a shell of 240 copies of capsid protein and a lipid envelope. Protruding from the envelope are 80 glycoprotein spikes shown in blue and green, each composed of heterodimers of the glycoproteins E1 and E2 arranged as trimers. In addition, the 6K protein and in some cases E3 are incorporated into the envelope. Figure adapted from Jose *et al*., (2009).

1.1.5 Alphavirus Life Cycle

The first step in the alphavirus life cycle is attachment to the host cell, this has been shown to be facilitated by the E2 envelope glycoprotein (Smith *et al*., 1995; Ashbrook *et al*., 2014). Alphaviruses infect a wide range of host including both vertebrate and arthropod cells, and a number of different surface heparan sulfate moieties have been shown to facilitate attachment (Heil *et al*., 2001). During CHIKV infection various cell surface proteins have been shown to mediate attachment, including prohibitin, various mucosal epithelia T-cell immunoglobulin and mucin domain (TIM). The TIM family members are expressed on various immune cells (van Duijl-Richter *et al*., 2015). Although they are not thought to be essential as infection also occurs in their absence (van Duijl-Richter *et al*., 2015). The diversity of cell surface receptors that SINV and other alphaviruses have been reported to use for attachment suggests that alphaviruses can not only utilise conserved molecules but can also readily adapt to use alternative molecules for attachment (Helenius *et al*., 1978; Ludwig *et al*., 1996; La Linn *et al*., 2005; Wintachai *et al*., 2012).

Following binding to the cell surface, alphaviruses are internalised by adsorptive endocytosis. In SFV and SINV infection this has been shown to be mediated by the formation of clathrin-coated pits, however, it is unclear as to whether this is essential for internalisation (White *et al*., 1980; Helenius *et al*., 1980; Helenius *et al*., 1985; Detulleo & Kirchhausen, 1998; Marsh *et al*., 1984; Kielian *et al*., 2010). *In vitro* studies of CHIKV infection have shown that depletion of clathrin by Small Interfering RNAs (siRNAs) had no effect during infection of human embryonic kidney cells (HEK-239T) but inhibited infection in both primary human umbilical vein endothelial (U2OS) cells and mosquito (C6/36) cells (Bernard *et al*., 2010; Lee *et al*., 2013; Ooi *et al*., 2013). Mosquito cells infected with SFV have also shown that virions can be found within both clathrin coated and uncoated vesicles, again suggesting that the participation of clathrin is not essential (Hase *et al*., 1989). Following endocytosis the viral envelope fuses with the endosome, releasing the nucleocapsid core and viral genome into the cytoplasm. Acidification of the endosome is crucial for release

of the nucleocapsid, as the decrease in pH induces dissociation of the E1-E2 heterodimer and allows E1 homodimers to form. The E1 homodimer inserts within the endosomal membrane, exposing the fusion peptide in the distal tip of E1. It is thought that these fusion peptides align to create a fusion pore between the viral envelope and the endosomal membrane, to form a hydrophobic channel through which the nucleocapsid core is released into the cytosol (Wahlberg *et al*., 1992; Lescar *et al*., 2001; Kielian *et al*., 2010).

The next step requires uncoating and release of the viral genome. Two mechanism for nucleocapsid uncoating have been proposed. The first mechanism suggests that core disassembly results from interactions with 60S ribosomal subunits in the host cell leading to autoproteolytic cleavage. At later stages in the replication, high levels of newly synthesised capsid protein are thought to saturate the ribosomal subunit, allowing new virions to assemble (Wengler & Wengler, 1984; Wengler *et al*., 1992; Singh & Helenius, 1992). The alternative mechanism proposed suggests that after fusion of the viral and the endosomal membranes the E1 and 6K proteins form pores. These pores create a region of low pH inside the endosome, leading to either disassembly of the capsid or unmasking of the ribosome-binding site. Subsequent binding to the 60S ribosomal subunit then primes the capsid for uncoating (Wengler & Wengler, 2002; Wengler *et al*., 2003). Once the viral RNA genome has gained entry to the host cytoplasm the structure of the junction region of alphavirus 49S RNA initiates the process of producing new virions. The alphavirus life cycle is shown schematically in Figure 1.3.

1.1.6 Alphavirus Replication

Alphaviruses produce two mRNAs after infection: the genomic (49S) RNA and the subgenomic (26S) RNA. The 49S RNA encodes the non-structural (replicase) proteins, whereas the 26S RNA encodes the structural proteins. (Ou *et al*., 1982). The genomic RNA contains two open readings frames (ORFs), each preceded and followed by untranslated regions (UTRs).

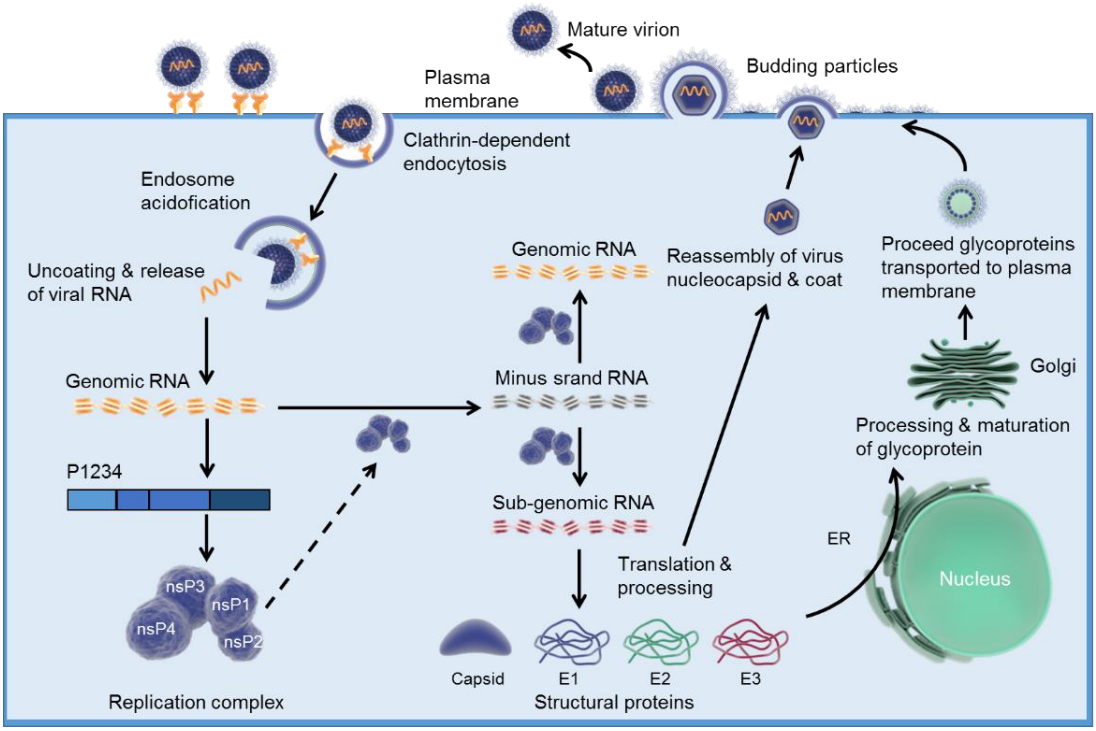

Figure 1.3 Alphavirus lifecycle. The lifecycle starts with the attachment of the virus particle to the cellular receptor (top left), after which receptor-mediated endocytosis, fusion of the viral envelope, disassembly of the core and liberating the viral genome occur. Next, the replication complex are then translated and processed (bottom left). These replication proteins enable the replication of the input genomic RNA and translation of the subgenomic mRNA into structural proteins (bottom center). E1, E2, E3 and K6 are translocated across the ER, processed and transported through the Golgi to the plasma membrane (right). Cytoplasmic assembly of virus nucleocapsid, coat and genomic RNA produces the nucleocapsid core, which associates with processed glycoproteins at the plasma membrane, resulting in budding (top right). Abbreviations: P1234, poly-protein 1234; nsP, non-structural protein; ER, endoplasmic reticulum. Figure adapted from Schwartz & Albert, (2010).

The first is the largest ORF and occupies approximately two thirds of the 5'end of the genome and encodes a polyprotein precursor of the viral replicase. The second of which is take up most of the final third of the genome and encodes a polyprotein that is subsequently processed to produce the structural proteins (Strauss & Strauss, 1994). There are three untranslated regions (UTRs) in the alphavirus genome. One existing at the 5' end, one at the 3' end and one at the junction region between the non-structural and structural ORFs (Figure 1.4) (Gebhart *et al*., 2015). The 5' ORF of the SFV 49S RNA is translated into a 2432 amino acid polypeptide termed P1234

(Takkinen, 1986; Kääriäinen *et al*., 1987; Takkinen *et al*., 1991). The expression of the non-structural proteins of the Sindbis (SIN) and Middelburg viruses are slightly different as the ORF of P1234 is interrupted by an opal termination codon (UGA) near the 3' end of the nsP3 gene. Thus, the major translation product is a P123 polyprotein. Following the opal codon is a cysteine residue, which results in a "leaky" opal codon, this allows low level translation (10-20%) of the complete P1234 polyprotein (Strauss *et al*., 1983; Li & Rice, 1989; Strauss & Strauss, 1994). The P1234 polyprotein undergoes rapid cleavage to form the four non-structural proteins: nsP1–P4, as well as a number of intermediate proteins. Cleavage is facilitated by the virus-encoded papain-like protease, located in the C-terminal end of nsP2. Cleavage occurs at three conserved sites, thereby liberating each of the component proteins. This cleavage occurs in a strictly regulated order, where the intermediate products, as well as the final proteins, regulate RNA synthesis within infected cells (Hardy & Strauss, 1989; Groot *et al*., 1990; Strauss & Strauss, 1994; Shirako & Strauss, 1994; Kim *et al*., 2004). In early infection nsP123 and nsP4 are produced. The nsP2-associated protease functions *in trans* to produce negative-sense RNA. Later in infection, when levels of P123 have reached a sufficiently high concentration nsP1 is released and a second transient complex consisting of nsP1, nsP23 and nsP4 is formed. This complex synthesises genome-length positive-sense RNA, although a low yield of negative-strand RNA may also be produced. Cleavage at the nsP2/nsP3 junction results in a more stable replication complex, composed of mature forms of the four non-structural proteins, which no longer synthesises negative-strand RNA. Negative-strand RNA is utilised as a template for the production of sub-genomic (26S) and genomic (49S) positive-strand RNA. As is seen in other positive-sense RNA viruses, the alphavirus replicase complex associates with the cytosolic surface of cytoplasmic membranes prior to the start of RNA synthesis (Salonen *et al*., 2004).

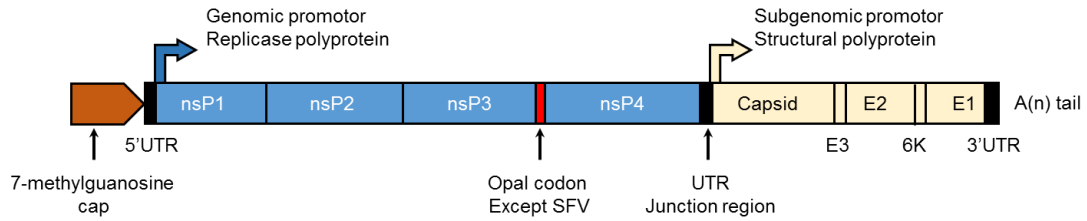

Figure 1.4 Schematic representation of the alphavirus genome. The +ssRNA contains two open reading frames (ORF) bordered by untranslated regions (UTRs). The 5' ORF (in blue) codes for a single polyprotein, which is processed to generate the non-structural proteins (nsP1-4). The second ORF (in yellow) encodes a polyprotein for the structural proteins (capsid, envelope glycoproteins (E1-3) and 6K protein). The genome contains a 7-methylguanosine cap and a poly-A tail. An opal termination codon is found in some isolates. Figure adapted from Gebhart *et al*., (2015).

The structural genes are arranged in the 26S mRNA in the following order: C-E3-E2-6K-E1. Like the non-structural proteins, the structural protein genes are translated into a single polyprotein that is subsequently processed to yield the final protein products. The capsid (C) protein is released into the cytosol through autoproteolysis (Choi *et al*., 1991). Cleavage occurs between two conserved residues: a C-terminal tryptophan in the C protein and a serine at the new N-terminal of the remaining polyprotein. The catalytic domain is present in the C-terminal half of the capsid protein and is composed of a β-barrel motif containing three crucial amino acids, histidine, aspartic acid and serine. Co-translational folding precedes cleavage, positioning these residues in the correct orientation (Nicola *et al*., 1999). The tertiary structure of the protein places the C-terminal tryptophan residue (W267 in SFV) in the catalytic site, blocking and rendering it inactive after cleavage has taken place (Thomas *et al*., 2010). Liberated capsid protein associates with newly synthesised positive-sense RNA. The N-terminal of the capsid protein contains a 100 amino acids region, rich in arginine or lysine residues, this results in a net positive charge. An electrostatic attraction between the positively charged capsid protein and the negatively charged genomic RNA is thought to contribute to the process of nucleocapsid packaging (Strauss & Strauss, 1994). A region near the C-terminal of the capsid protein protrudes from the

outer surface and enables association of similar domains on adjacent proteins to produce capsomeres and ultimately new nucleocapsids (Cheng *et al*., 1995). Following detachment of the capsid protein a signal sequence at the N-terminal of the remaining polyprotein is exposed and this translocates the remaining structural polyprotein (E3-E2-6K-E1) across the endoplasmic reticulum (ER) membrane. Within the lumen of the ER this product is processed by the host cell enzyme signalase to yield pE2 (a precursor of E3 and E2), 6K and E1 (Garoff *et al*., 1994; Strauss & Strauss, 1994).

Further signal sequences at the C-terminals of pE2 and 6K promote translocation of the 6K and E1 proteins into the ER. The E3 portion of pE2 provides a disulphide isomerase, which facilitates the formation of several disulphide bonds essential for the correct folding of E2 during spike formation (Parrott *et al*., 2009). The spikes are translocated to the plasma membrane within the Golgi complex which provides a similar acidic environment to that which triggers viral-host membrane fusion following receptor-mediated endocytosis in the initial stages of the infectious process. Here, interactions between the nucleocapsid core and the carboxy-terminal cytoplasmic domain of E2 promote virion assembly and budding (Jose *et al*., 2012). A schematic representation of the alphavirus replication and protein production is shown in Figure 1.5.

1.1.7 Alphavirus Non-Structural and Structural Proteins

The alphavirus genome encodes four multifunctional non-structural proteins: nsP 1-4. In SFV studies it was shown that nsP1 forms part of the replication complex (RC) together with nsP3, which targets the RC to cellular membranes (Spuul *et al*., 2007). Interactions between nsP1 and nsP4 have been shown to initiate the synthesis of negative-strand RNA from the positive-strand genome (Shirako *et al*., 2000). In addition to this, nsP1 is responsible for the addition of the 5’ cap to viral genomic and subgenomic RNAs (Vasiljeva *et al.,* 2000).

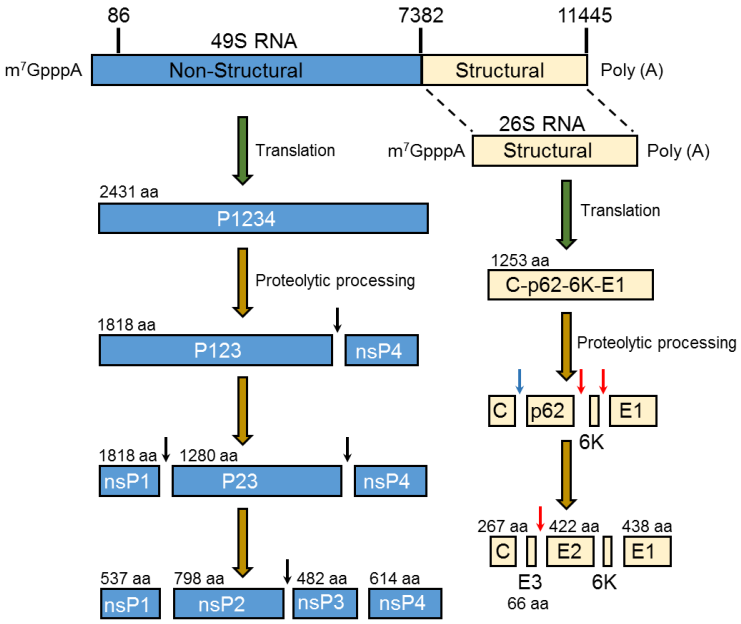

Figure 1.5 Schematic representation of alphavirus replication and polyprotein production. The non-structural proteins (nsP 1-4) are translated first and sequentially cleaved, which involved in the replication of the genome. The sub-genomic RNA are synthesized the sub-genomic RNA. Amino acid (aa) positions and black, blue and red arrows indicate cleavage sites and are labelled. Figure adapted from Takkinen, (1986).

RNA replication and processing of the nonstructural polyproteins requires nsP2. The C-terminal region of nsP2 contains a papain-like cysteine proteinase, which is responsible for the sequential cleavage of the non-structural polypeptide into the individual nsPs (Merits *et al*., 2001; Shirako & Strauss, 1990). Studies utilising SFV have shown that the N-terminal region of nsP2 contains NTPase, GTPase, ATPase and RNA helicase activity (Rikkonen *et al*., 1994; Rikkonen, 1996; Gomez De Cedrón *et al*., 1999). The helicase domain of nsP2 is also involved in unwinding and replicating the alphavirus genome. The replicase functions of nsP2 are involved in regulation of alphavirus negative-strand replication (26S mRNA transcription) (Suopanki *et al*., 1998; Gomez De Cedrón *et al*., 1999; Stapleford *et al*., 2015).

The nsP3 protein is essential for RNA synthesis: mutations in nsP3 resulted in defective initiation of minus-strand synthesis or subgenomic RNA

synthesis (Hahn *et al*., 1989; LaStarza *et al*., 1994; Wang *et al*., 1994). It was also been shown that cleavage of the nsP3/4 requires the presence of a proteinase containing nsP3 (Groot *et al*., 1990). Replication of the alphavirus genome requires a RNA-dependent RNA polymerase, studies with SFV and SINV have shown that nsP4 performs this function (Keränen & Kääriäinen, 1979). nsP4 is also required for the cleavage of nsP3/4 (Takkinen *et al*., 1990).

Alphaviruses has five structural proteins: C, E3, E2, 6K, E1. The capsid is multifunctional protein that plays a crucial role in the viral life cycle (Choi *et al*., 1997). The function of E3 is currently undefined, and appears to vary between alphaviruses. The E3 protein is found in SFV virions, whilst it is not incorporated into virions of other alphaviruses such as CHIKV, WEEV and SINV (Simizu *et al*., 1984; Garoff *et al*., 1974). The entry of alphaviruses into cells is facilitated by interactions between E2 and host cell surface receptors (Smith *et al*., 1995; Smith & Tignor, 1980). Various functions have been reported for the 6K protein, including uncoating, membrane fusion, budding and virus release (Wengler *et al*., 2003; Loewy *et al*., 1995; Liljestrom & Garoff, 1991; Gaedigk-Nitschko & Schlesinger, 1990; Sanz *et al*., 2003). The alphavirus E1 protein is a fusion protein (Boggs *et al*.,1989; Omar & Koblet, 1988), with a fusion peptide residing within a highly conserved hydrophobic domain (Garoff *et al*., 1980). The E1 and 6K membrane proteins contribute to the forming of pores during the fusion of the viral and the endosomal membranes in the early stage of virus infection, with the latter priming the capsid for uncoating (Wengler & Wengler, 2002; Wengler *et al*., 2003).

1.2 Chikungunya Virus

CHIKV was first recorded during a viral disease outbreak between 1952 and 1953 in the Makonde Plateau, in the southern region of Tanzania (Robinson, 1955). The word “chikungunya” originates from Swahili or Makonde language and signifies “that which bends up”, referring to the posture of infected people due to serious joint problems (Robinson, 1955). CHIKV is carried primarily by *Aedes aegypti* species which occurs in the tropics. However, *Aedes albopictus* mosquitoes, which are abundant in milder areas,

have also transmitted CHIKV (Vega-Rúa *et al*., 2014; Vega-Rúa *et al*., 2015; Lo Presti *et al*., 2016). This has resulted in CHIKV becoming a global problem, with infections recorded in over 100 countries and significant current outbreaks in Brazil and India (Burt *et al*., 2017). People infected by the virus can experience significant health implications, including raised temperature, rash, joint and muscle pain, and in some cases chronic disability (Suhrbier *et al*., 2012). At present, there is no effective vaccine or treatment to prevent infection. The following sections will describe the transmission cycle, epidemiology, pathogenesis, prevention and treatment.

1.2.1 CHIKV Transmission Cycles

Two specific CHIKV transmission models have been well documented for CHIKV: an enzootic sylvatic cycle and an endemic/ epidemic urban cycle (Figure 1.6) (Bordi *et al*., 2015). These models differ depending on the environment. A sylvatic cycle in rural areas of West and Central Africa occurs between *Aedes* (*Ae*.) species and monkeys living in forested habitats. It is believed that the species which serve as vectors include *Ae. furcifer, and Ae. africanus*. Humans in a jungle environment may be part of this cycle. However, in more densely populated human areas an urban cycle exists, where humans are passed the virus via a bite from an infected mosquito. Human to human transmission can occur in this cycle, although other vertebrates may be involved. For example, in regions of Asia affected by outbreaks of the disease, human-to-human transmission through mosquito bites seems to be a primary pattern of the virus spreading. However, in this situation there has been no evidence of zoonotic cycles with nonhuman primates occurring in these areas. The main vectors involved in the urban cycle are *Ae. aegyptii* and, since 2005 *Ae. albopictus*

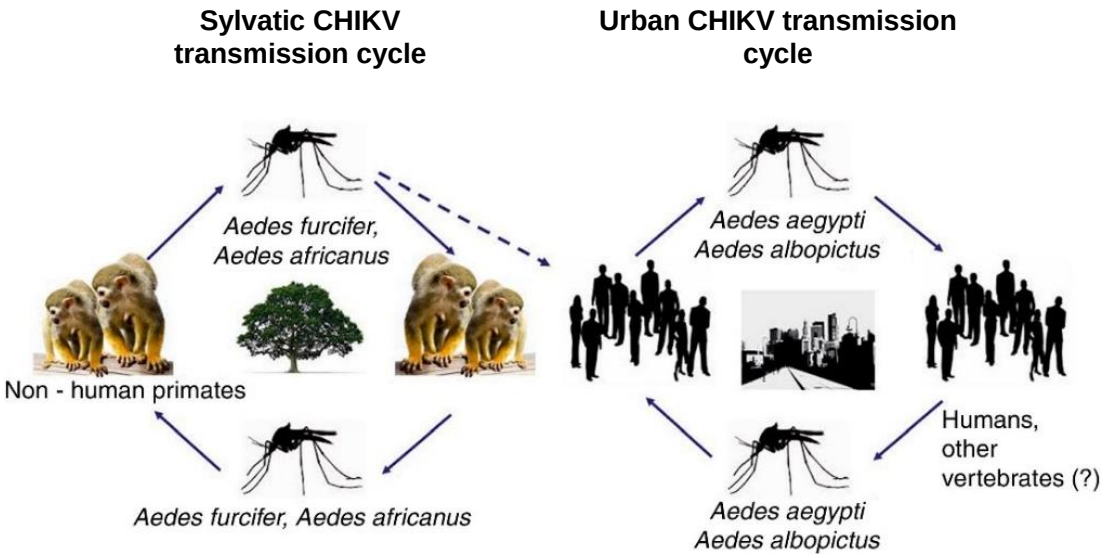

Figure 1.6 Transmission cycle of the Chikungunya virus. (taken from Madariaga *et al*., 2016)

1.2.2 Epidemiology of Chikungunya

Three distinct clades of CHIKV are currently recognized on the basis of phylogenetic criteria (Powers *et al.,* 2000). Names of these clades refer to locations where affected individuals were isolated initially and these are: West African, East/Central/South African (ECSA) and Asian. A universal pattern could be observed with epidemics happening between 1952 and 2003. These were fairly geographically restricted, self-limiting outbreaks, occurring not continuously and re-appearing after years or even decades. Nonetheless, a substantial outbreak representing a novel pattern was recorded in 2004, when several million people got ill as a result of an infection caused by viruses from ECSA clade. It is believed that the epidemic started in Kenya, on the island of Lamu (Sergon *et al*., 2008; Njenga *et al*., 2008), from which, over the next months and years, it reached other countries in Africa and towards the East, from islands on the Indian Ocean to India and Southeast Asia. It was the biggest outbreak that has been recorded. In 2005, on one of the islands of the Indian Ocean, La Rèunion, 38% of the inhabitants were affected (266,000 documented cases). It was also calculated that 1.4 million incidents happened in India between 2006 and 2007 (Schwartz & Albert, 2010).

Ae. aegyptii was the primary vector of CHIKV up to 2004. However, the re-emergence of CHIKV during the epidemic on La Reunion Island between 2005 and 2006 was not initiated by this species, which is only found in small numbers in these island. Instead, it was found that *Ae albopictus*, which was present in large numbers (Vega-Rúa *et al*., 2014), was responsible for this outbreak. It has been shown that a mutation in the E1 glycoprotein was present in CHIKV isolated from infected people during the early months of this outbreak. This mutation result in an Alanine to valine switch at position 226 of the E1 protein. CHIKV isolated from patients later contained valine instead. Through experiments comparing sensitivity of *Ae. albopictus* vectors to infection with the two CHIKV phenotypes, It was subsequently shown that CHIKV strains with the A226V mutation were the most efficient in replication and dissemination in *Ae. Albopictus species* (Vazeille *et al*., 2007; Tsetsarkin *et al*., 2007).

In 2007, CHIKV in India became a source of viral introduction to Europe. It has been investigated that a viremic individual travelling from India to their home in the North-eastern Emilia Romagna in Italy, initiated an outbreak involving additional 207 cases (Rezza *et al*., 2007; Cavrini *et al*., 2009). Two further cases within Europe, were detected in Frejus, South-eastern France, in 2010 (Grandadam *et al*., 2011). CHIKV infections were documented in the Oceania area for the first time in 2011 and 2012, on the islands of New Caledonia and Papua New Guinea (Horwood *et al*., 2013). Additionally, the virus emerged for the first time on a number of Caribbean islands and on South America mainland between 2013 and 2014 (Bortel *et al*., 2014). The autochthonous transmission of CHIKV has been recorded in 48 countries/territories in North, Central, South America, as well as in the Caribbean. Figure 1.7 shows the countries in which CHIKV has been reported up to 2016 (Burt *et al*., 2017).

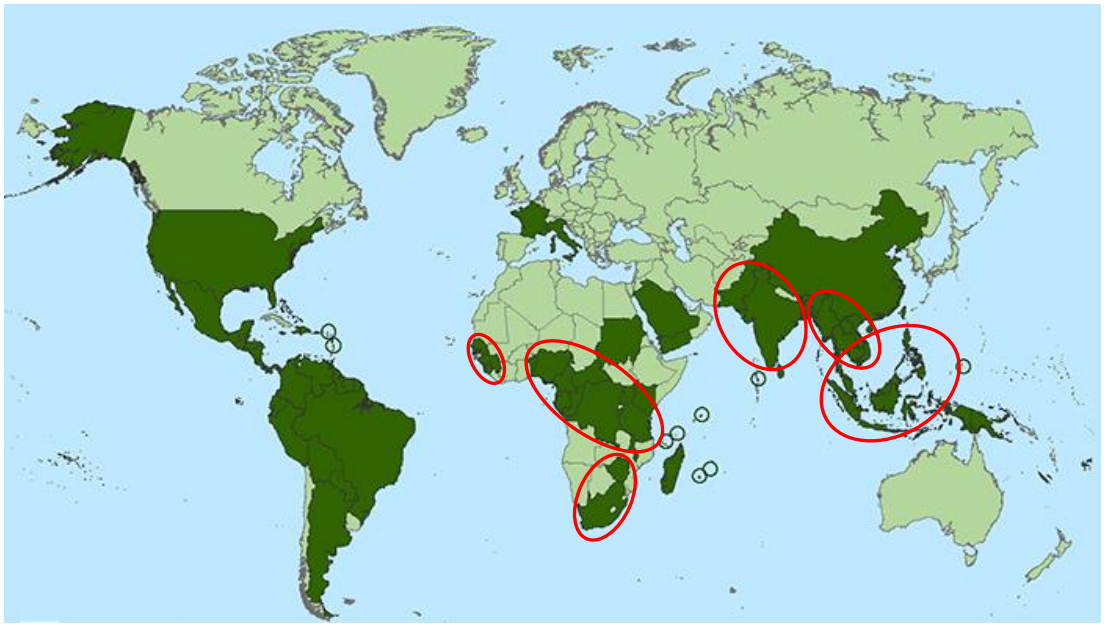

Figure 1.7 Map showing the approximate geographic locations of CHIKV. Highlighted by dark green colour in which chikungunya outbreaks have been reported as of April 22nd 2016. Areas with a history of CHIKV outbreaks prior to the 2004 re-emergence are enclosed by red cycle.

1.2.3 CHIKV Pathogenesis

Murine models (utilising the C57BL/6 mouse strain) have replicated some of the symptoms shown in CHIKV infected humans, including self-limiting arthritis, myositis, and tenosynovitis (Chan *et al*., 2015). The disease picture seen in mice is predominantly that of severe necrosis and destruction of tissues with significant cellular infiltration (Gardner *et al*., 2010; Morrison *et al*., 2011). There is not currently a murine model able to duplicate the long-lasting chronic arthralgic features found in up to two-third of the CHIKV-infected patients (Schilte *et al*., 2012). Models utilising macaques have shown virus persistence but not the severe joint damage seen in humans (Chen *et al*., 2010; Labadie *et al*., 2010). Nevertheless, both models suggest that inflammation macrophages as the main cellular reservoirs during the late stages of CHIKV infection in vivo, and local viral persistence are involved in the establishment of chronic disease.

The disease progression and the sequence of events following intradermal inoculation of mice which lacked Type 1 Interferons (IFNs) signalling with CHIKV was investigated. The data indicated that the fibroblast

is a major target cell of CHIKV and virus replication initially occurs in skin fibroblasts near the site of injection and then spreads via the blood to the liver, muscles, joints, lymphoid tissue and the brain (Figure 1.8) (Couderc *et al*., 2008).

Two further studies, utilising a cynomolgus macaques model, showed that intravenous or intradermal CHIKV inoculation resulted in high viraemia, peaking 1-2 day post-infection. Although infection was not lethal, but it was associated with a transient acute lymphopenia and neutropenia (Labadie *et al*., 2010; Akahata *et al*., 2010). In contrast *in vitro* studies have shown evidence of dendritic cell infection (Sourisseau *et al*., 2007). A possible explanation for this is that CHIKV is able to utilize the process of apoptosis as a means of virus dissemination within the infected host. Macrophages and dendritic cells may become infected by taking up progeny virus contained within apoptotic blebs from susceptible cells such as fibroblasts and hence transport them to other sites (Schwartz & Albert, 2010; Krejbich-Trotot *et al*., 2011). The innate immune system mediates the early host response to CHIKV infection through the induction of type 1 IFNs (IFN-α and IFN-β), which are detected at high levels during the acute phase of infection and return to normal towards the end of the viraemic phase (Schwartz & Albert, 2010; Schilte *et al*., 2010). Several studies have shed light on the interplay between type I IFNs and CHIKV during infection. In one of these, mice were intradermally infected with CHIKV and virus pathogenicity was compared between adult wild type (w/t) C57BL/6, neonatal w/t C57BL/6 and two groups of knock-out mice, one partial (IFN-α/β $R^{-/+}$) and the other completely lacking (IFN-α/β $R^{-/-}$) in type 1 IFN receptor genes (Couderc *et al*., 2008). It has been shown that adult w/t mice and those over 12 days old remained healthy whereas neonates developed severe CHIKV-associated disease, with risk decreasing with advanced age. Whereas mild and lethal disease symptoms were seen in the IFN-α/β $R^{-/+}$ and IFN-α/β $R^{-/-}$ knock-out mice respectively following CHIKV infection. Moreover, further studies have reported that a deficient in signal transducers and activators of transduction (STAT) dependent IFN responses exacerbates severity of CHIKV induced joint inflammation in mice when

compared to w/t mice, an observation not was seen with the vaccine candidate strain 181/25 (Levitt *et al*., 1986; Gardner *et al*., 2012).

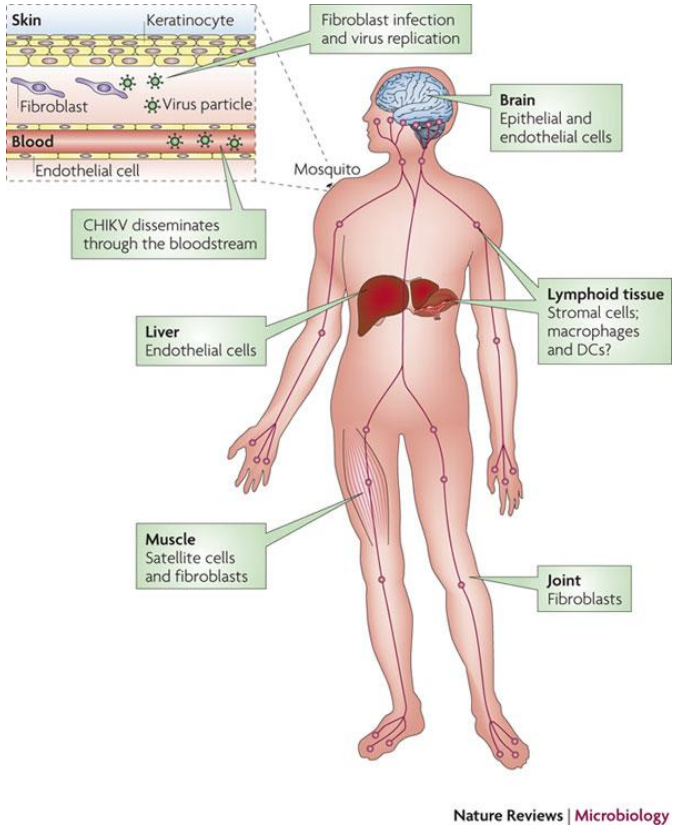

Figure 1.8 Spreading of Chikungunya virus in vertebrates. Transmission of CHIKV occurs following a mosquito (*Ae. aegypti* or *Ae. albopictus*) bite. CHIKV then replicates in the skin, in fibroblasts, and spread to the muscles, joints, liver, muscle, joints, lymph nodes, spleen and brain. The CHIKV target cells are indicated for each tissue (Schwartz & Albert, 2010).

Recent studies have shown that CHIKV is able to infect and replicate in a number of different types of immortalised human cells, these include epithelial cells, endothelial cells, fibroblasts and, to a lesser extent, monocyte-derived macrophages. Replication was not shown to occur in lymphoid and monocytoid cell lines, primary lymphocytes, monocytes, or monocyte-derived dendritic cells (Sourisseau *et al*., 2007). However, some studies have reported that macrophages are susceptible to CHIKV infection both *in vivo* and *in vitro* (Hoarau *et al*., 2010; Krejbich-Trotot *et al*., 2011). The ability of CHIKV to replicate in human muscle satellite cells, but not in differentiated myotubes has also been shown (Ozden *et al*., 2007). In addition to this, CHIKV has been

shown to replicate in a variety of cell lines, including mammalian cells (Vero, BHK21, HEK-293T, MRC5, BGM, HeLa), amphibian cells (XTC) and mosquito cells (C6/36, Ae, A20) (Thiberville *et al*., 2013).

It has been reported that the differences in susceptibility seen between humans and mice to CHIKV infection may be related to differences in the process of autophagy between the two species (Judith *et al*., 2013). When human cell lines were infected with CHIKV, the capsid protein was degraded following ubiquitination and binding of the autophagy receptor p62, which protected the cells from death. Whereas interactions between the autophagy receptor NPD52 and nsP2 were found to be permissive to virus replication. In contrast, both mouse orthologs carried out antiviral roles in infected mouse cells *in vitro* and *in vivo* (Sourisseau *et al*., 2007; Thon-Hon *et al*., 2012; Puiprom *et al*., 2013). Infection of susceptible mammalian cell cultures with alphaviruses usually induces a cytopathic effect (CPE), which in most cases, is due to apoptosis. There is more than one mechanism to induce apoptosis during alphavirus infection; in SFV apoptosis occurs following RNA synthesis, whereas in SINV it is dependent on virus entry and does not require virus replication (Glasgow *et al*., 1997; Jan & Griffin, 1999; Dhanwani *et al*., 2012).

1.2.4 Prevention and Treatment

Currently there are no drugs licensed for the treatment of CHIKV infection in humans, hence treatment of the disease is limited to symptomatic relief. This generally consists of supportive care and pain management through the use of non-salicylate analgesics and nonsteroidal anti-inflammatory drugs (Pialoux *et al*., 2007). There are a number of drugs that are known to be effective against CHIKV when tested *in vitro*, however none are currently licensed for the treatment of CHIKV infections. Harringtonine and ribavirin are examples of drugs that have been approved to use for the treatment of other medical conditions and have been reported to display potent inhibition of CHIKV infection *in vitro.* A study was conducted with a small group of patients in India, during which CHIK patients were treated with ribavirin (Ravichandran & Manian, 2008). Patients who had experienced arthritis and

lower limb pain for over two weeks, following the end of the febrile phase, were treated with ribavirin (200 mg, twice a day for 7 days), which resulted in a rapid reduction in soft tissue swelling and a significant reduction in pain. Harringtonine, an alkaloids derived from *Cephalotaxus harringtonia* (the Japanese plum-yew), has been found to inhibit production of nsP3 and E2 proteins, as well as positive- and negative-sense CHIKV RNA, leading to a reduction in CHIKV titers *in vitro* (Kaur *et al*., 2013). Recently, Varghese and colleagues have demonstrated that the effectiveness of berberine as an antiviral drug against CHIKV (Varghese *et al*., 2016). As there are limited treatments available for CHIKV infection, prevention of infection is imperative. Preventative measures are focused primarily on protecting against mosquito bites and controlling or eliminating the local mosquito populations (Weaver, 2016).

1.2.5 CHIKV Candidate Vaccines

The first chikungunya vaccines were developed with formalin-inactivated (Harrison *et al*., 1967) and live-attenuated virus (Levitt *et al*., 1986), although neither were made commercially available. The formalin an attenuated vaccine produced using TSI-GSD-218 (also known as 181/clone 25) was created by the serial passage of a clinical isolate originating from Thailand in 1962 in MRC-5 cultures and was shown to be highly immunogenic, however adverse side-effects (transient arthralgia) were seen in 8% of human volunteers in phase II trials (Levitt *et al*., 1986; Hoke *et al*., 2012; Edelman *et a*l., 2000). Inactivated vaccines were prepared by treatment of CHIKV with formalin, (Harrison *et al*.,1967) and Tween-80/ether (Eckels *et al*., 1970) and have been shown to be only moderately immunogenic. However, after the 2004 outbreak it was apparent that CHIKV can cause sporadic and sometimes explosive urban outbreaks and it has the potential to spread over an even wider geographical range. This has resulted in a resurgence of interest in the development of CHIKV vaccines and added to the perception of CHIKV as both a public health threat and a potential bioterrorism agent.

Recently another live attenuated vaccine was developed with the virus isolated from the La Reunion outbreak, this was developed using reverse

genetic techniques. The sub-genomic promoter within the vaccine strain was replaced with the internal ribosome entry site from encephalomyocarditis virus, which made it unable to replicate in mosquitoes. This vaccine produced high amounts of neutralising antibodies in mice and protected the animals from CHIKV and was highly immunogenic (Plante *et al*., 2011). Virus-like particles have also been investigated by two research groups as candidate vaccines (Akahata *et al*., 2010; Metz *et al*., 2013). Virus-like particles encoding the capsid of CHIKV and envelope glycoproteins (E1 and E2) were immunogenic in laboratory animals, inducing high concentrations of protective neutralising antibodies (Akahata *et al*., 2010; Akahata & Nabel, 2012). Similarly, a recombinant measles vaccine, which also expressed chikungunya virus-like particles, has been shown to be highly immunogenic and protected susceptible mice from lethal CHIKV challenge (Brandler *et al*., 2013). Two virus-like particle vaccines have been successful in clinical trials in which healthy adults were vaccinated and the vaccine was shown to be safe, well tolerated and produced neutralising antibodies to CHIKV (Chang *et al*., 2014; Ramsauer *et al*., 2015).

They have been shown to be effective in protecting a susceptible adult IFN-α/$\beta^{-/-}$ mouse model and neonatal C57BL/6 mice from a lethal dose of CHIKV (Couderc *et al*., 2009; Fric *et al*., 2013; Selvarajah *et al*., 2013; Akahata *et al*., 2010; Fox *et al*., 2015). Passive immunisation could therefore constitute an effective medical intervention for individuals with known exposure to CHIKV and in those whom the disease is likely to be particularly severe, such as immunocompromised patients and neonates born to viraemic mothers.

1.3 Semliki Forest Virus

SFV is often used as the prototype alphavirus in research studies (although in the USA it is SINV). It is found in central, eastern, and southern Africa, and was first isolated from *Ae. abnormalis* mosquitoes in 1942 in the Semliki Forest in Uganda (Smithburn and Haddow, 1944; Smithburn *et al*., 1946). SFV is an arbovirus and is transmitted by two species of Aedes mosquitoes, *Ae. aegypti and Ae. africanus* (Mathiot *et al*., 1990). Natural

reservoirs included non-human primates, small mammals, horses and humans, although the natural host of SFV remains unknown. In humans this virus causes a mild febrile illness with symptoms including: fever, myalgia, arthralgia, persistent headaches and asthenia during recovery. Only one a fatal case of SFV infection has been documented in humans; a laboratory worker in Germany, who was thought to be immunocompromised. The strain responsible is no longer used in laboratories (Willems *et al*., 1979). In 1987, 22 isolates of SFV were collected from the blood of French soldiers serving in the Central African Republic who were suffering from a mild febrile illness (Mathiot *et al*., 1990). There are several strains of this virus that infect experimental laboratory animals including: rabbits, guinea pigs and mice (Bradish *et al*., 1971; Atkins *et al*., 1985). Early work used chicken embryo fibroblasts (CEFs) and baby hamster kidney (BHK-21), as these cells were found to be permissive for SFV infection and were commonly used for *in vitro* studies (Atkins *et al*., 1999). However, since then SFV has been shown to be able to infect many other cell types, from BHK-21, Vero cells to mosquito and tick cells (Lundstrom *et al*., 1999; Peleg, 1969). SFV infection of laboratory mice is a useful prototype system for the study of the neuropathology and the mechanisms which underlie it (Fazakerley, 2004). CHIKV infectivity, RNA replication and non-structural polyprotein processing depend on the nsP2 protease. A study has observed that the substrate requirements of CHIKV nsP2 protease were similar to those reported for its SFV counterpart (Rausalu *et al*., 2016). Therefore, SFV is often used as a model in a lower biosafety level.

1.4 RNA Interference

Progress has been made recently in functional genomics by applying loss-of-function and gain-of-function screening techniques to study the interactions that occur between a virus and host cells during infection. The use of RNA interference (RNAi) to deplete targeted proteins from hosts has revolutionised the understanding of the role of individual proteins in a range of different situations. This, in addition to proteomics and transcriptomics, has resulted in a more extensive understanding of the complicated interactions

between viruses and their hosts (Ramage & Cherry, 2015). Advances of this nature provide important information about which host factors can be hijacked by the virus to facilitate infection, and anti-viral factors able to inhibit infection.

RNAi can be used to study loss of function to examine basic cellular functions of proteins, protein networks and functions of previously undefined genes (Hannon & Rossi, 2004). In this process, small interfering RNAs (siRNAs) can be used for sequence-specific knockdown of host cell mRNA, ultimately leading to a reduction in gene function through reduced RNA/protein expression and loss-of function (Figure 1.9) (Moffat & Sabatini, 2006; Falschlehner *et al*., 2010). Host factors are depleted by transient knockdown of expression of the gene of interest to uncover their importance in virus-host interactions (Moser *et al*., 2010). Alternatively, short hairpin RNAs (shRNAs) can be used for long term-silencing. These are encoded on plasmids, incorporated into the cells by transfection or by viral vectors, and then integrated into the host genome for long-term silencing (Hannon & Rossi, 2004). As with any technology, there are limitations to RNAi interference experiments including off-target gene effects and their potential to create false positives. To combat these non-specific effects, numerous siRNAs or shRNAs directed at the same gene of interest may be used, or increasing the number of independent assays carried out (Mohr *et al*., 2010).

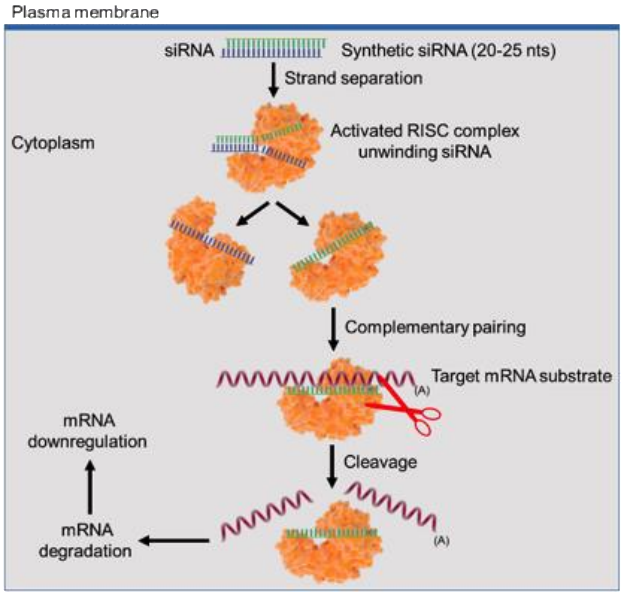

Figure 1.9 Mechanism of Small Interfering RNA (siRNA). A synthetic short pieces RNA of ~ 20-25 nucleotide pairs in length with characteristic 2nt 3' overhangs are introduced into cell. The siRNAs are then incorporated into the cellular enzyme called RNA-induced silencing complex (RISC), which can direct unwinding siRNA. The siRNA–RISC complex then targets a sequence, complementary to the siRNA, in a piece of mRNA. The protein synthesis is blocked either by degradation of mRNA or inhibition of translation. Figure adapted from Hannon & Rossi, (2004).

1.4.1 RNAi Screen Design

In terms of screen design, aspects that require some thought are the selection of cell type, screen type, and viral assay to be used. A simple assay allowing the use of multiple replicates would provide strong data and statistical analysis (Ramage & Cherry, 2015; Falschlehner *et al*., 2010). Chosen cell type should be based not only on a relevant cell type for infection, but also one that is easily transfectable. Knockdown efficiency should be tested as well as the effects of knockdown on infection (Mohr *et al*., 2010).

1.4.2 RNAi Screens against Virus Infection

Since 2008 RNAi screens have been used against a wide range of virus infections, including Human immunodeficiency virus-1 (HIV), Influenza, West Nile Virus (WNV) (Ramage & Cherry, 2015). In 2008, the first three screens were performed with siRNA libraries to identify of host proteins required for HIV infection (Brass *et al*., 2008; Konig *et al*., 2008; Zhou *et al*., 2008). Furthermore, several studies have been carried out using a multiple genome-wide screens to illustrate the mechanisms of influenza virus infection and the host cell requirements to support or control infection (Hao *et al*., 2008; Brass *et al*., 2009; Konig *et al*., 2010). RNAi screens have been used against alphavirus infection. Ooi and colleagues performed a genome-wide RNAi screen in human U2OS cells to identify the mechanisms of several novel host proteins that required for SNIV entry when targeted by multiple siRNAs (Ooi *et al*., 2013). In 2014, Balistreri et al conducted a genome-wide siRNA screen of HeLa cells infected with SFV. The outcomes of this siRNA screen identified that the regulator of nonsense transcripts 1 (UPF1), a central component of the nonsense-mediated mRNA decay pathway (NMD) act as a restriction factor for SFV replication (Balistreri *et al*., 2014). Recently, two studies performed a host genome-wide loss-of-function screen to identify either CHIKV pro- and anti-viral factors in human HEK-293 cells (Karlas *et al*., 2016) or trafficking machineries utilized by CHIKV infection in human HeLa cells (Radoshitzky *et al*. 2016).

1.5 Innate Immunity

The role of the innate immune system is to identify a pathogen entering the body and to start defence mechanisms to protect the body from infectious threats. Germline-encoded pattern-recognition receptors (PRRs) make the detection of microbes possible through analysis of extracellular and intracellular space. If conserved microbial determinants are found, this is treated as sign of infection (Kumar *et al*., 2011; Brubaker *et al*., 2015; Chen *et al*., 2017). Numerous microbial ligands (structural parts of bacteria, fungi, viruses) and biosynthetic molecules (nucleic acids) act as microbial

determinants, and are termed pathogen-associated molecular patterns (PAMPs). When PAMPs are recognised by PRRs, this stimulates the innate immune system by setting in train several different effector mechanisms to eliminate the infection (Janeway, 1989; Janeway & Medzhitov, 2002; Kawai & Akira, 2010).

To date, several families of PRRs have been discovered and characterized based on protein sequence homology. These families include Toll-like receptors (TLRs), RIG-I-like receptors (RLRs), NOD-like receptors (NLRs), and DNA receptors (cytosolic sensors for DNA) (Kumar *et al*., 2011; Chen *et al*., 2017). The PRRs are classified into two main classes: membrane bound receptors and unbound intracellular receptors. Membrane bound receptors consists of the TLRs, which are expressed exclusively on the cell surface or in intracellular vesicles such as the endosomes, lysosomes and endolysosomes. The RLRs and NLRs are intracellular receptors found in the cytoplasm (Kawai & Akira, 2010; Takeuchi & Akira, 2010; Medzhitov, 2007; Blasius & Beutler, 2010; Kumar *et al*., 2009).

1.5.1 Pattern Recognition Receptors

The TLR family is the most widely studied group of PRRs so far, and they are of substantial importance in early antiviral responses to several viruses (Jensen & Thomsen, 2012; Yoneyama *et al*., 2004). TLRs are separated into two subgroups based on their cellular localization and relevant PAMP ligands. The first group consists of TLR1, TLR2, TLR4, TLR5, TLR6 and TLR11, which are localized on cell surfaces and identify mainly microbial membrane components such as lipids, lipoproteins and proteins. Whereas, the second group is composed of TLR3, TLR7, TLR8 and TLR9, which are expressed exclusively in endocytic compartments, and recognize microbial nucleic acids (Kawai & Akira, 2010). It has been identified that human and mouse have 10 and 12 TLRs, respectively: TLR1 to 9 are expressed in both human and mice; in addition, human has TLR10 while mouse has TLR11-13 (Kawai & Akira, 2010; Kumar *et al*., 2011; Chen *et al*., 2017). The RLR family is presented in the cytoplasm and it has three members, retinoic acid- inducible

gene I (RIG-I), melanoma differentiation- associated gene 5 (MDA5), and laboratory of genetics and physiology 2 (LGP2) (Yoneyama & Fujita, 2009; Bryant & Fitzgerald, 2009).

Notably, recognition of viral RNA induces the production of inflammatory cytokines and type I interferons (INFs) by the infected cells. The IFNs (IFN-α and IFN-β) can bind directly to infected cells in an autocrine or paracrine manner through a common receptor and initiate the transcription of several interferon-stimulated genes (ISGs) (Wilkins & Jr, 2010). The NLRs family and their functions in inflammasome signalling highlighted play a role in controlling DNA or RNA virus infection and immunity (Delaloye *et al*., 2009; Allen *et al*., 2009).

1.5.2 Induction of Type-I IFNs and Pro-Inflammatory Cytokines

Viral ssRNA and dsRNA genomes or viral replication intermediates can be sensed in the endosome by TLRs. This serves as a platform for the initiation of signalling cascades and in turn causes the multimerization of cytoplasmic Toll/IL-1 receptor (TIR) domains, which will recruit downstream the TIR domain-containing adaptor-inducing interferon-β (TRIF) or myeloid differentiation primary response 88 (MyD88) through homotypic interaction. Further forming a signalling complex called signalosome and activating downstream transcription factors: one is interferon regulatory factor (IRF) that induces anti-viral type I Interferon (IFN), another is Nuclear factor kappa-light-chain-enhancer (NF-$_k$B) that induces pro-inflammatory cytokines (Kawai & Akira, 2010; Chen *et al*., 2017).

TLR-3, TLR-7 and LRT-8 are located in endosomal compartments and detect phagocytosed material including viruses through the endosomal pathway (Honda *et al.*, 2005). TLR-3 recognizes dsRNA, which is a replication intermediate produced during virus infection (Edelmann *et al*., 2004). Upon binding and activation, dimerization of TLR3 allows for recruitment of the downstream adaptor TRIF. Next, TRIF signalling complex involves other signalling components, such as TNF receptor-associated factor 3/6 (TRAF3, TRAF6-containing complex), which are mediated activation of the kinases

(TBK1, IKKε and IKK). The critical transcription factors IRF3/IRF7 and NF-$_k$B are subsequently phosphorylated and activated by the signalling complex and induce the expression of IFN and pro-inflammatory cytokines, respectively (Chen *et al*., 2017).

TLR7 and TLR8 are activated by ssRNA and they have very similar intracellular signalling. In addition, both may also detect short dsRNA such as siRNA from RNA interference (RNAi) (Sarvestani *et al*., 2012). At steady state, TLR7 and TLR8 exist as dimers; upon binding to agonists, the conformation of dimers change such that MyD88 is recruited to the TIR domain through homotypic interaction. The myddosome complex is formed (IRAK4, IRAK1, TRAF6 and TRAF3) which promotes transcription factors NF-$_k$B and IRF7 are activation to induce pro-inflammatory cytokines (IL-1β, IL-6, IL-10, and TNF-α) and IFNs, respectively (Qin *et al*., 2006; Cervantes *et al*., 2011; Chen *et al*., 2017).

RLRs are expressed in almost all mammalian cell types, and as the main family of cytosolic RNA sensors play key roles in virus recognition as well as initiation the immune responses. RIG-I and MDA-5 are composed of an RNA-binding helicase domain and two caspase recruitment domains (2CARDS) (Yoneyama *et al*., 2004), whereas LGP2 does not possess 2CARDs. The optimal RNA recognized by RIG-I and MDA5 are the 5' triphosphate group on-dsRNA and the long dsRNA, respectively. Whereas the third member LGP2 has no signalling activity, but is able to play as a key regulator of RIG-I and MDA5 act due to the capability of binding RNA (Schlee, 2013; Kell & Gale, 2015). RIG-I and MDA5 signal downstream through the mitochondrial adaptor protein MAVS (also known as IPS-1, VISA and Cardif) (Sohn & Hur, 2016), which serves as a platform for the initiation of signalling cascades. The downstream TRAF3/TBK1/IKKε and TRAF6/IKK further activate transcription factors IRF3/7 and NF-$_k$B, leading to the production of type I IFNs and other pro-inflammatory cytokines, respectively (Wu & Hur, 2016).

RIG-I specifically recognizes most -ssRNA viruses, which generate lots of viral replication intermediates such as short 5' triphosphate group on-dsRNA

during replication. Several studies identified a number of viruses that can be detected by RIG-I including, Ebola virus (EBOV), Measle virus (MV), Sendai virus (SeV), Newcastle disease virus (NDV), Respiratory syncytial virus (RSV), Influenza virus, Vesicular stomatitis virus (VSV), and Rabies virus (RV). In addition, RIG-I also recognizes positive single RNA viruses such as Hepatitis C virus (HCV) and Japanese encephalitis virus (JEV). Moreover, RIG-I is able to sense some DNA viruses such as Adenovirus, Vaccinia virus (VACV), Herpes simplex virus (HSV) in that these viruses produce small dsRNA through their type III RNA polymerase during replication (Vabret & Blander, 2013).

The activation of inflammasomes may also lead to the induction of a type 1 interferon response following of RNA viral infections (Allen *et al*., 2009). Inflammasomes are cytoplasmic multiprotein oligomer complexes that play an essential role in activation of inflammatory processes, apoptosis and necrosis and consist of a member of the Nod-like receptor (NLR) family of PRRs and one of a family of cysteine-aspartic acid proteases, known as caspases. NLRP3 and NOD2 are a subsets of the cytosolic NLRs family, and both of the most extensively studied. NLRP3 is able to recognize the cytosolic dsRNA/ssRNA of Influenza virus and Sendai virus, which is lead to activate the inflammasome and inducing IL-1 and IL-18 (Allen *et al*., 2009; Kanneganti *et al*., 2006). Upon recognition of PAMPs, NLRP3 binds downstream adaptor of the apoptosis-associated speck-like protein containing a CARD domain (ASC) and the CARD of procaspase-1, forming the wheel- like structure inflammasome. Next the caspase-1 is catalyzed the proteolysis of pro IL-1β (inactive) to IL-1β (active) (Chen *et al*., 2017). Several studies have found that NOD2 plays a key role in the restriction of human cytomegalovirus, respiratory Syncytial virus and Influenza A virus, likely through the detection of virus RNA and subsequent IFN induction (Sabbah *et al*., 2009; Kapoor *et al*. 2014). Similar to RLRs, NOD2 has structure to initiate the adaptor MAVS aggregation and down-stream activate NF-$_k$B to induce the transcription of pro-inflammatory cytokines (Sabbah *et al*., 2009).

1.5.3 Induction of ISGs by Type-I Interferon Signalling Pathway

Type I IFN signal transduction is initiated by the Interferon-alpha/beta receptor alpha chain (IFNARs) on the cell surface. IFNAR is heterodimeric and consists of two subunits, IFNAR1 and IFNAR2, located in close proximity on the cell surface. These two tyrosine kinases activate the IFN-stimulated gene factor 3 (ISGF3) consisting of the signal transducer and activator of transcription factors: STAT 1/2 and IRF9, which translocates into nucleus and binds to IFN-stimulated response elements (ISREs) and that leads to production more than 300 Interforn Stimulated Genes (ISGs) (Sadler and Williams, 2008; Li *et al*., 2015). ISG products are implicated in diverse roles, including establishing the antiviral state, antigen presentation, apoptosis, cell stress pathways and membrane trafficking, although many of the ISG are uncharacterised (Stark *et al.*, 1998; Williams, 1999; Sen, 2000; Enninga *et al.*, 2002). Importantly, ISG proteins such as ISG15, GTPase Mx1, and protein kinase R (PKR) have been validated as antiviral effectors in studies of gene knockout mice. ISG15 is one of the most highly induced ISGs and when coupled to protein substrates modulates pleiotropic cellular activities (Harty *et al*., 2009). Mx proteins are also highly induced by IFN then self-assemble into oligomers that are constitutively active (Haller *et al*., 2015; Fuchs *et al*., 2017). PKR is constitutively expressed as an inactive kinase that is activated by viral double-stranded RNA (dsRNA), then further induced by IFN (Pindel & Sadler, 2011).

1.5.4 Alphaviruses and the Innate Immune Response

For alphaviruses, it is known that high levels of serum IFN-α/β are associated with systemic replication of SINV and VEEV *in vivo* (Ryman *et al*., 2000; White *et al*., 2001). Type I IFNs are induced following alphaviruses infection in several cell types (Griffin, 2013), whereas the infection of established MEFs with the SINV did not result in IFN production (Frolova *et al*., 2002). Regarding PRRs involved in IFN induction by alphaviruses, one study reported that induction of IFN-α by SINV in MDA5$^{-/-}$ macrophages was minimally impaired, suggesting that this molecule was not vital to responses

against alphaviruses with this cell type (Gitlin *et al*., 2006). By contrast, MDA5$^{-/-}$ MEFs produced 2-fold less IFN following infection with mutant SINV compared to WT (Burke *et al*., 2009). Furthermore, in study observations suggested that ISG such as ISG15 was critical for controlling SINV (Lenschow *et al*., 2007).

1.5.4.1 Innate Immune Control of CHIKV Infection

The crucial role played by type 1 IFNs following CHIKV infections have been identified in several studies. In 1963, a study has reported in Nature that chick embryo fibroblasts infected with CHIKV produced detectable levels of type I IFNs 3 hours upon infection (Gifford and Heller, 1963). Recent studies with human and mouse cells, both *in vivo* and *in vitro,* have shown that infection of hematopoietic cells does not directly induce type I IFNs. By contrast, it was shown that type I IFNs are produced at high levels by infected primary human foreskin fibroblasts and MRC-5 fibroblast cells (Schilte *et al*., 2010). As described, CHIKV has a +ssRNA genome and likely replicates in two transcriptional stages; first a complementary (-ssRNA) version which is used as a template to generate progeny RNA and the second stage is made a dsRNA intermediary during this process. RLRs present in the cytoplasm including RIG-1 and MDA-5, are proposed to detect the replication intermediates (Figure 1.10). Similarly, it is possible that TLR3 present in endosomes plays a role in recognising virus entering via this pathway (Schwartz & Albert, 2010).

The activation of PRRs triggers the production of type I IFNs, which are crucial in control of CHIKV infections. Indeed, one study demonstrated that CHIKV is critically dependent on type I IFN action on non-hematopoietic cells such as stromal cells and, thus, acts as a direct antiviral, likely through the induction of one or more ISGs through IFN-α/β receptor (IFNAR) signalling (Schilte *et al*., 2010). For CHIKV, one group has been reported that HeLa cells transfected with ISG such as 2′, 5′-oligoadenylyl synthetase (OAS3) are more resistant to CHIKV replication (Bréhin *et al*., 2009). Whereas, SFV, it found that human MxA confers resistance (Landis *et al*.,1998).

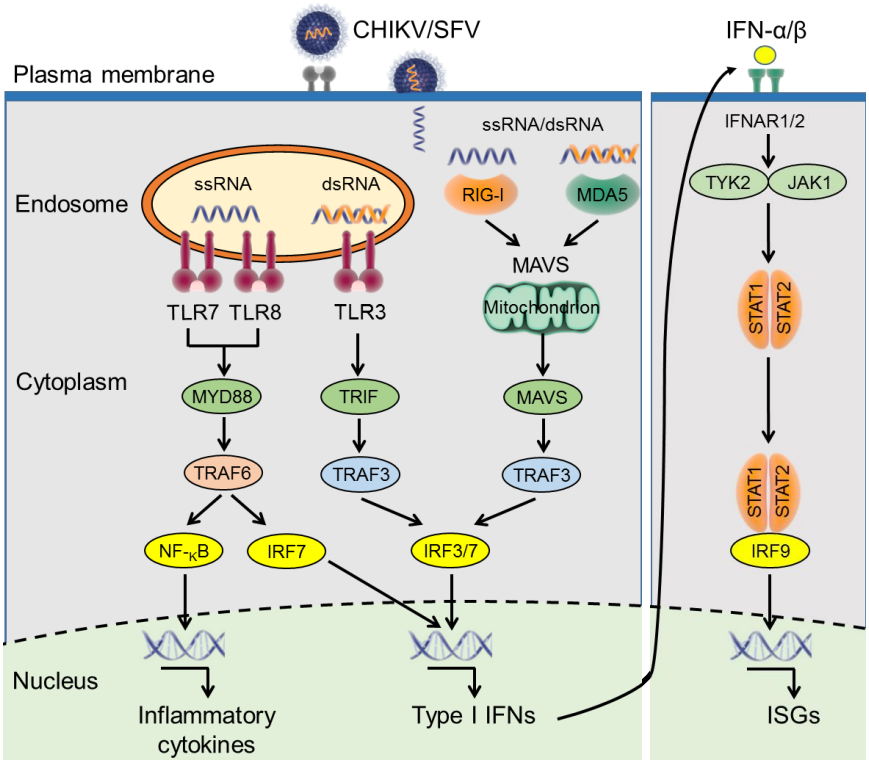

Figure 1.10 Schematic representation of recognition of CHIKV/SFV by PRR. CHIKV and SFV are ssRNA virus and may generate dsRNA intermediates during replication. In the endosome, ssRNA is engage with the pathogen recognition receptors Toll-like receptor 3 (TLR3), whereas TLR7 and TLR8 are sense dsRNA. In cytoplasm, the retinoic acid-inducible gene I (RIG-I)-like receptors (RLRs) melanoma differentiation-associated protein 5 (MDA5) and RIG-I are sense the ssRNA and dsRNA. These receptors activate a signalling cascade that leads to the activation of type I interferons (IFNs) and the transcription of cytokines and chemokines. Type-I IFN binds to and induces the dimerisation of IFNAR1/2 in the IFNAR receptor. This activates TYK2 and JAK-1, which phosphorylate STAT1/2. STAT1 and STAT2 form a heterodimer, which associates with IRF-9 either in the cytoplasm or the nucleus. The complex binds to the IFN-stimulated response element (ISRE), which induces the transcription of multiple IFN-stimulated genes. Figure adapted from Schwartz & Albert, (2010).

1.6 Ubiquitin Proteasome System

Regulation of the biological attributes of a translated protein is achieved through covalently adding or removing chemical entities to/from the protein termed the post-translational modification (PTM) process (Mann & Jensen, 2003). The process of ubiquitination, in which the 76 amino acid protein ubiquitin (Ub) is reversibly linked to substrate proteins, is a key PTM that regulates wide range of cellular processes. (Bergink & Jentsch, 2009). The discovery in 1975 of Ub as a highly conserved polypeptide in mammalian, bacterial, yeast and plant cells is attributed to Gideon and colleagues (Goldstein *et al*., 1975). Goldknopf and Busch (1977) distinguished a histone-protein complex bound by an isopeptide, that Ub could perform covalent alteration of other proteins, with Ub being later on identified as the conjugated protein (Goldknopf & Busch, 1977; Hunt and Dayhoff, 1977). During the 1980s, Hershko, Ciechanover and Rose shed light on the correlation between Ub-induced alteration of proteins and their proteasomal degradation (Hershko *et al*., 1980; Wilkineon & Urban, 1980). Since then, correlations have been established between Ub and various cellular processes such as endocytosis, cell cycle, transcription regulation and DNA damage repair (Ciechanover *et al*., 1980).

1.6.1 Conjugation of Ubiquitin to Proteins

Isopeptide bond linkages are the form that Ub alterations can take. The isopeptide bond occurs between the C-terminal glycine (Gly76 or G76) of Ub and the lysine (Lys or K) residues on substrate proteins. Mono-ubiquitination involves a single Ub moiety altering a substrate, while multi-ubiquitination involves multiple Ub moieties altering a substrate (Figure 1.11). Histone regulation and DNA damage repair are among the biological processes correlated with mono-ubiquitination (Hicke, 2001; Haglund *et al*., 2003; Huang and D'Andrea, 2006; Shilatifard, 2006). Meanwhile, a correlation seems to exist between both mono- and multi-ubiquitination and endocytosis.

Polyubiquitin (polyUb) chains can form because the seven Lys residues of Ub (K6, K11, K27, K29, K33, K48, and K63) (Figure 1.11) enables it to serve

as a substrate as well. For instance, K63 polyUb and K48 polyUb respectively present a chain-like structure and a compact and spherical structure. Meanwhile, correlations exist between certain chain isoforms and their physiological roles. For instance, K63 polyUb are predominant in cell signalling pathways, whereas K48 and K11 polyUb alterations usually accompany proteasomal degradation. (Ikeda & Dikic, 2008; Kim *et al*., 2007; Meyer & Rape, 2014).

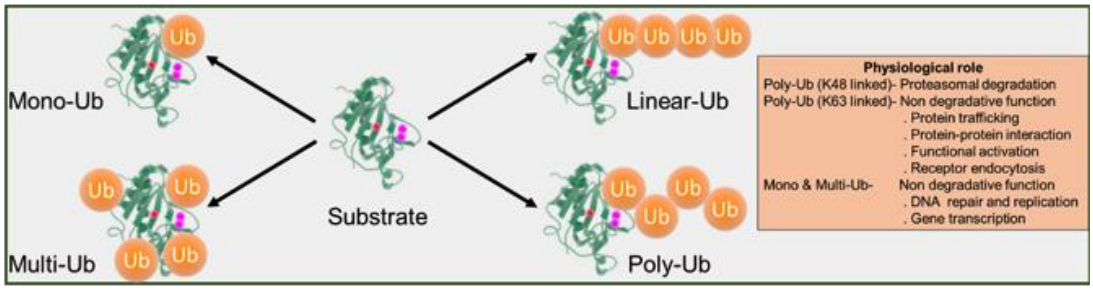

Figure 1.11 Schematic figure representing of types of Ub modification and their known physiological roles. Figure adapted from Haglund *et al*., (2003).

1.6.2 Ubiquitination Processing

A variety of Ub enzymes underlie the multitude of possible Ub alterations. Employing various enzyme assemblies, the Ub machinery can accurately regulate a couple of thousand target proteins. After ubiquitination was discovered as a crucial agent in proteasomal degradation, Ciechanover and colleagues uncovered the fundamental mechanism underpinning this process. In 1981, a discovery was made regarding the covalent attachment of the Ub-activating enzyme (E1) to Ub with dependence on ATP and mediated by a thioester bond (Ciechanover *et al*., 1981; Hershko *et al*., 1980). Two years later, affinity purification via an Ub-sepharose column permitted the isolation and detection of Ub-conjugating (E2) and Ub-ligase (E3) enzymes (Hershko *et al*.,1983). These aspects served to create the present ubiquitination model (see section 1.7, Figure 1.12). The initial step is active Ub conjugation to an E1 enzyme based on the mediation of a thioester bond between Gly76 and a catalytic cysteine (Cys) residue. This is followed by the conjugation of the Ub moiety to an E2 enzyme via an analogous thioester

bond, resulting in the formation of an E2-Ub conjugate. An E3 ligase subsequently enables a last transfer to a protein substrate Lys residue. A family of deubiquitinating enzymes (DUBs) eliminates such Ub PTMs (Inobe & Matouschek, 2014).

The Ubiquitin conjugating (UBC) domain is a catalytic domain with approximately 150 amino acids that is present in all E2 enzymes. It displays a topology of high consistency, while enzyme specificity is yielded by extra C- and N-terminal extensions (Stewart *et al*., 2016). Whereas some E2s have interaction with more than one E3 ligase family, others interact solely with one family. The reactivity of E2-Ub conjugates is usually low and, to mediate Ub transfer, they must interact with an E3. For instance, although the E2 family of UBE2D (ubiquitin-conjugating enzyme E2 D) has poor reactivity with Lys on its own, when it interacts with an E3, it exhibits fast reaction (Stewart *et al*., 2016; Wenzel *et al*., 2011). Ample structural research has highlighted the great dynamism of the configurations adopted by E2-Ub conjugates, with a reactive configuration arising from the attachment to its E3 correspondent (Pruneda *et al*., 2011; Pruneda, Jonathan *et al*., 2012; Dou *et al*., 2012; Branigan *et al*., 2015). Better understanding of such temporary complexes was promoted by the use of mutant E2-Ub conjugates imitating temporary thioester linkage by being bound not via a Cys residue, but a Lys. It is worth noting that Ub chains cannot be formed by a limited E2 subset, which exhibits specificity for lengthening of polyUb chains instead. Lacking inherent catalytic activity, these E2s can mediate Ub transfer solely when the substrate and E3 ligase partner are present. One such E2 with specificity for K63 chain lengthening is UBE2N-UBE2V1 (ubiquitin-conjugating enzyme E2 N-ubiquitin-conjugating enzyme E2 variant 1) heterodimer (Heride & Urbé, 2012; Hofmann & Pickart, 1999).

There is growing awareness that E2s have additional regulatory functions, besides Ub conjugation. For instance, UBE2D2 binds to the DUB OTUB1 (ubiquitin thioesterase OTUB1), thereby increasing its protease activity. Meanwhile, OTUB1 can attach to other E2-Ub conjugates, thus suppressing their activity (Stewart *et al*., 2016).

E3 ligases are involved in catalysis by mediating direct Ub transfer between the E2-Ub conjugate and substrate protein or through intermediary covalent bond to Ub followed by transfer to the substrate protein. Accordingly, three families of E3s can be distinguished, namely, RING (Really Interesting New Gene), HECT (Homologous to E6AP C-Terminus), and RBR (RING between RING) ligases (Morreale *et al*., 2016). The richest family is RING E3 ligases, consisting of around 600 enzymes so far. Covalent binding of HECT E3 ligases to Ub occurs before the transfer to the substrate. Consisting of around 30 human enzymes distinguished so far, HECTs constitute an E3 ligase family of smaller size (Morreale *et al.* 2016). A different E3 ligase family made up of about 12 enzymes is constituted by RBR ligases, which employ a combination of RING and HECT catalytic mechanisms (Wenzel *et al*., 2011).

1.7 Debiquitylation and Deubiquitylases

Ubiquitylation of protein is a reversible process, which facilitates the termination of ubiquitin-dependent signalling. The isopeptide that links ubiquitin and substrate and/or ubiquitin molecules in a polyubiquitin chain are cleaves by deubiquitylating enzymes (deubiquitylases or DUBs) (Komander *et al*., 2009). The most abundant type of linkage in proteins is the K48-linked polyUb chain, which targets proteins for proteasomal degradation (Finley, 2009; Kulathu & Komander, 2012). Before degradation commences, DUBs associated with the proteasome liberate Ub from the substrate, enabling Ub to be recycled (Inobe & Matouschek, 2014).

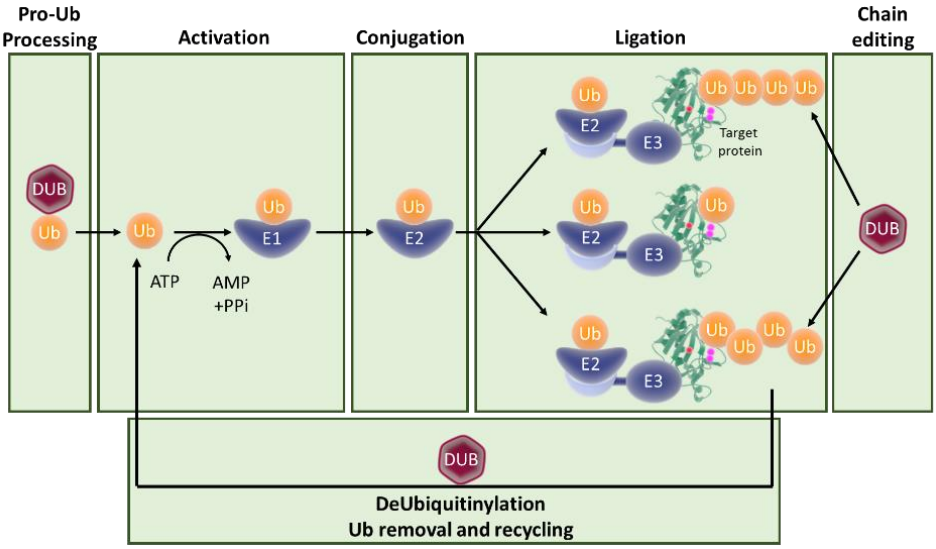

Figure 1.12 Schematic representation of the degradation cycle of the ubiquitin proteasome system. Polyubiquitin tag is attached by a E1–E2–E3 ubiquitination cascade and this process can be reversed by DUBs. Activation: ubiquitin is activated by an E1 activating enzyme in the presence of ATP and Mg2+, and forms a thioester bond to the catalytic cysteine (top left). Conjugation: activated ubiquitin is transferred to an E2 conjugating enzyme Top centre). Ligation: Ubiquitin is transferred to an acceptor lysine on the protein substrate (top right). Chain editing: the ubiquitin moiety is first transferred onto the E3 ligase which catalyses ubiquitylation of substrate (top right edge). Deubiquitinylation: repeated cycles of ubiquitylation are required for the construction of polyubiquitin chains. Figure adapted from Inobe & Matouschek, (2014).

1.7.1 DUB Families and Catalytic Activity

The human genome encodes about 100 DUBs that are distinguished by their catalytic mechanism and grouped into six families according to their catalytic domains. There are also genes for approximately 100 deubiquitylases in the human genome; around 80 of these have catalytic capability (Clague *et al*., 2013). Five of the families of DUBs are cysteine proteases; they are ubiquitin specific proteases (USPs), ubiquitin C-terminal hydrolases (UCHs), ovarian tumour proteases (OTUs, also known as otubains), Josephins (MJD) and motif interacting with Ub- containing novel DUB family (MINDY). A group of metalloproteases form the sixth group, known as JAMMs/MPN+ (JAB1/MPN/MOV34 metallo-enzymes) (Figure 1.13) (Rehman *et al*., 2016; Reyes-turcu *et al*., 2009).

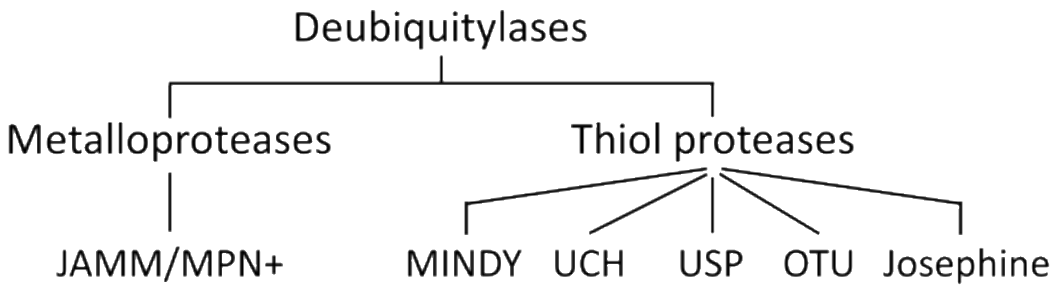

Figure 1.13 Schematic representation of the human DUB families and catalytic activity.

The functionality of cysteine proteases is typically reliant on a catalytic group of three residues, comprising histidine, cysteine and asparagine or aspartate. The pKa of the catalytic cysteine residue is reduced by the histidine residue, which exposes the isopeptide bond to nucleophilic attack (Komander *et al*., 2009). The purpose of the asparagine or aspartate residue is to align and polarise the histidine; though as the Otubain family member and TNFAIP3 (tumour necrosis factor alpha-induced protein 3, also known as A20) have demonstrated, the aligning and polarising action is not critical for DUB function (Komander & Barford, 2008). As a consequence of nucleophilic attack, the substrate is released and the cysteine residue and conjugated (distal) ubiquitin form a covalent bond that contributes to an acyl-intermediate forming. A supposed oxyanion hole, generated by surrounding residues, stabilises the intermediate, which is then hydrolysed by a molecule of water, releasing the free ubiquitin (Komander *et al*., 2009; Nijman *et al*., 2005).

The catalytic domain of STAMBPL1 (STAM binding protein-like 1, also known as AMSH-LP) has been crystallised alone and in combination with K63-linked diubiquitin, revealing the mechanisms of action of the metalloprotease DUBs (JAMMs) (Sato *et al*., 2008). A JAMM/MPN+ motif that co-ordinates a pair of catalytic zinc ions, is embedded in the catalytic domain. The isopeptide bond zinc is attacked by water molecule that has been activated by the zinc ions. This in turn results in a charged intermediate that collapses, releasing the amino group on the nearest ubiquitin (Komander *et al*., 2009; Sato *et al*., 2008).

1.7.2 Myb-like, SWIRM and MPN Domains-Containing Protein 1

In 2007, Zhu *et al*. distinguished Myb-like, SWIRM, and MPN domains-containing protein 1 (MYSM1) to be a histone H2A deubiquitinase (2A-DUB). The H2A deubiquitination activity stimulates a number of target genes in prostate cancer cells. Hydrolysis of the isopeptide bonds in the ubiquitin chains is performed by the JAMM/MPN+ domain, which has essential metalloprotease activity (Zhu *et al*., 2007). At the N-terminal of MYSM1 is a SANT domain (Swi3, Ada2, N-Cor and TFIIIB), which facilitates histone/DNA binding. A SWIRM domain (SW13, RSC8 and MOIRA) is located in the centre of the MYSM1; this domain is thought to regulate arbitrate interactions with chromatin-associated proteins. Finally, at the C-terminal is the MPN domain (JAB/Mov34), which bears the metalloprotease activity (Figure 1.14) (Boyer *et al*., 2004; Qian *et al*., 2005; Yoneyama *et al*., 2007; Zhu *et al*., 2007).

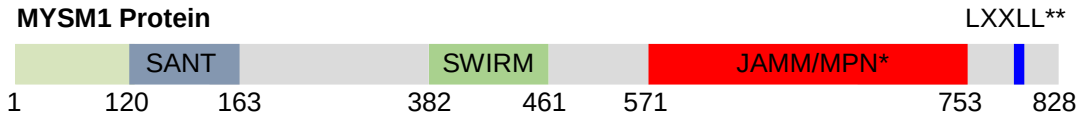

Figure 1.14 Schematic representation of the domain organization of the human MYSM1 protein structure. MPN region: (571-753) aa and JAMM region: (656-669) aa and LXXLL: region (774-778) aa. Figure adapted from Zhu *et al*., (2007).

A complex comprising MYSM1 and p300/CBP-associated factor (p/CAF), the histone acetyltransferase, was characterised in human embryonic kidney cells by Zhu *et al*., (2007). How gene transcription is regulated by H2A ubiquitinases has yet to be elucidated, but it has been postulated that a complex forms between MYSM1 and p/CAF, which regulates the initiation of gene transcription and elongation. The proposed mechanism is the stepwise coordination of histone acetylation, H2A deubiquitination and the linker histone, H1, disconnecting from the nucleosome (Zhou *et al*., 2009; Zhu *et al*., 2007).

A line of knockout mice, deficient in MYSM1, was created to resemble the clinical symptoms of human MYSM1 mutation (Alsultan *et al*., 2014; Le Guen *et al*., 2015). The mutation is manifest as reduced cellularity in all blood organs (Jiang *et al*., 2011; Nandakumar *et al*., 2013; Wang *et al*., 2013; Nijnik *et al*., 2012; Won *et al*., 2016). Various studies have highlighted the important roles of MYSM1-mediated H2A deubiquitination in the differentiation of haemopoietic stem cells (Wang *et al*., 2013), the maturity of natural killer (NK) cells (Nandakumar *et al*., 2013) and the duties of B-cells and dendritic cells (DCs) (Jiang *et al*., 2011; Jiang *et al*., 2015). Other researchers have found MYSM1 is needed for thymocyte development and interferon regulatory factor (IRF) expression to keep HSC dormant (Huang *et al*., 2016).

1.7.3 Deubiquitylation and Innate Immunity

Throughout the preliminary phases of viral infection, host PRRs detect PAMPs before signalling to induce IFNs and PIC (see section 1.5). As reported by Liu *et al*., (2005), a crucial operation in PRR signalling is protein ubiquitination and deubiquitination. DUBs perform an important functions in regulating innate immune-receptor signalling, especially the NF-κB pathway. As documented by Harhaj and Dixit, (2012), DUBs regulate the NF-κB pathway at a variety of levels, and the pathway itself regulates innate and adaptive immunity. The sequestration of NF-κB tends to take place in a complex with IκB, and this is followed by the phosphorylation of IκB and the subsequent dissociation from NF-κB. Before proteasome degrades IκB, it is subjected to K48 polyubiquitylation, thereby meaning that NF-κB is at liberty to translocate towards the nucleus. Oeckinghaus and Ghosh have described that in the nucleus, NF-κB's role is primarily concerned with target gene transcription regulation (Oeckinghaus & Ghosh, 2009). Whereas, K63 polyubiquitylation takes place for a range of NF-κB signal transduction promoting proteins (including NF-κB essential modulator [NEMO], TRAF3, and TRAF6) (Sun, 2008).

TNFAIP3 (tumour necrosis factor alpha-induced protein 3, also known as A20), a relative of Otubain, was the original DUB implicated in innate

immune regulation (Komander & Barford, 2008). Characterised by DUB and E3 ligase activity and the regulation of its substrates (TRAF6 and RIP1 [receptor interacting protein 1]), TNFAIP3 functions as a negative regulator of the NF-κB pathway. Substrate regulation occurs by a ubiquitin editing operation, characterised by the removal of K63 chains and their substitution for K48 linkages (Wertz *et al*., 2004; Novak *et al*., 2009). Ultimately, this drives substrate degradation. Another one of the NF-κB pathway's negative regulators is cylindromatosis turban tumour syndrome (CYLD), which is related to the USP group of DUBs. NF-κB transcriptionally upregulates CYLD, and CYLD serves as a negative feedback loop (Jono *et al*., 2004). As a tumour suppressor, it facilitates the degradation of the K63 chains, thereby driving the inactivation of the proteins and the pathway's downregulation (Trompouki *et al*., 2003; Kovalenko & Chable-bessia, 2003). Enesa *et al*., (2008) and Xu *et al*., (2010) suggested that other negative regulators of the NF-κB pathway include the Otubain OTU7B and USP21, both DUBs. A study has demonstrated that USP15 could be implicated in the regulatory aspects of NF-κB activation (Schweitzer *et al*., 2007). Zhou and colleagues were found evidence to indicate that USP4 deubiquitinates TRAF6, thus hindering NF-κB activation and the attendant proinflammatory responses (Zhou *et al*., 2012).

1.7.3.1 DUBs and the Regulation of Antiviral Innate Immunity

IKKε and TBK1 activation, along with IRF3 and IRF7 (namely, downstream transcription factors), are fundamental aspects of antiviral innate immunity (Hiscott, 2007). Häcker *et al*., (2006) reported that TRAF3 – a pivotal mediating molecule – serves as a linkage between upstream signalling molecules and TBK1 and IKKε. siRNA screening was applied to reveal DUBA's (also known as OTUD5) negative regulatory role regarding type I interferon (IFN) induction. OTUD5 facilitates the selective regulation of IRF3 and IRF7 activation (namely, the transcription factors regulating IFN expression by DUBA's physical interaction with TRAF3 and inhibition of TRAF3's self-ubiquitylation) (Kayagaki *et al*., 2007). Nevertheless, Zhang *et al*., (2008) found that CYLD facilitates the negative regulation of RIG-I's ubiquitylation while impeding irregular TBK1- IKKε activation. *In vitro* projects

implicated A20 as a negative regulator of antiviral innate immune responses, with TLR3 and RIG-I serving as intermediaries (Wang *et al*., 2004; Lin *et al*., 2006). Both studies found that A20 activity could centre around TRIF (an adaptor protein) or downstream kinases (namely, TBK1 and IKKε). Li *et al*., (2010) indicated that OTUB1 and OTUB2, by virtue of deubiquitinating TRAF3 and TRAF6, are implicated in the negative regulation of virus-triggered type I IFN induction, along with cellular antiviral response. Contrastingly, a study finding has suggested that USP25 induction by viral infection, since it intermediates TRAF3 and TRAF6 stability, underpins antiviral immune responses (Lin *et al*., 2015). During this thesis, the DUB MYSM1 was reported to be involved in negative regulation of PRR signalling (Panda *et al*., 2015). This will be referred to further during the discussion. A schematic overview of DUB regulations of PRR signalling is shown in Figure 1.15.

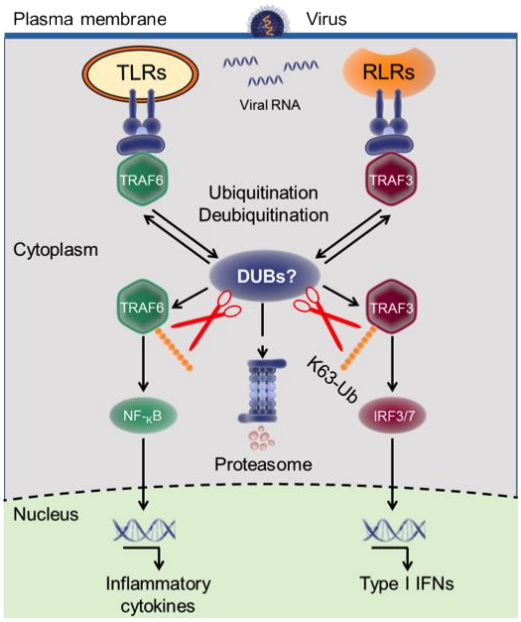

Figure 1.15 Regulation of innate immune-receptor signalling by DUBs upon viral infection. The Toll-like receptors (TLRs) are sense by endosomal viral RNA, while the RIG-like receptors (RLRs) are sense by cytoplasmic viral RNA. These receptors activate the K63-linked ubiquitylation of tumour-necrosis factor receptor-associated factor 3 (TRAF3) and TRAF6, which leads to the recruitment of downstream signalling molecules. Ubiquitylated TRAF6 recruits the inhibitor of NF-κB (nuclear factor-κB) kinase) complex thereby negatively regulating pro-inflammatory cytokines. While, ubiquitylated TRAF3 negatively regulate of IFN-regulatory factor 3 and 7 (IRF3/7) signalling events that control transcriptional induction of type I IFN responses. Figure adapted from Sun, (2008).

1.8 Viruses and the Ubiquitination System

All viruses rely extensively on host machinery to achieve successful infection. Accordingly, viruses have evolved to enhance or inhibit ubiqutylation of specific substrates to either enhance viral replication or inhibition specific cellular processes (Isaacson & Ploegh, 2009). Several studies have reported that many viruses have a capability to encode proteins which alter the host cells ubiquitin and deubiquitin processes. Indeed, a number of viruses have been shown to encode their own E3 ligases or DUBs enzymes (Gao & Luo, 2006).

1.8.1 Viral Manipulation of E3 Ligases

A number of virus families have been shown to encode proteins with E3 ligase activity or are capable of inducing cellular E3 ligase activity. These include viruses from the Herpesviruses family, adenoviruses, Human papillomaviruses (HPV), HIV-1, VACV (Wimmer & Schreiner, 2015). An example of this is the RTA protein encoded by Kaposi's sarcoma-associated herpesvirus (KSHV); this protein acts as a E3 ligase and promotes the polyubiquitination of interferon regulatory factor 7 (IRF7) (Yu *et al*., 2005), which is a transcription factor involved in the regulation of virus-inducible cellular genes such as the type-1 interferons (Sato *et al*., 2000). By promoting the degradation of IRF7, RTA aids the virus in evasion of the innate immune system during KSHV infection. KSHV also encodes two membrane-associated proteins with homology to RING-CH (MARCH) family E3 ubiquitin ligases: these are K3 and K5 (also known as MIR1 and MIR2). K3 and K5 proteins have been shown to target surface MHC class I molecules, leading to their ubiquitinylation, internalization and consequently endolysosomal degradation (Lehner *et al*., 2005; Wang *et al*., 2008).

The infected cell protein 0 (ICP0) encoded by the HSV-1 has been shown to act as an E3 ubiquitin ligase during infection. ICP0 targets specific cellular proteins such as specific nuclear structures known as PML (promyelocytic leukemia) nuclear bodies or ND10 that are responsible for

cellular repression of viral transcription (Parkinson & Everett, 2000; Hagglund & Roizman, 2002; Boutell *et al*., 2002; Boutell & Everett, 2003).

The adenovirus protein E1B-55K has multiple functions during infection. During the later stages of infection it has been shown to form a complex with the viral protein E4orf6 and cellular factors Rbx1/Roc1/Hrt1, Cullin2/5, Elongin B and C (Harada *et al*., 2002; Querido *et al*., 2001). This complex functions as an E3 ligase of the Skp1-Cullin-F-box type. E1B-55K serves as the substrate recognition unit of the complex whilst E4orf6 assembles the cellular components of the complex (Harada *et al*., 2002; Querido *et al*., 2001). This viral E3 ligase is known to play a role in accelerating the degradation of p53 and hence preventing apoptosis (Lowe & Ruley, 1993). HIV-1 has also been shown to encode at least three proteins that in a complex with cellular proteins form an Skp1-Cullin-F-box type E3 ligase (Yu, 2003). HIV Vif, Vpu, and Vpr have shown the ability to suppress cellular antiviral activity by redirecting cellular ubiquitin ligases to accelerate the degradation of apolipoprotein B mRNA editing enzyme, catalytic polypeptide-like 3G (APOBEC3G) (Sheehy *et al*., 2002; Yu, 2003).

HPV-16 and HPV-18, manipulate the ubiquitin pathway through the virus-encoded protein E6. The E6 protein in conjunction with the cellular E6-associated protein (E6-AP) (Huibregtse *et al*., 1991), facilitates the rapid degradation of the tumor-suppressor protein p53 by acting as an E3 ligase (Scheffner *et al*., 1994). The HPV-16 E7 protein has been shown to associate with a cullin 2 ubiquitin ligase complex, which can result in Ub-mediated degradation of retinoblastoma (Rb) protein (Berezutskaya *et al.*, 1997), a key tumour suppressor protein, which can lead to uncontrolled cellular proliferation.

Some viruses have the ability to block host ubiquitin E3 ligases by encoding inhibitors. Mansur and co-workers reported that during VACV infection the viral protein A49 promoted evasion of the immune system and enhanced virus virulence by blocking activation of NF-kB. A49 does this by exploiting molecular mimicry of IκBα, binding to the WD40 domain of the E3 ubiquitin ligase. Consequently, IκBα is not ubiquitinylated and degraded, thus

remains attached to the NF-κB complex in the cytoplasm (Mansur *et al*., 2013). Studies have shown that Rotavirus nonstructural protein NSP1 mimics the IκB phosphodegron to mediate degradation of immunomodulatory proteins, such as interferon factors 3/5/7/9, MAVS, and TRAF2 during rotavirus infection, which helps virus propagation (Graff *et al*. 2009; Bagchi *et al*. 2013).

1.8.2 Virus Encoded DUBs and Viral Activation of Cellular DUBs

Another way in which viruses can manipulate the host ubiquitination system is through deubiquitination. They can do this by encoding viral deubiquitinases or modulating the function of host deubiquitinases. Herpesviridae is an example of a family of virus that produces deubiquitinase enzymes. The herpesvirus ubiquitin-specific protease (USP) is conserved across all members of the family (Kattenhorn *et al*., 2005; Schlieker *et al*., 2005). Marek's disease virus (MDV), a tumorigenic alphaherpesvirus of chickens, produces a USP in which a single amino acid change has been shown to abolish USP activity. Without an active USP MDV replication *in vivo* is limited and the oncogenic potential of the virus significantly diminished (Jarosinski *et al*., 2007). Other herpesviruses which show DUB activity include HSV-1, Epstein-Barr virus (EBV) and human cytomegalovirus (Wang *et al*., 2006). These DUBs have been shown to lack homology with eukaryotic DUBS making them attractive drug targets (Kattenhorn *et al*., 2005). EBV is associated with a number of different cancers, studies have shown that the oncogenic properties of EBV may be related to stabilization of β-Catenin (a proto-oncogene) and subsequently, activation of the β-Catenin pathway by viral deubiquitinases (Shackelford *et al*., 2003). EBV has also been shown to produce herpesvirus-associated ubiquitin-specific protease (HAUSP, also known as USP7) during infection that is able to deubiquitylate both p53 and MDM2 and hence delay apoptosis (Hu *et al*., 2006; Saridakis *et al*., 2005).

Nairoviruses and arteriviruses, two unrelated groups of RNA viruses have been shown to produce ovarian tumour (OTU) domain-containing proteases. These proteases show DUB activity and are able to hydrolyze both Ub and ISG15 (a ubiquitin like protein with antiviral properties) from cellular target proteins (Frias-Staheli *et al*., 2007; Morales & Lenschow, 2013). These

viral OTU domain-containing proteases have been shown to function in a similar manner to A20 (mammalian DUB, also known as TNFAIP3), but have a broader target specificity (Frias-Staheli *et al*., 2007). Murine models of Sindbis virus infection have shown that expression of viral OTU domain-containing proteins antagonize the antiviral effects of ISG15 and inhibit NF-kB-dependent signalling and consequently increase susceptibility to infection (Frias-Staheli *et al*., 2007).

Respiratory syndrome coronavirus (SARS-CoV) has been shown to produce a papain-like protease (PLpro) with DUB activity; the protease has structural features that resemble known DUBs such as USP14 and HAUSP (Ratia *et al*., 2006) and cleaves at the consensus cleavage site LXGG, a target sequence recognized by many other deubiquitinating enzymes (Barretto *et al*., 2005; Lindner *et al*., 2005). PLpro has been shown to be a potent IFN antagonist but this function has been shown to be a result of PLpro interacting with IRF-3, to prevent phosphorylation of the protein and translocation to nucleus, as opposed to DUB activity of the protein (Devaraj *et al*., 2007). Middle East Respiratory Syndrome Coronavirus (MERS-CoV) has also been shown to produce a papain-like protease (Mielech *et al*., 2014).

Adenoviruses have also been shown to produce deubiquitinases in an effort to evade immune defences; studies using ubiquitin aldehyde, ubiquitin designed to identify the deubiquitinating proteases, aided the discovery of adenovirus L3 23K proteinase (Avp). In addition to processing viral precursor proteins during virion maturation, Avp has also been shown to deubiquitinate a number of cellular proteins *in vivo*. Structural models of the Avp binding site have shown that it shares similarities with ubiquitin hydrolases (Balakirev *et al*., 2002).

1.9 Aims and objectives

The role of the ubiquitin proteasome pathway, and in particular DUBs, during alphavirus infection has not been well studied. In this research project, I set out to investigate the role of the DUBs during the alphavirus infection, focusing initial on the BSL2 model virus SFV, and extending this to CHIKV (at BSL3). This work was stimulated by an original DUB siRNA screen against SFV infection of HeLa cells, carried out previously in the laboratory (See Chapter 3 section 3.1). This screen identified a number of DUBs that were predicted to be pro-viral (i.e. DUBs that were critical for virus replication) and thus could potential be candidate antiviral targets. The overall aim of this thesis was to validated the hits from the original screen and characterise the role of candidate DUBs during alphavirus infection.

The specific aims were:

- Validate hits for original DUB siRNA screen by deconvolution of siRNA pools
- To determine the role of selected DUBs during SFV and CHIKV infection.

Chapter 2

Materials and Methods

2.1 Materials

All material and reagents used throughout this thesis are listed in the Tables 2.1.1 to 2.1.3.

2.1.1 Chemical Reagents

Item	Company
Agarose	Invitrogen
Low melting point agarose	Invitrogen
Foetal Calf Serum	Sigma
Trypsin-EDTA	Sigma
Mercaptoethanol	Sigma
Dimethyl sulfoxide	Sigma
Sodium dodecyl sulfoxide	Sigma
Ammonium persulfate	Sigma
Penicillin/Streptomycin	Sigma
L-glutamine	Sigma
Ethidium Bromide	Sigma
N,*N*,*N*′,*N*′-Tetramethylethylenediamine	Sigma
1,4-Dithiothreitol	Sigma
7.5 % Sodium Bicarbonate	Sigma

2.1.2 Enzymes and Commercial Kits

Item	Company
CellTitre-Glo luminescence reagent	Promega
Small Interference RNA	QIAGEN
AllStars Positive Control siRNA	QIAGEN
AllStars Negative Control	QIAGEN
RNeasy Plus Mini Kit	QIAGEN
RevertAid™ H minus M-MuLV Reverse Transcriptase Enzyme	Thermo Fisher Scientific
Oligo (dT)15 primer	Promega
2x PCR ReddyMix	Thermo Fisher Scientific
iTaq™ Universal SYBR Green Supermix	BioRad
Pierce BCA Protein Assay	Thermo Fisher Scientific
Pierce ECL Western Blotting Substrate	Thermo Fisher Scientific
Lipopolysaccharide *E. coli* 0111:B4	InvivoGen

Polyinosinic-polycytidylic acid ,poly(I:C),High Molecular Weight	InvivoGen
poly(I:C)-LMW/LyoVec	InvivoGen
RNAiMax	Invitrogen
10x Trypsin	Sigma

2.1.3 Solutions and Buffers

Item	**Company**
5x Agarose Gel Loading Dye	New England BioLabs
10x Tris-Acetate-EDTA	GeneFlow
10x Tris-Borate-EDTA	GeneFlow
DNase/RNase-free H_2O	QIAGEN
RNasin ribonuclease inhibitor	Promega
Protogel Acrylamide solution	GeneFlow
10x SDS-PAGE running buffer	GeneFlow
Protogel Resolving buffer	Atlanta
Protogel Stacking buffer	Atlanta
Butanol	Sigma
10x Blotting buffer	GeneFlow
Tween-20	Sigma
Bromophenol blue	Sigma
Ponceau S stain	Sigma
Glycerol	Sigma
Methanol	Sigma
PCR Nucleotide mix	Promega
Opti-MEM media	Thermo Fisher Scientific

PBS-0.1% Tween (PBS-T) solution was made by adding 1 ml Tween-20 to 1000 ml PBS and stir.

Blotto solution was made by adding 10 g skimmed milk to 200 ml PBS-T.

2.1.4 Media

Growth Medium: Dulbecos' Modified Eagles Medium (DMEM) (Sigma, UK) was supplemented with 10% (v/v) heat-inactivated Fetal Calf Serum (FCS), 100 units/ml penicillin, 100 µg/ml streptomycin and 2 mM L-glutamine.

Maintenance Medium: Dulbecos' Modified Eagles Medium (DMEM) (Sigma, UK) was supplemented with 2.5% (v/v) FCS, 100 units/ml penicillin, 100 µg/ml streptomycin and 2 mM L-glutamine.

2x Dulbecos' Modified Eagles Medium (DMEM)

1000 ml of 2x DMEM was made by mixing:

400 ml 5x DMEM was filter-sterilised prior to use.

400 ml autoclaved distilled water.

100 ml heat-inactivated FCS

20 ml 2 mM L-glutamine

20 ml 100 units/ml penicillin, 100µg/ml streptomycin

60 ml 7.5% Sodium Bicarbonate solution ($NaCO_2$)

2.1.5 DNA and Protein Ladders

100 bp DNA Ladder (New England BioLabs, UK): Consists of 12 sharp bands with broad range between 100 and 1000 bp in multiples of 100 with an additional fragment at 1200 bp and 1517 bp. Three reference intense bands are 500, 1000 and 1517 bp.

Colour plus protein molecular weight ladder (11-245 kDa) (New England BioLabs, UK): Consists of 12 sharp bands with broad range of molecular weights (11, 17, 25, 32, 46, 58, 80, 100, 135, 190 and 245 kDa), covalently coupled with a blue chromophore. Two reference bands are included at 25 kDa (green) and one at 80 kDa (orange).

2.1.6 Antibodies

Primary and secondary antibodies used in this work, along with the working dilutions used for immunoblotting, are shown in Tables 2.1 and 2.2.

Table 2.1 Primary Antibodies

Target protein	Species	Source (Catalogue No.)	Dilution buffer	Dilution
Actin	Rabbit	Abcam, UK (ab6276)	Blotto solution	1:10,000
MYSM1	Rabbit	Merck Millipore, USA (ABE62)	Blotto solution	1:1000

Table 2.2 Secondary Antibodies

Antibody	Source (Catalogue No.)	Dilution buffer	Dilution
Goat anti-mouse	Santa Cruz Biotechnology, USA sc-2005	Blotto solution	1:5000
Goat anti-rabbit	Santa Cruz Biotechnology, USA sc-2030	Blotto solution	1:5000

2.1.7 Plasticware

Plasticware for molecular biology and tissue culture was obtained from either Sarstedt (Germany), Appleton Woods (UK) or Starlabs (UK), unless otherwise stated.

2.2 Methods

2.2.1 Cell Culture

2.2.1.1 Cells Used in This Study

The following cell lines were used in this study. HeLa cells (ATCC CCL-2), a human cervical cancer cell line, were obtained from Dr Chris Dawson, (University of Birmingham, UK). MRC5-AVS were provided by Prof J Coulson, (University of Liverpool), a human lung fibroblast cell line, transformed with SV40. Vero cells, African Green Monkey kidney cells, and BHK 21 cells, Baby Hamster Kidney cells, were provided by Dr Sareen Galbraith, (Leeds Beckett University, UK). Primary Murine Embryo Fibroblasts (MEFs) Wild Type (WT) and *Mysm1*$^{-/-}$ (KO) C57BL/6 mice were provided from Professor A. Nijnik (McGill University, Toronto, Canada) (Nijnik *et al*., 2012). These cells had been immortalized by treatment with SV40 large T antigen (A. Nijnik, personal communication). Primary MEFs derived from WT and *USP15*$^{-/-}$ mice were provided by Dr. Klaus-Peter Knobeloch (Freiburg University, Germany).

2.2.1.2 Cell Maintenance

All cell monolayers were grown under high humidity incubation (37°C, 5% CO_2) with DMEM supplemented with 10% (v/v) heat-inactivated FCS, 100 units/ml penicillin, 100 µg/ml streptomycin and 2 mM L-glutamine (termed growth medium). For maintenance, cells were routinely cultured in 10 cm tissue culture dishes and passaged when 80-100% confluent by discarding the

growth media, washing the cells with 6 ml of Dulbecos' Phosphate Buffered Saline (without Mg^{2+} and Ca^{2+}) (PBS) solution. The wash solution was removed and 2.5 ml of 1x Trypsin-EDTA solution (0.05% Trypsin, 0.02% EDTA; Sigma). Cells were then incubated at 37°C for 2-5 minutes (mins) to dislodge cells from the plastic and detach from each other, before addition of 7.5 ml of growth medium. Cells were then seeded into new 10 cm TC dishes at a seeding density of between 1:5 to 1:10, and 12 ml fresh growth medium added.

2.2.1.3 Storage of Cells in Liquid Nitrogen

Confluent adherent cell monolayers, in 10 cm TC dishes, were trypsinised, resuspended in growth medium, and centrifuged at 384 x g for 3 mins. Cells were then resuspended in 1 ml "freezing medium", DMEM supplemented with 20% FCS and 10% dimethyl sulphoxide (DMSO), and aliquoted into cryovials. The cryovial was put in a Mister Frosty and placed in a -80°C freezer overnight, before transfer to liquid nitrogen for long-term storage. To recover cells from liquid nitrogen, cryovials were rapidly thawed at 37°C and 0.5 ml growth medium added. After 2 mins cells were transferred to 15 ml tubes, 10 ml growth medium added before centrifugation at 225 x g for 3 mins. The medium was decanted and the wash step repeated. Cells were then resuspended in an appropriate volume of growth medium and placed in a 10 cm TC dish or T25 cm^2 flask (dependent on the size of the cell pellet), before being incubated at 37°C, 5% CO_2 overnight. After 24 hr, medium was removed and cells washed with PBS, and fresh growth medium added. Cells were then passage as described in 2.2.1.2.

2.2.1.4 Stimulation of Cells with Lipopolysaccharide, Poly (I:C) or Poly (I:C)-LMW/LyoVec

Cell monolayers at required confluency, generally approximately 90%, were stimulated with either Lipopolysaccharide *E. coli* 0111:B4 (LPS), Polyinosinic-polycytidylic acid (Poly I:C) or Poly (I:C)-LMW/LyoVec (Poly (I:C)/LV) in appropriate volume of maintenance medium. Growth media was removed from cells, and maintenance medium containing 1 µg/ml of relevant

stimuli added. Cells were incubated at 37°C, 5% CO_2 for the appropriate time until stimulated cells were processed further dependent on the experiment. In all cases, a mock stimulated control was included using maintenance medium only in place of the stimulation factors.

2.2.2 Viruses and Infection of Cells

2.2.2.1 Viruses Used in This Study

SFV clone 4 (Liljestrom *et al*., 1991) was provided by Dr Sareen Galbraith (Leeds Beckett University, UK). Chikungunya virus (CHIKV) strain SV0451-96 was provided by Dr Christopher Logue (Public Health England). This is a pre A226V mutation strain, original isolated from a human infection in Thailand. These viruses have been referred to as SFV and CHIKV throughout the rest of this thesis.

2.2.2.2 Preparation of Virus Stocks

Stocks of SFV and CHIKV were amplified in either Vero or BHK 21 cells. Cells at 80-90% confluent, generally one or two T75 cm^2 flasks. Cells were infected at a multiplicity of infection (MOI) of between 0.001-0.01 in 5 ml DMEM supplemented with 2.5% FCS. After 60 mins at 37°C, 5% CO_2, the inoculum was removed and replaced with 8 ml maintenance medium. Cells were incubated at 37°C, 5% CO_2 for 36-48 hr, and supernatants harvested when >70% cytopathic effect (CPE) was observed. An extra flask was used as a mock infected control to help monitor for CPE. Cells and other debris was removed by centrifugation (431 x g for 2 mins), and the supernatant containing virus was divided in 0.5 ml aliquots and stored at -80°C.

2.2.2.3 Titration of Virus Stocks - Plaque Assay

SFV and CHIKV stocks were titrated using either Vero, BHK 21 or HeLa cells. The virus titrations were obtained from HeLa cells used to infect the human cells while the virus titrations were obtained from either Vero or BHK 21 cells used to infect the animal cells. The rationale for titrating the viruses in

different cell lines was less than one Log. Cells were grown in 6-well plates until 80-90% confluent, before being infected with 10-fold dilutions of virus stock. Appropriate virus dilutions were prepared in maintenance medium. Cells were infected with 0.5 ml of each virus dilution, in triplicate, and incubated for 60 mins at 37°C, 5% CO_2. The virus inoculum (or DMEM only for mock infected wells) was then removed, and replaced with a 4 ml of overlay consisting of equal volumes of 2x DMEM (supplemented with 5% FCS) and 2% Low melting point (LMP) agarose. Cells were incubated at 37°C, 5% CO_2 for 48-72 hr before being fixed with 2 ml of 10% formaldehyde for a minimum of 2hrs. The formalin was aspirated followed by removal of the semi-solid overlay. Plaques were visualised by staining with 2 ml of crystal violet for 20 mins, followed by rinsing in H_2O. Plaques were counted, and virus titres calculated as plaque forming units per ml (pfu/ml), taking into account the original dilutions made.

2.2.2.4 Infection of Cells

Cell monolayers at required confluency, generally approximately 90%, were infected with either SFV or CHIKV in a minimal volume maintenance medium. For each specific experiment, the appropriate MOI was determined and virus stocks diluted accordingly. Growth media was removed from cells, and the appropriate volume of viral inoculum added. After infection for 60 mins at 37°C, 5% CO_2, the virus inoculum was removed and replaced with maintenance medium. Cells were incubated at 37°C, 5% CO_2 for the appropriate time until infected cells were processed further dependent on the experiment. In all cases, a mock infected control was included using maintenance medium only in place of virus inoculum.

2.2.3 Cell Viability Assay

Cell viability was monitored using the CellTiter-Glo Luminescent Cell Viability Assay (Promega). The CellTiter-Glo Luminescent reagent results in cell lysis and generation of a luminescent signal proportional to the amount of ATP present, and therefore the number of metabolically active cells. Cell viability assays were carried out in opaque-walled, clear bottom 96 well plates

(Corning). Wells containing target cells were set up in triplicate according to the individual experiment. At the appropriate timepoint, 100 µl CellTitre-Glo luminescence reagent was added to each well. Plates were then incubated for 10 mins at room temperature to stabilise the luminescent signal before detection using a Fluostar Omega luminometer (Germany). The plate was loaded to the luminometer and the ATP measurements were carried out at 37°C using the following parameters were luminescence of measurement type, endpoint of reading mod, corning 96 well microplate and 0.2s a positioning delay type. The excitation and emission filters were 485 and 520, respectively.

2.2.4 siRNAs

Gene-specific DUB siRNAs were obtained from QIAGEN. Further information and sequences are shown in Table 2.3. Control siRNAs used were the QIAGEN All Stars Positive Control (Hs Death; SI04381048) and All Stars Negative Control (siControl or siC; SI03650318) siRNAs.

2.2.4.1 siRNA Knockdown in 96 Well-Plate Format

siRNA knockdown was carried out in 96 well plate format using individual and pooled siRNAs by reverse transfection of HeLa cells. siRNAs were used in pools of four, each targeting the same gene, or as individual siRNAs. The concentration of each siRNA in the pools was 0.3 µM. The concentration of individual siRNAs (including controls) was 1.2 µM. A reaction mix of 3 µl of 1 in 20 diluted RNAiMAX (0.15 µl/well) and 2 µl of DUB siRNAs either pools or individuals and controls were combined with RNAiMAX in a total volume of 20 µl with OptiMEM, and dispensed into a well of a Corning opaque-walled and clear bottom 96 well microplate. An incubation of 20 mins followed, during which time cells were harvested and resuspended in antibiotic free DMEM at a concentration of $1x10^5$ cells/ml. 100 µl of cells were then added to each well thus obtaining a final siRNA concentration (either pools or individuals and controls) of 20 nM, and $1x10^4$ cells per well. The frame of wells around the edges of each plate were not used for transfections and instead filled with PBS to improve humidification and minimise edge effects. The plates were then incubated overnight at 37°C, 5% CO_2, and the following day 100 µl of

fresh media was added in each well. 72 hr post-transfection the cells were monitored and processed for the next step (either monitoring efficiency of knockdown or viral infection).

2.2.4.2 siRNA Knockdown in 6 Well-Plate Format

siRNA knockdown in 6 well plate format was carried out as follows. OptiMEM media (490 µl) was dispensed in each well of a 6 well plate. 6 µl of individual siRNAs at 10 µM was added to each well, while 3 µl of HsDeath or siControl siRNAs at 20 µM was added. 3 µl of RNAiMAX transfection reagent was added and the well contents were mixed gently. An incubation of 20 mins followed, during which time cells were harvested and resuspended in antibiotic free DMEM at a concentration of $1x10^5$ cells/ml. 2.5 ml of cells were then added to each well thus obtaining a final siRNA concentration of 20 nM, and $2.5x10^6$ cells per well. Cells were incubated at 37°C, 5% CO_2 for 72 hr (monitoring by microscope every 24 hr) before being used to either monitoring efficiency of knockdown or viral infection.

2.2.4.3 siRNA Knockdown in 10 cm Tissue Culture Dish

siRNA knockdown in 10 cm tissue culture dish format was carried out as follows. A reaction mix of 8 µl of RNAiMAX and either 16 µl or 8 µl of DUB individual or control siRNAs (at a concentration of 10 µM and 20 µM, respectively) was added into 1.5 ml eppendorf tubes that had 1350 µl of OptiMEM and mixed well by pipetting. An incubation of 20 mins followed, during which time cells were harvested and resuspended in antibiotic free DMEM at a concentration of $3x10^5$ cells/ml. 6.650 ml of cells were then added to each tissue culture dish. Next, the master mix solution was added to tissue culture dish, thus obtaining a final siRNA concentration of 20 nM and $2x10^6$ cells per dish. Cells were distributed evenly through the dish by swirling in a figure of eight, then dishes were incubated at 37°C, 5% CO_2, and the following day 6 ml of fresh media was added in each dish. After 48 hr, cells were harvested and reseeded at $1x10^6$ cell/well into 2 or more wells in 6 well plate. Plates were incubated at 37°C, 5% CO_2 for a further 24 hr and at 72 hr post-transfection the cells were monitored and processed for the next step (either monitoring efficiency of knockdown or viral infection).

Table 2.3 Details of DUB siRNAs used in this study

DUB	siRNA*	Sense sequence (5'-3')	Qiagen Code**
BRCC3	1	TACGATGTTGATTATAACATT	Hs_CXorf53_1
	2	CAGATTGAGATGAATTTGCAA	Hs_CXorf53_2
	3	CAGCATTTGCAGGAATTACAA	Hs_CXorf53_3
	4	TACGACGTTCTGATAAGAGGA	Hs_BRCC3_1
MYSM1	1	TATAATCGAAATAATCCCTTA	Hs_MYSM1_3
	2	AAGACCGGCCATAATCTTCAA	Hs_MYSM1_4
	3	TGGGATGATTGTTAGTCCCTA	Hs_MYSM1_5
	4	GAGGCGGATGTGGATATCGAA	Hs_MYSM1_6
UCHL1	1	CACGCAGTGGCCAATAATCAA	Hs_UCHL1_1
	2	CTCCGCGAAGATGCAGCTCAA	Hs_UCHL1_2
	3	CAGCCACACCCAGGCACTTAA	Hs_UCHL1_4
	4	AACGTGGATGGCCACCTCTAT	Hs_UCHL1_5
JOSD2	1	CTGCCGCTGCTGCCTCAATAA	Hs_SBBI54_1
	2	CTGGGAAAGGCCAGCACTTCA	Hs_SBBI54_2
	3	ACCGGCAACTATGATGTCAAT	Hs_SBBI54_3
	4	CCAGGTGGACGGTGTCTACTA	Hs_JOSD2_1
OTUD6A	1	CAAGACGACAGTAGCATTGAA	Hs_HSHIN6_1
	2	CTACGACGACTTCATGATCTA	Hs_OTUD6A_1
	3	AGGCCCAGATCCGGAGCTTAA	Hs_OTUD6A_2
	4	AAGAGTGAACAGCAGCGCATA	Hs_OTUD6A_3
USP1	1	AACCCTATGTATGAAGGATAT	Hs_USP1_11
	2	ACAGGCATTAATATTAGTGGA	Hs_USP1_10
	3	CTGGGACCCATGAATCTGATA	Hs_USP1_9
	4	ATGTGGCAGAATTACCTACTA	Hs_USP1_6
USP4	1	ACCGAGGCGTGGAATAAACTA	Hs_USP4_1
	2	TAGATGAATTAAGACGGTTAA	Hs_USP4_3
	3	CAGGCAGACCTTGCAGTCAAA	Hs_USP4_6
	4	CACCTACGAGCAGTTGAGCAA	Hs_USP4_7
USP5	1	ACCGACGATCCGGGTCCCTAA	Hs_USP5_1
	2	TACGTCTGCCACATCAAGAAA	Hs_USP5_2
	3	AGCGAGGAGAAGTTTGAATTA	Hs_USP5_3
	4	CCCAGCGAGTTGACTACATCA	Hs_USP5_5
USP34	1	CTGGATTGAGTCAGATAACAA	Hs_USP34_2
	2	AAGCCTAGATCTTGCATTTAA	Hs_USP34_4
	3	AGCAGTGATAATAGCGATACA	Hs_USP34_5
	4	GTGGATTGAACTGTTGACGAA	Hs_USP34_6
USP45	1	CAGGAAATTATCGGAACATAA	Hs_USP45_5
	2	CGGGTGAAAGATCCAACTAAA	Hs_USP45_6
	3	CACATGGATTATATGGTGTTA	Hs_USP45_9
	4	CAGCTAGTACTTACTTCTGAT	Hs_USP45_10
USP46	1	CAGCACGGCATTGTTCCTTAT	Hs_USP46_4
	2	TAGGGAAATGTTTGTACTATA	Hs_USP46_5
	3	CAGGGAACGCTTACCAATGAA	Hs_USP46_7
	4	CAGGTTGTCAATTACACGGAT	Hs_USP46_10
USP53	1	TTGTACTATGCTGGTAAACTA	Hs_USP53_5
	2	CAGATTACGACAAGCAACCTA	Hs_USP53_6
	3	ACCGAGGTTGGAAACCTATGA	Hs_USP53_7
	4	CTTCGTCCTGTTAAAGATAAA	Hs_USP53_8
OTUD7A	1	CACGCCGTCGCCCACAGACAA	Hs_OTUD7A_1
	2	CCACGTGGCAAGTGAATGCAA	Hs_OTUD7A_2
	3	CGGGACCTGGTGTTACGGAAA	Hs_OTUD7A_3
	4	CCGCGATTCGGTGTGCAGCAA	Hs_OTUD7A_4

**siRNA number used in this study*
***Reference code for QIAGEN siRNA*

2.2.5 Molecular Biology

2.2.5.1 RNA Extraction

Cell lysis and extraction of RNA was performed using an RNeasy Plus Mini kit (QIAGEN) as per the manufacturer's instructions. A QIAshredder column (QIAGEN) step was included to homogenise the sample. Briefly, cells were harvested using a cell scraper, washed twice with cold PBS before being lysed in 350 µl of RLT buffer (containing 10 µl -mercaptoethanol per ml RLT buffer). The lysate was added directly to a QIAshredder spin column and centrifuged at 13,226 x g for 2 mins. To eliminate any genomic DNA, the homogenised lysate was then added to a gDNA eliminator column and centrifuged at 13,226 x g for 30 secs. An equal volume of 70% ethanol was added to the flow through and mixed well by pipetting before being transferred to an RNeasy column and centrifuged for 15 secs at 13,226 x g. RW1 buffer (700 µl) then added to the column and centrifuged for 15 secs at 13,226 x g. The column was then washed by adding 500 µl of RPE buffer followed by centrifugation for 15 secs at 13,226 x g. A further, 500 µl of RPE buffer was added followed by centrifugation for 2 mins at 13,226 x g. After this the RNeasy spin column was placed in a new collection tube and centrifuged for 1 min at 13,226 x g to ensure all wash buffer was removed. To elute the RNA yield, the RNeasy spin column was placed in 1.5 ml collection tube and 30-50 µl of DNase/RNase free H_2O was added and then centrifuged for 1 min at 13,226 x g. All RNA samples were stored at -80°C until required.

2.2.5.2 Agarose Gel Electrophoresis

Agarose gels (between 1.5% and 2% agarose) were prepared by adding electrophoresis grade agarose to 0.5x either TBE buffer (45 mM Tris-borate, 1 mM EDTA) or TAE buffer (40 mM Tris, 20 mM Acetate and 1 mM EDTA). The mixture was heated in a microwave until all the agarose had dissolved. Ethidium bromide (EtBr) was then added to a final concentration of 0.2 µg/ml, the gel poured and allowed to set at room temperature. DNA or RNA samples were loaded onto the gel and resolved in a horizontal

electrophoresis tank containing 0.5x either TBE or TAE buffer run at 100V for approximately 30 mins.

2.2.5.3 RNA Quantification and Integrity

The RNA concentration and purity of each sample was assayed using a NanoDrop ND-1000 spectrophotometer (Thermo Scientific, Massachusetts, USA). Protein contamination was determined by monitoring the 260:280 ratio, and organic contamination by determining the 260:230 ratio. A ratio of between 1.8 and 2.0 was considered satisfactory. RNA integrity was assessed by gel electrophoresis. 1 µg of RNA, in a total volume of 12 µl containing 1x RNA loading buffer (50% glycerol, 10 mM Na_2PO_4 with 1% Bromophenol (BPB) blue dye) and DNase/RNase free H_2O, was resolved on a 1.5% agarose gel described in section 2.2.5.2, EtBr before being visualised using a GeneFlash UV transilluminator (Syngene, Cambridge, UK). A RNA sample of good quality was indicated by the presence of two clear bands representing 28S and 18S ribosomal RNA, at a ratio of approximately 2:1.

2.2.5.4 Conversion of RNA into cDNA

RNA was reverse transcribed to cDNA using the RevertAid™ H minus M-MuLV Reverse Transcriptase (RT) enzyme. The cDNA reaction mix was as follows: 1 µg of RNA was combined with 0.5 µg/µl oligo (dT)15 primer in a sterile 0.5 ml PCR tube and reaction volume made up to 11 µl with nuclease free distilled water. The RNA/oligo (dT) mix was incubated at 70°C for 5 mins, and then immediately chilled on ice. To each reaction mix, 4 µl of 5x reverse transcription buffered, 2 µl PCR nucleotide mix (containing dATP, dCTP, DGTP and dTTP each at 10 mM in water), 0.5 µl RNasin ribonuclease inhibitor (40 u/µl) and 1.5 µl DNase/RNase-free H_2O were added. The reaction was then incubated at 37°C for 5 mins, before 1 µl of RevertAid™ H minus M-MuLV RT was added and incubation continued for 1 hr at 42°C. The RT enzyme was then inactivated at 70°C for 10 mins. cDNA samples were immediately removed to ice for 5 mins, then diluted at 1:5 with nuclease free distilled water and stored at -20°C. These reactions were termed the RT+ reaction. To

control for the possible presence of genomic DNA contamination, RT- samples were prepared simultaneously, in which the RT enzyme was omitted, and replaced with equivalent amount of H_2O.

2.2.5.5 PCR Oligonucleotides

The majority of PCR oligonucleotide primers were designed in-house, aiming for the following: 20 bases with approximately 50% GC content, a melting temperature (Tm) of approximately 60°C and a GC clamp of 1-2 nucleotides at the 3' end. The PCR product predicted sizes were checked using NCBI (www.blast.ncbi.nlm.nih.gov/Blast.cgi). Other PCR primers were taken from published papers, and checked for accuracy by BLAST search. Details of all primers used in this study are shown in Tables 2.4 to 2.8. All PCR primers were checked by end-point PCR prior to using in QPCR.

2.2.5.6 Endpoint Polymerase Chain Reaction

Initial assessment of PCR primer pairs was performed using endpoint PCR. The PCR reaction was carried out as follows: 2 µl of cDNA, 1.5 µl each of forward and reverse primer (both at 10 µM concentration) and 10 µl of 2x Reddy Mix were made up to 20 µl in nuclease-free sterile distilled water. PCR was performed in a ThermoHybaid Px2 thermocycler (Thermo Scientific) using an initial denaturation step (95°C for 5 mins) followed by between 25-40 cycles at the following temperatures: 94°C for 30 secs, 50°C-60°C for 30 secs, 72°C for 30 secs; followed by 72°C/10 mins. Different annealing conditions were used specific to each primer pair, and different numbers of cycles are used dependent on the abundance of target sequence. In all PCR reactions, a no template reaction (using H_2O) was used as a negative control. The PCR product was assessed by gel electrophoresis. PCR product samples were loaded onto a 2% agarose gel described in section 2.2.5.2, EtBr before being visualised using a GeneFlash UV transilluminator (Syngene, Cambridge, UK). Primer pairs were judged satisfactory if there was a single PCR product at the expected product size, and there were minimal primer dimers visible. Primer pairs were also validated by QPCR (section 2.2.5.7), where melt curves were assessed for the presence of primer dimers or secondary products.

2.2.5.7 Quantitative Polymerase Chain Reaction

Quantitative PCR (QPCR) was performed using the iTaq™ Universal SYBR® Green Supermix (BioRad 172-5121, USA), and a Rotor-Gene Q real-time PCR cycler (QIAGEN). cDNAs was diluted 1:4 with DNase/RNase-free H_2O prior to using in QPCR reactions. Where SFV or CHIKV RNA levels were being monitored, samples were first diluted either 1:1,000 or 1:10,000 with DNase/RNase-free H_2O. A total reaction volume of 12 µl was made up for each sample, consisting of 4 µl of cDNA, 0.25 µl each of forward and reverse primers (at 10 µM) and 6 µl of SYBR green supermix (2x), made up with nuclease free distilled water. All QPCR reactions sample were run in triplicate and included blank controls (no template). A two-step QPCR cycling profile was performed for all primer pairs. An initial enzyme activation/denaturation step at 95°C for 3 mins was followed by 40 cycles of 94°C/15 secs, 55°C or 60°C/30 secs. Melt curves were read at 0.5°C intervals from 55°C to 95°C. Data were analysed using Rotor-Gene software, and a cycle threshold (Ct) set in the exponential amplification phase at 0.03 levels. Ct values were determined for each sample and compared to a reference gene, either actin for human cells (ACTB) or 18S for murine cells (m18S), using the $2^{-\Delta\Delta}$Ct method (Schmittgen and Livak, 2008).

Table 2.4 Details of DUB PCR primers

Target gene	Primer name	Primer sequence (5'-3')	Reference
BRCC3	BRCC3-For BRCC3-Rev	AATTTCTCCAGAGCAGCTGTCTG CATGGCTTGTGTGCGAACAT	Dong *et al* ; 2003
MYSM1	MYSM1-For MYSM1-Rev	ATCGAAGGGGACGTGGTAGC GCTGGTTTTGTAGGAGAGTG	*
mMYSM1	mMYSM1-For mMYSM1-Rev	TGTGGATGTGGAAGGAGATG TGGTGCTATCCAGAGTCCAA	Nijnik, unpublished
UCHL1	UCHL1-For1 UCHL1-Rev	CCTGAAGACAGAGCAAAATGC CCATCCACGTTGTTAAACAG	*
JOSD2	RT_JOSD2_F1 RT_JOSD2_R1	GAACCCTCATCGCAGCCTC GATCAGCCCCAGTACCTGG	*
OTUD6A	6A1-For 6A1-Rev	TGGTGTTCAGCGTGTCTGTGG TGAAGTCGTCGTAGCCGAAGG	*
USP1	USP1-For USP1-Rev	TGTGATCCTGAAGAGGACTTGG AACGCGTCCTTAATACCAGCTG	*
USP4	USP4-For USP4-Rev	ACCTTGCAGTCAAATGGATCTGG TCCAAGTCCACAGAGCCCAGG	Song *et al*; 2010
USP5	USP5-For USP5-Rev	CGGGACCAGGCCTTGAA TCGTCAATGTGACTGAAGATCCA	*
USP34	USP34-For USP34-Rev	TGTCGACAATTTATTGGTCCAC GATTTTGCACTAACCTGGGAGC	*
USP45	USP45-For USP45-Rev	GTCATGCTATCAGCGTGAATC GGCTTTCTGAGTTTTTACCAC	*
USP46	USP46-For USP46-Rev	CCCCTTGTAAAGATGGCGGT TTCCAGAGCAGAGGCATTGG	*
USP53	USP53-For USP53-Rev	GGAGTGGAAGGCCTGTATTT TAGACCATCATCACGGAACTTG	*

** PCR primers were designed in this study*

Table 2.5 Housekeeping Gene PCR Primers

Target gene	Primer name	Primer sequence (5'-3')	Reference
Beta-actin	ACTB-For ACTB-Rev	CACCTTCTACAATGAGCTGCGTGTG ATAGCACAGCCTGGATAGCAACGTAC	Faronato *et al.,* 2013
Mouse 18S	m18S-For m18S-Rev	GAACGTCTGCCCTATCAACTTTC GATGTGGTAGCCGTTTCTCAG	Peng *et al*., 2010

Table 2.6 SFV and CHIKV PCR Primers

Target gene	Primer name	Primer sequence	Reference
SFV	SFV-E1-For SFV-E1-Rev	CGCATCACCTTCTTTTGTG CCAGACCACCCGAGATTTT	Fragkoudis *et al.,* 2007
CHIKV	CHIKV-E1-For CHIKV-E1-Rev	TCGACGCGCCCTCTTTAA ATCGAATGCACCGCACACT	Edwards *et al.,* 2007

Table 2.7 Human and Mouse Type 1 IFNs and Pro-inflammatory Cytokines Primers

Target gene	Primer name	Primer sequence (5'-3')	Reference
Human genes			
IFN-α	Pan-IFNa-For Pan-IFNa-Rev	TCTTCAGCACAAAGGACTCATCTG CACACAGGCTTCCAGGTCATTC	Brzostek-Racine *et al.,* 2011
IFN-β	IFNb-For IFNb-Rev	ACTTTGACATCCCTGAGGAATTAAGCG ACTATGGTCCAGGCACAGTGACTGTACTC	Teng *et al.,* 2012
TNF-α	hTNFa-For hTNFa-Rev	CCTCTCTCTAATCAGCCCTCTG GAGGACCTGGGAGTAGATGAG	*
IL1-β	hIL1b-For hIL1b-Rev	AAACCTCTTCGAGGCACAAG GTTTAGGGCCATCAGCTTCA	*
Mouse genes			
IFN-α	mIFNa4-For mIFN4a4-Rev	TGATGAGCTACTACTGGTCAGC GATCTCTTAGCACAAGGATGGC	*
IFN-β	mIFNb1-For mIFNb1-Rev	CAGCTCCAAGAAAGGACGAAC GGCAGTGTAACTCTTCTGCAT	*
Mx1	mMx1-For mMx1-Rev	CCCAGAGGCAGTGGTATTGT GCCTCTCCACTCCTCTCCTT	*
TNF-α	mTNFa-For mTNFa-For	CCTGTAGCCCACGTCGTAG GGGAGTAGACAAGGTACAACCC	*
IL1-β	mIL1b-For mIL1b-Rev	GAAATGCCACCTTTTGACAGTG TGGATGCTCTCATCAGGACAG	*

** PCR primers were designed in this study*

2.2.6 Protein Analysis

2.2.6.1 Protein Extraction

Cell extracts for immunoblotting were prepared by generating whole cell extract using conventional cell lysis and hot lysis methods.

2.2.6.1.1 Conventional Cell Lysis

Whole cell extracts were prepared from adherent cells by scraping cells into the culture media. The media and cells were transferred to a labelled 15 ml tube. The cells were pelleted by centrifugation at 431 x g for 3 mins. The supernatant was decanted and cells were dislodged, then 5 ml of ice cold PBS was added, and the centrifugation step repeated. Cells were subjected to one further PBS wash before being resuspended with 1 ml ice-cold PBS, and transferred into a pre-labelled 1.5 ml microcentrifuge tube. Cells were pelleted again by micro-centrifugation at 3500 x g for 2 mins. Cell pellets were resuspended in 150 µl 1x Laemmli buffer [50 mM Tris-Cl pH 6.8, 2% Sodium dodecyl sulphate (SDS) and 10% glycerol] without Bromophenol blue (BPB) and Dithiothreitol (DTT). Cells lysate was boiled for 10 mins at 90-100˚C, then centrifuged at 13,226 x g for 10 mins. Supernatant (soluble proteins) was transferred into a new labelled 1.5 ml microcentrifuge tube and stored at -20˚C.

2.2.6.1.2 Hot Lysis

Cells in 6-well plates were rinsed twice in warm (37˚C) PBS before lysis. The PBS was aspirated from the cells, and the plates transferred immediately to a dry heat block at 90-100˚C, and preheated 150 µl 1x Laemmli buffer without BPB and DTT was added. The plate was immediately scraped using cell scrapers and the viscous lysate transferred to a preheated screw cap tube. The lysates were then heated at 100˚C for 10 mins, with vortexing every 2 mins. Next, cells debris and insoluble protein was pelleted by centrifuged at 13,226 x g for 10 mins. The supernatant was then transferred to a fresh 1.5 ml labelled microcentrifuge tube and stored at - 20˚C.

2.2.6.2 Determining Protein Concentration

Protein concentrations were assessed using a bicinchoninic acid (BCA) protein assay kit, (Pierce, UK) according to the manufacturer's instructions. A standard curve ranging from 2000 to 25 µg/ml of bovine serum albumin (BSA) was generated by serial dilution from a stock of known concentration. Protein experimental samples were prepared by mixing 5 µl of sample with 45 µl 1x Laemmli buffer without BPB and DTT. BCA working reagent was prepared by mixing 50 parts reagent A with 1 part reagent B. In a flat-bottom 96-well plate, 25 µl of standard and experimental samples were added to duplicate wells. Control wells were included 1x Laemmli buffer only. Next, 200 µl of working reagent was added to each well and mixed thoroughly. The plate was then incubated at 37°C for 30 mins. After cooling to room temperature, the absorbance was measured at 562 nm on the MultiSkan Plate Reader (Thermo Scientific, Massachusetts, USA). A standard curve was prepared by plotting the absorbance of samples containing known concentrations of the standard BSA protein, after being subtracted from the blank well absorbance. The protein content of the experimental cell lysates were determined by comparing the absorbance to a standard curve derived from known protein concentrations.

2.2.6.3 SDS Polyacrylamide Gel Electrophoresis (SDS-PAGE)

SDS-PAGE was performed using Mini-PROTEAN Tetra cell vertical electrophoresis system (Bio-Rad, UK) as per the manufacturer's instructions. Each gel consisted of a separate stacking and resolving gel section, made up according to Table 2.9 (for 1.5 mm gel thickness). The gels were prepared as recommended in the (National diagnostic, USA) data sheet. Protein samples for loading were adjusted to a final loading volume using 1x Laemmli buffer with 10% BPB (w/v) and 1 M (DTT), and heated at 90-100˚C for 5 mins prior to analysis. Equal amounts of each sample (generally 30 µg in a final volume of 25 µl) were loaded and run alongside the ColourPlus™ protein ladder (Broad range, 11-245 KDa). Protein was stacked through the stacking gel at 85V for 20 mins followed by separation through the resolving gel at 100V for

90 mins. 1x SDS-PAGE running buffer was used to run protein through the gel.

Table 2.8 Resolving and Stacking Gel Constituents (10 ml gel)

10% Acrylamide Resolving gel	
ProtoGel (ml)	3.4
Resolving buffer (ml)	2.6
Water (ml)	4
10% APS (µl)	100
TEMED (µl)	10
4% Acrylamide Stacking gel	
ProtoGel (ml)	1.3
Stacking buffer (ml)	2.5
Water (ml)	6.1
10% APS (µl)	50
TEMED (µl)	10

2.2.6.4 Immunoblotting

Following SDS-PAGE, protein was transferred to polyvinylidene difluoride (PVDF) membrane using the Mini Trans-Blot® electrophoresis system (Bio-Rad, UK) at 250 mAmp over 2 hr according to the manufacturer's instructions. Efficiency of transfer was monitored by Ponceau-S staining of PVDF membranes. Membranes were then blocked on a rocker for 2 hr in BLOTTO [5% (w/v) skimmed milk powder in PBS plus 0.05% (v/v) Tween 20]. After incubation in BLOTTO, membranes were incubated with appropriate primary antibodies overnight at 4˚C. Concentrations and conditions for each antibody are described in Table 2.1. After overnight incubation, blots were washed four times for 5 mins with PBS-0.05% Tween before addition of appropriate secondary antibody (Table 2.2), which was again diluted in the same blocking buffer. After 90 mins incubation on a rocker at room temperature, the blots were washed three times in with PBS-Tween, each time for 5 mins.

2.2.6.5 Enhanced Chemiluminescence (ECL) Detection

A ChemiDoc™ XRS+ System (BioRad, USA) was employed to detect secondary antibodies using enhanced chemiluminescence according to the manufacturer's protocol. Quantification of bands (densitometry) was performed using ImageJ software.

2.3 Data Analysis

Data sets were analysed in Microsoft Excel 2010 and GraphPad Prism 5. All error bars reflect standard deviation. Where reported, statistical tests utilised either a two-tailed student's t-test (comparing the means of two groups) or Tukey's One-way ANOVA test (comparing the means of several groups).

Chapter 3

Validation of DUB Hits from a siRNA Library Screen against Semliki Forest Virus

3.1 Introduction

As described in the introduction cellular DUBs play important roles during the life cycle of many viruses. At the start of this project no information was available on the specific role of DUBs during alphavirus infection. In a previous study in our laboratory a siRNA screen was undertaken to attempt to identify DUBs that may play a role during alphavirus infection (N Blake, unpublished). This study utilised a siRNA library targeting 92 known or predicted DUBs representing the five families known at the time. The model employed for this study was SFV infection of HeLa cells, and monitoring the effect of DUB depletion on cell viability after SFV infection. Cells in duplicate were reverse transfected with 92 pools of 4 siRNAs, each targeting a single DUB. After 72 hr cells in one plate was then infected with SFV at a MOI of 2, and the second plate was mock infected. Cell viability was measured at 16 hr post-infection using a tetrazolium salt (MTS) assay, and the percentage change in cell viability of infected v uninfected calculated for each DUB knockdown. This data, provided by N Blake, is shown in Figure 3.1. It was predicted that depletion of DUBs would lead to either an increase or decrease in cell viability, corresponding to a decrease or increase in virus CPE respectively (as a marker of replication). With the overall goal to identify pro-viral DUBs, that may be potential therapeutic targets, DUBs which when depleted lead to an increase in cell viability after SFV infection (and a predicted decrease in virus replication) were of specific interest. Using a cut-off of a 30% or greater increase in cell viability, 12 DUBs were identified for further analysis. These were: USP1, USP4, USP5, USP34, USP45, USP46, USP53, OTUD6A, UCHL1, JOSD2, BRRC3 and MYSM1 (Figure 3.1 and Table 3.1).

As this siRNA library screen used pools of 4 siRNAs, the next key step was to validate the selected hits from the screen by deconvoluting the siRNA pools. The criteria employed to define a true positive was that the original pool,

and 2 or more of the individual siRNAs showed the same phenotype as in the original screen (i.e. increase in cell viability after SFV infection).

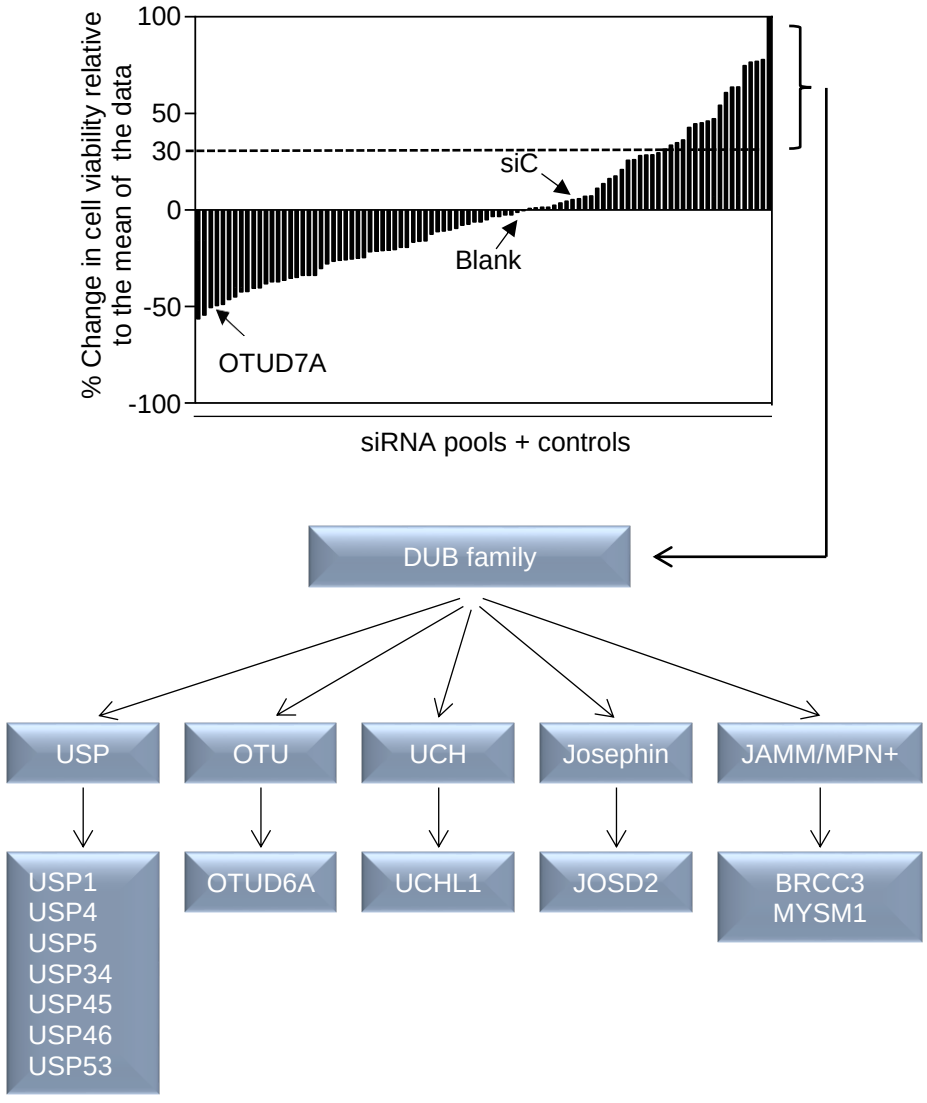

Figure 3.1 DUB siRNA screen identified 12 DUBs as required to aid SFV replication. HeLa cells were transfected with siRNAs targeting 92 known or predicted DUBs (in pools of 4 siRNAs per DUB). At 72 hr cells were either mock-infected or infected with SFV at MOI=2. After 16 hr cell viability was measured by MTS. The graph shows the data expressed as percentage change in cell viability of infected versus uninfected cells and is the mean of two independent experiments. Dotted line indicates an increase in cell viability of 30%. OTUD7A is highlighted as a DUB that leads to a decrease in cell viability after depletion. The lower panel shows the DUBs identified as resulting in a 30% or greater increase in cell viability divided into individual DUB family. (Data provided by Neil Blake, University of Liverpool).

Table 3.1 Percentage Increase in Cell Viability for the Hits in siRNA Screen*

DUB family	Positive hits	Increase In Cell viability (%)
USP	USP1	77
	USP4	64
	USP5	61
	USP34	75
	USP45	64
	USP46	45
	USP53	47
OTU	OTUD6A	110
UCH	UCHL1	45
Josephin	JOSD2	43
JAMM/MPN+	BRCC3	78
	MYSM1	46

*Details of the screen are shown in Figure 3.1

3.2 Determination of cell viability using the CellTitre-Glo assay

The original readout for the DUB siRNA library screen was monitoring cell viability utilising the measurement of MTS assay and monitoring viability based on a colorimetric read out. For the deconvolution experiments reported in this chapter cell viability would also be the read out, but to increase the sensitivity an alternative assay was chosen, the CellTitre-Glo Luminescent Cell Viability assay. This assay measures ATP levels and the readout is luminescence. It is reported to be more sensitive than the MTS assay (Kangas *et al*., 1984). Before employing the CellTitre-GLo assay experiments were carried out to validate the experimental set up.

3.2.1 Optimisation HeLa cell number with the CellTitre-Glo assay

It was first necessary to confirm a linear response for the luminescence signal in relation to HeLa cell number in our laboratory and under our

experimental conditions. This would allow for determination of the optimal cell number to enable an increase in cell viability to be monitored within a linear range. HeLa cells were titrated in triplicate in a 96 well plate, at the following cell numbers: $1x10^4$, $2x10^4$, $4x10^4$, $6x10^4$, $8x10^4$, $1x10^5$ and $2x10^5$ cells/well. Cells were allowed to settle in the wells for 30 min at 37°C, 5% CO_2 in a volume of 100 µl, before CellTitre-GLo reagent was added, after a further 10 min incubation the luminescence was measured. The mean cell viability for each cell number is shown in Figure 3.2. There was a clear linear relationship between luminescence readout and cell number over the range of $1x10^4$ to $2x10^5$, with a r^2=0.997. This data also indicated that a cell number of approximately $6x10^4$ per well would allow sufficient scope for monitoring changes in cell viability in subsequent experiments. This was thought to be appropriate to allow for a decrease in viability due to SFV infection to be monitored, and also to then detect an increase in cell viability due to depletion of specific DUBs.

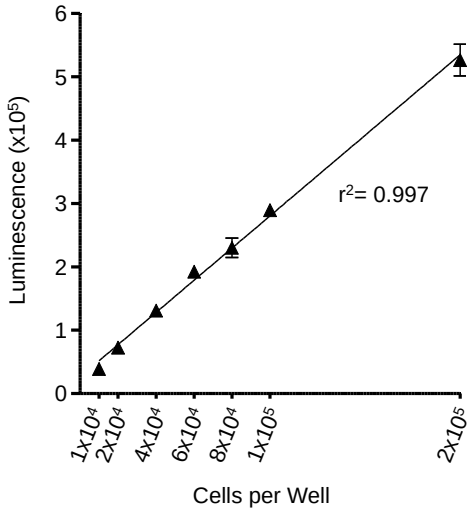

Figure 3.2 HeLa cell number correlates with luminescent output using the CellTiter-Glo assay. HeLa cells at the indicated cell density were seeded into a 96 well plate before addition of CellTiter-Glo Luminescent Cell Viability reagent. Luminescence was measured 10 minutes after addition of the reagent using a FLUOstar Omega Luminometer Detection System. Data is presented as the mean of triplicate wells (±SD). HeLa cell numbers show a linear relationship with luminescent output (r^2 = 0.997).

3.2.2 Optimisation of SFV multiplicity of infection

To determine the most appropriate SFV MOI required to achieve around 40-50% reduction in cell viability, $5x10^4$ cells were added to triplicate wells of a 96 well plate. After overnight incubation it was determined that there were approximately $6x10^4$ cells, and then cells were infected with SFV at a MOI of 0.001, 0.01, 0.1, 1, 2, 5, and 10. At 16 hr post-infection cell viability was monitored by addition of CellTitre-Glo reagent. The percentage viable cells were determined relative to mock-infected cells. As anticipated, infection of HeLa cells with an increasing SFV MOI resulted in decreased cell viability. Infection of cells with an MOI of 1 gave a cell viability of 70%, whereas an MOI of 2 gave a cell viability of 61%, and an MOI of 5 gave a cell viability of 44% (Figure 3.3). As a MOI of 2 was used in the original siRNA library screen, it was decided to continue with this MOI for the deconvolution experiments. This would give appropriate scope for detecting an increase in cell viability due to depletion of DUBs.

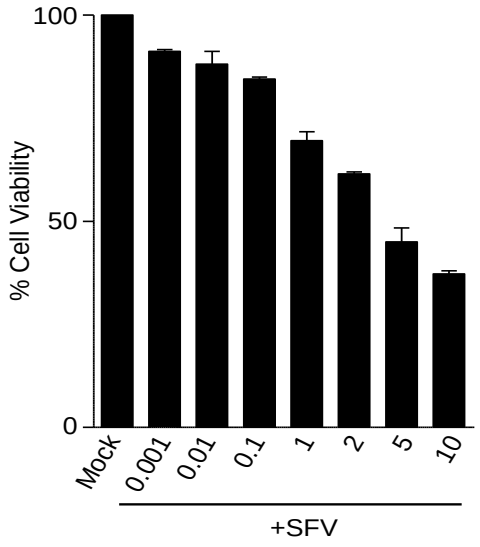

Figure 3.3 Monitoring the effect of SFV infection on the viability of HeLa cells using the Celltiter-Glo assay. HeLa cells seeded into a 96 well plate were infected in triplicate with SFV at MOIs of 0.001, 0.01, 0.1, 1, 2, 5 and 10. At 16 hr post-infection cell viability was measured using the CellTiter-Glo Luminescent Assay. Data is presented as the percentage cell viability relative to mock infected cells (100% viability), and is the mean of three technical replicates (± SD).

3.3 Deconvolution of DUB siRNA pools for positive library hits

The 12 DUBs identified in the original library screen contained members from each of the five DUB families, shown in Figure 3.1. These were: USP1, USP4, USP5, US34, USP45, USP46 and USP53 from the USP family; UCHL1 from the UCH family; OTUD6A from the OTU family; BRCC3 and MYSM1 from the JAMM family; and JOSD2 from the Josephin family.

The approach used for the deconvolution of DUB siRNA pools is shown in the flowchart in Figure 3.4. HeLa cells in duplicate 96 well plate were reverse-transfected in triplicate with DUB siRNAs corresponding to the original pool used in the preliminary screen (P), along with each individual siRNA (siRNAs 1-4). At 72 hr post transfection, one plate was infected with SFV at a MOI of 2, the second plate was mock infected. At 16 hr post-infection cell viability was measured using the CellTitre-Glo assay. Both a control non-targeting siRNA (siC) and untransfected controls (H_2O) were included. In addition, a siRNA pool targeting OTUD7A, which lead to a decrease of 50% in cell viability in the original screen (N Blake, personal communication, see Figure 3.1) was also used as a control. HsDeath siRNA, is a mixture of siRNAs targeting ubiquitously expressed human genes that are essential for cell survival. Depletion of these genes induces a high degree of cell death, which is visible by light microscopy and it was used as a positive control to monitor transfection efficiency.

Using this approach, DUBs were deemed to be positive for playing a role in SFV infection if the pool of 4 siRNAs and two or more of the individual siRNAs resulted in a 20% or more increase in cell viability. This value (20%) was chosen as it was thought that when the siRNAs were used individually, they may not achieve the same level of effect as when used as a pool of 4, and thus may not reach the 30% level as used in the original screen. In addition, it was thought that a 20% difference also represented a significant effect on virus due to DUB depletion. The following sections will present the results of the deconvolution experiments grouped by DUB family.

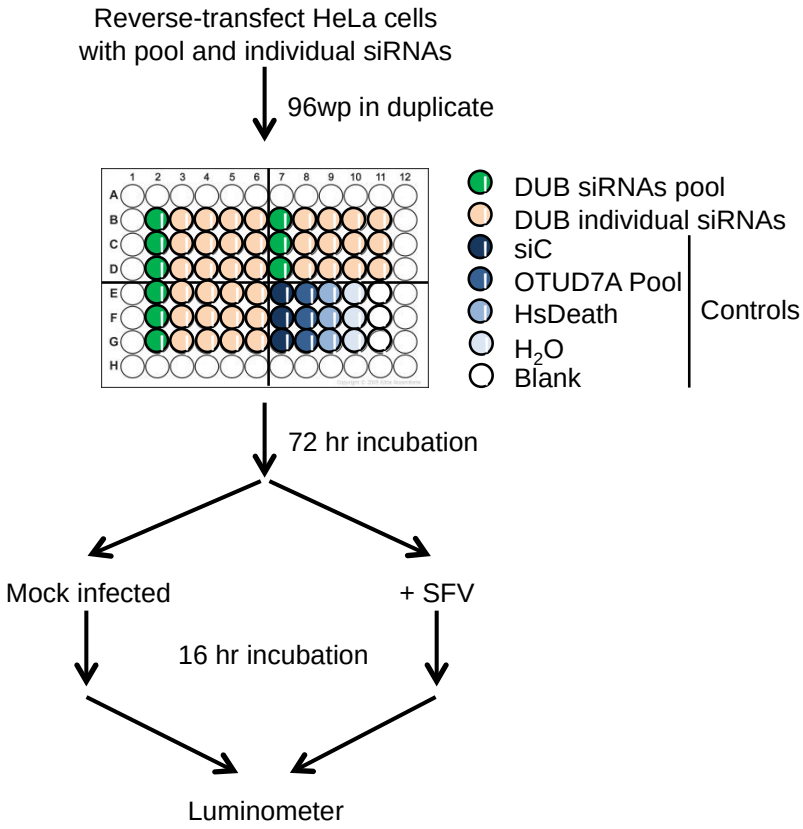

Figure 3.4 Flowchart showing the approach used for deconvolution of DUB siRNA pools. HeLa cells in duplicate 96 well plate were reverse-transfected with DUB siRNAs corresponding to the original pool used in the preliminary screen (P), along with each individual siRNA (siRNAs 1-4). At 72 hr post-transfection, one plate was infected with SFV at 2 MOI, the second plate was mock infected. At 16 hr post-infection cell viability was assayed using the CellTiter-Glo assay. Control wells included a non-targeting siRNA siContol (siC) and an siRNA pool targeting OTUD7A, which lead to a decrease in cell viability in the original screen. HsDeath siRNA was used as a positive control for transfection. Cell viability was monitored by microscopic inspection of the cells at 72 hr post-transfection.

3.3.1 Deconvolution of the siRNA pools for the USP family hits

Deconvolution experiments were carried out for USP1, USP4, USP5, US34, USP45, USP46 and USP53. Data for USP1 is shown in Figure 3.5. There was an increase in cell viability of 24% due to depletion of USP1 with the pool of 4 siRNAs. This was significantly lower than the increase in viability observed in the original screen, of 77% (Table 3.1). Although lower, it was still deemed to be a positive hit. However, when the individual USP1 siRNAs were analysed only treatment with a single siRNA, USP1 siRNA 1, resulted in a

significant increase in cell viability (of 54%). USP1 siRNA 2 resulted in a very marginal increase in cell viability (4%), whereas siRNAs 3 and 4 resulted in a decrease in cell viability of 14% and 55% respectively (Figure 3.5). Treatment with the siRNA pool for OTUD7A resulted in the expected decrease in cell viability, of 62%. Thus, using the cell viability readout to deconvolute the USP1 siRNA pool, USP1 did not meet the criteria of a positive hit, with only a single siRNA resulting in an increase in cell viability.

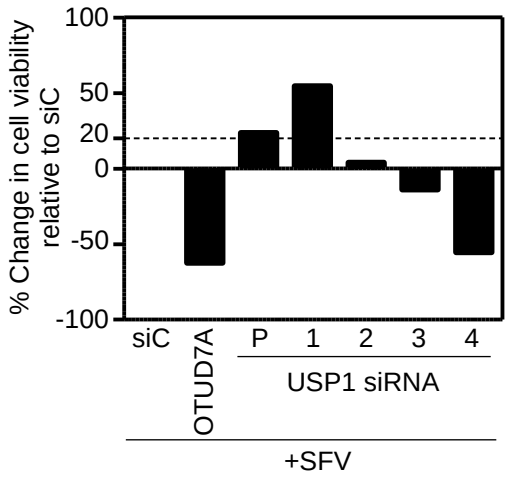

Figure 3.5 Deconvolution of the USP1 siRNA pool involved in SFV replication. HeLa cells in duplicate 96 well plate were reverse-transfected with USP1 siRNAs corresponding to the original pool used in the preliminary screen (P), along with each individual siRNA (siRNAs 1-4). At 72 hr post-transfection, one plate was infected with SFV at 2 MOI, the second plate was mock infected. At 16 hr post-infection cell viability was assayed using the CellTiter-Glo assay. The percentage change in cell viability of infected vs. uninfected cells, relative to the siC treated control is shown. An siRNA pool targeting OTUD7A, shown previously to lead to a decrease in cell viability, was included as an additional control. Data is one of two independent experiments.

The next positive hit from the screen to be analysed was USP4. In the initial screen, depletion of USP4 with the siRNA pool resulted in an increase in cell viability of 64%. In the deconvolution study here, shown in Figure 3.6A, the increase in cell viability observed due to treatment with the USP4 siRNA pool was only 18%. However, depletion of USP4 with both siRNAs 1 and 4 lead to an increase in cell viability of 37% and 22% respectively (Figure 3.6A). Knockdown with USP4 siRNAs 2 and 3 resulted in a decrease in cell viability of 38% and 11% respectively. Depletion of OTUD7A resulted in the expected decrease in cell viability of 62% (Figure 3.6A). Thus, the data for the USP4

siRNA pool was significantly lower than that seen in the original screen (18% v 64%), and slightly lower than 20% cut-off criteria adopted in this study. However, two individual USP4 siRNAs (siRNAs 1 and 4) lead to increases in cell viability of greater than 20%. Thus, this was deemed to be supportive of USP4 having a functional role during SFV infection.

The next hit to be tested was USP5, which resulted in an increase in cell viability of 61% in the original screen. Deconvolution of the USP5 siRNA pool is shown in Figure 3.6B. Knockdown of USP5 in HeLa cells with the siRNA pool again lead to an increase in cell viability after SFV infection, this time of 29%. Two individual USP5 siRNAs, siRNAs 1 and 4, also resulted in increases in cell viability of 27% and 15% respectively (Figure 3.6B). Treatment of HeLa cells with USP5 siRNAs 2 and 3 resulted in a decrease in cell viability of 59% and 24%, respectively. Again the OTUD7A siRNA pool lead to a decrease in cell viability of 21%. Although the USP5 siRNA pool and individual siRNA 1 resulted in increases in cell viability greater than 20%, only one other individual siRNA lead to an increase. This was siRNA4, but only showing a 15% increase. This was not thought to be close enough to the 20% threshold. Thus, USP5 was not predicted to have a functional role during SFV infection.

The siRNA pool for USP34 was next to be deconvoluted. In the original screen the USP34 pool resulted in an increase of 75% in viability after SFV infection. In the deconvolution experiment, depletion of USP34 with the pool of 4 siRNAs resulted in a small increase in cell viability of 11%, contrasting significantly with the original data. However, knockdown of USP34 with three of the individual siRNAs resulted in an increase in cell viability after SFV infection of 17%, 33% and 23% for siRNAs 2, 3 and 4 respectively (Figure 3.6C). Whereas, USP34 siRNA 1 resulted in a decrease in cell viability of 79% (Figure 3.6C). Again the OTUD7A pool lead to the expected decrease in cell viability of 81%. Although the USP34 siRNA pool resulted in an increase of only 11% in cell viability, two individual siRNAs lead to increase in viability over 20%, with a third siRNA resulting in close to 20% increase. This data was

suggestive that USP34, although not complying with the deconvolution criteria, did warrant further investigation.

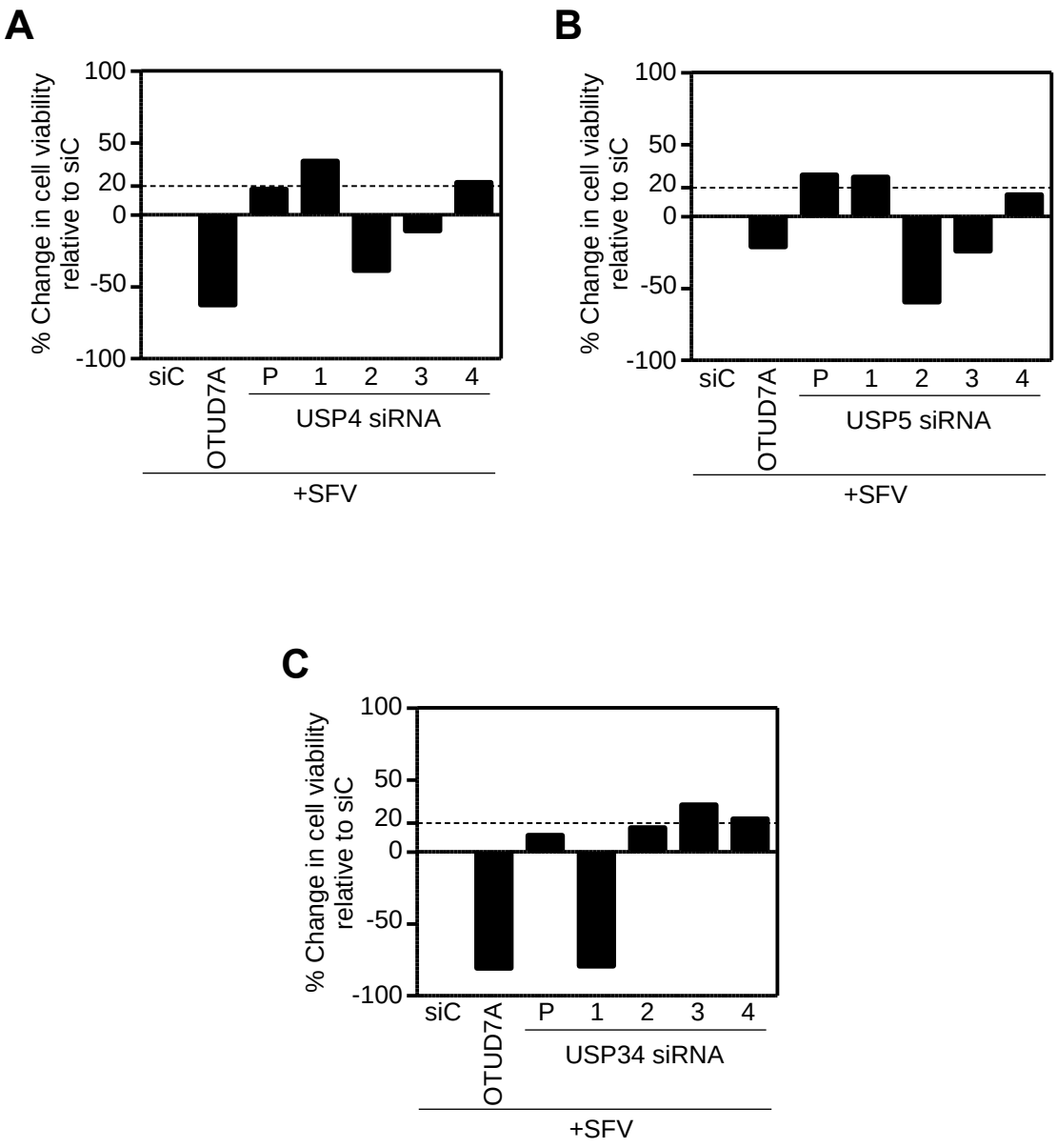

Figure 3.6 Deconvolution of the USP4, USP5 and USP34 siRNA pools involved in SFV replication. siRNA pools for the USP family DUBs USP4 (A), USP5 (B) and USP34 (C) were deconvoluted as described in Figure 3.5.

Deconvolution experiments were then carried out for USP45. In the initial screen, an increase in cell viability of 64% was seen after depletion of USP45 by the pool of 4 siRNAs. However, the deconvolution experiments in this thesis resulted in a very small increase in cell viability of 5% following to treatment of HeLa cells with the USP45 siRNA pool and subsequent SFV infection. When the four individual USP45 siRNAs were analysed, only siRNA 3 lead to an increase in cell viability (of 62%). Knockdown of USP45 by siRNAs 1, 2 and 4 resulted in a decrease in cell viability after SFV infection of 2%, 52% and 30%, respectively (Figure 3.7A). In this deconvolution assay, the OTUD7A siRNA pool resulted in a decrease in cell viability after SFV infection of 69%. Thus, this data indicates that USP45 did not meet the criteria of a positive hit.

USP46 was the next positive hit that was tested. In the initial screen, an increase in cell viability of 45% was observed due to depletion of USP46 by the siRNA pool. When the siRNA pool was tested again in the deconvolution experiments, an increase in cell viability of 16% was detected (Figure 3.7B). Knockdown of USP46 with the individual siRNAs resulted in an increase in cell viability after SFV infection of 25% and 44% for USP46 siRNA 3 and 4 respectively. Whereas, siRNAs 1 and 2 resulted in a 5% decrease and increase respectively (Figure 3.7B). Again, the OTUD7A pool lead to the expected decrease in cell viability of 31%. Although depletion of USP46 by the siRNA pool lead to an increase in cell viability of only 16%, two individual siRNAs 3 and 4 resulted in increases in cell viability greater than 20%. This suggested that USP46 might play a role during SFV infection and warranted further investigation.

In the first screen, depletion of USP53 by pool of 4 siRNAs showed an increase of cell viability of 47% whereas in the second screen a change in cell viability of 31% was seen following to treatment HeLa cell with USP53 pool of 4 siRNAs. An increase in cell viability of 53%, 29% and 45% was observed in regards to depletion of USP53 with siRNA 1, 3 and 4. Although, treatment of HeLa cells with siRNA 2 resulted in a decrease in cell viability of 35% (Figure 3.7C). The depletion of OTUD7A by pool resulted in a decrease in cell viability after SFV infection of 53%. Thus, as the USP53 siRNA pool and 3 individual siRNA result in increases in cell viability greater than 20%, this strongly

supports USP53 as a positive hit from the screen and suggests a functional role in SFV infection. Several factors may explain the variable differences in cell viability increases between the initial screens and the screens undertaken in this study. It is possible that there may have been technical issues when generating the pools to be used in this study, as the original screen pools were no longer available. In addition, two different reagents were utilised to assess changes in cell survival resulting from the depletion DUBs and infection with SFV. The MTS assay was utilised in the preliminary screen while, CellTiter-Glo assay was utilised in the deconvolution study and hence this may account for variation in the results.

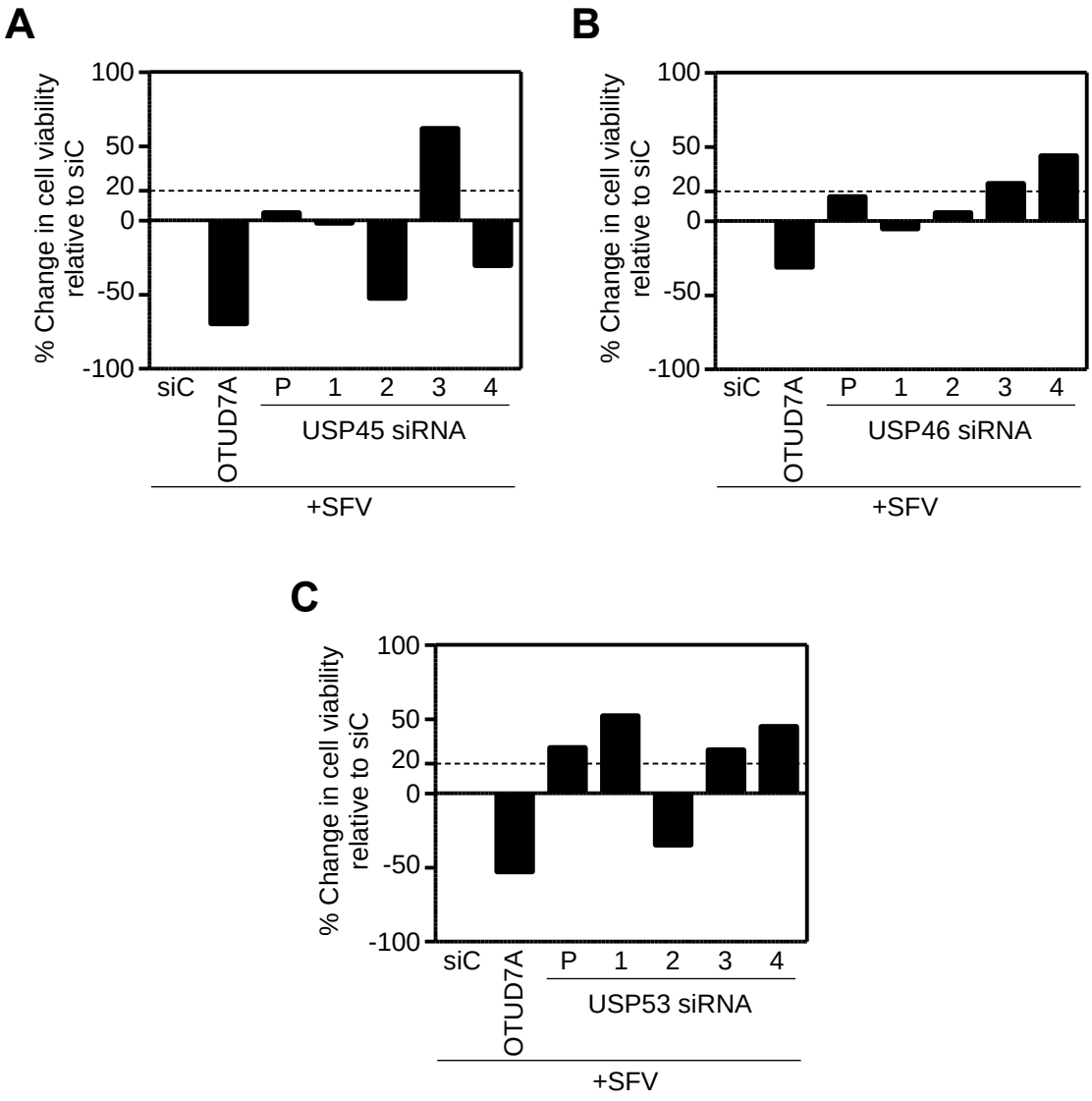

Figure 3.7 Deconvolution of the USP45, USP46 and USP53 siRNA pools involved in SFV replication. siRNA pools for the USP family DUBs USP45 (A), USP46 (B) and USP53 (C) were deconvoluted as described in Figure 3.5.

3.3.2 Deconvolution of the siRNA pools for the OTU family DUB, OTUD6A

OTUD6A was the only member of the OTU DUB family identified in the original screen, where knockdown with the siRNA pool lead to a 110% increase in cell viability after SFV infection. A deconvolution experiment for the OTUD6A siRNA pool is shown in Figure 3.8A. Knockdown of OTUD6A with the pool of 4 siRNAs resulted in an increase in cell viability of 35%, significantly lower than the original screen but still showing an increase. Each individual OTUD6A siRNA was tested in the same experiment and showed variable results. Depletion of OTUD6A with siRNA 1 resulted in an increase in cell viability of 13%, while treatment HeLa cells with siRNA 4 resulted in an increase in cell viability of 61%. However, depletion of OTUD6A by siRNAs 2 and 3 resulted in a decrease in cell viability of 4% and 38%, respectively. Depletion of OTUD7A with the siRNA pool resulted in a decrease of 81% (Figure 3.8A). Thus with only the pool and one individual siRNA (siRNA 4) resulting in greater than 20% increase in cell viability, and the next greatest effect being only 13% for siRNA 1, it suggested that OTUD6A was not a hit based on this deconvolution approach.

3.3.3 Deconvolution of the siRNA pools for the UCH family DUB UCHL1

Deconvolution experiments were carried out for UCHL1, which when knocked down in the original screen resulted in an increase of 45% in cell viability after SFV infection. In this study, treatment of HeLa cells with the pool of 4 siRNAs resulted in an increase in cell viability of 29% (Figure 3.8B). However, individually only a single UCHL1 siRNA, siRNA 3, resulted in an increase in cell viability after SFV infection, of 29%. The other UCHL1 siRNAs (siRNAs 1, 2 and 4) all resulted in decreases in cell viability, of 16%, 3% and 2% respectively. The siRNA pool for OTUD7A as expected lead to a decrease in cell viability of 21% (Figure 3.8B). Based on this data, the effect of knockdown of UCHL1 did not meet the criteria for a positive deconvolution using this approach.

3.3.4 Deconvolution of the siRNA pools for the Josephin family DUB JOSD2

JOSD2 was the only member of the Josephin DUB family identified in the original screen, where knockdown with the siRNA pool lead to a 43% increase in cell viability after SFV infection. A deconvolution experiment for the JOSD2 siRNA pool is shown in Figure 3.8C. Knockdown of JOSD2 with the pool of 4 siRNAs resulted in an increase in cell viability of 25%, a relatively similar value to the original data. Treatment of HeLa cells by siRNA 2 and 4 resulted in increases in cell viability after SFV infection of 35% and 56% respectively (Figure 3.8C). JOSD2 siRNA 3 lead to a very minor increase in cell viability of 5% (Figure 3.8C). Depletion of JOSD2 with siRNA 1 had an opposite effect and resulted in a decrease in cell viability of 66%. Depletion of OTUD7A by pool of 4 siRNAs resulted in a 76% decrease in cell viability (Figure 3.8C). Thus, as the pool and, individual siRNAs 2 and 4, lead to increases in cell viability greater than 20%, JOSD2 was deconvoluted successful. This suggests a potential role for JOSD2 during SFV infection, and warrants further investigation.

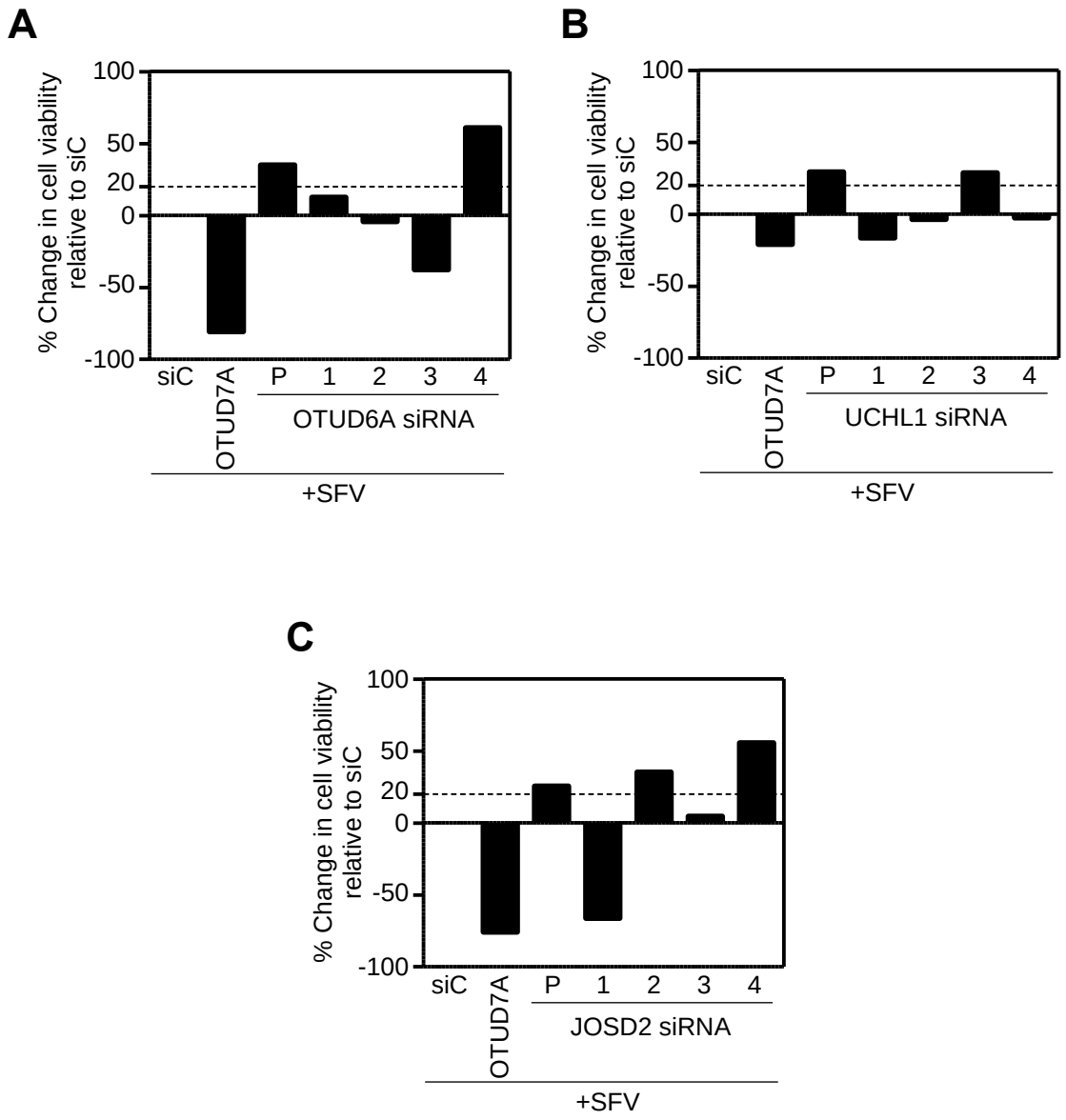

Figure 3.8 Deconvolution of the siRNA pools for OTUD6A, UCHL1, and JOSD2. siRNA pools for the OTU DUB OTUD6A (A), UCH DUB UCHL1 (B) and Josephin DUB JOSD2 (C) were deconvoluted as described in Figure 3.5.

3.3.5 Deconvolution of the siRNA Pools for the JAMM/MPN+ family hits

In the original screen, knockdown of two JAMM/MPN+ family DUBs, BRCC3 and MYSM1, led to an increase in cell viability after SFV infection of 78% and 46% respectively. Thus, deconvolution experiments were carried out for both BRCC3 and MYSM1 siRNA pools, shown in Figure 3.9A (BRCC3) and B (MYSM1). Depletion of BRCC3 using the siRNA pool lead to a small

increase in cell viability after SFV infection of 11%. Individual BRCC3 siRNAs 2 and 3 lead to an increase in cell viability of 52% and 67% respectively. Whereas, siRNAs 1 and 4 had the opposite effect, resulting in a decrease in cell viability of 35% and 45%, respectively (Figure 3.9A). The control siRNA pool of OTUD7A lead to a decrease in cell viability of 21%. Although knockdown of BRCC3 by siRNA pool lead to increase in cell viability lower than the 20% threshold, two individual siRNAs (2 and 3) lead to significant increases in cell viability. Thus suggesting that BRCC3 may warranted further investigation.

The last DUB deconvoluted was MYSM1 (Figure 3.9B). In this study, depletion of MYSM1 with the siRNA pool lead to an increase in cell viability after SFV infection of 69%, comparable with 46% seen in the original screen. Knockdown with each of the four individual siRNAs (siRNAs 1-4) for MYSM1 resulted in increases in cell viability of 26%, 46%, 64% and 20%, respectively (Figure 3.9B). Depletion of OTUD7A by the pool of 4 siRNAs led to a decrease in cell viability of 57%. Thus, the MYSM1 siRNA pool and each individual siRNA resulted in increases in cell viability after SFV infection of greater than 20%, strongly supporting a role for MYSM1 during SFV infection.

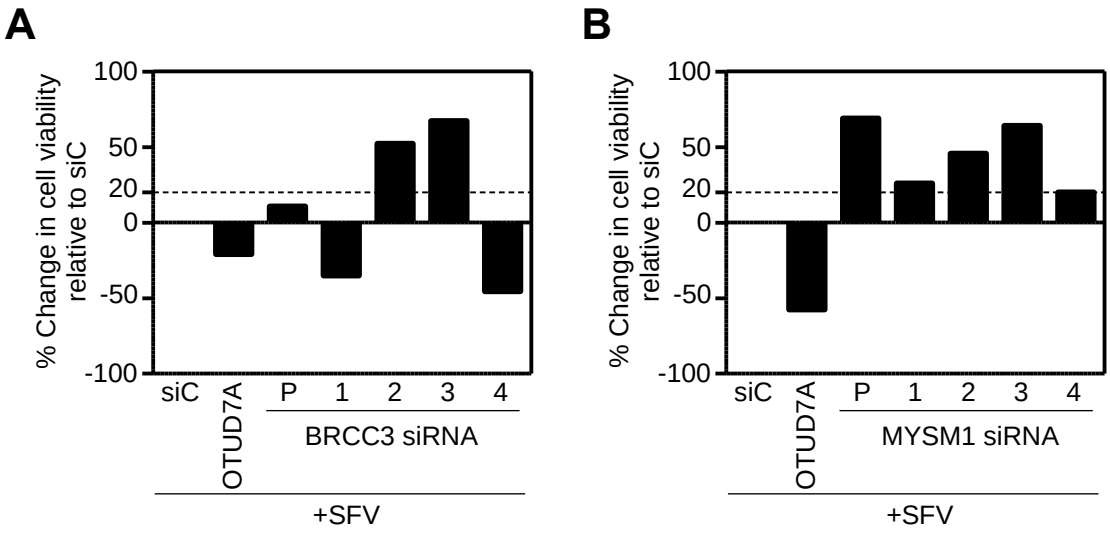

Figure 3.9 Deconvolution of the siRNA pools for the JAMM/MPN+ family BRCC3 and MYSM1. siRNA pools for the JAMM/MPN+ family DUBs BRCC3 (A), and MYSM1 (B) were deconvoluted as described in Figure 3.5.

3.4 Quality control of deconvolution for DUB hits siRNA pools

Three important variables could potentially influence the data from these deconvolution experiments. These are poor transfection efficiency, poor knockdown efficiency of the target transcript and toxicity due to siRNA treatment (either due to depletion of the specific DUB or off-target effects). Using the experimental approach in this chapter, it was not possible to monitor the target knockdown efficiency (this was addressed in Chapter 4). However, steps were included in the protocol to monitor both transfection efficiency and toxicity issues (see section 3.3).

As described, the siRNA pool for OTUD7A was used as a control throughout the cell viability deconvolution experiments. This was a control for the data in the original screen, where the OTUD7A pool lead to a decrease in cell viability, so also served partly to monitor transfection efficiency. In all deconvolution experiments cells treated with OTUD7A siRNA pool resulted in the expected decrease in cell viability after SFV infection (section 3.3.1 to 3.3.5). The OTUD7A siRNA pool data were quite variable from assay to assay (21-81% decrease in cell viability). That may be these deconvolution experiments had a variable transfection efficiency of the target transcript. The transfection was consider successful if the OTUD7A siRNA pool showed 20% or more decrease in cell viability after SFV infection. Transfection efficiency was also monitored by utilising the ALLStar HsDeath siRNA, which induces a high degree of cell death by targeting and depleting essential human survival genes. HsDeath siRNA induced cell death was monitored visually by light microscopy. Triplicate wells of the 96 well plate were treated with HsDeath siRNA (see Figure 3.4). Successful transfection of the HeLa cells should result in a high level of cell death. This was monitored visually at 72 hr post-transfection. HsDeath transfected cells showed an estimated reduction in confluence of 80-90% in all experiments (with increased numbers of floating cells observed).

Monitoring of siRNA induced toxicity was carried out two ways. Firstly, examination of cells by light microscopy was performed at 72 hr post-transfection. The majority of the DUB siRNAs were associated with little visible

direct toxicity. There was evidenced by an estimated confluency of cells of greater than 80%, with few floating cells in the media and healthy looking cells. One notable exception was BRCC3 siRNA 1, which showed a reduced cell confluence to approximately 40-50%. Depletion of several other DUBs was associated with a degree of cell toxicity of >20% as determined visually. These were USP1 siRNA 1, USP34 siRNAs 1 and 2, OTUD6A siRNA 1 and JOSD2 siRNA 4. These microscopy observations were supported by monitoring the cell viability in the transfected but uninfected plate. This was determined as part of the overall assay (to determine the ratio of cell viability of infected vs uninfected), but here it is analysed on its own, as a percentage relative to untransfected cells (H_2O control wells is transfection without siRNA to control potential effect of transfection reagents on the cell) to assess siRNA induced toxicity (after 88 hr transfection). The percentage cell viability indicates the level of toxicity following knockdown of DUBs by either the pool or individual siRNAs. Data from the experiments presented in section 3.3 is shown in Figure 3.10. As predicted by the visual monitoring at 72 hr, transfection with BRCC3 siRNA 1 resulted in a reduction in cell viability to 45%. Whilst USP1 (pool of 4 siRNAs and siRNA 1), USP34 (siRNAs 1 and 2), OTUD6A (siRNA 1) and JOSD2 (siRNA 4) all caused a reduction in cell viability to 60-70%. Depletion of all other DUBs by either the pool of 4 siRNAs or individual siRNAs resulted in cell viabilities of >70%. The mean cell viability across all experiments for the siC and OTUD7A siRNA pool transfected wells was 92% and 90% respectively. The cell viability for the HsDeath was only measure in 5 of the deconvolution experiments and showed an average of 5% cell viability.

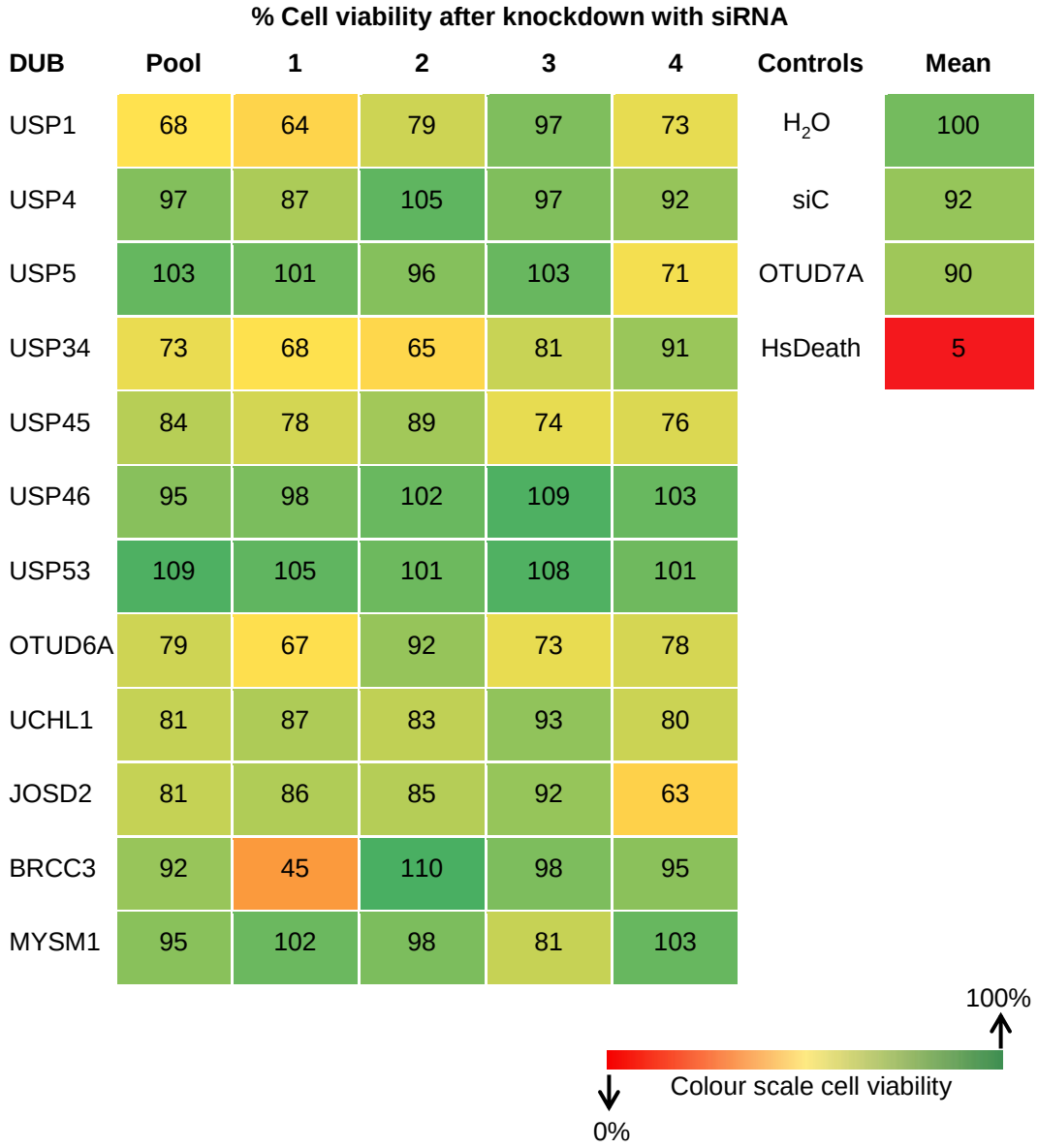

Figure 3.10 Heat map showing effect of DUB knockdown on cell viability. A heat map representing the cell viability of DUB and control siRNA treated cells 88 hr post-transfection. Data shows the percentage cell viability from one representative experiment.

3.5 Summary of the cell viability deconvolution experiments for the siRNA pools for DUBs identified in the original siRNA screen

Twelve DUBs had been identified in an siRNA library screen as potentially playing a pro-viral role during SFV infection. In this chapter, each of the DUB siRNA pools were deconvoluted using a similar assay read out monitoring changes in cell viability. A positive deconvolution was where the original pool and at least 2 individual siRNAs results in an increase in 20% or

greater in cell viability after SFV infection. Using these criteria strictly, only three of the DUBs deconvoluted successfully (Figure 3.11).

% Change in cell viability of DUBs knockdown + SFV infection

DUB	Pool	1	2	3	4
USP1	24	54	4	-14	-55
USP4	18	37	-38	-11	22
USP5	29	27	-59	-24	15
USP34	11	-79	17	33	23
USP45	5	-2	-52	62	-30
USP46	16	-5	5	25	44
USP53	31	52	-35	29	45
OTUD6A	35	13	-4	-38	61
UCHL1	29	-16	-3	29	-2
JOSD2	25	-66	35	5	56
BRCC3	11	-35	52	67	-45
MYSM1	69	26	46	64	20

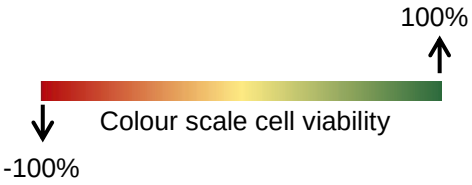

Figure 3.11 The % cell viability vs siControl of cells treated with DUB siRNAs and infected with SFV. Cell viability of infected vs uninfected relative to siC treated cells was measured following 72 hr reverse transfection and 16 hr post-infection cell viability was assayed using the CellTiter-Glo assay. Numerical data shows change in % cell viability from one representative experiment. Negative values indicate a decrease in cell viability whilst positive values indicate an increase in cell viability. Red squares indicate <0% cell viability, orange squares indicate 0-20% cell viability, and green squares indicate >20% cell viability.

These were MYSM1, USP53 and JOSD2. All 4 siRNAs were positive for MYSM1, 3 were positive for USP53 and 2 for JOSD2. Analysis of cell viability after DUB depletion for these DUBs and the positive individual siRNAs highlighted high levels of viability with the exception of JOSD2 siRNA 4 (63%

cell viability). In a number of cases 2 or more individual siRNAs were positive but the original pool did not result in greater than 20% change (nor agree with the original screen values). It is possible that, as these pools were not the identical pools as originally used in the screen, there may have been technical issues when generating the aliquots. Thus, where at least two individual siRNAs gave positive data these DUBs were not automatically rule out. These were USP4, USP34, USP46 and BRCC3. With the exception of USP34, cell viability after siRNA depletion for these DUBs was greater than 70%. For USP34, as single positive siRNA (siRNA 2) resulted in a cell viability of 65%. Five of the 12 DUBs did not deconvolute. These were USP1, USP5, USP45, OTUD6A, UCHL1. This data is summarised in Table 3.2.

Table 3.2 Summary of Deconvolution of siRNA Pools by Cell Viability

Did Not Deconvolute	**Pool + 2 siRNAs**	**Pool + 3 siRNAs**	**Pool + 4 siRNAs**
USP1	(USP4)*	USP53	MYSM1
USP5	(USP34)		
USP45	(USP46)		
OTUD6A	JOSD2		
UCHL1	(BRCC3)		

*DUBs in brackets the pools were below 20%, but 2 or more individual siRNAs were positive

Using the approach in this chapter only allowed for monitoring the effect on cell viability after SFV infection of siRNA treated cells. Although it was inferred that this reflected a changes in SFV replication this was not directly measured. Nor did this provide any information on the efficiency of DUB depletion. Thus, a second screening assay was employed to monitor SFV infection and confirm depletion of the target DUB by measuring virus RNA levels and DUB mRNA in HeLa cells using QPCR. This is described in the following chapter.

Chapter 4

Deconvolution of the DUB siRNA Pools Utilising a Secondary Read-Out: SFV RNA Level

4.1 Introduction

In chapter 3, the preliminary deconvolution of 12 DUBs identify in a siRNA screen against SFV was described. These were USP1, USP4, USP5, USP34, USP45, USP46, USP53, OTUD6A, UCHL1, JOSD2, BRCC3 and MYSM1. In those experiments, using the same approach as the original screen by measuring the effect on cell viability, USP53, JOSD2 and MYSM1 were successfully validated by deconvolution, meeting the criteria that the original pool of 4 siRNAs and at least two of the individual siRNA recapitulated the effects observed in the original screen. Additionally, while the value for the siRNA pool was below 20%, two individual siRNAs were positive for USP4, USP34, USP46 and BRCC3. In this chapter, a secondary readout was used to repeat the deconvolution. This readout was monitoring levels of SFV RNA genome after infection of HeLa cells depleted of the selected DUBs. Based on the original interpretation of the cell viability screen, it was predicted that the increase in cell viability reflected a reduction in SFV replication. Thus, the hypothesis was that there will be a decrease in SFV RNA levels. This approach would also have a dual purpose. In addition to validating the DUB hits, i.e. an effect on SFV replication based on measuring RNA levels, it would also allow for the efficiency of knockdown of the DUB transcript to be monitored. The overall, aim was to combine the data generated in this chapter, with the data from chapter 3 to provide a robust approach to validate the hits from the original DUB siRNA screen.

4.2 Monitoring transcript levels in HeLa cells for DUBs identified in the siRNA screen

Before undertaking the secondary readout approach, experiments were undertaken to monitor the normal transcript levels of each of the 12 DUBs in

untreated HeLa cells. This would confirm transcription of these DUBs in the HeLa cells being used in these assays, and determine the transcript baseline which would help with interpretation of efficiency of siRNA knockdown. RNA was extracted from HeLa cells, before being converted to cDNA using oligo (dT) primer. For all cDNA generations a RT negative (RT-) control was included to monitor for potential genomic DNA contamination. End-point PCR was then carried out for the following DUBs: USP1, USP4, USP5, USP34, USP45, USP46, USP53, OTUD6A, UCHL1, JOSD2, BRCC3 and MYSM1. PCR was performed using the following cycling conditions for each DUB, with the relevant annealing temperature: a denaturing step (95°C for 5 mins), 40 cycles of [94°C for 30 secs, 55°C or 60°C for 30 secs, 72°C for 30 secs], with a final 72°C/10 mins. All DUB PCR reactions were performed on the same cDNA sample, and a PCR for actin (ACTB) was simultaneous performed for each reaction. RT- and H_2O controls were used throughout. The results of all DUB E-P PCRs are shown in Figure 4.1, with a representative ACTB reaction shown. Products of the expected size were detected for 11 of the 12 DUBs (predicted DUB product sizes is provided in Appendix B), with the exception being OTUD6A where no product was detected. Transcript levels of the other 11 DUBs varied from very high for BRCC3, to low but detectable for JOSD2.

As the efficiency of DUB knockdown was going to be analysed at the same time as level of SFV RNA, the representative Ct value for each DUB in QPCR reactions was also determined in the HeLa cells. Using a two step QPCR reaction with 40 cycles and SYBR green detection, the Ct value for each DUB was as follows: USP1=17, USP4=21.5, USP5=23, USP34=22, USP45=27, USP46=22, USP53=23.5, OTUD6A=not detected, UCHL1=21, JOSD2=28, BRCC3=21 and MYSM1=27 (Figure 4.1). As OTUD6A was not detected by either E-P PCR or QPCR, this suggested that OTUD6A was either not expressed in the HeLa cells, or the transcript was at very low (undetectable levels). In addition, it is possible that OTUD6A expression is induced following SFV infection. Thus, it was decide that OTUD6A would not be analysed further in this chapter.

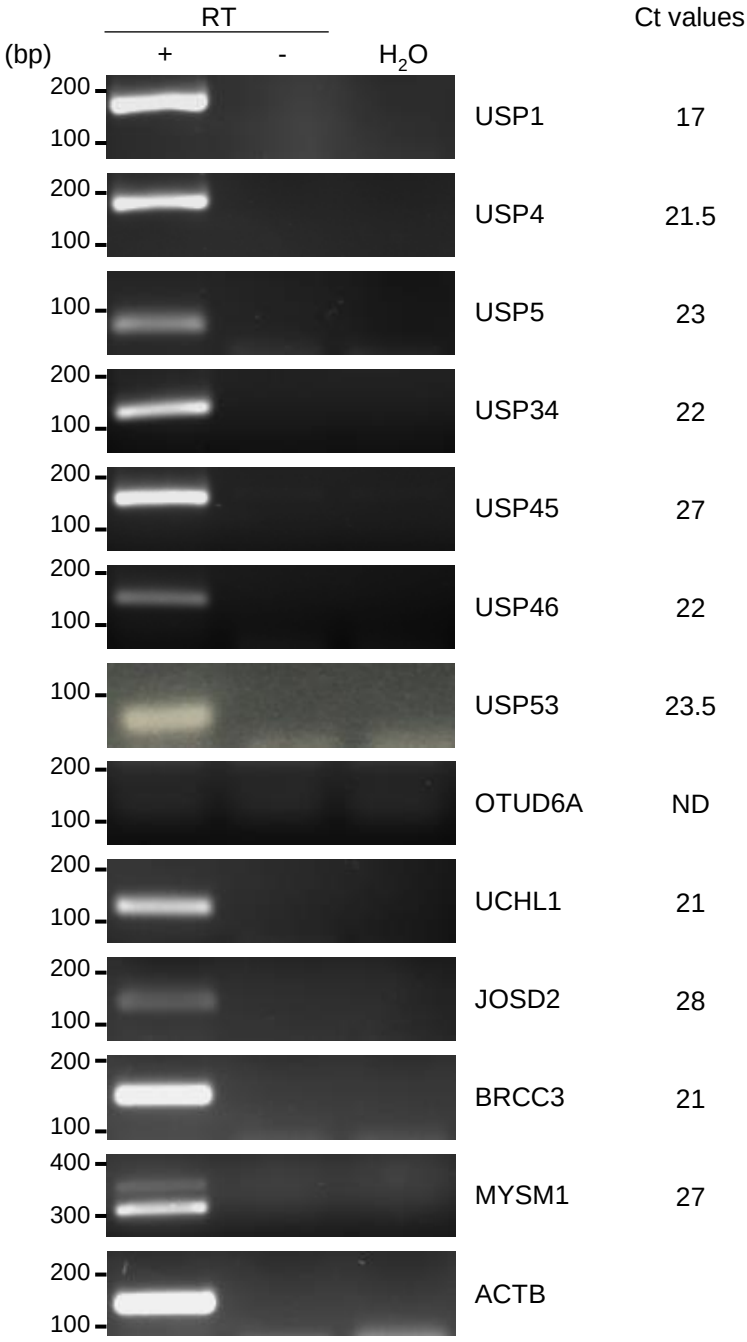

Figure 4.1 Transcript of DUB positive hits in HeLa cells. HeLa cells were harvested in the resting condition. Total RNA was extracted, converted to cDNA before the individual DUB transcript levels were monitored by E-P PCR. RT(+) and RT(-) are RNA samples converted to cDNA in the presence of reverse transcriptase. Actin (ATCB) was used as a positive control, and a H_2O control was used in all PCR reactions. The Ct value for each DUB determined in QPCR reactions is shown.

4.3 Experimental approach to deconvolute the DUB siRNA pools based on monitoring SFV RNA levels

The DUB siRNA pools were deconvoluted using the following approach. HeLa cells were reverse-transfected in 6 well plate with each of the 4 individual siRNAs present in the original pool or the non-targeting siRNA, siC. Note, the original siRNA pool itself was not use in these assays. Cells were then incubated for 72 hr before being infected with SFV (MOI = 2). Total RNA was extracted at 8 hour post-infection, converted to cDNA using oligo (dT), before being analysed by PCR. A schematic representation of this approach is shown in Figure 4.2. Note, oligo (dT) was used to prime the production of cDNA as in addition to converting DUB mRNA transcripts to cDNA, it would also convert SFV +ve sense genomes as they are poly-adenylated. For all cDNA generation a RT- control was included. All cDNAs (both RT+ and RT-) were first screened by end-point PCR to monitor RT- samples (a representative example is shown in Figure 4.3A). Accurate quantitation of DUB mRNA and SFV RNA levels was carried out by using the comparative (Ct) method and expressed relative to the siC treated cells. The criteria to determine a positive hit using this approach were that depletion of the DUB by two or more siRNAs results in a reduction in SFV RNA by at least 50%. In addition, these siRNAs must also lead to a reduction of the DUB mRNA of 50% or more. The data from analysis of the following 11 DUBs will be presented in the following sections as follows: the USP family DUBS USP1, USP4, USP5, US34, USP45, USP46 and USP53; the UCH DUB UCHL1 and the Josephin DUBs JOSD2; the JAMM family DUBs BRCC3 and MYSM1.

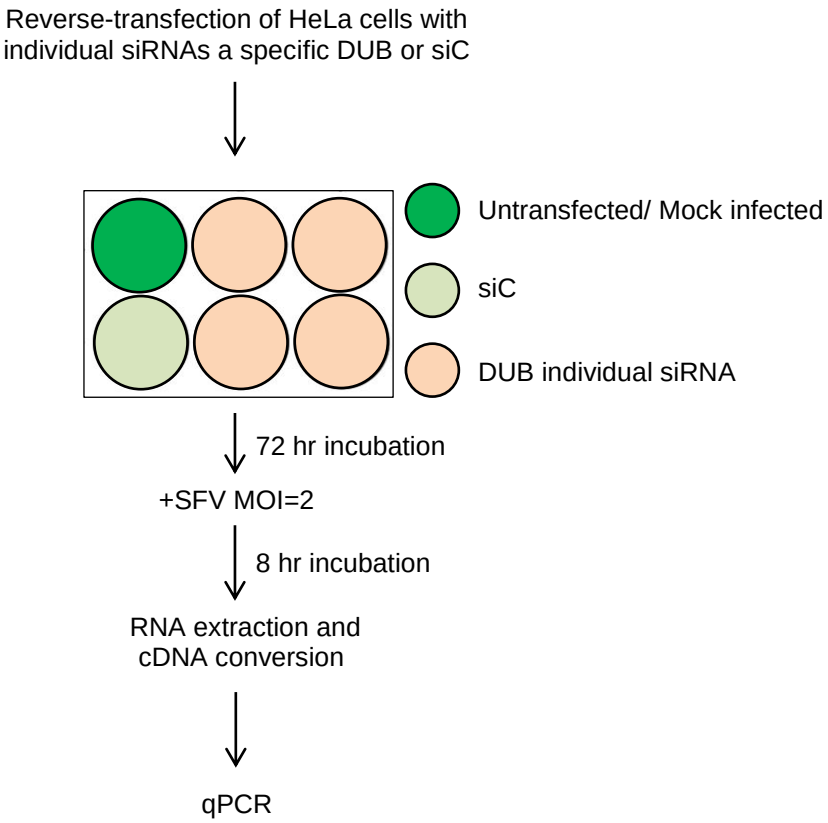

Figure 4.2 Flowchart showing the approach used to deconvolute the DUB siRNA pools based on monitoring changes in SFV RNA levels. HeLa cells were seeded into a 6 well plate and either reverse-transfected with the individual DUB siRNAs 1-4 from the original pool, the control siRNA siC or left untransfected. Following a 72 hr incubation, the cells were then infected with SFV (MOI = 2). One well was use as a mock infected control. Total RNA was extracted at 8 hr post-infection, converted to cDNA and analysed by PCR for levels of DUB transcripts and SFV RNA levels.

4.4 Analysis of the effect of depletion of USP family DUBs on SFV RNA levels

Using the approach described above (section 4.3) the following USP family DUB siRNA pools were deconvuloted based on monitoring SFV RNA levels: USP1, USP4, USP5, USP34, USP45, USP46 and USP53. Data for USP1 is shown in Figure 4.3. cDNAs generated from HeLa cells treated with the four individual USP1 siRNAs, and infected with SFV, were first analysed by end-point PCR for USP1, ACTB and SFV (SFV was only analysed in the RT+ samples). This showed that the relevant samples were infected efficiently with SFV, showing strong PCR products, but also that there was evidence of

knockdown of USP1 transcript, as indicted by faint bands for siRNAs 1-4 in comparison to siC. Importantly, no PCR products were detected in RT- controls. Actin showed a constant product for all RT+ samples (Figure 4.3A).

To quantitate any changes in SFV RNA and USP1 mRNA the cDNA samples were then analysed by QPCR. This data is shown in Figure 4.3B. All four siRNAs reduced USP1 mRNA levels relative to the siC control, with a reduction of 85%, 75%, 90% and 80% for siRNA 1-4 respectively. Thus, suggesting that there would be efficient reduction in levels of USP1 protein in each case. Depletion of USP1 by siRNA 1 and 2 showed a significant reduction in the levels of SFV RNA, with a reduction of 85% and 65% respectively. Depletion of USP1 by siRNA 3 lead to a small increase in SFV RNA levels (10%) and depletion of USP1 by siRNA 4 resulted in an increase of 165% in SFV RNA levels. Thus, two USP1 siRNAs (1 and 2), lead to a decrease in both USP1 mRNA and a SFV RNA, of over 50%, indicating that USP1 meets the criteria for a positive hit in this approach.

For subsequent analysis of the other USP targets, all cDNA samples (both RT+ and RT-) were analysed by E-P PCR as described above for USP1. This confirmed that no products were detectable in the RT- samples, prior to analysis by QPCR. E-P PCR gels for USP4, USP5, USP34, USP45, USP46 and USP53 are shown in Appendix C. QPCR analysis of the effect of depletion of USP4, USP5 and USP34 are shown in Figure 4.4. For USP4 transfection of HeLa cells with siRNAs 1 to 4 showed a reduction in USP4 mRNA of 95%, 84%, 74% and 85% respectively (Figure 4.4A). Analysis of SFV RNA levels showed depletion of USP4 by siRNA 1 and 4 caused a significant reduction of 74% and 67% in SFV RNA levels, while siRNA 3 resulted in a reduction of 40%. However, siRNA 2 caused 70% increase in SFV RNA levels (Figure 4.4A). Thus, there was clear correlation between reduction in USP4 mRNA and SFV levels, of over 50% for siRNAs 1 and 4. Therefore, USP4 does meet the criteria for a positive hit.

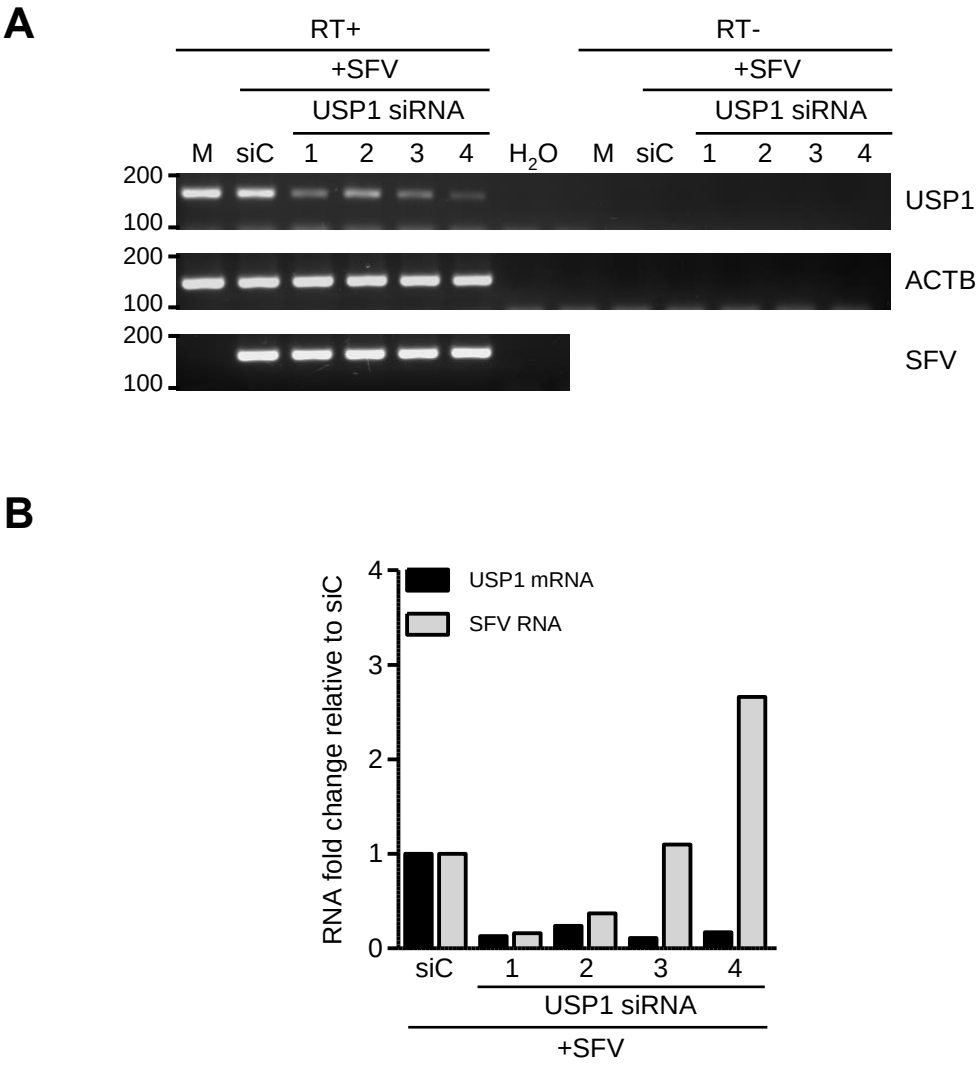

Figure 4.3 The effect of USP1 siRNAs on SFV replication. HeLa cells were reverse-transfected with individual USP1 siRNAs 1-4, corresponding to the original pool used in the preliminary screen or siC. Cells were then incubated for 72 hr before being infected with SFV (MOI = 2). Total RNA was extracted at 8 hr post-infection and converted to cDNA using oligo (dT), before being amplifed by PCR. (A) End -point PCR of RT+ and RT- for USP1, SFV and ACTB. Water and (RT-) controls were used throughout to ensure validity. (B) QPCR analysis of levels of USP1 mRNA and SFV RNA for RT+ samples, the $2^{-\Delta\Delta}$Ct method was used to analyse the data. Actin was employed as the reference gene and results were further normalized to the siC. Data for the siC well was normalised to 1, and data for individual siRNAs is shown as fold change relative to the siC. Data is from one independent experiment.

QPCR analysis data of USP5 knockdown showed a significant reduction in USP5 transcript levels of 97%, 85%, 96% and 94% for the siRNAs 1-4 respectively (Figure 4.4B). Analysis of SFV RNA levels data revealed a reduction on of 70% and 60% after depletion of USP5 by siRNAs 1 and 4 respectively. Treatment of HeLa cells with siRNA 3 showed a small reduction on SFV levels of 30%, while depletion of USP5 with siRNA 2 leads to a small increase (10%) in SFV RNA levels (Figure 4.4B). Thus, two USP5 siRNAs (1 and 4), lead to a decrease in both USP5 mRNA and a SFV RNA, of over 50%, implying that USP5 meets the criteria for a positive hit using this secondary assay. QPCR data for depletion of USP34 by siRNAs 1 to 4 showed a reduction in USP34 mRNA levels of 90%, 85%, 80% and 50% respectively, relative to siC (Figure 4.4C). Analysis of SFV RNA levels after USP34 depletion revealed there was no consistent effect. siRNA 1 led to a small reduction on SFV RNA levels of 15%, while siRNA 2 lead to a 50% increase in SFV RNA levels. Whereas treatment of HeLa cells with siRNA 3 had no effect of SFV RNA levels, and siRNA 4 a minor increase of 14% (Figure 4.4C). Thus, there was no correlation between reduction in USP34 mRNA and SFV levels, especially with regard reduction in SFV RNA. Therefore, USP34 does not meet the criteria for a positive hit.

QPCR analysis of the effect of depletion of USP45, USP46 and USP53 is shown in Figure 4.5. Treatment of HeLa cells with USP45 siRNAs 1-4 resulted in a decrease in USP45 mRNA for all siRNAs (33%, 70% 85% and 96% for siRNAs 1-4 respectively) (Figure 4.5A). Analysis of SFV RNA levels revealed that levels were increased in all cases. Significant increases of 310% and 220% were observed for siRNAs 1 and 4 respectively. Whereas, siRNA 2 and 3 both caused a small increase in SFV RNA levels of 20%. (Figure 4.5A). Although USP45 siRNAs 1 depleted USP45 transcript (albeit of only 33% for siRNA1), and lead to a substantial increase in SFV RNA levels, this did not agree with the assumptions being made with regard the implication of increase cell viability (seen in the original screen) and the predicted effect of a decrease in SFV replication. Thus, as there was no correlation between reduction in USP45 mRNA and reduction in SFV levels, it was decided that USP45 does not meet the criteria for a positive hit in this model.

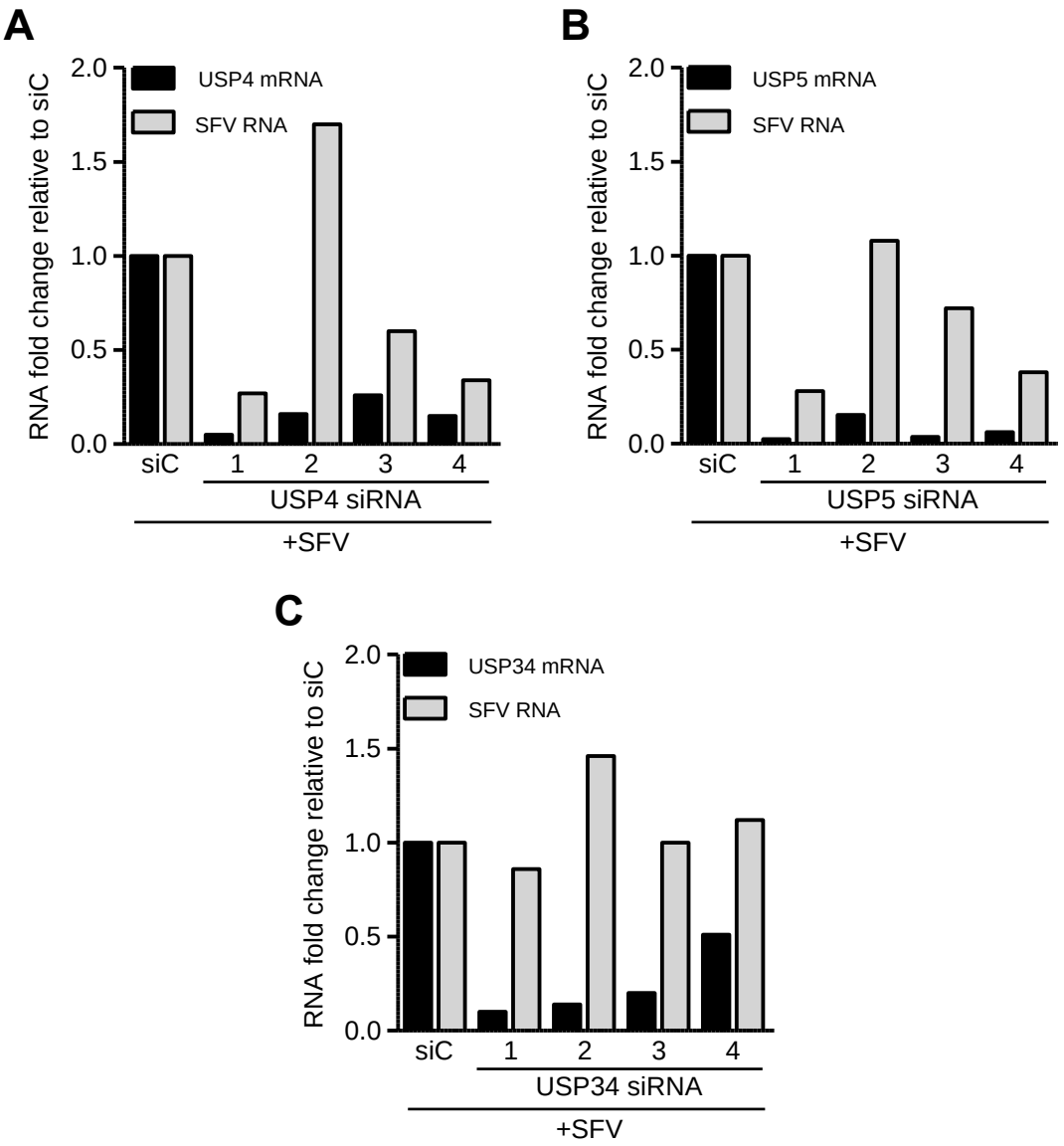

Figure 4.4 The effect of USP4, USP5 and USP34 siRNAs on SFV replication. HeLa cells were reverse-transfected with individual USP4, USP5 and USP34 siRNAs 1-4, corresponding to the original pool used in the preliminary screen or siC. Cells were then incubated for 72 hr before being infected with SFV (MOI = 2) and analysed as in figure 4.2 for levels for DUB transcript and SFV RNA for (A) USP4 (B) USP5 (C) USP34. Data is from one independent experiment.

Analysis of the effect of depletion with USP46 siRNAs is shown in Figure 4.5B. QPCR data shows that depletion of USP46 by siRNA 1-4 led to a reduction in transcript levels relative to siC of 70%, 90%, 85% and 25% respectively. Analysis of SFV RNA revealed that similar to USP45, there was an increase in SFV RNA after knockdown with the USP46 siRNAs, of 20%, 170%, 350% and 240% for siRNAs 1-4 respectively (Figure 4.5B). Again, this

did not agree with the assumptions being made with regard the implication of increase cell viability and the predicted effect of a decrease in SFV replication. Thus, as there was no correlation between reduction in USP46 mRNA and reduction in SFV levels, it was decided that USP46 does not meet the criteria for a positive hit in this model.

Data for USP53 is shown in Figure 4.5C. Treatment of HeLa cells with USP53 siRNA 1 to 4 resulted in a reduction in USP53 mRNA levels of 60%, 80%, 60% and 90% respectively relative to siC. Analysis of SFV RNA levels showed mixed results. Treatment HeLa cells with siRNA 1 lead to a reduction in SFV RNA of 90%, while siRNA 3 lead to a smaller reduction, of 15%. In contrast, depletion of USP53 with siRNAs 2 and 4 lead to an increase on SFV RNA of 200% and 115% respectively. Thus, although USP53 transcript levels were reduced with all four siRNAs, only one lead to a reduction in SFV RNA levels greater than 50% (siRNA 1). Therefore it was decided that USP53 does not meet the criteria for a positive hit in this model.

4.5 Analysis of the effect of depletion of UCH DUB UCHL1 on SFV RNA levels

Only one UCH family DUB, UCHL1, was identified during the siRNA library screen as potentially having a pro-viral function. To investigate whether depletion of UCHL1 in HeLa cells does affect on SFV replication, a knockdown experiment was carried out for UCHL1 using the individual siRNAs 1 to 4 as described in section 4.3. As for the USP DUBs, the cDNAs generated were tested by E-P PCR, showing no amplification in the RT- controls to confirm (Appendix C). QPCR analysis of the cDNA samples showed that there was a reduction in UCHL1 mRNA of 98%, 11%, 98% and 92% for siRNAs 1-4 respectively (Figure 4.6A). Analysis of SFV RNA levels after depletion of UCHL1 revealed an increase on SFV RNA levels of 100%,180%, 100% and 30% for siRNAs 1-4 respectively (Figure 4.6A). Thus, although UCHL1 transcript levels were significantly reduced with all three out of the four siRNAs, SFV RNA levels were increased for all siRNAs. Therefore, it was decided that

UCHL1 does not meet the citeria for a positive hit in this model, based on the assumption that there will be a decrease in SFV RNA/replication.

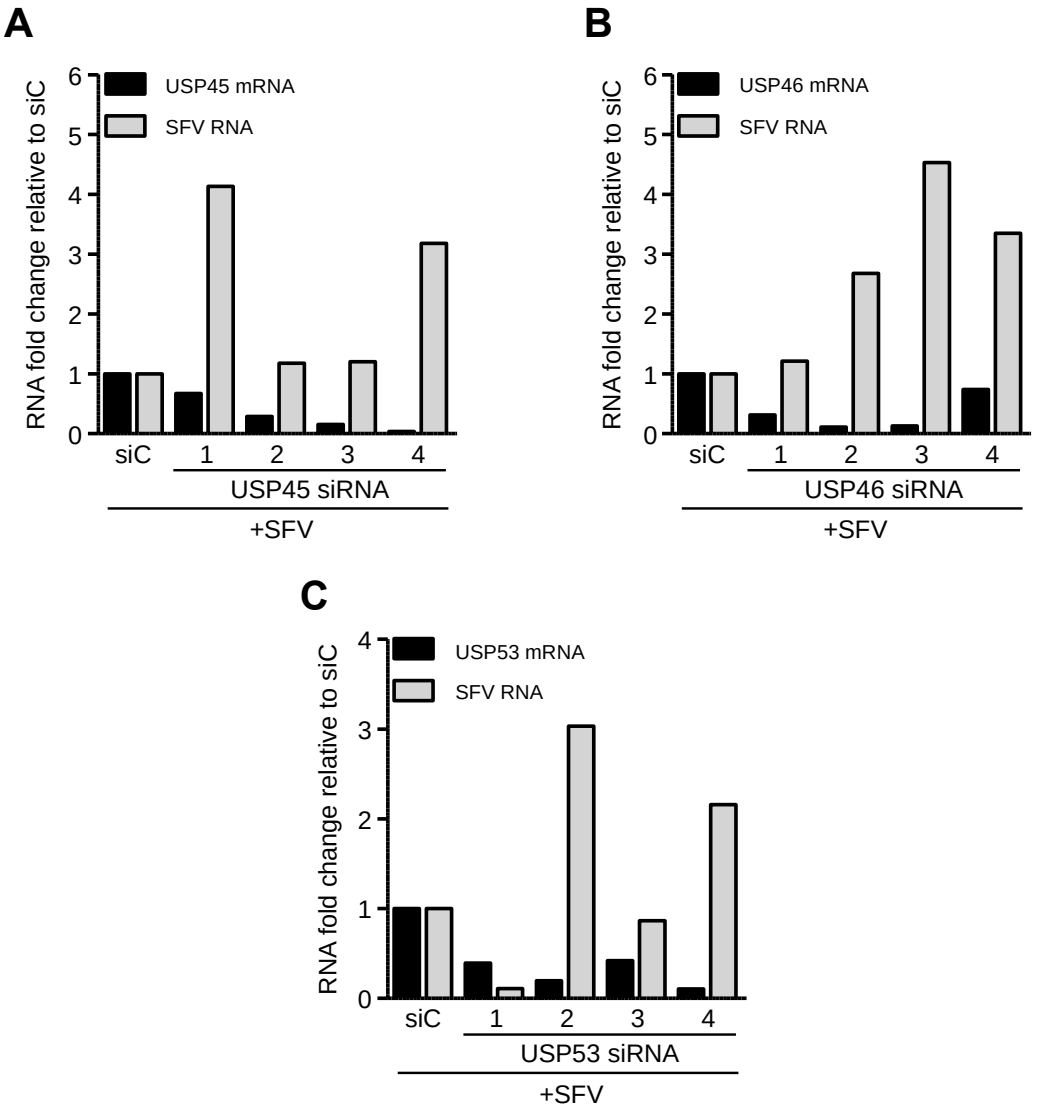

Figure 4.5 The effect of USP45, USP46 and USP53 siRNAs on SFV replication. HeLa cells were reverse-transfected with individual USP45, USP46, USP53 siRNAs 1-4, corresponding to the original pool used in the preliminary screen or siC. Cells were then incubated for 72 hr before being infected with SFV (MOI = 2) and analysed as in figure 4.2 for levels for DUB transcript and SFV RNA for (A) USP45 (B) USP46 (C) USP53 Data is from one independent experiment.

4.6 Analysis of the effect of depletion of the Josephin Family DUB JOSD2 on SFV RNA levels

JOSD2 was the sole member of the Josephin family identified during the siRNA library screen as potentially having a pro-viral function. To investigate whether depletion of JOSD2 in HeLa cells does affect on SFV replication, a knockdown experiment was carried out for JOSD2 using the individual siRNAs 1 to 4 as described in section 4.3. As for the previous DUBs analysed in this way, the cDNAs generated were tested by E-P PCR, showing no amplification in the RT- controls (Appendix C). QPCR analysis showed that the individual JOSD2 siRNAs lead to reductions in JOSD2 transcript of 30%, 50%, 13% and 50% for siRNAs 1-4 respectively (Figure 4.6B). Depletion of JOSD2 with the individual siRNAs lead to a reduction of 80% and 78% in SFV RNA levels for siRNA 2 and 4. Whereas, depletion of JOSD2 by siRNAs 1 and 3 led to an increase on SFV RNA levels of 55% and 520% respectively (Figure 4.6B). Thus, for JOSD2 two siRNAs (siRNAs 2 and 4) lead to decreases of greater than 50% in SFV RNA leads, and caused similar decreases in the JOSD2 transcript, implying that JOSD2 meets the criteria for a positive hit using this secondary assay. The differences in antiviral or pro-viral activities of the various JOSD2 siRNAs used in this assay may reflect differential protein repress efficiency or alternatively different effects on JOSD2 splice variants, and will require further investigation.

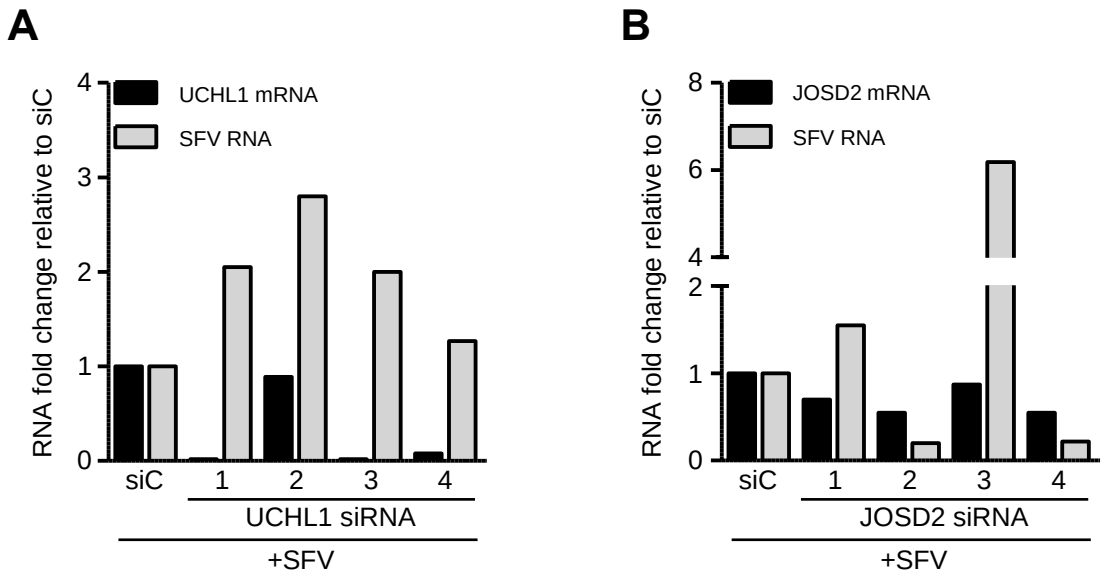

Figure 4.6 The effect of UCHL1 and JOSD2 siRNAs on SFV replication. HeLa cells were reverse-transfected with individual UCHL1 and JOSD2 siRNAs 1-4, corresponding to the original pool used in the preliminary screen or siC. Cells were then incubated for 72 hr before being infected with SFV (MOI = 2) and analysed as in figure 4.2 for levels for DUB transcript and SFV RNA for (A) UCHL1 (B) JOSD2. Data is from one independent experiment.

4.7 Analysis of the effect of depletion of the JAMM/MPN+ family DUBs BRCC3 and MYSM1 on SFV RNA levels

Two members of the JAMM/MPN+ family of DUBs were identified in the original screen. These were BRCC3 and MYSM1. The effect of depletion of these DUBs on SFV RNA levels was thus investigated using the individual siRNAs 1 to 4 as described in section 4.3. As for the previous DUBs analysed in this way, the cDNAs generated were tested by E-P PCR, showing no amplification in the RT- controls (Appendix C). QPCR analysis showed that the individual BRCC3 siRNAs lead to reductions in BRCC3 transcript, with 94%, 98%, 95% and 97% reduction compared to the siC for siRNAs 1-4 respectively (Figure 4.7A). Depletion of BRCC3 by all four siRNAs had little effect on SFV RNA levels, with either increase of 13%, 5% and 17% resulted from knockdown of BRCC3 by siRNA 1, 2 and 3 or decrease of 12% following to depletion of BRCC3 by siRNA 4 (Figure 4.7A). Thus, BRCC3 does not meet the criteria for a positive hit in this model.

Analysis of MYSM1 is shown in Figure 4.7B. QPCR data showed that all four siRNAs lead to reduction in MSYM1 transcript of 87%, 60%, 72% and 55% (for siRNAs 1-4 respectively). Analysis of SFV RNA levels showed that three of the siRNAs induced similar significant reductions in SFV RNA levels, with reductions of 81%, 78% and 85% compared to siC for siRNAs 1, 2 and 3 respectively. MYSM1 siRNA 4 lead to a reduction of 20% in SFV RNA levels. Thus, as three siRNA lead to reductions of greater than 50% in both MYSM1 transcript and SFV RNA, MYSM1 was consider a positive hit in this secondary assay.

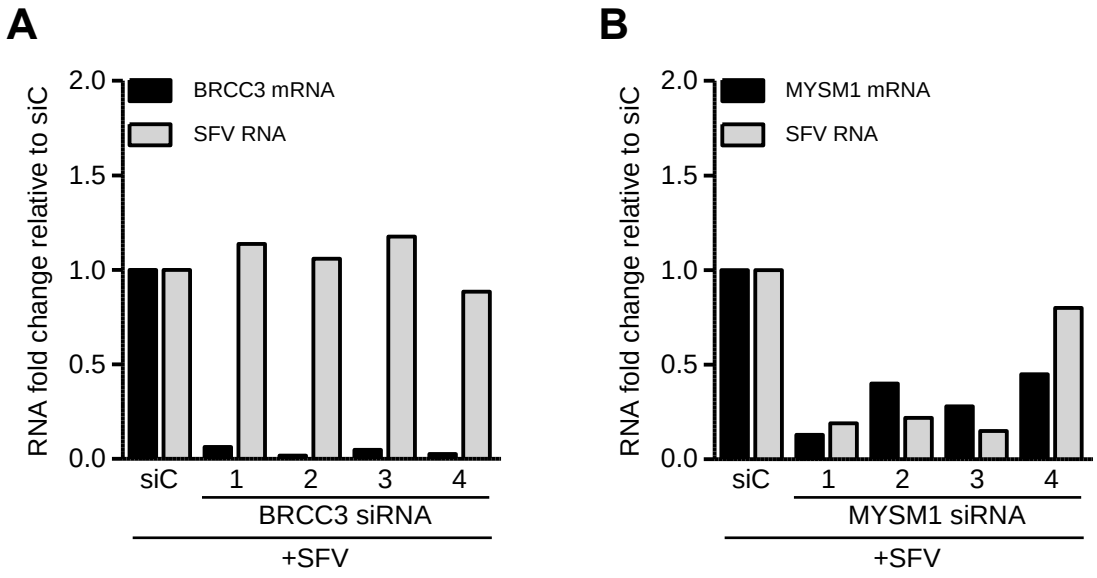

Figure 4.7 The effect of BRCC3 and MYSM1 siRNAs on SFV replication. HeLa cells were reverse-transfected with individual BRCC3 and MYSM1 siRNAs 1-4, corresponding to the original pool used in the preliminary screen or siC. Cells were then incubated for 72 hr before being infected with SFV (MOI = 2) and analysed as in figure 4.2 for levels for DUB transcript and SFV RNA for f (A) BRCC3 (B) MYSM1 Data is from one independent experiment.

4.8 Summary of the secondary deconvolution assay of DUB siRNA pools

Eleven DUBs were validated in this secondary deconvolution assay based on measuring the effect of DUB depletion on levels of SFV RNA. It was predicted that the reduction in cell viability observed in the original screen, and the deconvolution studies in chapter 3, would be reflected in a reduction in SFV RNA levels. The experimental approach used in this section also enabled the efficiency of DUB gene silencing to be measured. The data for the 11 DUBs

is summarised in Table 4.1, showing the percentage changes (either decrease or increase) in DUB mRNA and SFV RNA levels after deletion with each individual siRNA from the original pools. The criteria stated at the start of the chapter for a positive deconvolution was that depletion with 2 or more siRNA lead to an 50% or greater decrease in SFV RNA levels, and that for these siRNA the efficiency of DUB mRNA knockdown was ≥50%. Thus, the DUBs USP1, USP4, USP5, JOSD2 and MYSM1 all fulfilled these criteria. The remaining candidates (USP34, USP45, USP46, USP53, UCHL1 and BRCC3), while showing variable levels of depletion for the DUB mRNA, this did not lead to reduction in SFV levels in more than 1 of the siRNAs tested. In some cases, there was a significant increase in SFV levels (USP45, USP46, USP53, UCHL1). However, although this may be of interest, this did not fit in the original hypothesis and these DUBs were not followed up.

4.9 Overall summary of data from the primary and secondary validation assays

Twelve DUBs were identified in the original DUB siRNA screen against SFV infection. Two further assays were undertaken to deconvolute the siRNA pools and validate the hits. This data is presented in this and the previous chapter. To rigorously identify true hits from the screen, the data from both assays were combined. For a DUB to be a true positive hit, the criteria were defined as the original siRNA pool (for the cell viability assay only) and at least 2 or more individual siRNA lead to a 20% or greater increase in cell viability, and a 50% or greater decrease in both the DUB mRNA and SFV RNA. This is summarised in Table 4.2, where a (+) indicates that depletion of the DUB by the indicated siRNA results in a positive results in the indicated screen. Of the 12 DUBs identified in the siRNA screen, only two have deconvoluted successfully using the criteria outlined in this chapter. These were JOSD2 and MYSM1. For JOSD2 the pool and two individual siRNAs were positive in relevant screens. For MYSM1 the pool and three individual siRNAs were positive. USP4 was also potentially a positive hit as two siRNAs were positive in relevant screens. However, the siRNA pool did not confirm the original screen data. As MYSM1 was the best candidate, with three individual siRNAs

giving a positive result, it was decide that this DUB would be followed up to further investigate its role during alphavirus infection.

Table 4.1 Summary of changes in DUB and SFV RNA levels after deconvolution of selected DUBs siRNAs pool

DUB	mRNA/vRNA	% Change in RNA levels*			
		siRNA 1	siRNA 2	siRNA 3	siRNA 4
USP1	DUB	85	75	90	80
	SFV	85	65	10	165
USP4	DUB	95	84	74	85
	SFV	74	70	40	67
USP5	DUB	97	85	96	94
	SFV	70	10	30	60
USP34	DUB	90	85	80	50
	SFV	15	50	0	14
USP45	DUB	33	70	85	96
	SFV	310	20	20	220
USP46	DUB	70	90	85	25
	SFV	20	170	350	240
USP53	DUB	60	80	60	90
	SFV	90	200	15	115
UCHL1	DUB	98	11	98	92
	SFV	100	180	100	30
JOSD2	DUB	30	50	13	50
	SFV	55	80	520	78
BRCC3	DUB	94	98	95	97
	SFV	13	5	17	12
MYSM1	DUB	87	60	72	55
	SFV	81	78	85	20

**Changes are expressed relative to the siC. Values in RED represent decreases in RNA levels; values in GREEN represent increases in RNA levels.*

Yellow shading indicates where the individual siRNA lead to a reduction of ≥ 50% for both the DUB mRNA AND SFV RNA.

Table 4.2 Summary of Data from Individual Assays Used to Deconvolute the DUB siRNA Pools*

DUB	siRNA													
	Pool		1			2			3			4		
	CV		CV	KD	SFV	CV	KD	SFV	CV	KD	SFV	CV	KD	SFV
USP1	+		+	+	+	-	+	+	-	+	-	-	+	-
USP4	-		+	+	+	-	+	-	-	+	-	+	+	+
USP5	+		+	+	+	-	+	-	-	+	-	-	+	+
USP34	-		-	+	-	-	+	-	+	+	-	+	+	-
USP45	-		-	-	-	-	+	-	+	+	-	-	+	-
USP46	-		-	+	-	-	+	-	+	+	-	+	-	-
USP53	+		+	+	+	-	+	-	+	+	-	+	+	-
OTUD6A	+		-	nt	nt	-	nt	nt	-	nt	nt	+	nt	nt
UCHL1	+		-	+	-	-	-	-	+	+	-	-	+	-
JOSD2	+		-	-	-	+	+	+	-	-	-	+	+	+
BRCC3	-		-	+	-	+	+	-	+	+	-	-	+	-
MYSM1	+		+	+	+	+	+	+	+	+	+	+	+	-

**(+/-) indicates where DUB siRNA was positive or negative in the individual assays. Assays were CV -cell viability screen; KD – efficiency of DUB mRNA depletion; SFV - SFV RNA levels.*

nt – not tested

Blue shading indicates where the DUB was positive for the pool assay and individual siRNA was positive for the CV, KD and SFV readouts.

Chapter 5

Characterisation of the Effect of Depletion of MYSM1 on Semliki Forest Virus and Chikungunya Virus Infection in Different Cell Backgrounds

5.1 Introduction

The analysis of the siRNA pools for the DUBs identified in the siRNA screen against SFV, described in Chapters 3 and 4, revealed that the MYSM1 pool deconvoluted successfully in two different assays. These assays measured the effect of MYSM1 depletion on SFV infection by monitoring changes in cell viability and SFV RNA levels. All four MYSM1 siRNAs successfully recapitulated the data from the screen in the cell viability assay, whereas three siRNAs (1, 2 and 3) lead to a reduction SFV RNA in the secondary assay. In this chapter the role of MYSM1 during alphavirus replication was further investigated. Two different approaches were taken. Firstly, the effect of depletion of MYSM1 by siRNA treatment was further investigated in HeLa cells. Secondly, the analysis was extended to investigate the role of MYSM1 in fibroblasts utilising MYSM1 genetic knockout murine embryo fibroblasts. These studies were carried out using both SFV and CHIKV.

5.2 Confirmation of MYSM1 siRNA deconvolution assays

The siRNA deconvolution assays described in Chapters 3 and 4 identifying MYSM1 as a true positive from the original DUB siRNA screen were only carried out one (RNA assay) or two (cell viability) independent times. Thus, before following up this result to characterise the role of MYSM1 during alphavirus infection, it was necessary to ensure that the data supporting a role for MYSM1 during SFV infection were reproducible and statistically significant. Therefore, each assay was carried out on three independent occasions.

5.2.1 Biological replicates of MYSM1 deconvolution by cell viability readout

Deconvolution experiments in HeLa cells as described in section 3.3 were carried out for the MYSM1 siRNA pool on three independent occasions. The mean percentage change in cell viability of MYSM1 depleted cells after SFV infection relative to the siC control is shown in Figure 5.1A. Depletion of MYSM1 by the siRNA pool led to an increase in cell viability of 59% after SFV infection. As seen in the first deconvolution experiments, depletion using the four individual siRNAs also lead to an increase in cell viability, of 40%, 51%, 47% and 33% for siRNAs 1, 2, 3 and 4 respectively. The controls used during these experiments gave the expected results, with depletion of OTUD7A pool resulting in a decrease in cell viability of 60% (Figure 5.1A) and the HsDeath siRNA causing greater than 90% cell death after 72 hr (which was visible by light microscopy). Analysis of the data compared to the siC, using Tukey-one-way ANOVA, showed that the data for each MYSM1 siRNA (including the pool) was statistically significant, ranging from $p<0.05$ to $p<0.001$ (Figure 5.1A). Thus, this data agrees with the original deconvolution experiment, and strongly supports a role for MYSM1 during SFV infection.

5.2.2 Biological replicates of MYSM1 deconvolution by monitoring SFV RNA levels

Deconvolution experiments utilising the secondary read out of changes to SFV RNA levels as described in section 4.3 were also carried out on three independent occasions. HeLa cells were reverse-transfected with MYSM1 siRNAs and after 72 hr infected with SFV. RNA extracted at 8 hr post infection was analysed by QPCR for levels of SFV RNA and MYSM1 mRNA (Figure 5.1B). All four MYSM1 siRNAs lead to a significant depletion of MYSM1 transcript of 89%, 68%, 75% and 65% for siRNAs 1-4 respectively ($p<0.005$). For SFV RNA levels, similar to the experiment described in Chapter 4, depletion of MYSM1 with siRNAs 1, 2 and 3 lead to significant reductions in SFV RNA, of 63%, 75%, 60% respectively (Figure 5.1B). Again, MYSM1 siRNA 4 had no effect on SFV RNA levels. Analysis of the data compared to

the siC, using Tukey-one-way ANOVA, showed that this data was statistically significant, siRNA 1 $p<0.05$, siRNA 2 $p<0.005$, siRNA 3 $p<0.05$ (Figure 5.1B).

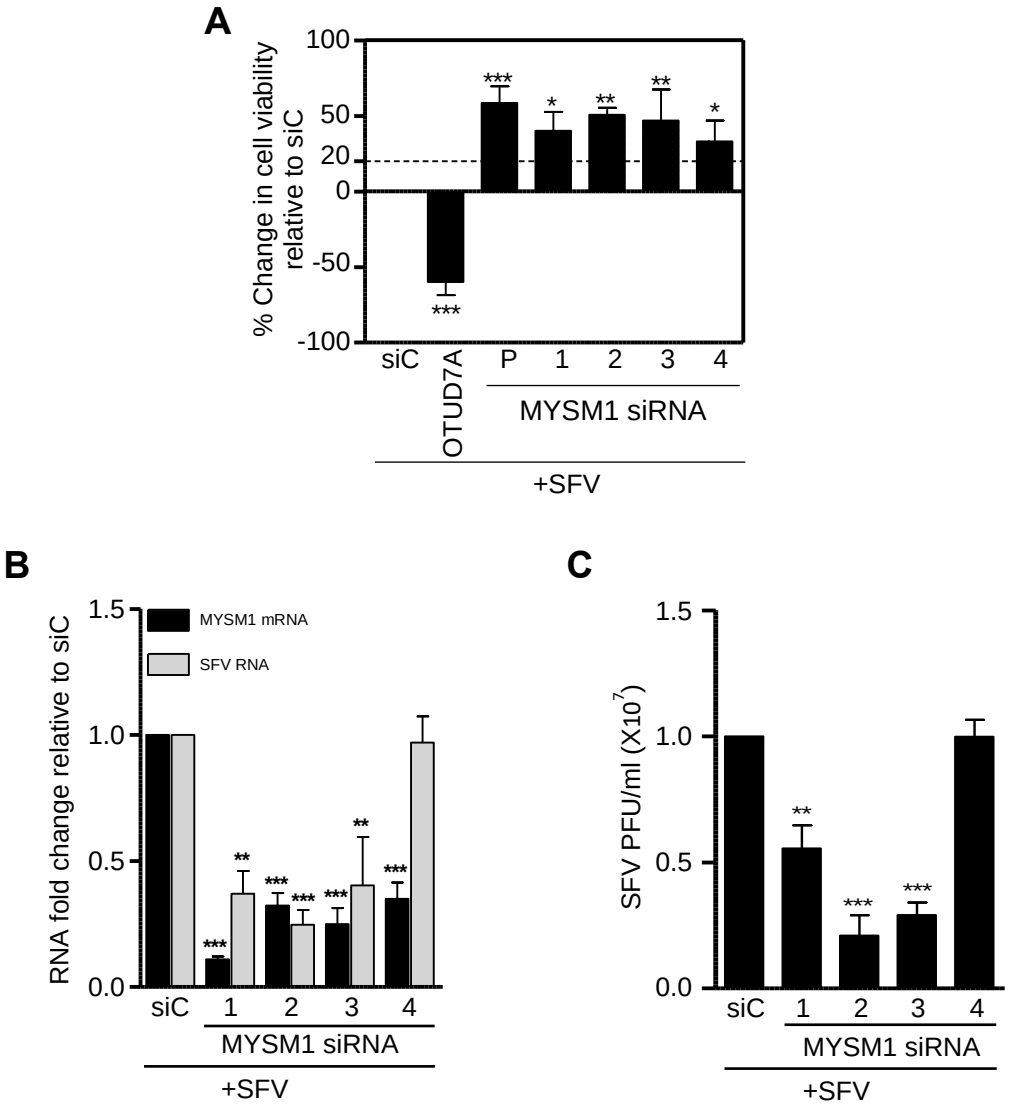

Figure 5.1 Replicate deconvolution assays for the MYSM1 siRNA pool based on readouts of cell viability and SFV RNA levels. (A) HeLa cells were transfected in duplicate with MYSM1 siRNAs pool and individual siRNAs 1-4. At 72 hr post transfection, plates were either infected with SFV (MOI=2) or mock infected, and cell viability assessed at 16 hr post infection. An siRNA pool targeting OTUD7A was included as an additional control. The percentage change in cell viability of infected vs. uninfected cells, relative to the siC treated control is shown. (B) HeLa cells were transfected with MYSM1 siRNAs 1-4 or siC, incubated for 72 hr before infecting with SFV at MOI 2. Total RNA was extracted at 8 hr post-infection and analysed by qPCR for levels of SFV genomic RNA and MYSM1 mRNA. (C) SFV present in the supernatants from these experiments were titrated on monolayers of BHK cells. The data shown represents the mean of 3 independent experiments (+/- SEM) [*$p<0.05$, **$p<0.005$, ***$p<0.001$].

It was also possible to determine the levels of SFV virus released from cells in these experiments. Supernatants were saved at 8 hr post-infection and titrated on BHK cells. The mean pfu/ml in the supernatant for cells treated with MYSM1 siRNA 1-4 was 0.55 x 10^7 pfu /ml, 0.2 x 10^7 pfu /ml, 0.3 x 10^7 pfu /ml and 1 x 10^7 pfu /ml respectively. This was in comparison to 1 x 10^7 pfu /ml for supernatant from siC treated cells (Figure 5.1C). This showed that for MYSM1 siRNAs 1, 2 and 3 there was a small but consistent reduction in SFV titres, but no difference for siRNA 4. This was in general agreement with the intracellular SFV RNA levels (Figure 5.1B). Thus, when the data from the cell viability screen (section 5.2.1) and SFV RNA levels (section 5.2.2) is combined, showing that three out of the four individual MYMS1 siRNAs resulted in complementary phenotypes, this strongly supports a pro-viral role for MYSM1 during SFV infection of HeLa cells. The individual MYSM1 siRNA 1, 2 and 3 were positive in both assays, whereas although siRNA 4 gave a positive result in the cell viability assay, this was not seen with the SFV RNA read out. This data for siRNA 4 is likely to be due to an off-target effect or may differentially affect alternative MYSM1 splice variants compared to siRNA 1, 2 and 3 (Figure 5.2).

The next step was to confirm depletion of MYSM1 protein using these siRNAs and to further characterise the role of MYSM1 during SFV infection. This would then be extended to investigate if the same phenotype was observed with CHIKV infection after depletion of MYSM1.

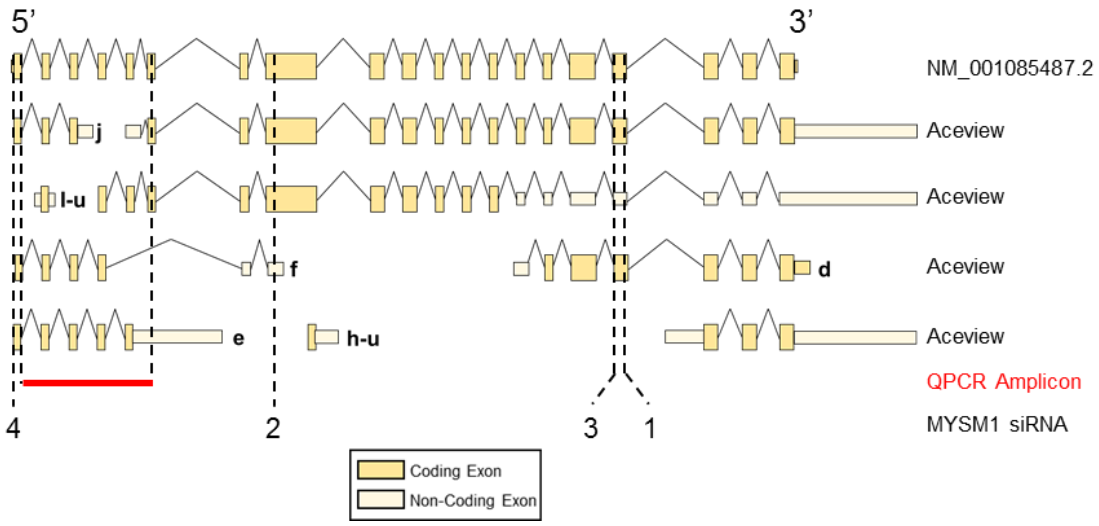

Figure 5.2 MYSM1 transcript and location of siRNA. Schematic representation of MYSM1 splice variants (named in hand right column). The location of MYSM1 Qiagen siRNAs 1-4 and PCR amplicon is also shown. The position of the QPCR amplicon is highlighted in red.

5.3 MYSM1 siRNAs 1, 2 and 3 lead to a reduction in MYSM1 protein levels

It was important to confirm that the individual MYSM1 siRNA 1, 2 and 3, in addition to causing a reduction in transcript also lead to a reduction in MYSM1 proteins levels. Western blot analysis of protein extracts from HeLa cells 72 hr after addition of each individual MYSM1 siRNAs is shown in Figure 5.3A and B. Individual siRNA 1 and 3 lead to an efficient reduction in MYSM1 protein, of 85% and 95% compared to siC treated cells respectively. Whereas, MYSM1 siRNA 2 lead to a 40% reduction in protein levels compared to siC. Thus, MYSM1 siRNAs 1 and 3 were chosen to use for the follow up studies investigation the role of MYSM1 during alphavirus infection.

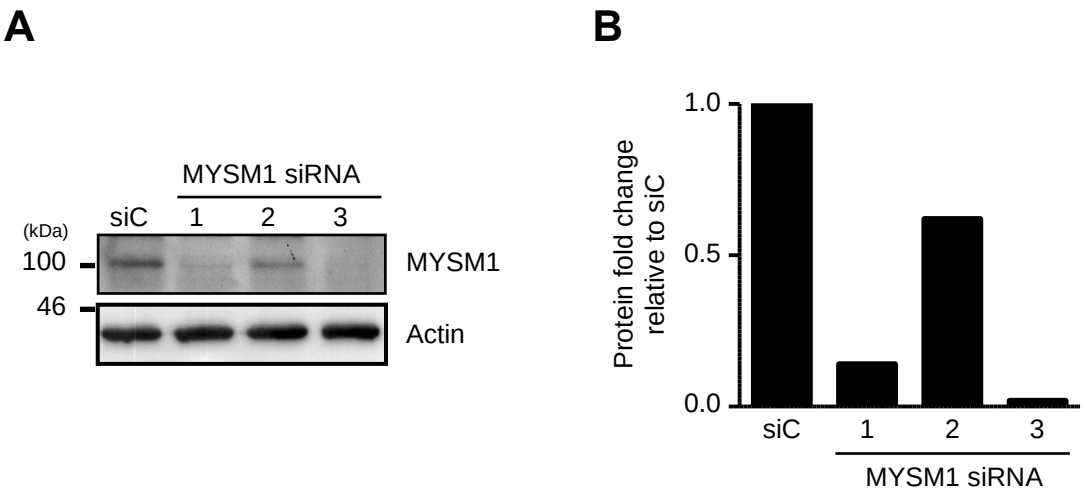

Figure 5.3 Efficiency of siRNA depletion of MYSM1 protein. (A) HeLa cells were transfected with the Qiagen MYSM1 siRNAs 1, 2 and 3 or siC. Following 72 hr incubation, the cells were lysed in Laemmli buffer. 30 µg were then resolved by SDS-PAGE and immunoblotted for MYSM1 and actin. Proteins were visualised using ECL detection. (B) Quantification of MYSM1 protein levels was performed by densitometry using ImageJ software. The efficiency of MYSM1 depletion was determined by quantitating relative to actin and then compared to siC. Data from one independent experiment.

5.4 The effect of MYSM1 depletion on SFV plaque formation

The effect of MYSM1 depletion on SFV infection was further investigated by monitoring the effect on SFV plaque formation. These experiments were carried out as follows. HeLa cells were reverse-transfected with MYSM1 siRNAs 1 and 3, or the control siC, in a 10 cm^2 tissue culture dish. After a 48 hr incubation, cells were harvested and treated in two ways. Cells were (i) re-seeded into 6 well plates at appropriate cell number to ensure 90-100% confluent monolayers in a further 24 hr, and then infected with SFV at appropriate dilution to allow for monitoring (and counting) plaque formation and (ii) the remaining cells were seeded in 6 well plate for harvesting 24 hr later to analyse levels of MYSM1 protein (Figure 5.4).

The number and morphology of SFV plaques in MYSM1 depleted cells was compared to siC treated cells (Figure 5.5A and B). Depletion of MYSM1 by siRNAs 1 and 3 lead to a reduction in SFV plaque numbers of 50% and

60% compared to siC respectively (mean of three independent experiments). In each experiment, the appearance of plaques revealed that MYSM1 depletion lead to plaques of slightly smaller size for siRNA 1 than those seen for siC. Plaques for siRNA1 were not noticeably different to the control. In each experiment cells treated with MYSM1 siRNAs were also analysed by immunoblotting, which showed efficient depletion of MYSM1 protein. A representative immunoblot for the plaque assay experiment shown in part A, is shown in part C (Figure 5.5). The reduction in MYSM1 protein levels for the three independent assays was quantified and is shown in part D. A reduction of around 60-70% was seen for both siRNAs 1 and 3.

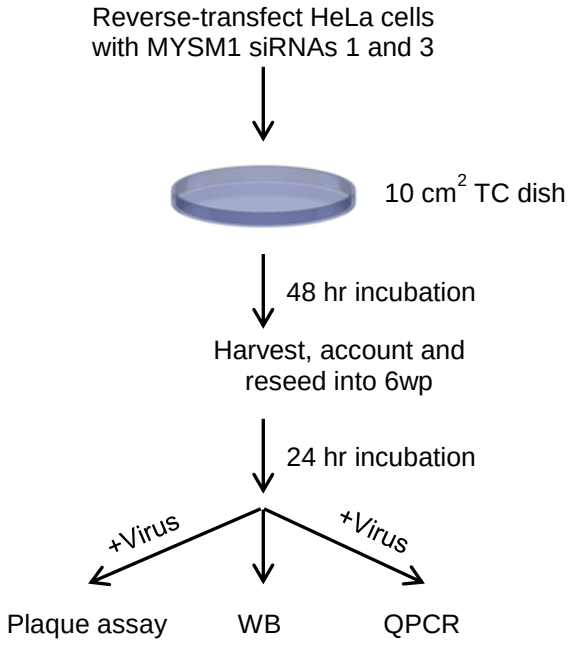

Figure 5.4 Flowchart showing the approach used for knockdown of MYSM1 in TC format. In 10 cm^2 TC dishes, HeLa cells were transfected individually with MYSM1 siRNAs 1 and 3, or siC. At 48 hr transfected cells were harvested, counted and reseeded at known cell density into duplicate 6 well plates. After a further 24 hr, one plate was infected with SFV either to monitor SFV genomic RNA levels or to visualise plaques formation. Cells in the second plate were used to determine the efficiency of MYSM1 knockdown by immunoblotting and quantification via Image J analysis.

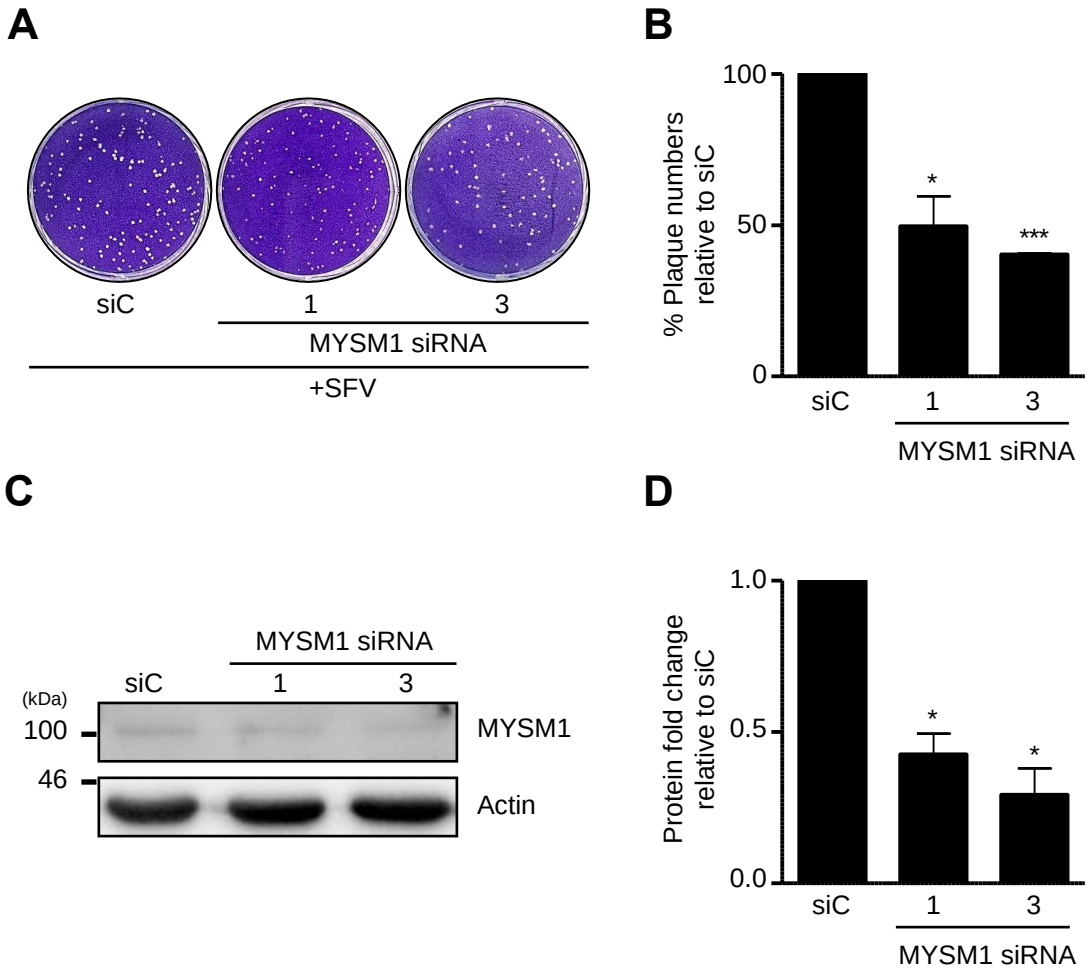

Figure 5.5 The effect of MYSM1 depletion on SFV plaque formation. HeLa cells were transfected with either MYSM1 siRNAs 1 or 3, or siC. At 48 hr cells were reseeded into duplicate 6 well plate. After a further 24 hr, one plate was infected with SFV and incubated for a further 72 hr to allow SFV plaques to form. The second plate was used to determine the efficiency of MYSM1 depletion at 72 hr post transfection. (A) Representative images of SFV plaques in the siC well and MYSM siRNA 1 and 3 wells. (B) Quantification of plaque numbers relative to siC shown as the mean of 3 independent experiments (+/- SEM). (C) Representative immunoblot analysis of MYSM1 and Actin in lysates from siRNA treated cells. (D) Quantification of MYSM1 protein level relative to siC via Image J analysis. The data shown represents the mean of 3 independent experiments (+/- SEM) [*p<0.05, ***p<0.001].

5.5 Investigation of the role of MYSM1 during CHIKV replication

SFV was used as a model alphavirus. The next step was to investigate if MYSM1 also played an important role during infection with the more pathogen CHIKV. Similar experiments to those described previously in this chapter were now carried out using CHIKV infection. The work focused on using the MYSM1 siRNA 1 and 3, shown to be effective at depletion of MYSM1 and resulting in the same phenotype for the role of MYSM1 during SFV infection.

5.5.1 MYSM1 depletion leads to a decrease in CHIKV RNA levels

To assess the effect of depletion of MYSM1 on CHIKV replication, and monitor the efficiency of MYSM1 protein knockdown in the same experiment, a similar approach to that described in Figure 5.4 was used. HeLa cells were reverse-transfected with MYSM1 siRNAs 1 and 3, or siC, in a 10 cm^2 tissue culture format. After 48 hr, cells were harvested and re-seeded into duplicate 6 well plates, and incubated for a further 24 hr. The cells in one plate where then infected with CHIKV at an MOI of 2. After 8 hr cells were harvested and RNA extracted, before being converted to cDNA and analysed for CHIKV RNA levels and MYSM1 mRNA transcript by QPCR. The mean of three independent experiments are shown in Figure 5.6A. Similar to SFV, there was a reduction in CHIKV RNA levels after depletion of MYSM1 with siRNAs 1 and 3, of 70% and 75% respectively compared to the siC treated cells. Analysis of the MYSM1 transcript showed a reduction of 65% and 55% for siRNA 1 and 3 respectively. The efficiency of knockdown of MYSM1 proteins was analysed using the second 6 well plate, protein extract was harvested at 72 hr post-transfection and immunoblotted for MYSM1 levels. A representative blot is shown in Figure 5.6B, and the quantitation of the three independent experiments is shown in Figure 5.6C. In each experiment there was efficient depletion of MYSM1 protein by both siRNA 1 and 3, with a mean of 65 % and 75% respectively compared to the siC (Figure 5.6).

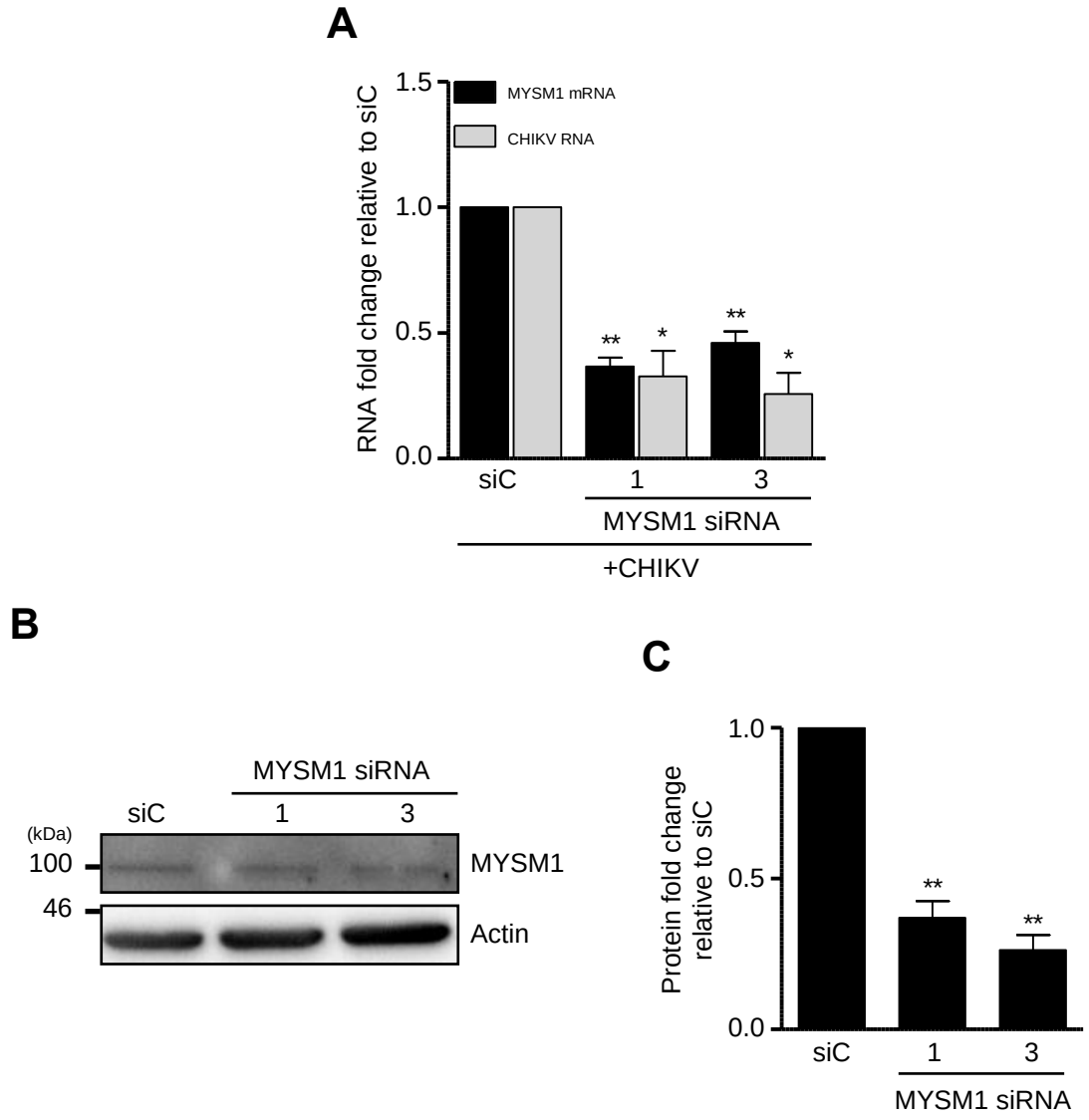

Figure 5.6 MYSM1 depletion leads to a decrease in CHIKV genomic RNA levels after infection. HeLa cells were transfected with either MYSM1 siRNAs 1 or 3, or siC. At 48 hr cells were reseeded into duplicate 6 well plate. After a further 24 hr, one plate was infected with CHIKV at 2 MOI. The second plate was used to determine the efficiency of MYSM1 depletion at 72 hr post transfection. (A) QPCR analysis of CHIKV RNA levels and MYSM1 mRNA, normalised to actin and presented relative to siC. (B) Representative immunoblot analysis of MYSM1 and Actin in lysates from siRNA treated cells. (C) Quantification of MYSM1 protein level relative to siC via Image J analysis. All data shown represents the mean of 3 independent experiments (+/- SEM) [*p<0.05, **p<0.005].

5.5.2 MYSM1 depletion leads to a reduction in CHIKV plaque numbers and size

The effect of MYSM1 depletion on CHIKV infection was further investigated by monitoring the effect on plaque formation, as carried out above for SFV. HeLa cells were reverse-transfected with MYSM1 siRNAs 1 and 3, or the control siC, in a 10 cm^2 tissue culture dish. After a 48 hr incubation, cells were harvested and treated in two ways. Cells were (i) re-seeded into 6 well plates at appropriate cell number to ensure 90-100% confluent monolayers in a further 24 hr, which were infected with CHIKV at appropriate dilution to allow for monitoring of plaque formation and (ii) the remaining cells were seeded in 6 well plate for harvesting 24 hr later to analyse levels of MYSM1 protein. Three independent experiments were carried out, and representative data is shown in Figure 5.7. The number and morphology of CHIKV plaques in MYSM1 depleted cells was compared to siC treated cells (Figure 5.7 A and B). Depletion of MYSM1 by siRNAs 1 and 3 lead to a reduction in CHIKV plaque numbers of 56% and 54% compared to siC respectively (mean of three independent experiments). In each experiment, the appearance of plaques revealed that MYSM1 depletion lead to plaques of slightly small size than those seen for siC. In each experiment cells treated with MYSM1 siRNAs were also analysed by immunoblotting, which showed efficient depletion of MYSM1 protein. A representative immunoblot for the plaque assay experiment shown in Figure 5.7 A, is shown in Figure 5.7 C. The reduction in MYSM1 was quantified using a mock infected sample due to the presence of blotting artefact in the siC lane. This showed a reduction in MYSM1 of around 40-50% for both siRNAs 1 and 3, compared to mock (Figure C and D). Visual inspection of the immunoblot suggest that there was also a decrease relative to the siC but this could not be quantified.

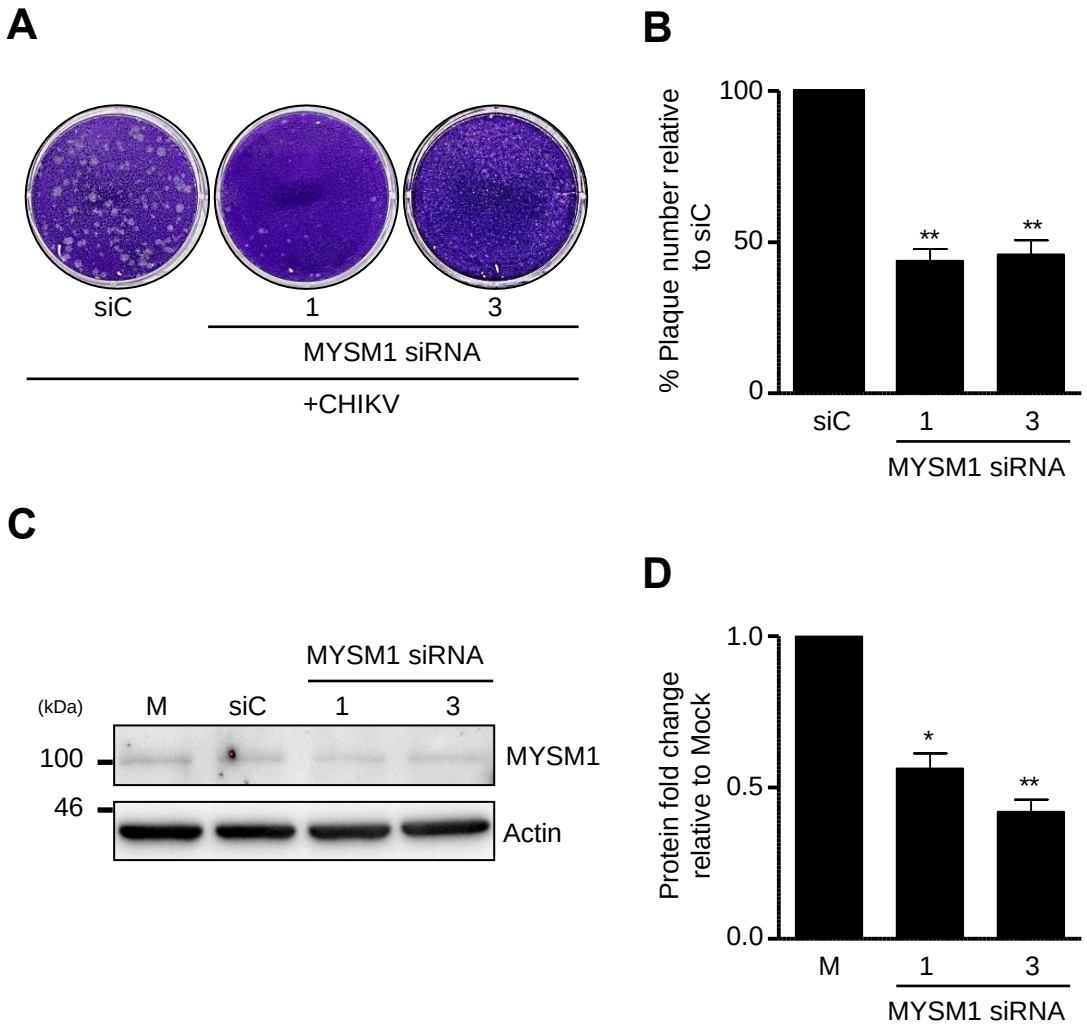

Figure 5.7 The effect of MYSM1 depletion on CHIKV plaque formation. HeLa cells were transfected with either MYSM1 siRNAs 1 or 3, or siC. At 48 hr cells were reseeded into duplicate 6 well plate. After a further 24 hr, one plate was infected with CHIKV and incubated for a further 72 hours to allow CHIKV plaques to form. The second plate was used to determine the efficiency of MYSM1 depletion at 72 hr post transfection. (A) Representative images of CHIKV plaques in the siC well and MYSM siRNA 1 and 3 wells. (B) Quantification of plaque numbers relative to siC. (C) Representative immunoblot analysis of MYSM1 and Actin in lysates from siRNA treated cells. (D) Quantification of MYSM1 protein level relative to Mock via Image J analysis. The data shown represents one of two independent experiments.

5.6 Utilising *Mysm1*$^{-/-}$ Murine embryo fibroblasts to investigate the role of MYSM1 during alphavirus infection

The previous sections employed siRNA depletion of MYSM1 in HeLa cells to characterise the role of MYSM1 during alphavirus infection, using both SFV and CHIKV. An alternative approach to studying the role of individual proteins is to utilise cells containing a genetic knockout of the gene of interest. To use this methodology to study the role of MYMS1 during alphavirus infection, *Mysm1*$^{-/-}$ murine embryo fibroblasts (MEFs) were obtained from Professor A. Nijnik (McGill University, Toronto, Canada) (Nijnik *et al*., 2012)**.** These contain a targeted insert disrupting the splicing of two early exons, and fail to produce Mysm1 transcript or protein (A. Nijnk, Personal communication). Both KO MEFs, and comparable WT cells, were derived according to the same protocol, from littermate-embryos and then SV40-immortalized. MEF KO cells had normal morphology and their growth rate was slightly faster from WT cells.

5.6.1 Validation confirmation of lack of expression of MYSM1 protein in *Mysm1*$^{-/-}$ MEFs

Before using the KO MEFs cells in experiments with SFV and CHIKV infection, the lack of expression of MYSM1 was confirmed at both the RNA and protein level. RNA was extracted from actively growing WT and KO cells, converted to cDNA using oligo d(T) and analysed by both end-point and QPCR. MYSM1 PCR primers were designed to span the junction of exons 1 and 3 of the MYSM1 transcript (Figure 5.8A). End-point PCR show a lack of detectable product in the KO cell line, while displaying a product in the WT cell line. The control m18S primers revealed bands in both of the WT and KO cells (Figure 5.8B). This was confirmed by QPCR, which showed a reduction in MYSM1 transcript of over 99% (Figure 5.8C). The lack of MYSM1 protein was confirmed by immunoblotting, which should good levels of MYSM1 in WT cells but undetectable in the KO MEF cells (Figure 5.8D).

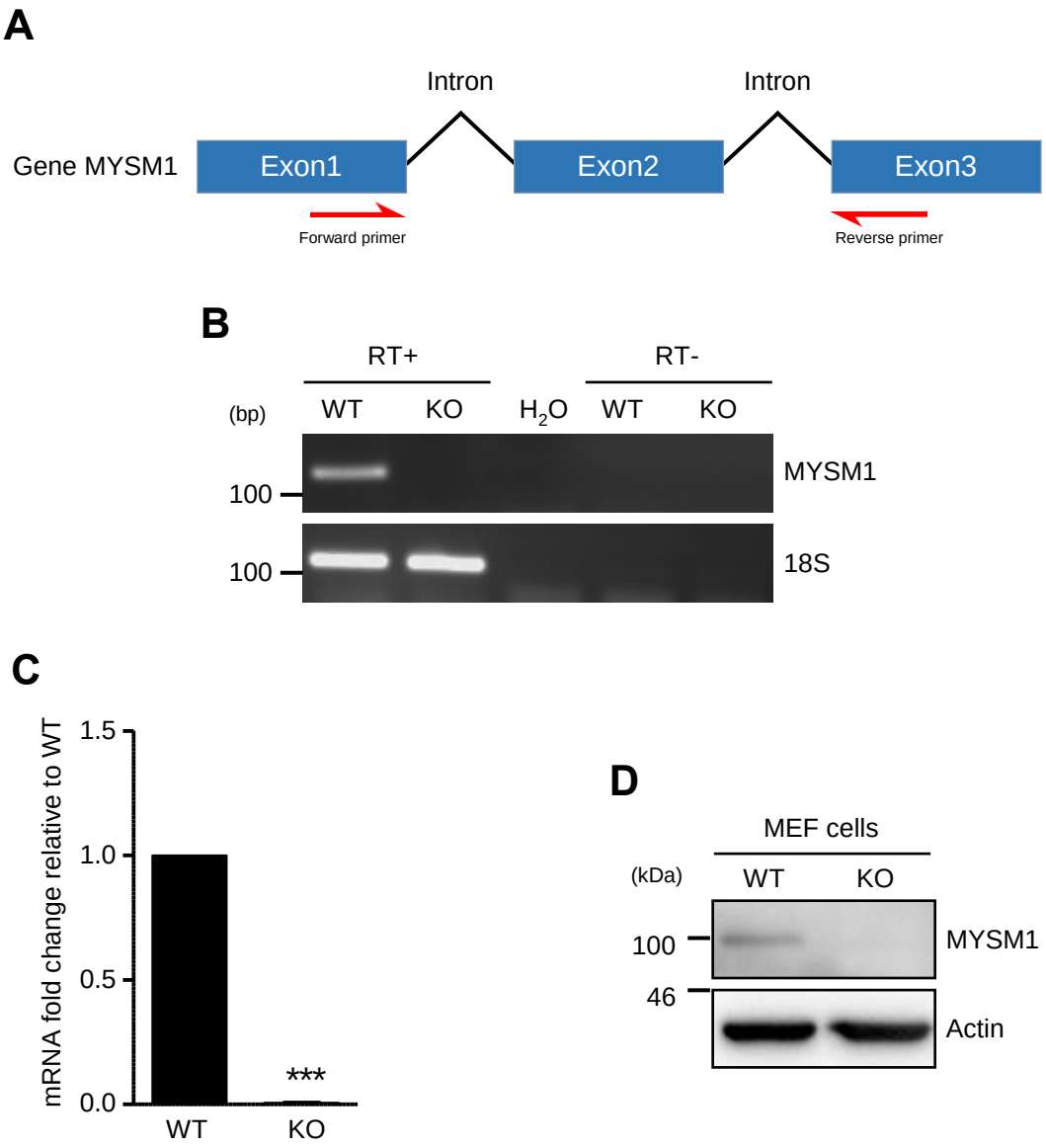

Figure 5.8 Confirmation of MYSM1 knockout in MEF cells. Total RNA was extracted from MEF WT and KO cells and converted to cDNA using oligo d(T), before being amplifed by PCR. (A) MYSM1 PCR primers (primers spanning the junction of exons 1 and 3 of the *Mysm1* transcript). (B) End -point PCR of RT+ and RT- for MYSM1 and ACTB. Water and (RT-) controls were used throughout to ensure validity. (C) QPCR analysis of levels of MYSM1 for RT+ samples, the $2^{-\Delta\Delta}$Ct method was used to analyse the data. 18s was employed as the reference gene and results were further normalized to the WT. Data for the WT well was normalised to 1, and fold reduction in *Mysm1*-transcript levels relative to WT is shown. Data shown represents the mean of 3 independent experiments (+/- SEM) [***p<0.001]. (D) Immunoblot analysis of MYSM1 protein levels in WT and KO MEFs.

5.6.2 Infection of KO MEFs with SFV leads to increased CPE compared to WT

The first experiment carried out with these cells was simply to infect both the WT and KO cells with SFV at 2 MOI, and monitor the infection visually. Development of CPE was observed over a period of 24 hr and phase contrast images were taken at 8, 12, 18 and 24 hr post-infection (Figure 5.9). Surprisingly, the CPE observed in the KO cells was more significant than the WT. Clear signs of CPE were observed from 8 hr onwards in the KO cells, whilst this was delayed in the WT. Comprehensive CPE could be seen at 24 hr in the KO cells (Figure 5.9 Panel J). Although there was CPE in the WT cells (Figure 5.9 Panel I), this was significantly less than in the KO. These results suggested SFV replicated more efficiently, inducing more cytotoxicity in the MEFs lacking the MYSM1 protein via targeted knockout, in direct contrast to what had been observed in HeLa cells using siRNA depletion.

5.6.3 MYSM1-deficient MEF cells are more permissive to SFV and CHIKV infection

The effect of the MYSM1 knockout in MEFs on SFV replication was next investigated at the level of viral RNA. Both WT and KO cells were infected with SFV at MOI of 2, and RNA extracted 8 hr post-infection. SFV RNA levels were then monitored by QPCR. The lack of MYSM1 in these fibroblasts resulted in a 6-fold enhancement in SFV RNA compared to WT cells (Figure 5.10A). To see if the same phenotype was observed with CHIKV, WT and KO cells were infected with CHIKV at MOI of 2 and viral RNA levels monitored at 8 hr post-infection. This data, shown in Figure 5.10B, indicates that there is increase in CHIKV RNA in the KO compared to the WT, of approximately 3 fold. In the three independent experiments carried out in this thesis this was not found to be significant. However, this data was influenced by a single experiment with a very high value for the KO line. Taken together, these data suggest that MYSM1 plays a different role during alphavirus infection of different cell types i.e. HeLa cells versus MEFs

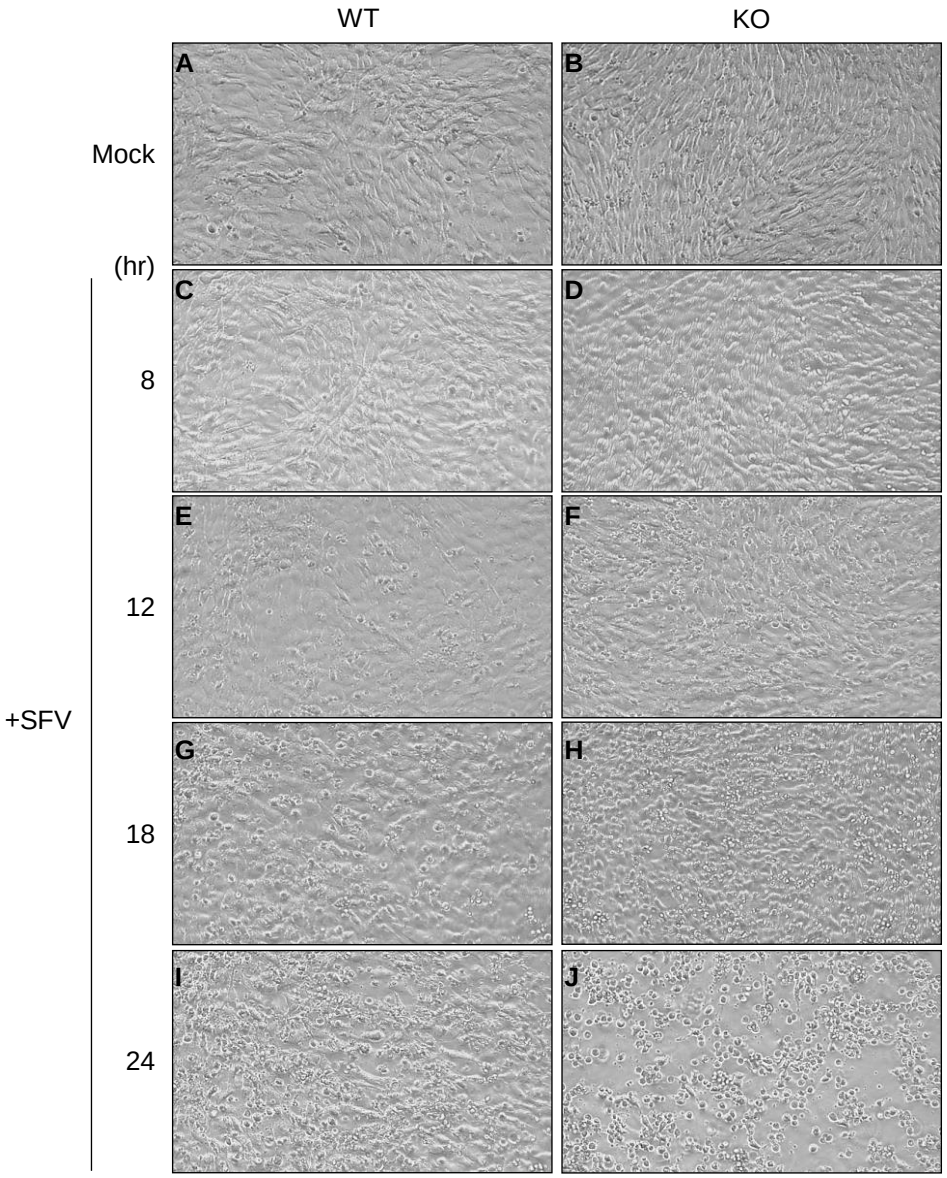

Figure 5.9 Phase contrast images of SFV induced cytopathic effect in WT and KO MEFs. WT and KO MEFs were infected with SFV at MOI 2. Phase contrast microscopic images taken at various times post infection are shown. WT cells are on the left hand panels, and KO cells in the right hand panels. A and B are mock infected cells; C, E, G and I are WT cells and D, F, H and J are KO cells, infected with SFV at 8, 12, 18 and 24 hr post-infection respectively.

However, two different approaches were used in these cells, siRNA depletion in HeLa compared to genetic knockout in the MEFs. It is possible that during the generation of the KO cells they adapted/compensated in some way to the loss of MYSM1.

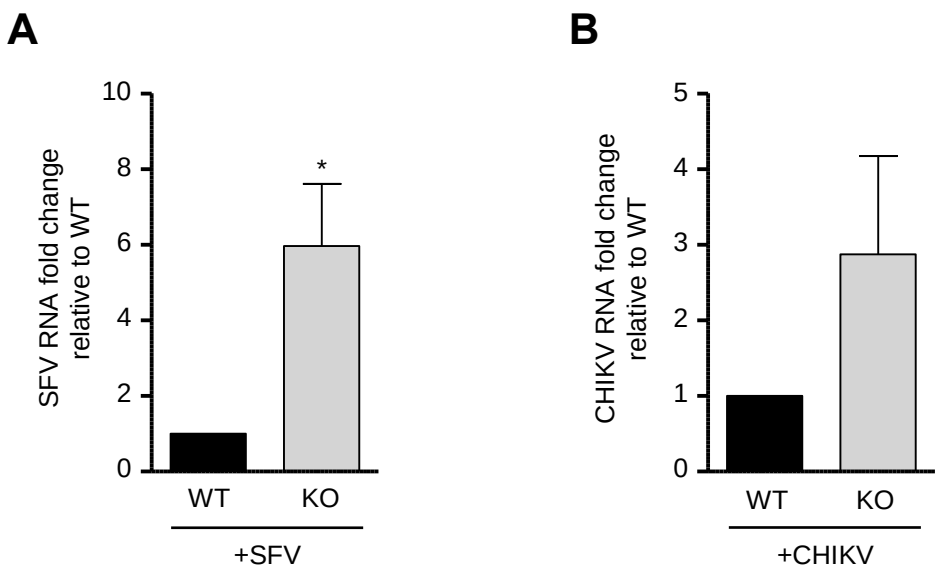

Figure 5.10 Knockout of MYSM1 in MEFs leads to an increase in SFV and CHIKV replication. WT and KO MEFs were infected with either SFV or CHIKV at MOI 2. Total RNA was extracted at 8 hr post-infection and analysed by qPCR for levels of either (A) SFV genomic RNA or (B) CHIKV genomic RNA. The data was normalised to 18s, and presented relative to WT. The data shown represents the mean of 3 independent experiments (+/- SEM) [*$p<0.05$].

5.7 The effect of MYSM1 depletion in MRC5 cells on SFV replication

To confirm if this phenotype in fibroblasts was indeed a true reflection of the role of MYSM1 and that fibroblast lacking MYSM1 are more susceptible to alphavirus infection, a further second fibroblast line was used and this time siRNA depletion was used to remove MYSM1. Human MRC5 fibroblasts were transfected with MYSM1 siRNAs 1 and 3, along with the siC. After 48 hr, transfected cells were harvested and re-seeded into 2 x 6 well plate and incubated for a further 24 hr. One plate was infected with SFV at MOI of 2, and SFV RNA levels determined 8 hr post-infection. QPCR analysis of three independent experiment revealed an increase in SFV RNA levels of 2-fold and 1.5-fold compared for MYSM1 siRNAs 1 and 3 respectively, compared to cells treated with siC (Figure 5.11A). Although not significant, it was in general agreement with the data from the KO MEF cells. The cells in the second 6 well plate were harvested after 24 hr (total of 72 hr post-transfection with siRNAs), and protein lysates analysed for levels of MYSM1 by immunoblotting. This confirmed depletion of MYMS1 protein in these cells. A representative

immunoblot is shown in Figure 5.11B and C. Densitometry analysis of three independent experiment highlighted an average reduction of MYSM1 protein of 50% and 65% for siRNAs 1 and 3 respectively.

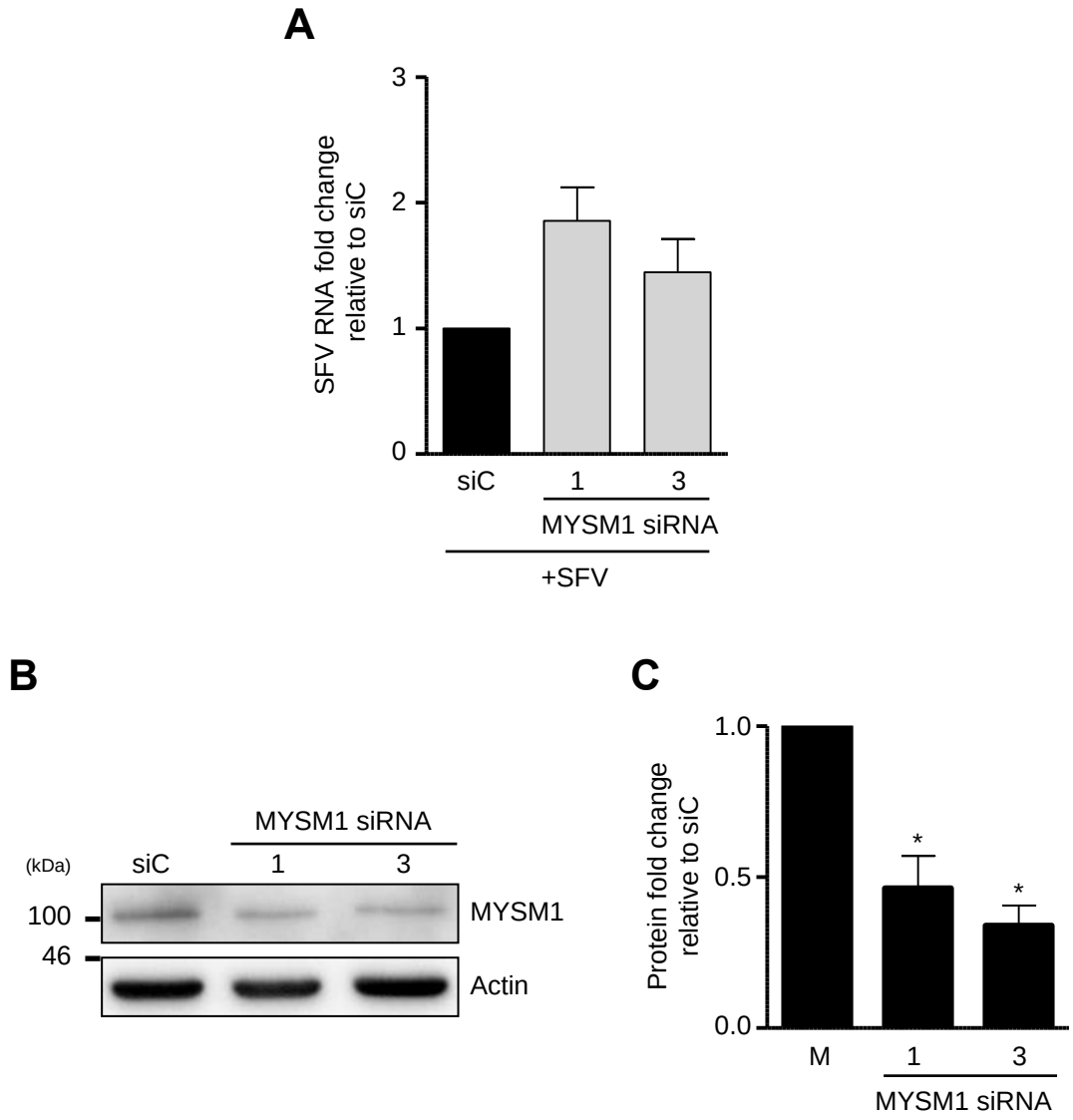

Figure 5.11 MYSM1 depletion in MRC5 fibroblast leads to an increase in SFV replication. MRC5 cells were transfected with either MYSM1 siRNAs 1 or 3, or siC. At 48 hr cells were reseeded into duplicate 6 well plate. After a further 24 hr, one plate was infected with SFV at 2 MOI and RNA extracted 8 hr post infection. The second plate was used to make protein lysates to determine the efficiency of MYSM1 depletion at 72 hr post transfection. (A) QPCR analysis of SFV RNA levels normalised to ACTB and presented relative to siC. (B) Representative immunoblot analysis of MYSM1 and actin in lysates from siRNA treated cells. (C) Quantification of MYSM1 protein level relative to siC via Image J analysis. All data shown represents the mean of 3 independent experiments (+/- SEM) [*p<0.05].

To check to see if this was a general feature of using fibroblasts compared to HeLa, i.e that DUBs had an inverse role during alphavirus infection, or if there were unexplained issue related the approach used, an experiment was carried out utilising USP15 KO MEFs. In the original DUB siRNA screen, depletion of USP15 with a pool of 4 siRNAs lead to a decrease in cell viability of 33.7 after SFV infection (N Blake, personal communication). This suggested USP15 may have an antiviral role, and while this DUB hit has yet to be confirmed by deconvolution of the siRNA pool. The availability of primary WT and *USP15*$^{-/-}$ MEF cells from Dr. Klaus-Peter Knobeloch (Freiburg University, Germany) laboratory (Torre *et al*., 2016) allowed for the opportunity to test if the same phenotype was observed in fibroblast as was seen in HeLa cells (again comparing KO with depletion). WT and *USP15*$^{-/-}$ MEF were infected with SFV at MOI of 2. SFV RNA levels were then monitored at 8 hr post-infection. QPCR analysis showed that in the absence of USP15 in MEFs there was a 2.6-fold increase in SFV RNA levels as compared to WT (Figure 5.12). Although only a single experiment was possible, this data suggested that lack of USP15, either by depletion in HeLa cells or knockout in MEFs, resulted in similar overall phenotypes. Thus, providing supporting data for the results with MYSM1 knockout in MEFs, such that not all DUBs generate different phenotypes in fibroblasts as compared to HeLa cells.

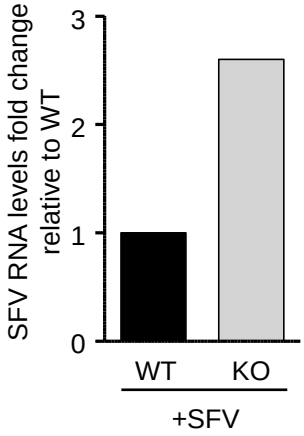

Figure 5.12 The effect of the absence of USP15 in MEF cells on SFV replication. MEF WT and *USP15*$^{-/-}$ cells were infected with SFV at MOI 2. Total RNA was extracted at 8 hr post-infection and analysed by qPCR for levels of SFV genomic RNA.

5.8 Summary

In this chapter, the study aimed to investigate the role of MYSM1 during alphavirus replication. Using siRNAs, depletion of MYSM1 in HeLa cells resulted in a reduction in both SFV and CHIKV replication, as assayed by measuring RNA levels and plaque formation. However, in contrast, when utilising MEFs with a MYSM1 genetic knockout, infection with SFV lead to increased CPE and virus replication in the KO when compared to the WT cells. This increase in virus replication was also observed for CHIKV infection. Support for this different phenotype in fibroblast was shown when human fibroblasts were depleted of MYSM1 by siRNA treatment and a similar increase in virus RNA levels was seen. The reasons for this alternate phenotype were unclear. MYSM1 has primarily been reported to a nuclear localised DUB which plays a role in histone deubiquitination and be important for lymphocyte development (Zhu *et al*., 2007; Nijnik *et al*., 2012). However, a recent paper has suggested a role during innate immune signalling, which is particularly relevant to virus infection. The next chapter will investigate the role of MYSM1 and innate signalling during alphavirus infection.

Chapter 6

Investigation of the Role of MYSM1 in Pattern Recognition Receptor Signalling

6.1 Introduction

In chapter 5, the role of MYSM1 during both SFV and CHIKV infection was found to differ depending on the cell background. Using siRNA depletion of MYSM1 in HeLa cells, it was found that this lead to a decrease in both SFV and CHIKV replication. In contrast, using both siRNA depletion and genetic KO of MYSM1 in fibroblasts, it was observed that SFV and CHIKV replication was increased. Thus, in HeLa cells MYSM1 was shown to be pro-viral, whereas in fibroblasts derived cells it was shown to have an anti-viral role. This suggested different functional roles for MYSM1 in cells of different background. When this project was initiated MYSM1 had been shown to have a role in deubiqutination of histones, influencing transcription, and to be important for the development of cells of lymphoid origin (section 1.7.2). However, whilst the work in this thesis was underway, Panda and colleagues published a manuscript showing that MYSM1 could function as a negative regulatory of pattern recognition receptor signalling (Panda *et al*., 2015). Thus, based on the data in the previous chapter, if MYSM1 was involved in regulation of PRR signalling to influence SFV and CHIKV replication this was dependent on the cell background. In this chapter the effect of MYSM1 depletion and knockout on the production of Type 1 IFNs and pro-inflammatory cytokines after SFV and CHIKV infection was therefore investigated in both HeLa and fibroblast cell lines.

6.2 Characterisation of the type I IFN and pro-inflammatory cytokine response in HeLa cells after exposure to LPS, Poly (I:C) and Poly (I:C)/LV

Before beginning the experiments to determine any role for MYSM1 in PRR signalling in HeLa cells in response to SFV and CHIKV infection, a series of experiments were undertaken to determine the ability of HeLa cells to

respond to PRR agonists and validate the individual PCR primers being used in this study. HeLa cells were treated with either LPS (to stimulate via TLR4), Poly (I:C) (to stimulate via TLR3) or Poly (I:C)/LV (to stimulate via RIG-1/MDA-5). The production of Type I IFNs (IFNα and IFNβ), and the pro-inflammatory cytokines (TNFα and lL1β), were monitored at the transcript level by PCR.

HeLa cells were treated with the above PRR agonists for 8 hr, before RNA was extracted and converted to cDNA using oligo (dT) primer. End-point PCR was then carried out for IFNα, IFNβ, TNFα and lL1β, with ACTB and H_2O used as controls throughout. This data is shown in Figure 6.1A (see Appendix B for the primers PCR product size). This end point PCR data indicated that in HeLa cells IFNα was detectable in resting cells possible that cells were under stress or was a technical error, and was only marginally induced by Poly (I:C). Whereas IFNβ was not detected in resting cells, and was induced by both Poly (I:C) and Poly (I:C)/LV, but not detectably so by LPS. TNFα was detected at low levels in resting HeLa cells, and appeared to be strongly induced by Poly (I:C). Meanwhile IL1β was barely detectable, with a very faint band in resting cells and in cells treated with LPS, Poly (I:C) and Poly (I:C)/LV. QPCR analysis was also carried out for the above genes. This data is shown in Figure 6.1B. IFNα was only induced by Poly (I:C) treatment, and even this was at a very low level, of 1.4-fold (Figure 6.1B). Whereas IFNβ was induced by treatment with all three PRR agonists, with Poly (I:C) and Poly (I:C)/LV resulting in significant induction of the IFNβ transcript of 34- and 170-fold respectively, with LPS inducing a very low level of increase of 1.3-fold (Figure 6.1C). The QPCR analysis data for TNFα mRNA levels obtained from treated HeLa cells with LPS, Poly (I:C) and Poly (I:C)/LV revealed levels of induction, 1.9-fold, 8.3-fold and 1.5-fold respectively (Figure 6.1D). No transcript was detected for lL1β in these experiments, with Ct values in the high 30s. Thus, this shows that HeLa cells can respond to mimics of viral RNA via RLR and TLR3 receptors to primarily induce transcription of IFNβ mRNA.

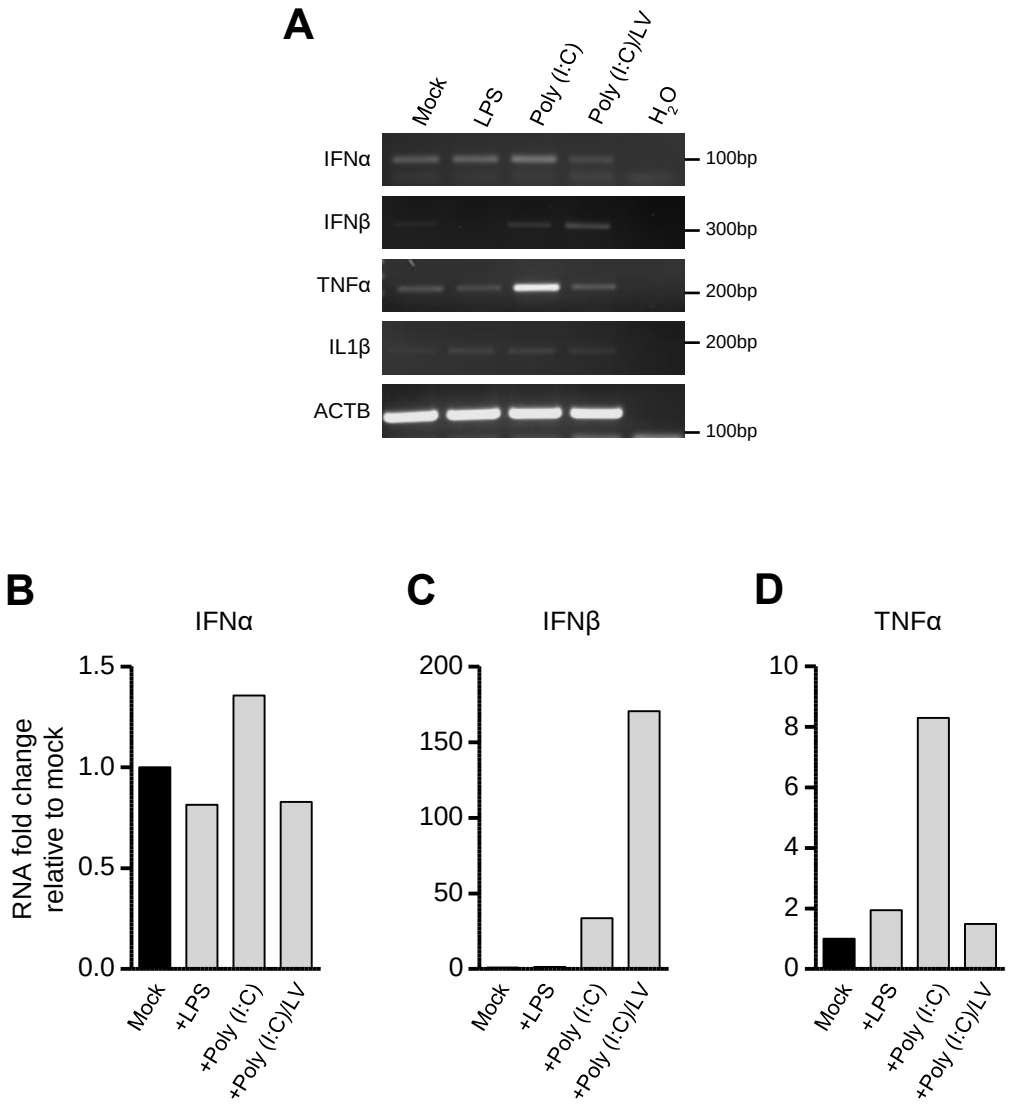

Figure 6.1 Type I IFN and pro-inflammatory cytokine responses after stimulation of HeLa cells with LPS, Poly (I:C) and Poly (I:C)/LV. HeLa cells were stimulated with either LPS, Poly (I:C) or Poly (I:C)/LV at 1 µg/ml. Total RNA was extracted at 8 hr post-stimulation and converted to cDNA using oligo d(T), before being amplifed by PCR. (A) End-point PCR for IFNα, IFNβ, TNFα, IL1β and ACTB. Water control was used throughout to ensure validity. (B) QPCR analysis of levels of IFNα, IFNβ, TNFα, IL1β mRNA for cDNA samples, and the $2^{-\Delta\Delta}$Ct method was used to analyse the data. Actin was employed as the reference gene and results were further normalized to the mock-stimulated cells and shown as fold change relative to the mock-stimulated. Data is from one independent experiment.

6.3 Induction of type I IFNs and pro-inflammatory cytokine responses in HeLa cells after infection with SFV

To test the effect of SFV infection of HeLa cells on the induction of the IFNα, IFNβ, TNFα and lL1β transcripts, cells were infected at 2 MOI and RNA extracted at 3, 6, 9, 12, 18 and 24 hr post SFV infection. In a simple approach, cDNAs were analysed by end-point PCR for IFNα, IFNβ, TNFα and lL1β (Figure 6.2). IFNα PCR product was detected in mock-infected cells, it is likely these cells were under stress. Although not quantified, the intensity of PCR bands appeared to increase overtime to 12 hpi (peaking at 9 hr), then decreasing and being undetectable at 24 hpi. There is a feint band in this lane that is identical to one in the H_2O lane. It is possible that no cDNA was added to the PCR reaction for the 24 hpi sample. Likewise, IFNβ was again not detected in normal HeLa cells (mock-infected) but was detectable from 9 hr onwards, appearing to increase in intensity over time up to 24 hr. TNFα was detected at low levels in normal HeLa cells but appeared to be induced from 9 hr onwards. ILβ was not detected in mock infected cells, but a faint band was seen from 3 hpi onwards, with the exception of 6 hr where no product was seen, and appeared to increase at 18 and 24 hr. It is likely that the 6 hr timepoint was a technical error, but these experiments were not repeated.

These samples were not quantified by QPCR, and while dependent on normalising to ACTB product levels, this data implied that SFV infection of HeLa cells lead to an induction in transcript levels of both IFNs α and β, and both pro-inflammatory cytokines test (TNFα and IL1β). Although not carried out for CHIKV, we assumed that CHIKV infection of HeLa cells would induce similar induction. Thus, this experiment suggested that this model is suitable to investigate the effect of MYSM1 depletion on recognition of SFV and CHIKV by PRRs.

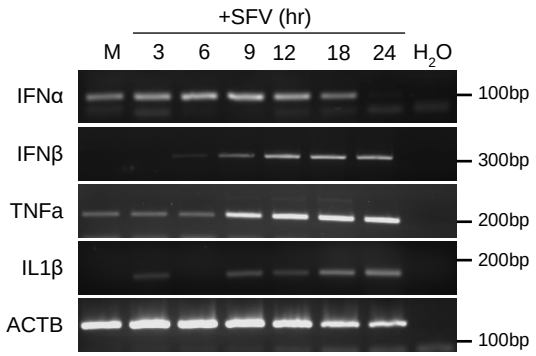

Figure 6.2 Induction of type I IFN and pro-inflammatory cytokine responses in HeLa cells after SFV infection. HeLa cells were infected with SFV at MOI=2. Total RNA was extracted at 3, 6, 9, 12, 18 and 24 hr post-infection and converted to cDNA using oligo d(T), before being amplified by end-point PCR for IFNα, IFNβ, TNFα, IL1β and ACTB. A water control was used throughout to ensure validity.

6.4 The effect of MYSM1 Knockdown in HeLa cells on the induction of type I IFNs and pro-inflammatory cytokines after infection with SFV and CHIKV

The next step was to investigate the effect of depletion of MYSM1 in HeLa cells on the induction of IFNs α and β, TNFα and IL1β after both SFV and CHIKV infection. The individual MYSM1 siRNAs 1 and 3 were used to deplete MYSM1 for 72 hr, before cells were infected with either SFV or CHIKV for 8 hr, RNA extracted and cDNA generated. These samples were the same ones generated in experiments described in section 5.2.2 for SFV and section 5.5.1 for CHIKV. As previously, QPCR analysis was carried on the three independent experiments.

The data for SFV is shown in Figure 6.3. For IFNα and IFNβ, the data revealed a general reduction in transcripts levels after MYMS1 knockdown with siRNAs 1 and 3 for IFNα, and with siRNA1 for IFNβ. The mean of data of IFNα showed that the depletion of MYSM1 with siRNA 1 lead to a reduction of 28% compared to cells treated with siC. There was more significant reduction, of 56%, with siRNA 3 (Figure 6.3A).

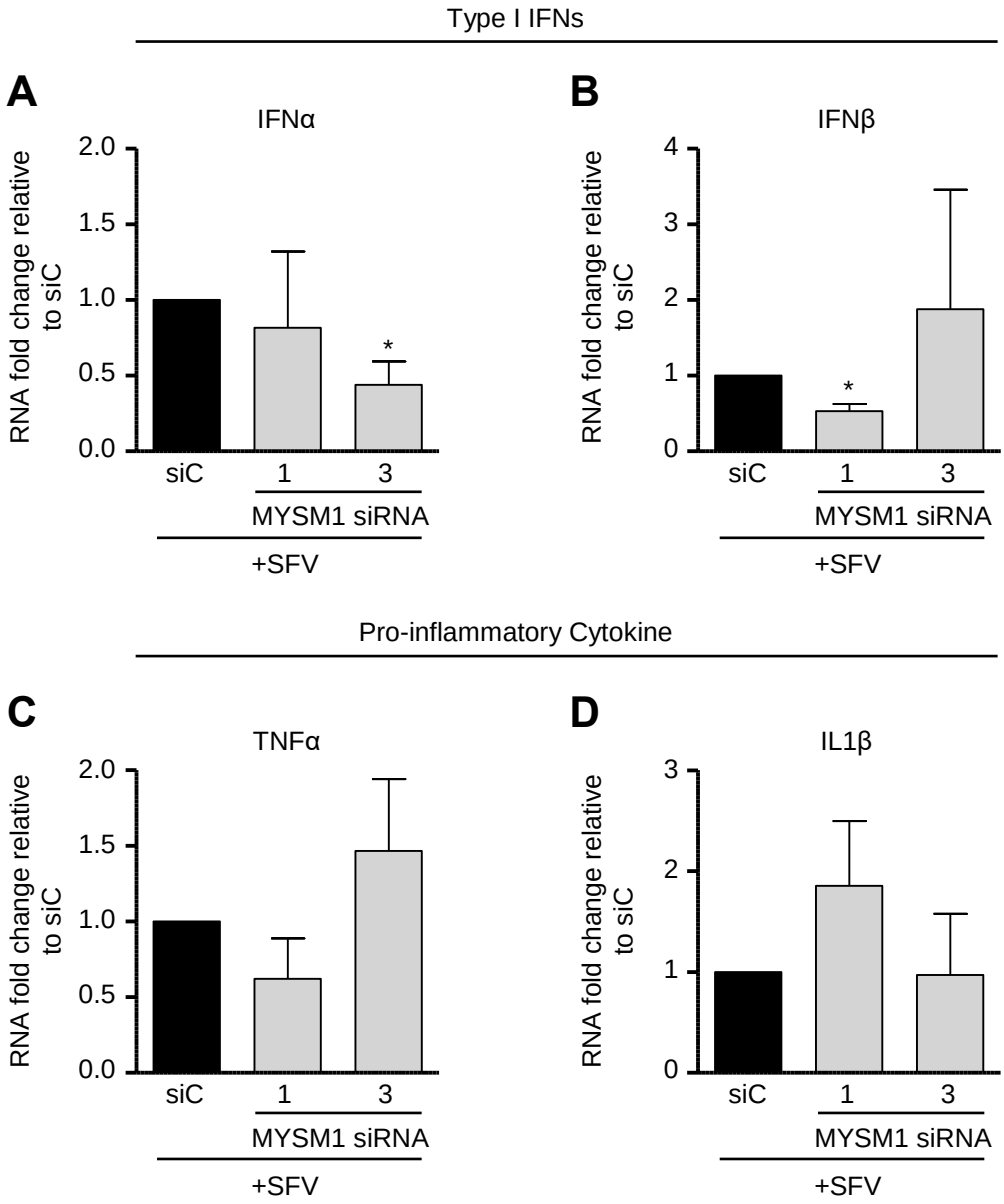

Figure 6.3 Induction of pro-inflammatory cytokine and type I IFN responses after SFV infection of MYSM1 depleted HeLa cells. HeLa cells were transfected with either MYSM1 siRNAs 1 or 3 or siC, incubated for 72 hr before infecting with SFV at MOI 2. Total RNA was extracted at 8 hr post-infection and analysed by qPCR for levels of (A) IFNα, (B) IFNβ, (C) TNFα and (D) IL1β mRNA for RT+ samples are shown. Data was analysed using the $2^{-\Delta\Delta}$Ct method. Actin was employed as the reference gene and results were further normalized to the siC treated cells and shown as fold change relative to the siC. All data shown represents the mean of 3 independent experiments (+/- SEM) [*$p<0.05$]. Note, these cDNA samples are derived from the experiments described in Section 5.2.2.

Whereas, the mean of the data for IFNβ mRNA levels showed a significant reduction of 47% following depletion of MYSM1 by siRNA 1, but with siRNA 3 there was an increase in IFNβ of 88% (Figure 6.3B). However, there were large standard deviations for this data, and analysis of the individual experiments shows inconsistent data (Figure 6.4). It was not possible to interpret a conclusive result for this analysis. Although it was suggestive of a decrease in induction of IFNα after knockdown with siRNA 1 and 3, and a decrease in IFNβ with siRNA1 but not 3.

The data for the pro-inflammatory cytokines is also shown in Figure 6.3 (D and E), and was slightly contradictory. TNFα transcript levels were reduced 38% with siRNA1, whereas IL1β levels were increased 86%. In contrast, TNFα levels were increased 47% with siRNA3, whereas IL1β levels were essential unaffected being reduced 3%. However, across the three experiments there was no significant effects seen. Overall, this data did not provide a clear message for the role of MYSM1 in the production of type I IFNs and pro-inflammatory cytokines after infection with SFV. It may be the 8 hr post-infection was not suitable to monitor the production of type I IFNs and pro-inflammatory cytokines, although the data shown in figure 6.2 would suggest that these cytokines were being induced at this timepoint.

Analysis of the data for type I IFNs and pro-inflammatory cytokines after infection with CHIKV also produced unexpected results. Depletion of MYSM1 in HeLa cells with siRNAs 1 and 3 lead to a reduction in IFNα transcript levels of 52% and 61% respectively, compared to cells treated with siC (Figure 6.5A). There was also a reduction in levels of IFNβ of 41% and 70% for siRNA 1 and 3 respectively (Figure 6.5B). With the exception of siRNA1 for IFNβ, this data was statistically significant. In contrast, both pro-inflammatory cytokines showed increased levels after depletion of MYSM1 with both siRNAs. TNFα mRNA levels showed a non-significant induction of 10-fold and 6-fold for siRNAs 1 and 3 respectively compared to cells treated with siC (Figure 6.5C). Whilst, for IL1β there was non-significant induction of 8-fold and 5-fold for siRNAs 1 and 3 respectively compared to cells treated with siC (Figure 6.5D).

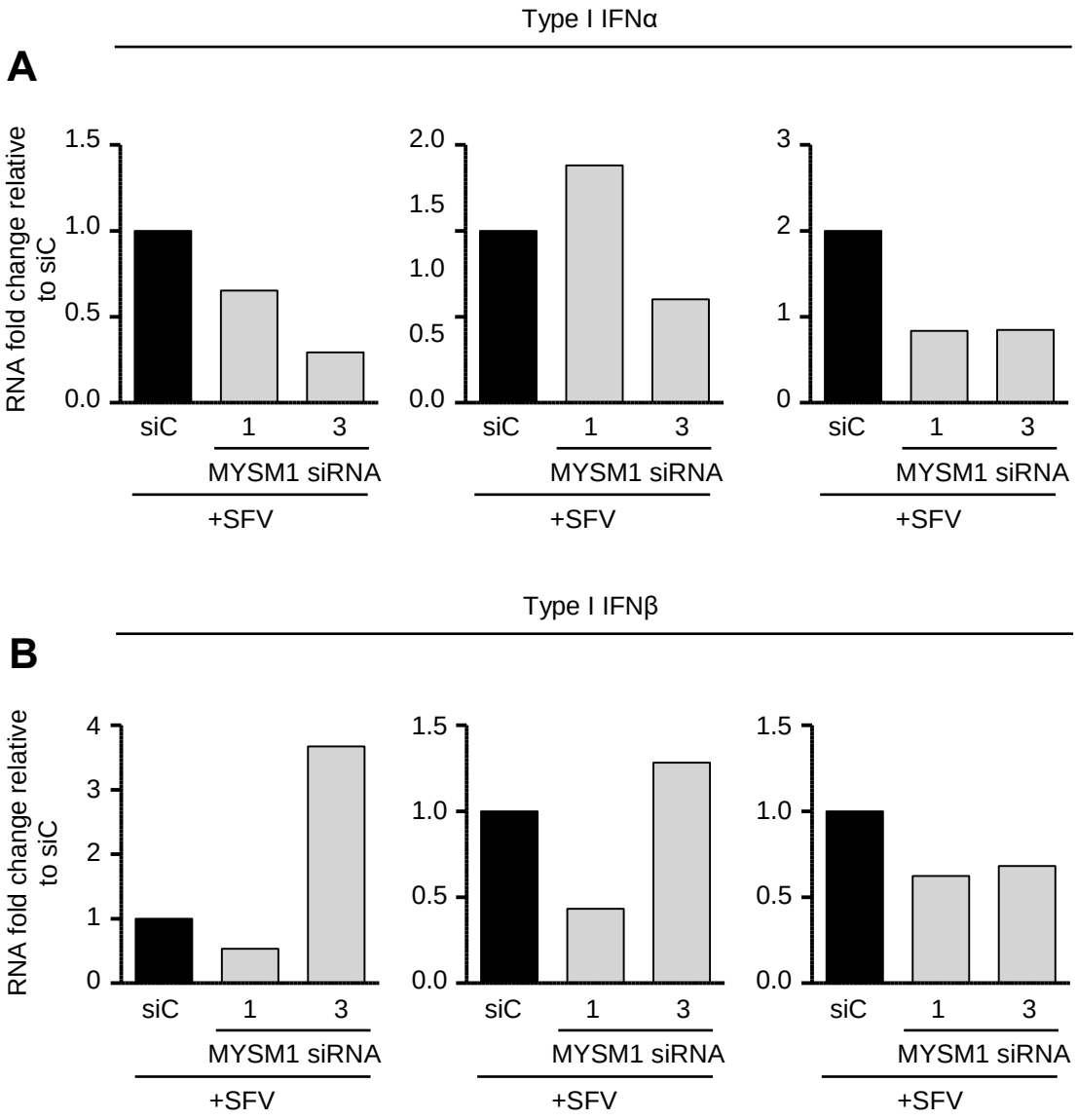

Figure 6.4 Induction of Type I IFN responses after SFV infection of MYSM1 depleted HeLa cells. HeLa cells were transfected with either MYSM1 siRNAs 1 or 3 or siC, incubated for 72 hr before infecting with SFV at MOI 2. Total RNA was extracted at 8 hr post-infection and analysed by qPCR for levels of (A) IFNα and (B) IFNβ mRNA for RT+ samples are shown. Data was analysed using the $2^{-\Delta\Delta}$Ct method. Actin was employed as the reference gene and results were further normalized to the siC treated cells and shown as fold change relative to the siC. Data shown is from each individual experiment. Note, these cDNA samples are derived from the experiments described in Section 5.2.2.

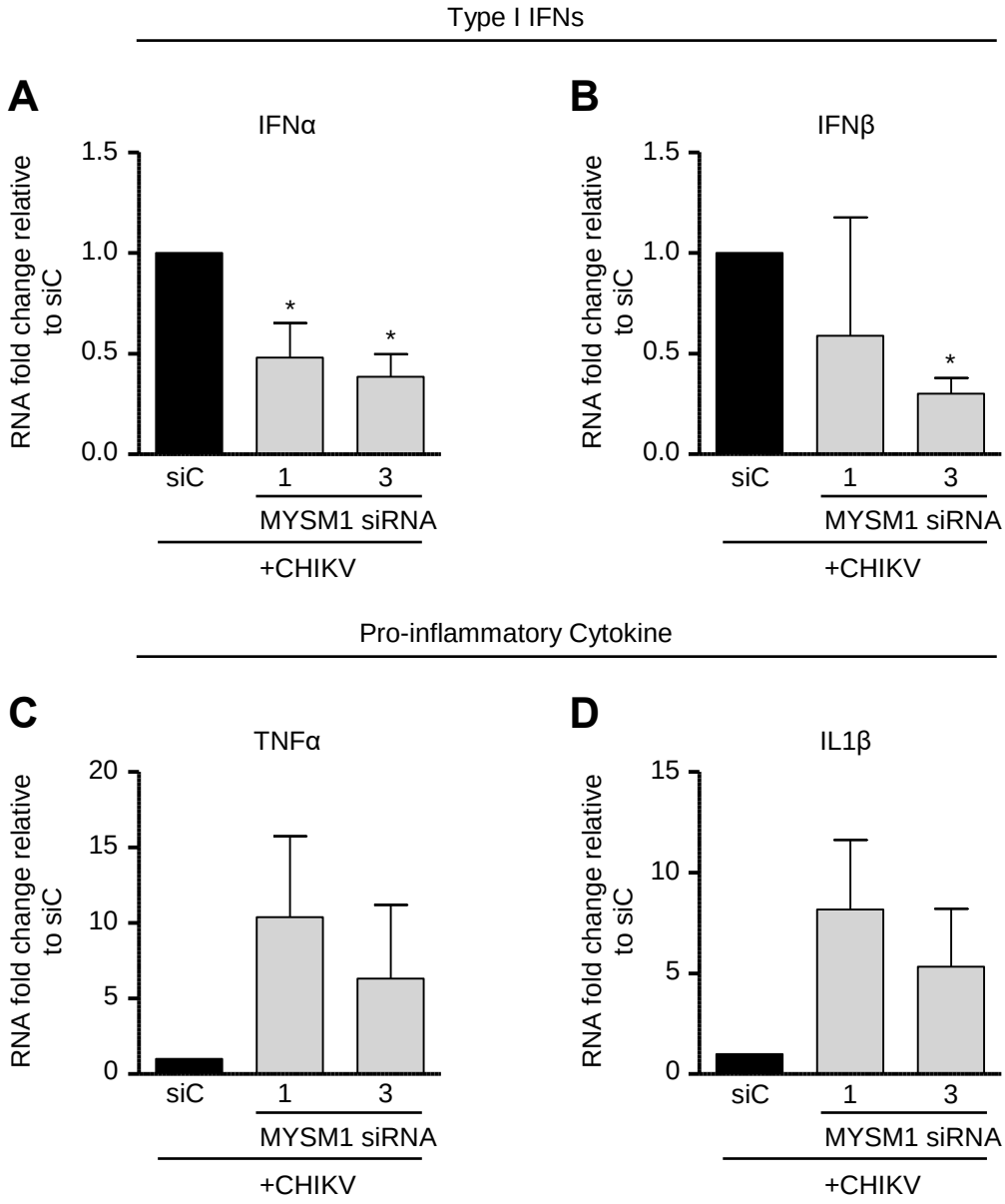

Figure 6.5 Analysis of pro-inflammatory cytokine and type I IFN responses after CHIKV infection of MYSM1 depleted HeLa cells. HeLa cells were transfected with either MYSM1 siRNAs 1 or 3, or siC. At 48 hr cells were reseeded into duplicate 6 well plate. After a further 24 hr, one plate was infected with CHIKV at 2 MOI. Total RNA was extracted at 8 hr post-infection and analysed by qPCR for levels of (A) IFNα, (B) IFNβ, (C) TNFα and (D) IL1β mRNA for RT+ samples are shown. Data was analysed using the $2^{-\Delta\Delta}$Ct method. Actin was employed as the reference gene and results were further normalized to the siC treated cells and shown as fold change relative to the siC. All data shown represents the mean of 3 independent experiments (+/- SEM) [*$p<0.05$]. Note, these cDNA samples are derived from the experiment described in Section 5.5.1.

Overall the findings show no consistent pattern in the effect of MYSM1 depletion in Hela cells on induction of Type 1 IFNs or pro-inflammatory cytokines after SFV and CHIKV infection. The SFV data was difficult to interpret. Whereas for CHIKV, although perhaps contradictory, there was evidence of down regulation of IFNs but upregulation of TNFα and IL1β.

6.5 The role of MYSM1 in induction of type I IFNs and pro-inflammatory responses in MEF cells after stimulation with PRR agonists

The experimental data in chapter 5 showed that the MYSM1-deficient MEF cells were more permissive to SFV and CHIKV replication, perhaps indicating a differential cytokine response. To investigate the role of MYSM1 in PRR signalling in MEF cells, experiments were undertaken to stimulated WT and MYSM1-KO MEFs with either LPS, Poly (I:C) or Poly (I:C)/LV and analyse transcript levels for IFNα, IFNβ, TNFα and lL1β. The production of cytokines was monitored at 8 hr post-stimulation. QPCR analysis data are shown in (Figure 6.6). WT MEF cells stimulated with LPS led to an induction in IFNα, IFNβ, TNFα and IL1β transcript levels of 4.3-fold, 14.2-fold, 3.2-fold and 2.6-fold respectively, compared to the WT mock-stimulated cells. Whereas LPS treatment of MYSM1-KO cells had little to no effect on type I IFNs and caused increases in TNFα and IL1β mRNA levels of 1.5-fold and 2.4-fold change respectively compared to the WT mock-stimulated cells (Figure 6.6A).

The QPCR data analysis for IFNα, IFNβ TNFα and IL1β transcript levels obtained from MEF cells treated with Poly (I:C) revealed an induction of 1.8-fold, 2.8-fold, 2.2-fold and 1.9-fold change respectively, compared to the WT mock-stimulated cells. Again, Poly (I:C) treatment of MYSM1 KO MEFs had no effect on type I IFNs, whilst enhanced TNFα and IL1β levels were seen, of 1.5-fold and 1.9-fold change respectively relevant to the WT mock-treated cells (Figure 6.6B).

The data in Figure 6.6C shows the effect of the lack of MYSM1 on the induction of cytokines after treatment with Poly (I:C)/LV. The QPCR analysis data for IFNα, IFNβ and TNFα transcript levels obtained from WT MEF cells treated with Poly (I:C)/LV showed an enhancement of 55-fold, 250-fold and

4.6-fold respectively. Whereas, there was no effect on IL1β mRNA levels. While the data obtained from MYSM1 KO MEFs revealed only very minor inductions in IFNα, IFNβ and TNFα levels of 1.2-fold, 12.5-fold and 2.2-fold respectively. Again, there was no effect on IL1β mRNA levels.

Thus, while the overall level of induction was low (with the exception of poly(I:C)/LV and IFNs), this data suggested that genetic silencing of MYSM1 in MEF cells was associated with a reduction in induction of IFNα and β, and TNFα but not IL1β after stimulation with defined agonists for different PRR pathways including LPS, Poly (I:C) and Poly (I:C)/LV.

6.6 Investigation of the effect of MYSM1 KO in MEFs on the induction of type 1 IFNs and pro-inflammatory cytokines after infection with SFV and CHIKV

Having shown that induction of IFNα and β, and TNFα, was impaired in MEF MYSM1 KO cells when stimulated with PRR agonists, the next step was to investigate the induction of these cytokines during infection with SFV and CHIKV. Using the cDNA samples obtained from MEFs (WT and KO) at 8 hr post-infection with each virus (as described in section 5.6.3), QPCR analysis was undertaken. WT MEF cells after infection with SFV showed a significant enhancement in type I IFN (IFNα and IFNβ) mRNA levels of 650-fold and 1110-fold respectively compared to the WT mock-infected cells. Whereas, MEF MYSM1 KO cells showed an induction in IFNα and IFNβ transcript levels after SFV infection of 160-fold and 460-fold respectively (Figure 6.7A). The difference between WT and KO was statistically significant ($p<0.05$), indicating that in the absence of MYSM1 there is less induction of IFNα and β after SFV infection. Whereas, there was the same level of induction of the pro-inflammatory cytokine gene TNFα transcript levels (of 240 –fold) in both WT and KO MEF cells compared to the mock- infected (Figure 6.7A). No transcript was detected for IL1β in these experiments. QPCR data from one representative experiment (of two) from WT and KO MEF cells infected with CHIKV is shown in figure 6.6B.

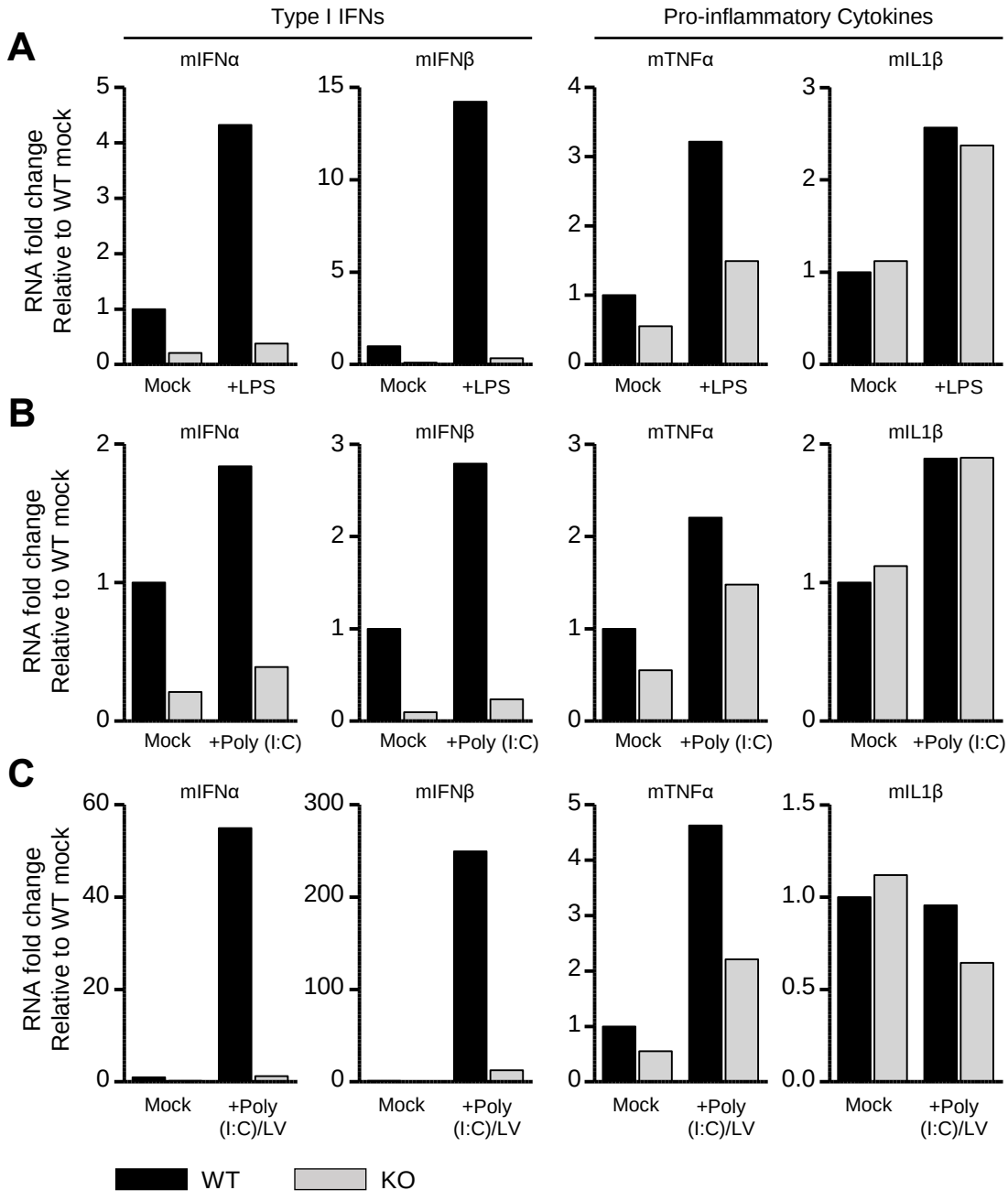

Figure 6.6 Genetic knockout of MYSM1 in murine embryo fibroblasts results in suppression of pro-inflammatory cytokine and type I IFN genes upon stimulation with agonists of PRR pathways. WT and MYSM1 KO MEFs were stimulated for 8 hr with either (A) LPS, (B) Poly (I:C) or (C) Poly (I:C)/LV. Total RNA was extracted and converted to cDNA using oligo d(T), before being analysed by qPCR for levels of IFNα, IFNβ, TNFα or IL1β mRNA for RT+ samples. Data was analysed using the $2^{-\Delta\Delta}$Ct method. The data was normalised to 18s, and presented relative to WT. Data is from one independent experiment.

The data showed there was a similar low induction in IFNα and IFNβ mRNA levels of 1.6-fold change in the WT cells respectively compared to WT mock-infected cells. For KO cells data was revealed no change in IFNα mRNA levels compared to WT mock-infected, while there was an increase of 2.2-fold change in IFNβ transcript levels. The QPCR analysis data was shown an increase of 3-fold and 1.5-fold change in TNFα transcript levels in WT and KO cells respectively (Figure 6.7B). Again, IL1β was not detected.

Thus, in these experiments the results suggest that MYSM1 might be a positive regulator of PRR signalling pathways events that control transcriptional induction of type I IFN responses during SFV infection. However, there was no significant induction of relevant cytokines after CHIKV infection of WT cells, and no overall effect of the MYSM1 KO. This was suggestive of an unexpectedly poor induction of cytokines with this combination, so difficult to make any interpretation.

6.7 The lack of MYSM1 function as a negatively regulator of the interferon stimulating gene (Mx1) in MEF cells

The data presented in previous sections for MEF cells treated with either PRR agonists (Figure 6.6) or infected with SFV (Figure 6.7) highlighted a decrease in the levels of IFNβ transcript due to the absence of MYSM1. The data for infection with CHIKV was less conclusive. To see if this was reflective in a reduction in the response to the presence of IFNβ, the next set of experiments investigated the levels of Mx1, an Interferon stimulated gene (ISG). The QPCR analysis data for Mx1 mRNA levels showed an induction of 6.2-fold, 1.5-fold and 10-fold in WT MEF cells in response to LPS, Poly (I:C) and Poly (I:C)/LV respectively (Figure 6.8A, B and C). There was no induction in Mx1 transcript levels in KO MEF cells. QPCR analysis QPCR analysis was also carried out for Mx1 after SFV and CHIKV infection. SFV infection resulted in an induction in Mx1 mRNA levels of 90-fold in WT cells, compared to 30-fold in KO MEF cells (Figure 6.8D). Whereas infection of WT MEF cells with CHIKV revealed a small induction in the Mx1 transcript levels of 1.4-fold, reflective of the low levels of IFNα/β seen in figure 6.7, with little or no change in Mx1 transcript levels in the KO line (Figure 6.8E).

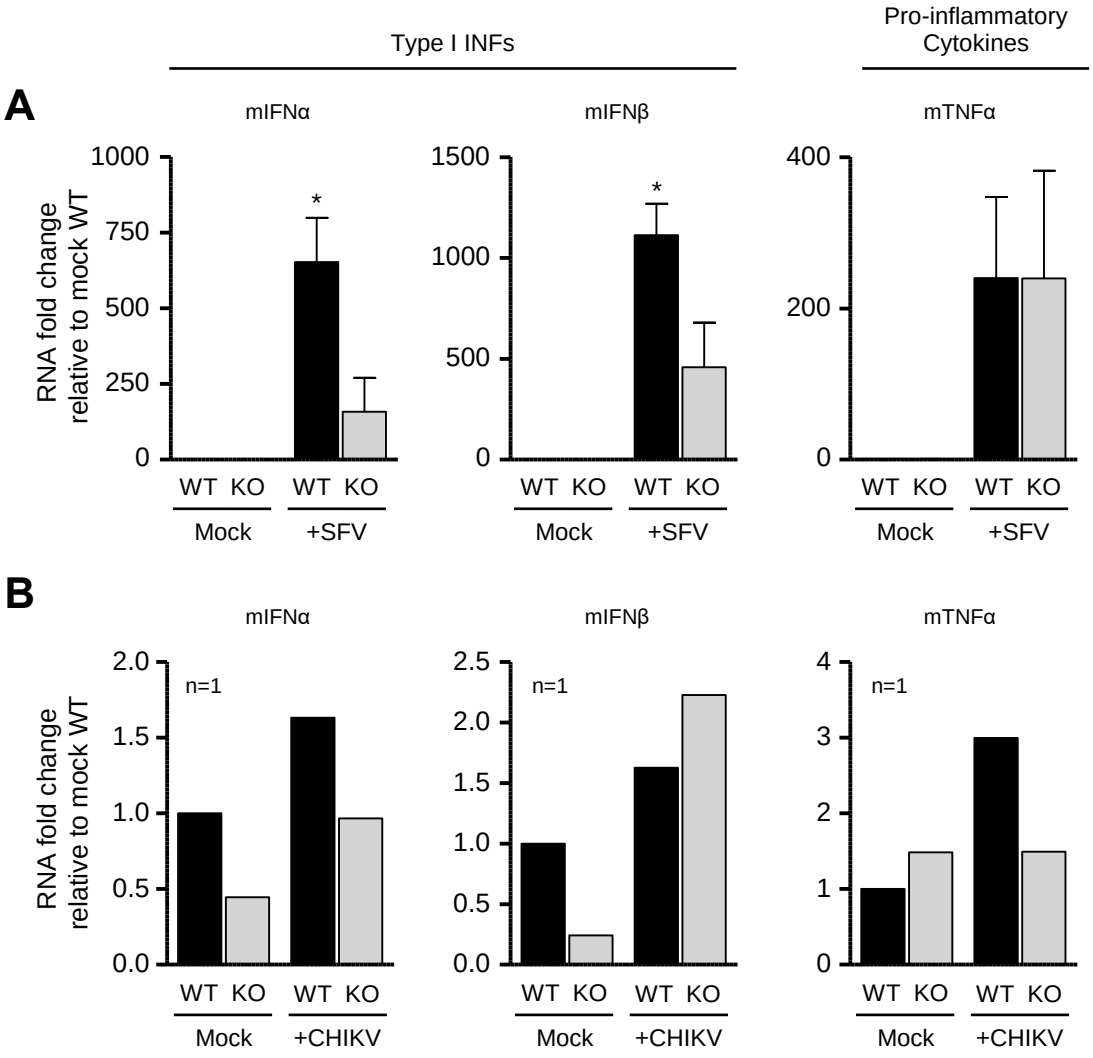

Figure 6.7 Pro-inflammatory cytokine and type I IFN responses in WT and MYSM1 KO MEFs infected with SFV and CHIKV. WT and KO MEFs were infected with either SFV or CHIKV at MOI 2. Total RNA was extracted at 8 hr post-infection and analysed by qPCR for levels IFNα, IFNβ and TNFα mRNA for RT+ samples, the $2^{-\Delta\Delta}$Ct method was used to analyse the data. The data was normalised to 18s, and presented relative to WT. (A) SFV infected data shown represents the mean of 3 independent experiments (+/- SEM) [*p<0.05]. (B) CHIKV infected data shown represents one of two independent experiments. Note, these cDNA samples are derived from the experiments described in Section 5.6.3.

6.8 The effect of MYSM1 knockdown in human fibroblast (MRC-5) cells on the regulation of the innate immune response upon infection with SFV

Experiments described in chapter 5 (section 5.7) highlighted that the role of MYSM1 during SFV replication seen in MEFs was also evident in human fibroblasts (MRC5 cells) using siRNA depletion. Thus, Experiments were carried out to investigate if depletion of MYSM1 in MRC5 cells also results in differential induction of type I IFNs (IFNα and IFNβ) and pro-inflammatory cytokine (TNFα and IL1β) genes after SFV infection. QPCR analysis of cDNA from MRC5 cells depleted of MYSM1 and infected with SFV showed an overall induction in IFNα mRNA levels of 90% and 65%, when presented as the mean of three independent experiments (Figure 6.9A). However, there was significant variability in these data, as evident with the large error bars. In contrast, depletion of MYSM1 by siRNA 1 and 3 resulted in decreased IFNβ production of 22% and 35% compared to the treated cells with siC (Figure 6.9B). However, with only the data for siRNA 3 being statistically significant. SFV infection lead to decreased TNFα levels in MRC5 cells with MYSM1 siRNA 1 and 3, of 57% and 72% respectively (Figure 6.9C). There was an induction in IL1β of 2.38-fold following depletion of MYSM1 by siRNA 1. In contrast, treatment of MRC5 cells with siRNA 3 lead to a small reduction in IL1β production of 10% (Figure 6.9D). Together, these data don't provide a consistent pattern for the role of MYSM1 with respect to induction Type 1 IFNs and pro-inflammatory cytokine in MRC5 fibroblast. Although, TNFa is shown to be significantly reduced for both MYSM1 siRNAs.

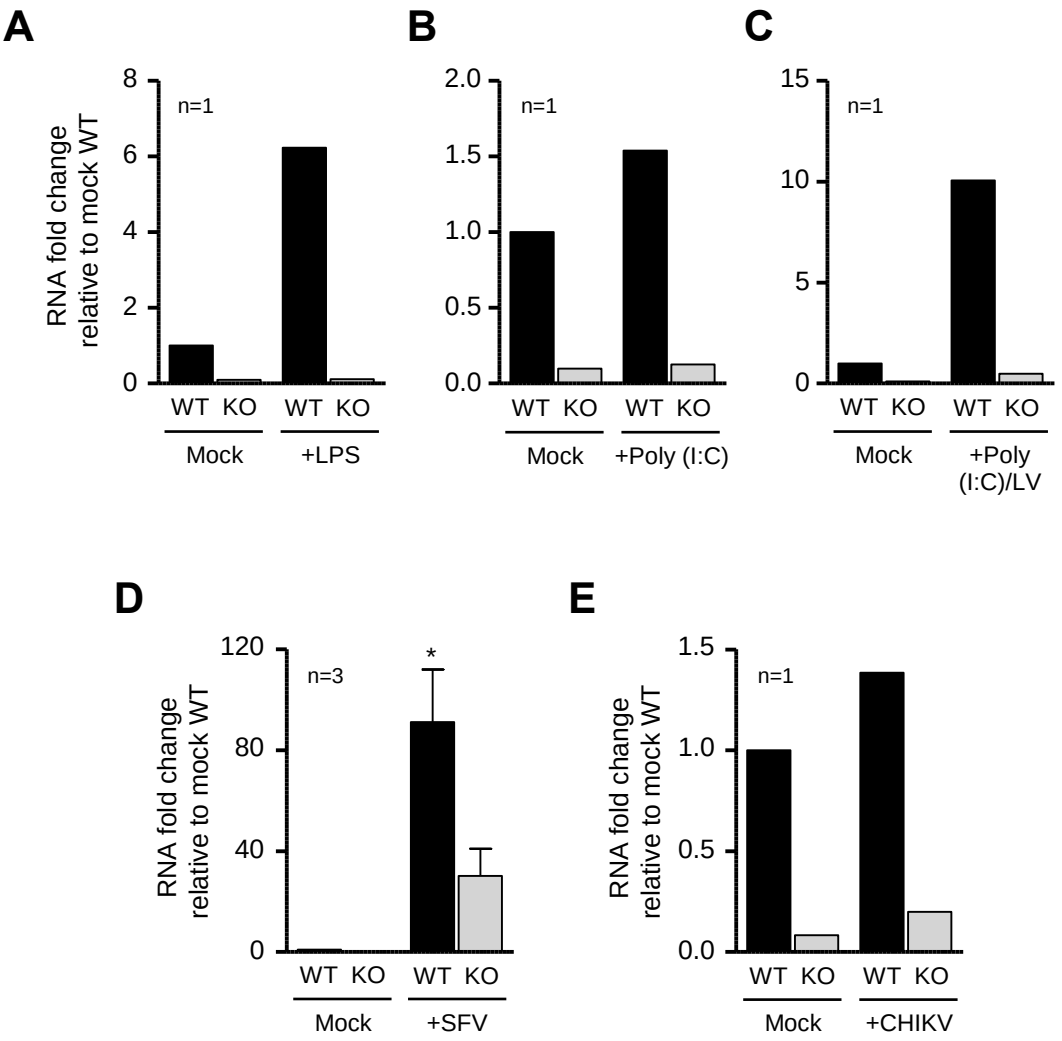

Figure 6.8 Induction of Mx1 is suppressed in MYMS1 KO MEFs. WT and MYSM1 KO MEFs were either stimulated for 8 hr (A) LPS, (B) Poly (I:C) and (C) Poly (I:C)/LV or infected for 8 hr with either (D) SFV or (E) CHIKV. Total RNA was extracted at 8 hr post-stimulation/infection before being analysed by qPCR of Mx1 mRNA levels for RT+ samples, the $2^{-\Delta\Delta}$Ct method was used to analyse the data. The data was normalised to 18s, and presented relative to WT (A), (B) and (C) Data is from one independent experiment. (D) Data shown represents the mean of 3 independent experiments (+/- SEM) [*$p<0.05$]. (E) Data shown represents one of two independent experiments. Note, cDNA samples are derived from the experiments described in section 6.5 (A, B and C) and/or Section 5.6.3 (D and E).

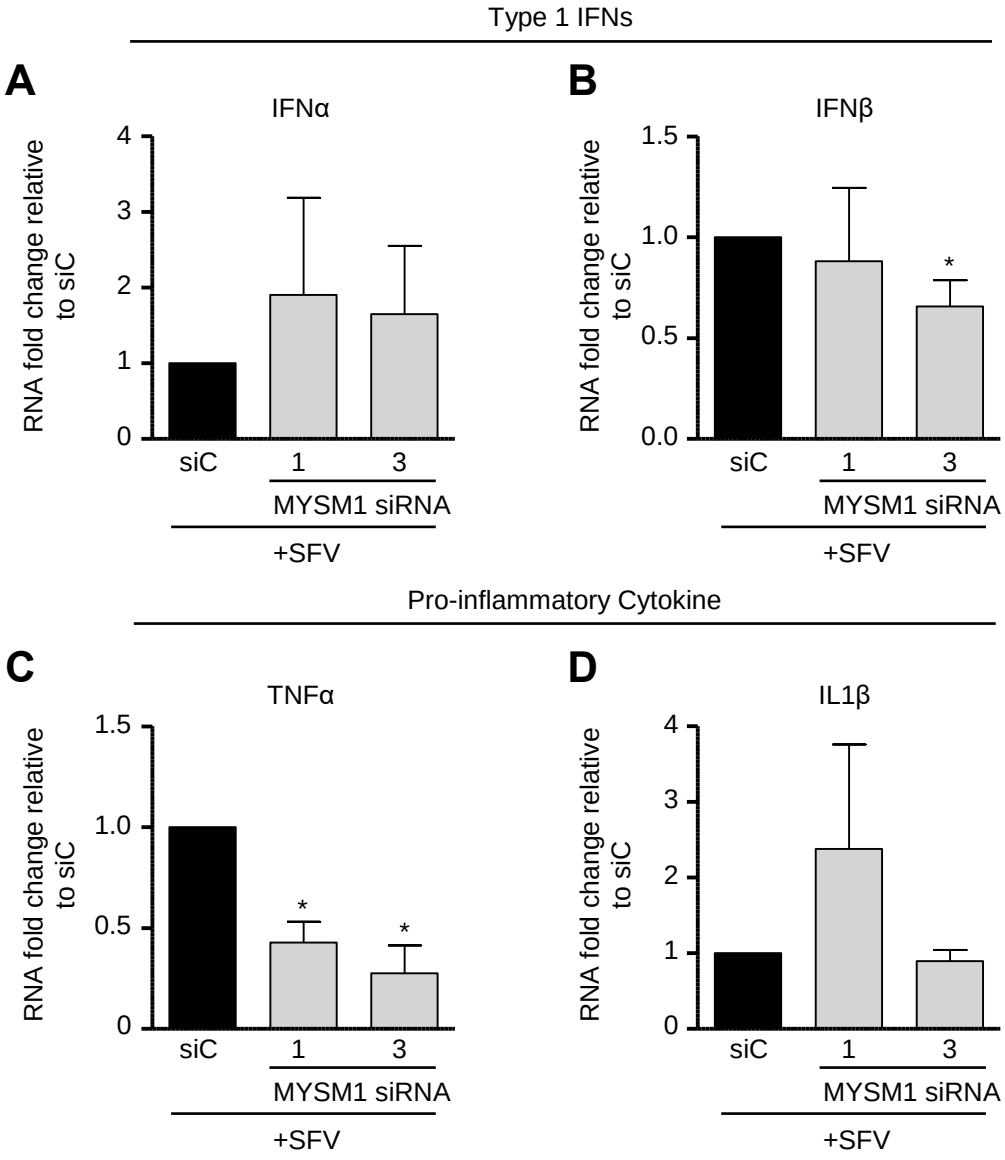

Figure 6.9 Analysis of pro-inflammatory cytokine and type 1 IFN levels after SFV infection of human fibroblasts treated with MYSM1 siRNA. MRC5 cells were transfected with either MYSM1 siRNAs 1 or 3, or siC. At 48 hr cells were reseeded into duplicate 6 well plate. After a further 24 hr, one plate was infected with SFV at 2 MOI. Total RNA was extracted at 8 hr post-infection and analysed by qPCR for levels of (A) IFNα, (B) IFNβ, (C) TNFα and (D) IL1β mRNA for RT+ samples are shown. Data was analysed using the $2^{-\Delta\Delta}$Ct method. Actin was employed as the reference gene and results were further normalized to the siC treated cells and shown as fold change relative to the siC. All data shown represents the mean of 3 independent experiments (+/- SEM) [*$p<0.05$]. Note, these cDNA samples are derived from the experiments described in section 5.7.

6.9 Summary

In this chapter, I found that depletion of MYSM1 by siRNAs in HeLa cells did not show a clear message for the involvement of MYSM1 in PRRs pathway with either SFV or CHIKV infection. Although, the data showed depletion of MYSM1 results in a non-significant augmentation in the pro-inflammatory genes expression during CHIKV infection. Furthermore, the data indicated that the genetic silencing of MYSM1 in MEFs associated with suppression of type I IFNs, pro-inflammatory cytokine genes expression and ISG (Mx1) upon stimulation with defined agonists for different PRR pathways including LPS, Poly (I:C) and transfected Poly (I:C)/LV. Meanwhile, infection of MEF cells lacking of MYSM1 with SFV lead to a reduction in type I IFNs and Mx1 gene expression compared to WT but there was no clear evidence for the role of MYSM1 in MEFs during CHIKV. Overall, these experiments produced disappointingly inconclusive data with regard the role of MYSM1 during alphavirus infection and much remains to be clarified

Chapter 7

Discussion

7.1 General overview

Over the past decade CHIKV has been the alphavirus of most concern to humans, with significant outbreaks in Africa, the Indian Ocean and Asia have occurred, as well as the recent emergence of CHIKV in the Americas. Infections have also been reported in Italy, France and Greece. We are only just beginning to decipher the cellular factors and pathways involved in the replication of CHIKV. CHIKV infection in humans is associated with both acute and chronic symptoms, the pathophysiology of which remains poorly understood. Furthermore, there is no commercially available vaccine or drug to tackle this a major public health issue.

The ubiquitin-proteasome system is key to the coordination of normal cellular functions. As with all cellular pathways viruses have targeted this process to aid their replication within cells. Previous studies have shown that both the forward reaction of ubiquitination, and the reverse reaction of deubiquitination are targeted during virus infection to enhance their replication, either by targeting of cellular proteins or encoding viral homologues of key pathway proteins. The reverse reaction is undertaken by a large family of enzymes termed deubiquitylases or DUBs, and many of these have been shown to act in key pathways for virus infection such as the immune system and vesicle trafficking. However, the role of DUBs during alphavirus infection had not been specifically studied previously. In on-going experiments in the research group a DUB siRNA library screen had been performed against SFV infection of HeLa cells. In this thesis, the hits from this screen which when depleted lead to an increase in cell viability (and presumed decreased in SFV replication) were further validated, with the long term aim to identify potential targets for therapeutic intervention. This work was expanded to focus on the DUB MYSM1 and its role during alphavirus infection.

7.2 Deconvolution of a DUB siRNA screen against SFV infection

RNAi libraries have previously been employed in unbiased reverse genetic screens to identify host cell factors that participate in viral infection and lead to the discovery of novel mechanisms of both host antiviral defences and the manipulation of host factors required for infection (reveiwed by Ramage & Cherry, 2015; Brummelkamp *et al*., 2003; Tauriello *et al*., 2010; Nijman *et al*., 2005). Pathway specific siRNA libraries have also been utilised to investigate specific cellular process. DUB siRNA libraries have been used in many different circumstances from cancer, cell cycle, immune pathways and endocytosis (Qin *et al*., 2015; Brummelkamp *et al*., 2003; Gewurz *et al*., 2012; Liu *et al*., 2009) . However, to date there have been no published data showing DUB siRNA library screens against virus infection. The DUB siRNA library used in the screen against SFV infection carried out prior to the start of this thesis was a custom designed library from Qiagen, which consisted of siRNAs pools against 92 known or predicted DUBs representing the five families known at the time. Each pool contained 4 individual siRNAs targeting each specific DUB. The original screen utilised a readout based on cell viability. SFV infection is known to induce rapid cytopathic effect on cells, with greater than 50% reduction in viability after 12 hour infection with SFV at a MOI of 1-2. The cell viability assay was established to measure each step in infection or to assess viral spread to neighbouring cells. Pohjala and colleagues have reported that using a quantitative cell viability assay to screen for proteins involved in SFV replication was effective assay (Pohjala *et al*., 2008). Thus, depletion of DUBs was predicted to either increase or decrease viability. For this thesis, DUBs which when depleted resulted in an increase in cell viability after SFV infection were of central interest. These DUBs were assumed to play a pro-viral role, and thus could potentially be targets of therapy. This lead to the identification of 12 candidate DUBs, These were USP1, USP4, USP5, USP34, USP45, USP46, USP53, UCHL1, OTUD6A, MYSM1, JOSD2 and BRCC3 (see section 3.1, Figure 3.1). The screen also identified a number of DUBs which when depleted lead to decreased cell viability after SFV infection, presumed to be due to increase SFV replication. These hits were being followed up in a separate study.

Although siRNA screens are a powerful tool, there are a number of limitations with this approach. The most significant factor which must be considered is the potential for false negatives due to inefficient siRNA knockdown and false positives as a result to siRNA off-target effects (Mohr *et al*., 2010; Campeau & Gobeil, 2011; Boutros & Ahringer, 2008). To reduce false negative results, the original DUB siRNA screen employed pools of four siRNAs against each DUB target rather than a single siRNA. This would compensate for potential poor knockdown efficiencies of individual siRNAs, (König *et al*., 2007). The screen was also carried out on two independent occasions, which would help to reduce both false positive and negative results (Campeau & Gobeil, 2011). However, it is necessary to consider the potential of siRNA off-target effects and steps must be taken to confirm and validate data from siRNA screens. Thus, it was important to validate the 12 candidate DUBs using secondary assays. The deconvolution studies involved using each siRNA from the pool of 4 individually, as well as the pool of 4, and repeating the cell viability study.

The original hits were considered validated if the original pool, and two or more of the individual siRNAs showed a similar phenotype to that seen in the original screen i.e. a 20% or greater increase in cell viability after SFV infection. The value of 20%, rather than the 30% defined cut off in the original screen, was chosen as it was thought that when the siRNAs were used individually, they may not achieve the same level of effect as when used as a pool of four. In addition, it was thought that a 20% difference also represented a significant effect on virus due to DUB depletion. The data present in chapter 3 revealed that, by using these criteria strictly, only three of the DUBs deconvoluted successfully, these were MYSM1, USP53 and JOSD2 (Figure 3.11 and Table 3.2). In a number of cases two or more individual siRNAs were positive but surprisingly the original pool did not repeat the result seen in the screen. Several factors may explain the lack of overlap between the results of the preliminary screen and the deconvolution. It is possible that there may have been technical issues when generating the pools to be used in this study, as the original screen pools were no longer available. Furthermore, a study by Bushman and colleagues analysed data from a screen performed in

duplicate with the same experimental conditions and estimated that comparison of these data sets yields only 50% overlap (Bushman *et al*., 2009). Thus, suggesting that there inherent factors which may prevent duplication of data with siRNA screens and validations. Three important variables that could potentially influence the data from these deconvolution experiments are poor transfection efficiency, poor knockdown efficiency of the target transcript and toxicity due to siRNA treatment (either due to depletion of the specific DUB or off-target effects) (Mohr *et al*., 2010; Cherry, 2009; Panda & Cherry, 2012). Using this experimental approach taken for these validation experiments it was not possible to monitor the target knockdown efficiency (this was addressed in Chapter 4). However, steps were included in the protocol to monitor both transfection efficiency and toxicity issues (see section 3.3).

Transfection efficiency was monitored by utilising the ALLStars HsDeath siRNA, which induces a high degree of cell death by targeting and depleting essential human survival genes (Moser *et al*., 2013). HsDeath siRNA induced cell death was monitored visually by light microscopy after 72 hrs knockdown, and in all experimental data used in this chapter, there was estimated to be a reduction in cell confluence of 80-90% in all experiments, with increased numbers of floating cells observed. Thus, suggesting successful transfections. An addition transfection control was utilised, whereby an siRNA pool for OTUD7A was included throughout the cell viability deconvolution experiments. This was included as a quality control for the data in the original screen, where the OTUD7A pool lead to a decrease in cell viability, and so also served to monitor transfection efficiency. In all deconvolution experiments, cells treated with OTUD7A siRNA pool resulted in the expected decrease in cell viability after SFV infection (sections 3.3.1 to 3.3.5). The effect of siRNA induced toxicity, either due to the direct effect of depletion of the DUB or by off-target effects, was monitored as part of the experimental approach. The duplicate wells that were not infected with virus were assayed for viability of the cells. This was used to determine the percentage change in infected versus uninfected. However, it also allowed for a direct measurement of the toxicity induced by siRNA treatment. In general, the percentage viability was greater than 60% in most cases. Beyond these

potential off-target effects, another factor that may have influenced the data, although unlikely in this setting, was measurement error intrinsic to the alternative readouts used. Two different reagents were utilised to assess changes in cell survival resulting from the depletion DUBs and infection with SFV. The MTS assay was utilised in the preliminary screen while, CellTiter-Glo assay was utilised in the deconvolution study and hence this may account for variation in the results (Hao *et al*., 2013). In addition, trypan blue exclusion was not used for all cell counts. As such, the number of viable cells in each experiments may have varied.

Taking all these factors into consideration, the DUBs for which two individual siRNAs gave positive data, but the pool did not repeat, should not be automatically ruled out. These were the USP4, USP34, USP46 and BRCC3 pools. In addition, as the deconvolution data was presented as one of two independent experiments to obtain data that could be assessed for significance would have required the assay to be performed on three or more independent occasions. However, it was decided that these issue could be addressed by undertaking a deconvolution approach utilizing a secondary readout.

7.3 Utilising a secondary readout to confirm roles for DUBs during Alphavirus infection

As described for Chapter 3, the siRNA pools for the 12 selected hits from the original DUB siRNA screen were deconvoluted utilising the assay readout as in the original screen (i.e. change in cell viability). To further support a role for these DUBs during SFV infection, a secondary assay was utilised to repeat the deconvolution and subsequent validation of the group of 12 DUBs. The secondary readout to be used was monitoring the effect of DUB silencing on levels of SFV RNA genome at 8 hours post-infection. It was assumed that the decrease in cell viability observed in the original screen and the deconvolution assays in chapter 3 reflected decreased virus replication. In the experiments undertaken only the four individual DUB siRNAs were used, and not the pools. This approach had a dual purpose. In addition to validating

the DUB hits, based on a direct effect on SFV replication, it also allowed for the efficiency of each siRNA at reducing DUB transcript levels to be monitored.

Before carrying out this secondary assay, the normal transcript levels of each of the 12 DUBs in untreated HeLa cells were measured by both E-P and Q-PCR. This was done to confirm transcription of the selected DUBs in the HeLa cells, and determine the transcript baseline level, to aid interpretation of the efficiency of siRNA knockdown. Of the 12 DUBs tested, only OTUD6A was not detected by either E-P or QPCR, suggesting that OTUD6A was either not expressed in the HeLa cells being used in this project, or the transcript was at undetectable levels. Transcripts were detected for the remaining 11 DUBs, at varying levels of abundance (Figure 4.1). The European Bioinformatics Institute (EMBL-EBI) gene atlas indicates that OTUD6A is expressed in HeLa cells (Kapushesky *et al*., 2009). However, OTUD6A was not investigated further by this secondary readout, as it appears to not be expressed at significant levels and would have been difficult to prove siRNA mediated knockdown. It is possible that it does play a role during SFV infection that still needs to be determined. It may be that SFV infection itself can induce up regulation of the OTUD6A transcript and protein, to enhance replication. This has been observed in other viral infections (EBV, Hepatitis virus and Influenza virus). However, in other projects in the laboratory looking at the effect of SFV infection on the DUB transcriptome in HeLa cells, no increase in OTUD6A mRNA was observed (M Wali, personal communication). Furthermore, in separate experiments commercially available antibodies to OTUD6A where tested but not shown to work (N Blake, unpublished), so could not be used to look at protein levels in HeLa cells.

The criteria defined for identifying a ‘hit’ using this secondary readout was that at least two of the individual siRNAs resulted in a reduction in SFV RNA by at least 50%. In addition, these siRNAs should also lead to a reduction of the DUB mRNA, again by at least 50%. Of the 11 DUBs screened, in six cases either no or only 1 siRNA lead to a reduction in SFV RNA levels. These were USP34, USP45, USP46, USP53, UCHL1 and BRCC3 (Figures 4.4C, 4.5A, B and C, 4.6A and 4.7A). Surprisingly, for each of these DUBs either 3 or all 4 of the siRNAs were shown to lead to a reduction in mRNA transcript.

This perhaps does not reflect directly on the level of protein, and it may be that for some of the DUBs in these experiments there was not a sufficient turnover of protein such that there was still active DUB present. It has been reported by several groups that mRNA levels cannot be used as substitutes for corresponding protein levels (Eng *et al.,* 2004; Vogel *et al.,* 2010; Lundberg *et al.,* 2010; Schwanhausser *et al.,* 2011). Thus, for each of these DUBs this would have to be experimental verified, for example by western blotting with suitable antibodies. However, as the overall goal of the screen was to identify candidates to characterise further (see below), this experimental work was not pursued. In some cases, a significant increase in SFV RNA levels was observed for more than one siRNA, with corresponding decrease in DUB transcript, such as USP46 and UCHL1. However, although this may be of interest, this did not fit in the original hypothesis and these results were not followed up in this thesis.

Five DUBs were shown to fulfil the criteria defined for the assay used in this chapter, where at least 2 or more siRNAs lead to decreases in SFV RNA levels of 50% or more, with corresponding decrease in DUB transcript levels. These were USP1, USP4, USP5, JOSD2 and MYSM1. However, when the data from both the cell viability deconvolution assays (Chapter 3) and the secondary readout (Chapter 4) were analysed together, limited overlap between DUBs identified was observed. Only JOSD2 and MYSM1 fully complied with the criteria set (see Table 4.2). JOSD2 is a member of the Josephins DUB family, with nothing currently known regarding function roles. It is predicted to be localised mainly in the cytoplasm, but is also found in the nucleus (Urbe *et al*., 2012). The paucity of published literature on JOSD2 makes it an attractive candidate to follow up. However, the second DUB which full filled the selection criteria, MYSM1, was selected for further follow up studies. MYSM1 is a member of the JAMM/MPN+ DUB metalloprotease family (Clague *et al*., 2013). MYSM1 was originally characterised as a histone H2A deubiqutinase, important for the removal of Ub from chromatin to influence regulation of a range of process including transcription and the DNA damage response (reviewed in Belle and Nijnik, 2014). A range of studies utilising MYSM1 knockout mice revealed an important role in hematopoietic stem cell

differentiation and maintenance (Jiang *et al*., 2011; Nandakumar *et al*., 2013; T. Wang *et al*., 2013; Won *et al*., 2016). At this point of the thesis no data was available to indicate a role related to viral infection (see later), and the data generated at this stage suggested MYSM1 could also act as a pro-viral DUB during SFV infection of HeLa cells.

USP4 was also of potential interest as it fulfilled the parameters where transfection with two individual siRNAs lead to both an increase in cell viability and a reduction in SFV RNA levels (Figures 3.6A and 4.4A). However, the siRNA pool did not duplicate the original result when used in the cell viability experiments described in chapter 3. Given that two of the individual siRNAs reproduced the anticipated phenotype, this may have been due to technical reason within this experiment. However, this was not repeated. Nevertheless, although not followed up during this thesis, the data was suggestive of USP4 playing a pro-viral role during SFV infection and thus may warrant further attention. However, this implied role for USP4 was in contrast to data from Wang and colleagues (Wang *et al*., 2013). This research group reported that USP4 was down-regulated during infection with VSV or by treatment of cells with RIG-1 stimuli [Poly (I:C)]. Further work showed that USP4 enhanced RIG-1 mediated expression of IFNβ, inducing antiviral state in cells. The discrepancy between this study and the preliminary data in this thesis is unclear and could be further investigation.

7.4 MYSM1 appears to play different roles in different cell types

Based on the data from chapters 3 and 4, MYSM1 was selected for further characterisation of its role during alphavirus infection. Firstly, investigation of the effect of depletion of MYSM1 by siRNA treatment in HeLa cells on both SFV and CHIKV replication was studied in more detail. This was then extended to a murine embryo fibroblast line with a MYSM1 genetic knockout (Nijnik *et al*., 2012), again with both SFV and CHIKV. Fibroblasts were chosen to reflect a cell line known to be relevant for CHIKV infection (Schilte *et al*., 2010).

For SFV infection of HeLa cells, the effect of depletion of MYSM1 on virus replication (QPCR of viral RNA) was repeated on three independent occasions to confirm that the result seen earlier was statistically significant. Again, depletion of MYSM1 by 3 out of the 4 siRNAs lead to a significant reduction in virus replication (Figure 5.1B). The individual siRNA that did not lead to a reduction was siRNA 4. However, this did lead to an increase in cell viability, likely to be due to an off-target effect. This data was supported by immunoblotting for MYSM1 in the depleted cells, which showed a reduction in MYSM1 protein level of 85-95% with the siRNAs 1 and 3, but less depletion with siRNA 2. Analysis of SFV virus released into the supernatant of infected cells also showed a small but consistent reduction in SFV titres (after MYSM1 depletion) (Figure 5.1C). Depletion of MYSM1 also lead to a significant reduction in virus plaque formation (Figure 5.5). Similar results were also observed when these experiments were extended to CHIKV infection (Figures 5.6 and 5.7). Taken together, these data implied that in HeLa cells MYSM1 is required for efficient alphavirus infection. How it exerted this strong pro-viral effect was not directly obvious at this stage. However, data from Panda and colleagues (Panda *et al*., 2015) provided insight into this. This manuscript reported that MYSM1 acted as a negative regulator of PRR signalling, via inactivation of TRAF3 and TRAF6 by removal of ubiquitin chains. In there model, this lead to reduction in replication of VSV and Listeria monocytogenes. Normally, E3 ligases activate TRAF3/6 by addition of K63 linked polyubiquitin chains, and leading to production of IRF3/7 and NF-kβ. This subsequent causes induction of pro-inflammatory cytokines and type 1 IFNs (Liu *et al*., 2013; Abe & Barber, 2014). Thus, in the absence of MYSM1 there is overproduction of cytokines such as IFNβ, which induces a strong anti-viral environment. Thus, it appears a key role of MYSM1 is to prevent pathology induced due to over production of IFNs and pro-inflammatory cytokines. In this role MYMS1 is one of an increasing number of DUBs that are involved in control of IFN signalling e.g. A20 and CYLD (Trompouki *et al*., 2003; Jono *et al*., 2004; Lin *et al*., 2006). The fact that MYSM1, which to date had primarily been thought of as a nuclear DUB responsible for epigenetic changes, was implicated in regulation of cytoplasmic signalling was unexpected. However, the authors go on to show that there is transient expression of a cytoplasmic

version of MYSM1, which must then interact with the TRAFs (Panda *et al*., 2015).

The implication of this data tied in well with the observations in this thesis with respect to the role of MYSM1 during infection of HeLa cells, where there was decreased SFV and CHIKV replication in the absence of MYSM1. The prediction would be that this was due to increased induction of IFNβ primarily. Alphaviruses are very sensitive to IFNs and pre-treatment of cells with IFN previous to infection inhibits replication (Deuber & Pavlovic, 2007). Findings by Reynaud *et al* suggest that IFNβ pre-treatment could block alphavirus infection before the beginning of RNA replication but did not affect on the steps of virus entry and virion disassembly (Reynaud *et al*., 2015). An *in-vivo* study showed that inoculation of mice with SFV results in a high-titre plasma viraemia, which triggers an IFN response (Bradish & Titmuss, 1981). In mice which lack of a type I IFNs response, SFV spreads rapidly to infect many tissues, and animals die within 48 hr post-infection (Fragkoudis *et al*., 2007).

To extend this work to a cell type relevant to CHIKV infection, the role of MYSM1 during infection of fibroblast was investigated. This was aided by the availability of MYSM1 KO MEFs (and corresponding WT). The first experiments were carried out with SFV, and surprisingly in SFV-infected MEFs there was a clear increase in CPE seen in the KO cells at 24 hr post-infection (Figure 5.9). The clear explanation for this initial observation was that SFV replicated more efficiently, inducing more cytotoxicity, in the MEFs lacking the MYSM1 protein. This was supported by increased SFV RNA levels found in the KO cell line (Figure 5.10A). A similar increase in viral RNA were observed when CHIKV was used to infect the MYSM1 KO MEFs (Figure 5.10B). It was possible that this contrasting data (HeLa v MEF), may be due to the technical approaches taken i.e. siRNA depletion v genetic KO. To address this, the human fibroblast line MRC-5 was used, and after deletion of MYSM1 with siRNAs, cells were infected with SFV and RNA levels monitored. In support of the data in the MEF cells, depletion of MYSM1 in MRC5 cells also lead to an increase in SFV RNA levels (Figure 5.11).

Taken together, these data suggest that MYSM1 plays a different role during alphavirus infection of different cell types i.e. HeLa cells versus fibroblasts. Whether this also applies to other virus remains to be determined. It should also be noted that in the study by Panda and colleagues, they used murine macrophages lines, both the established line RAW 264.7 with shRNA depletion, and BMDMs from KO mice (Panda *et al.,* 2015). Therefore, using comparable approaches to remove MYSM1 from the system. Thus, this may reflect a fundamental difference the role of MYSM1, which relates to the cell lineage. However, more important was to determine if there was a difference in the induction of type 1 IFNs and pro-inflammatory cytokines in HeLa cells compared to MEFs in the absence of MYSM1.

7.5 The role of MYSM1 in pattern recognition receptor signalling in different cell background

The aim of chapter 6 was to investigate if MYSM1 plays a role PRR signalling in response to SFV and CHIKV replication, and if it had a differential role in HeLa and fibroblast cell lines. Initially using HeLa cells and agonists of PRRs (LPS, Poly (I:C) and Poly (I:C)/LV), the ability to respond via specific receptors was studied. This data showed that there was enhanced induction of IFNα by Poly (I:C) treatment only, and even this was at a very low level (Figure 6.1B). Whereas IFN β was induced by treatment with all three PRR agonists (Figure 6.1C). HeLa cells also responded to Poly (I:C) to induce TNFα (Figure 6.1D). Whereas lL1β was not detectable. TLR3 recognizes Poly (I:C) in the endolysosomes, while TLR4 recognizes LPS on the cell surface. Both resulting in the induction of pro-inflammatory cytokine genes and type I IFNs (Blasius & Beutler, 2010; Takeuchi & Akira, 2010). In contrast, RLR (RIG-I/MDA-5) recognizes both Poly (I:C) when delivered to the cytoplasm (in this case as Poly (I:C)/LV) and leads to the induction of type I IFNs (Kato *et al*., 2011). These experiments indicate that TLR3 and RLR are expressed in HeLa cells but not TLR4. However, many studies have been reported that RLR, TLR3 and TLR4 are expressed in HeLa cells after viral infection or treatment with the mimic of viral RNA and LPS (Jiang *et al*., 2004; Matsumiya & Stafforini, 2010). Thus, suggesting that their activation may play a role in the detection

of SFV and CHIKV infection, to induce expression of pro-inflammatory cytokine and type I IFNs. When HeLa cells with infected with SFV this lead to the induction of the type I IFN and pro-inflammatory cytokine. An infection experiment over 3, 6, 9, 12, 18 and 24 hr highlighted the time course of induction of the cytokines (Figure 6.2). The end point PCR data revealed that strong IFN-α/β and TNF-α PCR bands were detectable from 9 hpi onwards. Whereas, for IL1β a faint band was seen from 3 hpi onwards, with the exception of 6 hr where no product was seen, and demonstrated a dramatic increase at 18 and 24 hpi. It is likely that the lack of product at 6 hr timepoint was a technical error. ACTB PCR bands were decreased from 9 hpi onwards. This temporal reduction in ACTB gene expression is consistent with other previous findings provide that SFV infection suppresses global cellular gene transcription (Breakwell *et al*., 2007; Barry *et al*., 2009), a phenomenon also observed with other alphaviruses like SIN (Gorchakov *et al*., 2005; Trobaugh & Klimstra, 2017). These experiments would have been better analysed by QPCR to accurately quantify the induction, and also should have been undertaken with CHIKV. Nevertheless, this showed that the HeLa cells being used where capable of producing cytokines in response to infection.

The studies were extended to look at the induction of IFNα, IFNβ, TNFα and IL1β after infection with SFV and CHIKV, in the absence of MYSM1 in HeLa cells. Unfortunately, there was no consistent pattern from these experiments, and overall there did not appear to be strong induction of the cytokines tested (Figures 6.3 to 6.5). Thus, it is very difficult to make any direct conclusions from these experiments. Why there was poor induction is unclear, given that in Figure 6.1 there was evidence of induction particular of IFNβ by poly (I:C)/LV, and SFV infection of HeLa cells results in enhance bands for IFNβ and TNFα particular (Figure 6.2). Although that data was not quantified by QPCR. It is unclear if the time point selected, 8 hr, was the most appropriate for detection of cytokine transcripts. The time course study in Figure 6.2 included an 6 hr and 9 hr point, and based on that data it was assumed that transcript would be seen at 8 hr, and any difference would be detectable.

The data derived from analysis of the MEF cells was slightly clearer. The MYSM1 KO MEF cells were also analysed for their ability to respond to

LPS, Poly (I:C) and Poly (I:C)/LV (Figure 6.6). Although only a single experiment, this provided very clear data. There was a much reduced IFNα and β response in the KO line, particularly in response to poly (I:C) delivered to the cytoplasm (via poly (I:C)/LV), which is a good model for SFV and CHIKV infection. The data was less convincing for TNFα and IL1β. This could imply that MYMS1 may not be involved in this part of the signalling pathway in these cells, which contrast directly with the data in Panda et al for macrophages (Panda *et al*., 2015). However, it should be noted that overall there was a low induction for TNFα and IL1β in response to the all the stimuli. When these cell were then analysed for the effect of KO of MYSM1 on responses to SFV and CHIKV, there was contrasting data (Figure 6.7). For SFV there was a clear reduction in the IFNα and β response in the KO line, but with CHIKV there was no evidence of any differences, and in fact very poor induction. Whereas, the data for CHIKV infection was less conclusive, with overall poor induction of cytokines and no difference due to MYSM1.

The data for SFV support the premise that in MEFs the increased viral RNA levels are due to poor induction of type 1 IFNs in the absence of MYSM1. Why there was poor induction of IFNs in response to CHIKV infection in the WT cells is not clear. Due to the lower titre of CHIKV virus stocks, a lower MOI of infection was used compared to SFV. However, this was still a reasonable virus input, 2 MOI, and would be expected to stimulate the various PRR pathways. Although, this may lead to lower concentrations of genomic RNA and possible result in decreased levels of intracellular ssRNA, as well as the generation the intermediate dsRNA. Thus, lead to a weaker activation of antiviral mRNA levels. It has been reported that the IFN gene expression response is proportional to the viral RNA load (Fragkoudis *et al*., 2007). Furthermore, CHIKV is known to inhibit STAT phosphorylation and translocation to the nucleus to prevent IFN-α/β upregulation (Fros *et al*., 2010). It may be that there are distinct differences in the signalling pathways between SFV and CHIKV data. It has been reported that infected fibroblasts respond to CHIKV infection via a Cardif-dependant sensor (i.e. RIG-I and MDA5), producing type I IFNs and limiting infection (Schilte *et al*., 2010). However, it has been reported that dendritic cells infected by SFV, result in the production

of dsRNA that may engage TLR3 (Schulz *et al*., 2005). This is pertinent, as it indicates that the CHIKV sensor and in addition the host response in viral pathogenesis may be different from other alphaviruses (MacDonald & Johnston, 2000; Ryman *et al*., 2005; Shabman *et al*., 2007). Recently, It has been observed that infected keratinocytes respond to CHIKV infection, producing a highly upregulated of type III IFN (IFN-λ) and limiting infection (Bernard *et al*., 2015). Regardless of the reasons for the poor induction, no difference was observed between the WT and KO lines despite a clear phenotype when CHIKV RNA was measured.

In direct contrast, the lack of MYSM1 in MEFs resulted in much reduced levels of the ISG Mx1, for both SFV and CHIKV (Figure 6.8). This was also observed for the PRR agonists. Induction of ISGs can be considered to be an indirect measure of bioactive IFNβ. While Mx1 was the only ISG measured in this study, it is know that a number of ISGs, including Mx1, have important anti-viral roles in the control of alphavirus infection (Ryman & Klimstra, 2008; Reynaud *et al*., 2015). For SFV, Mx1 confers resistance (Landis *et al*., 1998), meanwhile ISG15 plays a critical role in controlling SIN (Lenschow *et al*., 2007) and viperin has been shown to be important during CHIIKV infection (Teng *et al*., 2012). Although normally requiring signalling via IFNβ, some ISGs are directly induced by viral infection in the absence of IFN production (Sen & Peters, 2007). This may be relevant for the CHIKV experiments here, although this has not been reported. The requirement for induction of IFNβ fits with the SFV data present here i.e. greater induction in the WT, and again contrasts directly with the data from Panda. In that study, they also measure Mx1, and as expected saw an increase in transcript levels.

The analysis of IFNα, β TNFα and IL1β was also undertaken for the MRC-5 cells infected with SFV after MYSM1 depletion with siRNA. This data was even more confusing, as there were apparent increases in IFNs, a decrease in TNFα and mixed data for IL1β. However, again over all the levels of induction were very low and thus difficult to make any specific conclusion. The reasons for the confounding results for the fibroblast lines is not clear. It has been shown that cultured MRC-5 and mouse skin fibroblasts were both permissive to CHIKV (Sourisseau *et al*., 2007). Furthermore, one study

concluded that primary human foreskin fibroblasts, MRC-5 and MEFs were sensitive to infection with CHIKV at low MOI (Schilte *et al*., 2010). Also, it should be noted that the MRC5 line used in this study had been transformed with SV40. It is possible that immortalized and transformed MRC-5 cells with SV40 progressively accumulate changes in gene expression and that could be effected negatively on the mRNA levels of the gene under studying (Gordon *et al*., 2014). Overall, the findings presented in Chapter 6 do not provide conclusive answers for the role of MYSM1 in the induction of type 1 IFNs and pro-inflammatory cytokines in the cell lines tested, and does not provide a clear rational for the differences between HeLa and fibroblasts.

7.6 General summary

siRNA library screens have proved extremely valuable in analysing the role of individual proteins across the range of cellular process and in many virus infections (Falschlehner *et al*., 2010; Brass *et al*., 2008; Konig *et al*., 2010; Karlas *et al*., 2016). This thesis was focused on the analysis of hits from a DUB siRNA library screen carried out previously in the laboratory. The experiments described focused on the deconvolution siRNA pools for the 12 DUB hits, and the subsequent follow up experiments with one strong candidate DUB from this list, MYSM1. A number of important lessons came from the deconvolution analysis of the siRNA pools. Firstly, the failure to duplicate the results from the original screen was of concern. Only three of these hits deconvoluted based on the same assay readout and criteria used in this study (MYMS1, USP53 and JOSD2). Secondly, the lack of overlap between the two independent screens used in this assay lead to a reduction in the number of potential candidates for further analysis to two (MYSM1, JOSD2). Although, as described USP4 could also be included in this group. These may be seen as inherent risks with siRNA studies, and there are many reasons that may contribute to this, as describe earlier in the discussion. However, with any siRNA screen and list of candidate hits, the need to validate the data using appropriate systems such as alternative siRNAs, knock-down cells lines and rescue experiments is critical. Nevertheless, siRNA screens have proved extremely valuable in identify host cell factors involved in virus replication and

this thesis has provided data in the context of cellular DUBs. The work with MYSM1 generated interesting data, implying a role during virus infection that appeared to depend on the cell type being infected. As yet it is unclear what the effector mechanisms are that contribute to these observations and a number of key experiments remain to be carefully completed to answer this questions.

7.7 Future work

There are a number of areas that could be followed up from this work, in addition to the many of unanswered questions regarding the role of MYSM1. Much of this work would be to carry out a range of experiments to fully clarifying and support the role of MYSM1 during virus infection of various cell lines. Immunofluorescence and/or FACS analysis of cells would have provided information about whether there was an inverse correlation between MYSM1 depletion and virus replication in an individual cell basis. In addition, Immunofluorescence studies would provide data on the location of MYSM1 in HeLa and fibroblast cells. If this differed, the data may have provided an explanation of the differential effects of MYSM1 depletion in HeLa vs fibroblast cells on SFV and CHIKV replication. Many of these experiments would be to repeat the work described in Chapter 6, to obtain more reliable and convincing data. The experiments investigating the role of MYSM1 in the regulation of type 1 IFNs and pro-inflammatory cytokines in different cell lines needs to be repeated. All of the IFN and pro-inflammatory readouts were RT-qPCR. These should be repeated with ELISAs or Luminex assays to determine concentrations of these cytokines at the protein level. To fully confirm a role for MYSM1, as with any depletion or knockout study, rescue experiments should be undertaken where the functional protein is re-introduced into the system. Mapping the functional region of the MYSM1 protein would also be important. As would confirming that the enzymatic activity was required, using catalytically inactive mutants.

In addition to the work with MYSM1, it would also be of interest to follow up the other candidates that were validated in chapters 3 and 4. These were

JOSD2 and USP4, although it is noted that USP4 was not considered fully validated as the siRNA pool did not repeat the phenotype as originally observed. As described, a role for USP4 during virus infection has been described (Wang *et al.,* 2013). However, this was not in agreement with the proposed role during alphavirus infection. A number of simple experiments could be undertaken to determine of USP4 was worthy of further study in this system. JOSD2 presents a clean slate, in that there is no published data on this DUB. This would make JOSD2 an attractive to begin basic experiments to characterise its role during alphavirus infection.

The overall goal of this type of work is to try to identify druggable proteins that it may be possible to target during virus infection. DUBs are heavily studied as drug targets in cancer, and a number of drugs are under investigation (Tian *et al*., 2011; Davis & Simeonov, 2015). This makes the continued characterisation of the role of DUBs during virus infection a worthwhile objective.

Bibliography

Abe, T. & Barber, G.N., 2014. Cytosolic-DNA-Mediated, STING-Dependent Proinflammatory Gene Induction Necessitates Canonical NF-kB Activation through TBK1. *JVI*, 88(10), pp.5328–5341.

Akahata, W. et al., 2010. A virus-like particle vaccine for epidemic Chikungunya virus protects nonhuman primates against infection. *Nature Medicine*, 16(3), pp.334–338.

Akahata, W. & Nabel, G.J., 2012. A specific domain of the Chikungunya virus E2 protein regulates particle formation in human cells: implications for alphavirus vaccine design. *Journal of virology*, 86(16), pp.8879–83.

Allen, I.C. et al., 2009. The NLRP3 Inflammasome Mediates In Vivo Innate Immunity to Influenza A Virus through Recognition of Viral RNA. *Immunity*, 30(4), pp.556–565.

Alsultan, A. et al., 2014. MYSM1 is mutated in a family with transient transfusion-dependent, mild thrombocytopenia, and low NK- and B-cell counts. *Blood*, 122, pp.3844–3845.

Anthony J. Sadler and Bryan R. G. Williams, 2008. Interferon-inducible antiviral effectors Anthony. *Nat rev immunology*, 8(7), pp.559–568.

Anthony V. Nicola1, W.C.& A.H. et al., 1999. Co-translational folding of an alphavirus capsid protein in the cytosol of living cells. *Nature cell biology*, 1(6), pp.341–345.

Arif, S. et al., 2016. Short Article MINDY-1 Is a Member of an Evolutionarily Conserved and Structurally Distinct New Family of Deubiquitinating Enzymes Short Article MINDY-1 Is a Member of an Evolutionarily Conserved and Structurally Distinct New Family of Deubiquitinating Enz. *Molecular Cell*, 63(1), pp.146–155.

Ashbrook, A.W. et al., 2014. Residue 82 of the Chikungunya Virus E2 Attachment Protein Modulates Viral Dissemination and Arthritis in Mice. *Journal of Virology*, 88(21), pp.12180–12192.

Atkins, G.J., Sheahan, B.J. & Dimmock, N.J., 1985. Semliki Forest virus infection of mice: a model for genetic and molecular analysis of viral pathogenicity. *J Gen Virol*, 66 (Pt 3)(1985), pp.395–408.

Atkins, G.J., Sheahan, B.J. & Liljeström, P., 1999. The molecular pathogenesis of Semliki Forest virus: A model virus made useful? *Journal of General Virology*, 80(9), pp.2287–2297.

Bagchi, P. et al., 2013. Rotavirus NSP1 inhibits interferon induced non-canonical NF??B activation by interacting with TNF receptor associated factor 2. *Virology*, 444(1–2), pp.41–44.

Balakirev, M.Y. et al., 2002. Deubiquitinating Function of Adenovirus Proteinase. *Journal of Virology*, 76(12), pp.6323–6331.

Balistreri, G. et al., 2014. The Host Nonsense-Mediated mRNA Decay

Pathway Restricts Mammalian RNA Virus Replication. *Cell Host Microbe*, 16, pp.403–411.

Barretto, N. et al., 2005. The Papain-Like Protease of Severe Acute Respiratory Syndrome Coronavirus Has Deubiquitinating Activity The Papain-Like Protease of Severe Acute Respiratory Syndrome Coronavirus Has Deubiquitinating Activity. *Journal of Virology*, 79(24), pp.15189–98.

Barry, G. et al., 2009. PKR acts early in infection to suppress Semliki Forest virus production and strongly enhances the type I interferon response. *Journal of General Virology*, 90(6), pp.1382–1391.

Berezutskaya, E. et al., 1997. Differential regulation of the pocket domains of the retinoblastoma family proteins by the HPV16 E7 oncoprotein. *Cell growth & differentiation : the molecular biology journal of the American Association for Cancer Research*, 8(12), pp.1277–86. \

Bergink, S. & Jentsch, S., 2009. Principles of ubiquitin and SUMO modifications in DNA repair. *Nature*, 458, pp.461–467.

Bernard, E. et al., 2010. Endocytosis of chikungunya virus into mammalian cells: Role of clathrin and early endosomal compartments. *PLoS ONE*, 5(7), pp.1–11.

Bernard, E. et al., 2015. Human keratinocytes restrict chikungunya virus replication at a post-fusion step. *Virology*, 476, pp.1–10.

Blasius, A.L. & Beutler, B., 2010. Intracellular Toll-like Receptors. *Immunity*, 32(3), pp.305–315.

Boggs, W.M. et al., 1989. Low pH-dependent Sindbis virus-induced fusion of BHK cells: differences between strains correlate with amino acid changes in the E1 glycoprotein. *Virology*, 169, pp.485–488.

Bordi, L. et al., 2015. Chikungunya and Its Interaction With the Host Cell. *Current Tropical Medicine Reports*, 2(1), pp.22–29.

Van Bortel, W. et al., 2014. Chikungunya outbreak in the Caribbean region , December 2013 to March 2014 , and the significance for Europe. *Eurosurveillance*, 19(13), pp.1–11.

Boutell, C. & Everett, R.D., 2003. The herpes simplex virus type 1 (HSV-1) regulatory protein ICP0 interacts with and ubiquitinates p53. *Journal of Biological Chemistry*, 278(38), pp.36596–36602.

Boutell, C., Sadis, S. & Everett, R.D., 2002. Herpes Simplex Virus Type 1 Immediate-Early Protein ICP0 and Its Isolated RING Finger Domain Act as Ubiquitin E3 Ligases In Vitro. *Journal of virology*, 76(2), pp.841–850.

Boutros, M. & Ahringer, J., 2008. The art and design of genetic screens: RNA interference. *Nature reviews. Genetics*, 9(7), pp.554–66.

Boyer, L.A., Latek, R.R. & Peterson, C.L., 2004. The SANT domain: a unique histone-tail-binding module? *Nature Reviews Molecular Cell Biology*, 5(2), pp.158–163.

Bradish, C.J., Allner, K. & Maber, H.B., 1971. The virulence of original and derived strains of Semliki forest virus for mice, guinea-pigs and rabbits. *Journal of General Virology*, 12(2), pp.141–160.

Bradish, C.J. & Titmuss, D., 1981. The effects of interferon and double-stranded RNA upon the virus-host interaction: Studies with togavirus strains in mice. *Journal of General Virology*, 53(1), pp.21–30.

Brandler, S. et al., 2013. A recombinant measles vaccine expressing chikungunya virus-like particles is strongly immunogenic and protects mice from lethal challenge with chikungunya virus. *Vaccine*, 31(36), pp.3718–3725.

Branigan, E. et al., 2015. Structural basis for the RING-catalyzed synthesis of K63-linked ubiquitin chains. *Nature Structural & Molecular Biology*, 22, pp.597–602.

Brass, A. et al., 2008. Identification of Host Proteins Required for HIV Infection Through a Functional Genomic Screen. *Science*, 319 (921), pp.921–26.

Brass, A.L. et al., 2009. The IFITM Proteins Mediate Cellular Resistance to Influenza A H1N1 Virus , West Nile Virus , and Dengue Virus. *Cell*, 139(7), pp.1243–1254.

Breakwell, L. et al., 2007. Semliki Forest virus nonstructural protein 2 is involved in suppression of the type I interferon response. *Journal of virology*, 81(16), pp.8677–8684.

Bréhin, A.C. et al., 2009. The large form of human 2′,5′-Oligoadenylate Synthetase (OAS3) exerts antiviral effect against Chikungunya virus. *Virology*, 384(1), pp.216–222.

Brubaker, S.W. et al., 2015. Innate Immune Pattern Recognition : A Cell Biological Perspective. *Annu. Rev. Immunol*, 33, p.10.1–10.34.

Brummelkamp, T.R. et al., 2003. Loss of the cylindromatosis tumour suppressor inhibits apoptosis by activating NF-kappaB. *Nature*, 424(6950), pp.797–801.

Bryant, C. & Fitzgerald, K.A., 2009. Molecular mechanisms involved in inflammasome activation. *Trends in Cell Biology*, 19(9), pp.455–464.

Brzostek-Racine, S. et al, 2011. The DNA Damage Response Induces Interferon. *J Immunol*, 187(10), pp.320–331.

Burke, C.W. et al., 2009. Characteristics of alpha / beta interferon induction after infection of murine fi broblasts with wild-type and mutant alphaviruses. *Virology*, 395(1), pp.121–132.

Burt, F.J. et al., 2017. Chikungunya virus: an update on the biology and pathogenesis of this emerging pathogen. *The Lancet Infectious Diseases*, 17(4), pp.e107–e117.

Bushman, F.D. et al., 2009. Host cell factors in HIV replication: Meta-analysis of genome-wide studies. *PLoS Pathogens*, 5(5), pp.1–12.

Campeau, E. & Gobeil, S., 2011. RNA interference in mammals: Behind the

screen. *Briefings in Functional Genomics*, 10(4), pp.215–226.

Cavrini, F. et al., 2009. Chikungunya : an emerging and spreading arthropod-borne viral disease. *J. Infect. Dev. Ctries. 3(10): 744-752*, 3(10), pp.744–752.

Cervantes, J.L. et al., 2011. Phagosomal signaling by Borrelia burgdorferi in human monocytes involves Toll-like receptor (TLR) 2 and TLR8 cooperativity and TLR8-mediated induction of IFN- β. *Proc Natl Acad Sci*, 108(9), pp.3683–3688.

Chan, Y.-H., Lum, F.-M. & Ng, L., 2015. Limitations of Current in Vivo Mouse Models for the Study of Chikungunya Virus Pathogenesis. *Medical Sciences*, 3(3), pp.64–77.

Chang, L.J. et al., 2014. Safety and tolerability of chikungunya virus-like particle vaccine in healthy adults: A phase 1 dose-escalation trial. *The Lancet*, 384(9959), pp.2046–2052.

Chen, C.I. et al., 2010. Comparative pathogenesis of epidemic and enzootic Chikungunya viruses in a pregnant Rhesus macaque model. *American Journal of Tropical Medicine and Hygiene*, 83(6), pp.1249–1258.

Chen, N. et al., 2017. RNA Sensors of the Innate Immune System and Their Detection of Pathogens. *IUBMB Life*, pp.1–8.

Cheng, R.H. et al., 1995. Nucleocapsid and glycoprotein organization in an enveloped virus. *Cell*, 80(4), pp.621–630.

Cherry, S., 2009. What have RNAi screens taught us about viral-host interactions? *Current Opinion in Microbiology*, 12(4), pp.446–452.

Choi, H. et al., 1991. Structure of Sindbis virus core protein reveals a chymtrypsin-like serine proteinase and the organization of the virion. *Nature*, 354, pp.37–43.

Choi, H., Lu, G. & Lee, S., 1997. Structure of Semliki Forest virus core protein. *Proteins-Structure, Function and Genetics*, 359(September 1996), pp.345–359.

Ciechanover, A. et al., 1981. Activation of the heat-stable polypeptide of the ATP-dependent proteolytic system. *Proc Natl Acad Sci U S A*, 78(2), pp.761–765.

Ciechanover, A. et al., 1980. Characterization of the Heat- stable Polypeptide of the ATP- dependent Proteolytic System. *J. Biol. Chem.*, 255, pp.7525–7528.

Clague, M.J. et al., 2013. Deubiquitylases from genes to organism. *Physiol Rev*, 93(3), pp.1289–1315.

Couderc, T. et al., 2008. A mouse model for Chikungunya: Young age and inefficient type-I interferon signaling are risk factors for severe disease. *PLoS Pathogens*, 4(2), pp.1–12.

Couderc, T. et al., 2009. Prophylaxis and Therapy for Chikungunya Virus Infection. *The Journal of infectious diseases*, 200, pp.516–23.

Davis, M.I. & Simeonov, A., 2015. Ubiquitin-Specific Proteases as Druggable Targets. *Drug target review*, 2(3), pp.60–64.

Delaloye, J. et al., 2009. Innate Immune Sensing of Modified Vaccinia Virus Ankara (MVA) Is Mediated by TLR2-TLR6 , MDA-5 and the NALP3 Inflammasome. *PLoS Pathog.*, 5(6), pp.1–15.

Detulleo, L. & Kirchhausen, T., 1998. The clathrin endocytic pathway in viral infection. *The EMBO journal*, 17(16), pp.4585–4593.

Deuber, S.A. & Pavlovic, J., 2007. Virulence of a mouse-adapted Semliki Forest virus strain is associated with reduced susceptibility to interferon. *general virology*, 88, pp.1952–1959.

Devaraj, S.G. et al., 2007. Regulation of IRF-3-dependent innate immunity by the papain-like protease domain of the severe acute respiratory syndrome coronavirus. *Journal of Biological Chemistry*, 282(44), pp.32208–32221.

Dhanwani, R. et al., 2012. Characterization of Chikungunya virus infection in human neuroblastoma SH-SY5Y cells: Role of apoptosis in neuronal cell death. *Virus Research*, 163(2), pp.563–572.

Dong, Y. et al., 2003. Regulation of BRCC, a holoenzyme complex containing BRCA1 and BRCA2, by a signalosome-like subunit and its role in DNA repair. *Molecular Cell*, 12(5), pp.1087–1099.

Dou, H. et al., 2012. BIRC7 – E2 ubiquitin conjugate structure reveals the mechanism of ubiquitin transfer by a RING dimer. *Nature Structural & Molecular Biology*, 19(9), pp.876–83.

van Duijl-Richter, M.K.S. et al., 2015. Early events in chikungunya virus infection???from virus cell binding to membrane fusion. *Viruses*, 7(7), pp.3647–3674.

Eckels, K.H., Harrison, V.R. & Hetrick, F.M., 1970. Chikungunya virus vaccine prepared by Tween-ether extraction. *Applied microbiology*, 19(2), pp.321–5.

Edelman, R. et al., 2000. Phase II safety and immunogenicity study of live chikungunya virus vaccine TSI-GSD-218. *American Journal of Tropical Medicine and Hygiene*, 62(6), pp.681–685.

Edelmann, K.H. et al., 2004. Does Toll-like receptor 3 play a biological role in virus infections ? *Virology*, 322, pp.231–238.

Edwards, C.J. et al., 2007. Molecular diagnosis and analysis of Chikungunya virus. *Journal of Clinical Virology*, 39(4), pp.271–275.

Enesa, K. et al., 2008. NF-kB Suppression by the Deubiquitinating Enzyme Cezanne. *The Journal of biological chemistry*, 283(11), pp.7036–7045.

Eng, J. et al., 2004. Integrated Genomic and Proteomic Analyses of Gene Expression in Mammalian Cells. *Mol Cell Proteomics*, 3(10), pp.960–969.

Falschlehner, C. et al., 2010. High-throughput RNAi screening to dissect cellular pathways : A how-to guide. *Biotechnology*, 5, pp.368–376.

Faronato, M. et al., 2013. The deubiquitylase USP15 stabilizes newly synthesized REST and rescues its expression at mitotic exit. *Cell Cycle*, 12(12), pp.1964–1977.

Fazakerley, J.K., 2004. Semliki forest virus infection of laboratory mice: a model to study the pathogenesis of viral encephalitis. *Archives of virology. Supplementum*, (18), pp.179–190.

Finley, D., 2009. Recognition and Processing of Ubiquitin-Protein Conjugates by the Proteasome. *Annu. Rev. Biochem.*, 78, pp.477–513.

Forrester, N.L. et al., 2012. Genome-Scale Phylogeny of the Alphavirus Genus Suggests a Marine Origin. *Journal of Virology*, 86(5), pp.2729–2738.

Fox, J.M. et al., 2015. Broadly Neutralizing Alphavirus Antibodies Bind an Epitope on E2 and Inhibit Entry and Egress. *Cell*, 163(5), pp.1095–1107.

Fragkoudis, R. et al., 2007. The type I interferon system protects mice from Semliki Forest virus by preventing widespread virus dissemination in extraneural tissues, but does not mediate the restricted replication of avirulent virus in central nervous system neurons. *Journal of General Virology*, 88(12), pp.3373–3384.

Frias-Staheli, N. et al., 2007. Ovarian Tumor Domain-Containing Viral Proteases Evade Ubiquitin- and ISG15-Dependent Innate Immune Responses. *Cell Host and Microbe*, 2(6), pp.404–416.

Fric, J. et al., 2013. Use of human monoclonal antibodies to treat Chikungunya virus infection. *The Journal of infectious diseases*, 207(2), pp.319–22.

Frolova, E.I. et al., 2002. Roles of Nonstructural Protein nsP2 and Alpha / Beta Interferons in Determining the Outcome of Sindbis Virus Infection. , 76(22), pp.11254–11264.

Fros, J.J. et al., 2010. Chikungunya virus nonstructural protein 2 inhibits type I/II interferon-stimulated JAK-STAT signaling. *Journal of virology*, 84(20), pp.10877–87.

Fuchs, J. et al., 2017. Evolution and antiviral specificity of interferon-induced Mx proteins of bats against Ebola- , Influenza- , and other RNA viruses. *Journal of virology*.

Gaedigk-Nitschko, K. & Schlesinger, M.J., 1990. The sindbis virus 6K protein can be detected in virions and is acylated with fatty acids. *Virology*, 175(1), pp.274–281.

Gao, G. & Luo, H., 2006. The ubiquitin--proteasome pathway in viral infectionsThis paper is one of a selection of papers published in this Special Issue, entitled Young Investigator's Forum. *Canadian Journal of Physiology and Pharmacology*, 84(1), pp.5–14.

Gardner, C.L. et al., 2012. Interferon-alpha/beta deficiency greatly exacerbates arthritogenic disease in mice infected with wild-type chikungunya virus but not with the cell culture-adapted live-attenuated 181/25 vaccine candidate. *Virology*, 425(2), pp.103–112.

Gardner, J. et al., 2010. Chikungunya Virus Arthritis in Adult Wild-Type Mice. *Journal of Virology*, 84(16), pp.8021–8032.

Garoff, H., Frischauf, A.M., Simons, K., Lehrach, H., Delius, H., 1980. Glycoproteins, Nucleotide sequence of cDNA coding for Semliki Forest virus membrane. *Nature*, 288, pp.236–241.

Garoff, H. et al., 1994. Assembly and entry mechanisms of Semliki Forest virus. *Archives of virology. Supplementum*, 9, pp.329–38.

Garoff, H., Simons, K. & Renkonen, O., 1974. Isolation and characterization of the membrane proteins of Semliki Forest virus. *Virology*, 61(2), pp.493–504.

Gebhart, N.N. et al., 2015. Alphavirus RNA synthesis and non-structural protein functions. *Journal of General Virology*, 96(9), pp.2483–2500.

Gewurz, B.E. et al., 2012. Genome-wide siRNA screen for mediators of NF-κB activation. *Proc. Nat. Acad. Sci. USA*, 109(7), pp.2467–72.

Gifford GE and Heller E, 1963. Effect of Actinomycin D on Interferon Production by “Active” and “Inactive” Chikungunya Virus in Chick Cells. *Nature*, 200, pp.50–51.

Gitlin, L. et al., 2006. Essential role of mda-5 in type I IFN responses to polyriboinosinic : polyribocytidylic acid and encephalomyocarditis picornavirus. *Proc. Natl. Acad. Sci. U. S. A.*, 103, pp.8459–8464.

Glasgow, G.M. et al., 1997. Death mechanisms in cultured cells infected by Semliki Forest virus. *J Gen Virol*, 78 (Pt 7)(1997), pp.1559–1563.

Goldknopf, I.R.A.L. & Busch, H., 1977. Isopeptide linkage between nonhistone and histone 2A polypeptides of chromosomal conjugate-protein A24. *Proc Natl Acad Sci U S A*, 74(3), pp.864–868.

Goldstein, G. et al., 1975. Isolation of a Polypeptide That Has Lymphocyte-Differentiating Properties and Is Probably Represented Universally in Living Cells. *Proc. Nat. Acad. Sci. USA*, 72(1), pp.11–15.

Gomez De Cedrón, M. et al., 1999. RNA helicase activity of Semliki Forest virus replicase protein NSP2. *FEBS Letters*, 448(1), pp.19–22.

Gorchakov, R. et al., 2005. Inhibition of Transcription and Translation in Sindbis Virus-Infected Cells Inhibition of Transcription and Translation in Sindbis. *Journal of virology*, 79(15), pp.9397–9409.

Gordon, K. et al., 2014. Immortality , but not oncogenic transformation , of primary human cells leads to epigenetic reprogramming of DNA methylation and gene expression. *Nucleic Acids Research*, 42(6), pp.3529–3541.

Graff, J.W., Ettayebi, K. & Hardy, M.E., 2009. Rotavirus NSP1 inhibits NF??B activation by inducing proteasome-dependent degradation of ??-TrCP: A novel mechanism of IFN antagonism. *PLoS Pathogens*, 5(1), p.e1000280 1-12.

Grandadam, M. et al., 2011. Chikungunya Virus, Southeastern France. *Emerg.*

Infect. Dis., 17(5), pp.910–913.

Griffin DE, 2013. *Alphaviruses. In: Fields Virology 6th Edition.* Knipe DM and Howley PM, ed., Philadelphia: Lippincott, Williams and Wilkins.

Groot, R.J. De et al., 1990. Cleavage-site preferences of Sindbis virus polyproteins containing the non-structural proteinase. Evidence for temporal regulation of polyprotein processing in vivo. *EMBO Journal*, 9(8), pp.2631–2638.

Le Guen, T. et al., 2015. An in vivo genetic reversion highlights the crucial role of Myb-Like, SWIRM, and MPN domains 1 (MYSM1) in human hematopoiesis and lymphocyte differentiation. *Journal of Allergy and Clinical Immunology*, 136(6), pp.1619–1626.

Häcker, H. et al., 2006. Specificity in Toll-like receptor signalling through distinct effector functions of TRAF3 and TRAF6. *Nature*, 439(7073).

Hagglund, R. & Roizman, B., 2002. Characterization of the novel E3 ubiquitin ligase encoded in exon 3 of herpes simplex virus-1-infected cell protein 0. *Proceedings of the National Academy of Sciences of the United States of America*, 99(12), pp.7889–94.

Haglund, K. et al., 2003. Distinct monoubiquitin signals in receptor endocytosis. *Trends Biochem Sci*, 28(11), pp.598–604.

Hahn, Y.S., Strauss, E.G. & Strauss, J.H., 1989. Mapping of RNA-temperature-sensitive mutants of Sindbis virus: assignment of complementation groups A, B, and G to nonstructural proteins. *Journal of virology*, 63(7), pp.3142–3150.

Haller, O. et al., 2015. Mx GTPases : dynamin-like antiviral machines of innate immunity. *Trends in Microbiology*, 23(3), pp.154–163.

Hannon, G.J. & Rossi, J.J., 2004. Unlocking the potential of the human genome with RNA interference. *Nature*, 431, pp.371–78.

Hao, L. et al., 2008. Drosophila RNAi screen identifies host genes important for influenza virus replication. *Nature*, 454, pp.890–894.

Hao, L. et al., 2013. Limited Agreement of Independent RNAi Screens for Virus-Required Host Genes Owes More to False-Negative than False-Positive Factors. *PLOS Comput. Biol.*, 9(9), pp.1–21.

Harada, J.N. et al., 2002. Analysis of the Adenovirus E1B-55K-Anchored Proteome Reveals Its Link to Ubiquitination Machinery. *Journal of Virology*, 76(18), pp.9194–9206.

Hardy, W.R. & Strauss, J.H., 1989. Processing the Nonstructural Polyproteins of Sindbis Virus : Nonstructural Proteinase Is in the C-Terminal Half of nsP2 and Functions Both in cis and in trans. , 63(11), pp.4653–4664.

Harhaj, E. W. and Dixit, V.M., 2012. Regulation of NF-κB by deubiquitinases. *Immunol Rev*, 246(1), pp.107–124.

Harrison, VR. Binn, LN. and Randall, R., 1967. Comparative Immunogenicities of Chikungunya Vaccines Prepared in Avian and Mammalian Tissues.

Am. J. Trop. Med. Hyg, 16(6), pp.786–791.

Harty, R.N., Pitha, M. & Okumura, A., 2009. Antiviral Activity of Innate Immune Protein ISG15. *ijournal of innate immunity*, 1, pp.397–404.

Hefti, E. et al., 1975. 5' nucleotide sequence of sindbis viral RNA. *Journal of virology*, 17(1), pp.149–59.

Heil, M.L. et al., 2001. An Amino Acid Substitution in the Coding Region of the E2 Glycoprotein Adapts Ross River Virus To Utilize Heparan Sulfate as an Attachment Moiety. , 75(14), pp.6303–6309.

Helenius, A. et al., 1985. Effects of monovalent cations on Semliki Forest virus entry into BHK-21 cells. *The Journal of biological chemistry*, 260(9), pp.5691–7.

Helenius, A.R.I. et al., 1978. Human (HLA-A and HLA-B) and murine (H-2K and H-2D) histocompatibility antigens are cell surface receptors for Semliki Forest virus. , 75(8), pp.3846–3850.

Helenius, A.R.I. et al., 1980. On the entry of Semiliki Forest Virus into BHK-21. *the journal of cell*, 84, pp.404–420.

Heride, C. & Urbé, S., 2012. Ubiquitin code assembly and disassembly. *Curr Biol*, 24(6), pp.R215–R220.

Hershko, A.; Heller, H.; Elias, S.; Ciechanover, A., 1983. Components of ubiquitin-protein ligase system. Resolution, affinity purification, and role in protein breakdown. *J Biol Chem*, 258, pp.8206–14.

Hershko, A. et al., 1980. Proposed role of ATP in protein breakdown : Conjugation of proteins with multiple chains of the polypeptide of ATP-dependent proteolysis. *Proc Natl Acad Sci U S A*, 77(4), pp.1783–1786.

Hicke, L., 2001. Protein regulation by monoubiquitin. *Nat Rev Mol Cell Biol*, 2, pp.195–201.

Hiscott, J., 2007. Triggering the Innate Antiviral Response through IRF-3 Activation. *The Journal of biological chemistry*, 282(21), pp.15325–15329.

Hoarau, J.J. et al., 2010. Persistent Chronic Inflammation and Infection by Chikungunya Arthritogenic Alphavirus in Spite of a Robust Host Immune Response. *The Journal of Immunology*, 184(10), pp.5914–5927.

Hofmann, R.M. & Pickart, C.M., 1999. Noncanonical MMS2-Encoded Ubiquitin-Conjugating Enzyme Functions in Assembly of Novel Polyubiquitin Chains for DNA Repair. *Cell*, 96, pp.645–653.

Hoke, C.H. et al., 2012. US Military contributions to the global response to pandemic Chikungunya. *Vaccine*, 30(47), pp.6713–6720. Available at: http://dx.doi.org/10.1016/j.vaccine.2012.08.025.

Horwood, P. et al., 2013. The threat of chikungunya in Oceania. *WPSAR*, 4(2), pp.8–10.

Hu, M. et al., 2006. Structural basis of competitive recognition of p53 and MDM2 by HAUSP/USP7: Implications for the regulation of the p53-MDM2

pathway. *PLoS Biology*, 4(2), pp.228–239.

Huang, T. T.; D'Andrea, A.D., 2006. Regulation of DNA repair by ubiquitylation. *Nat Rev Mol Cell Biol*, 7, pp.323–34.

Huang, X.F. et al., 2016. Mysm1 is required for interferon regulatory factor expression in maintaining HSC quiescence and thymocyte development. *Cell Death and Disease*, 7(6), p.e2260 (6-12).

Huibregtse, J.M., Scheffner, M. & Howley, P.M., 1991. A cellular protein mediates association of p53 with the E6 oncoprotein of human papillomavirus types 16 or 18. *The EMBO journal*, 10(13), pp.4129–35.

Hunt, Lois T and Dayhoff, M.O., 1977. Amino-terminal sequence identity of ubiquitin and the nonhistone component of nuclear protein A24. *BBiochem. Biophys. Res. Commun*, 74(2), pp.650–655.

Ikeda, F. & Dikic, I., 2008. Atypical ubiquitin chains: new molecular signals. *EMBO reports*, 9(6), pp.536–542.

Inobe, T. & Matouschek, A., 2014. Paradigms of protein degradation by the proteasome. *Current Opinion in Structural Biology*, 24, pp.156–164.

Isaacson, M.K. & Ploegh, H.L., 2009. Ubiquitination, Ubiquitin-like Modifiers, and Deubiquitination in Viral Infection. *Cell Host and Microbe*, 5(6), pp.559–570.

Jan, J.T. & Griffin, D.E., 1999. Induction of apoptosis by Sindbis virus occurs at cell entry and does not require virus replication. *Journal of virology*, 73(12), pp.10296–10302.

Janeway, C.A., 1989. Approaching the Asymptote ? Evolution and Revolution in Immunology. *Cold Spring Harb. Symp. Quant. Biol*, 54(Pt 1), pp.1–13.

Janeway CA Jr and Medzhitov R, 2002. Innate Immune Recognition. *Annu Rev Immunol*, 20, pp.197–216.

Jarosinski, K. et al., 2007. A herpesvirus ubiquitin-specific protease is critical for efficient T cell lymphoma formation. *Proceedings of the National Academy of Sciences of the United States of America*, 104(50), pp.20025–20030.

Jensen, S. and & Thomsen, A.R., 2012. Sensing of RNA Viruses : a Review of Innate Immune Receptors Involved in Recognizing RNA Virus Invasion. *Journal of virology*, 86, pp.2900–2910.

Jiang, X. et al., 2015. Epigenetic Regulation of Antibody Responses by the Histone H2A Deubiquitinase MYSM1. *Sci Rep*, 5(13755), pp.1–15.

Jiang, X.X. et al., 2011. Control of B Cell Development by the Histone H2A Deubiquitinase MYSM1. *Immunity*, 35(6), pp.883–896.

Jiang, Z. et al., 2004. Toll-like receptor 3-mediated activation of NF-kappaB and IRF3 diverges at Toll-IL-1 receptor domain-containing adapter inducing IFN-beta. *Proc. Nat. Acad. Sci. USA*, 101(10), pp.3533–3538.

Jono, H. et al., 2004. NF-kB Is Essential for Induction of CYLD , the Negative

Regulator of NF-kB. *The Journal of biological chemistry*, 279(35), pp.36171–36175.

Jose, J. et al., 2012. Interactions of the Cytoplasmic Domain of Sindbis Virus E2 with. *Journal of Virology*, 86, pp.2585–2599.

Jose, J., Snyder, J.E. & Kuhn, R.J., 2009. A structural and functional perspective of alphavirus replication and assembly. *Future microbiology*, 4(7), pp.837–856.

Judith, D. et al., 2013. Species-specific impact of the autophagy machinery on Chikungunya virus infection. *EMBO reports*, 14(6), pp.534–544.

K. C. Smithburn, A.J.H. and A.F.M., 1946. A neurotropic virus isolated from Aedes mosquitoes caught in the Semliki forest. *The American journal of tropical medicine and hygiene*, 26(2), pp.189–208.

Kääriäinen, L. et al., 1987. Replication of the genome of alphaviruses. *Journal of cell science.*, 7, pp.231–50.

Kangas, L., Grönroos, M. and Nieminen, A.L., 1984. Bioluminescence of cellular ATP: A new method for evaluating cytotoxic agents in vitro. Med. Biol. 62, 38-43.

Kanneganti, T. et al., 2006. Critical Role for Cryopyrin / Nalp3 in Activation of Caspase-1 in Response to Viral Infection and Double-stranded RNA. *The Journal of biological chemistry*, 281(48), pp.36560–36568.

Kapoor, A., Forman, M. & Arav-boger, R., 2014. Activation of Nucleotide Oligomerization Domain 2 (NOD2) by Human Cytomegalovirus Initiates Innate Immune Responses and Restricts Virus Replication. *PLoS ONE*, 9(3), p.e92704.

Kapushesky, M. et al., 2009. Gene expression Atlas at the European Bioinformatics Institute. *Nucleic Acids Research*, 38(10.1093), pp.690–698.

Karlas, A. et al., 2016. A human genome-wide loss-of-function screen identifies effective chikungunya antiviral drugs. *Nature Communications*, 7(11320), pp.1–14.

Kato, H., Takahasi, K. & Fujita, T., 2011. RIG-I-like receptors : cytoplasmic sensors for non-self RNA. *Immunological Reviews*, 243, pp.91–98.

Kattenhorn, L.M. et al., 2005. A deubiquitinating enzyme encoded by HSV-1 belongs to a family of cysteine proteases that is conserved across the family Herpesviridae. *Molecular Cell*, 19(4), pp.547–557.

Kaur, P. et al., 2013. Inhibition of Chikungunya virus replication by harringtonine, a novel antiviral that suppresses viral protein expression. *Antimicrobial Agents and Chemotherapy*, 57(1), pp.155–167.

Kawai, T. & Akira, S., 2010. The role of pattern-recognition receptors in innate immunity : update on Toll-like receptors. *Nature immunology*, 11(5), pp.373–384.

Kayagaki, N. et al., 2007. DUBA : A Deubiquitinase That Regulates Type I

Interferon Production. *Science*, 318, pp.1628–1631.

Kell, A.M. & Gale, M., 2015. RIG-I in RNA virus recognition. *Virology*, 479–480, pp.110–121.

Keränen, S. & Kääriäinen, L., 1979. Functional defects of RNA-negative temperature-sensitive mutants of Sindbis and Semliki Forest viruses. *Journal of virology*, 32(1), pp.19–29.

Kielian, M., Chanel-Vos, C. & Liao, M., 2010. Alphavirus entry and membrane fusion. *Viruses*, 2(4), pp.796–825.

Kim, H.T. et al., 2007. Certain Pairs of Ubiquitin-conjugating Enzymes (E2s) and Ubiquitin-Protein Ligases (E3s) Synthesize Nondegradable Forked Ubiquitin Chains Containing All Possible Isopeptide Linkages. *the journal of bio*, 282(24), pp.17375–17386.

Kim, K.H. et al., 2004. Regulation of Semliki Forest virus RNA replication : a model for the control of alphavirus pathogenesis in invertebrate hosts. *Virology*, 323, pp.153–163.

Komander, D. & Barford, D., 2008. Structure of the A20 OTU domain and mechanistic insights into deubiquitination. *Biochem journal*, 85(2), pp.77–85.

Komander, D., Clague, M.J. & Urbé, S., 2009. Breaking the chains : structure and function of the deubiquitinases. *Nature reviews. Molecular cell biology*, 10(8), pp.550–563.

Konig, R. et al., 2008. Global Analysis of Host-Pathogen Interactions that Regulate Early-Stage HIV-1 Replication. *Cell*, 135(2), pp.49–60.

Konig, R. et al., 2010. Human host factors required for influenza virus replication. *Nature*, 463, pp.813–817.

König, R. et al., 2007. A probability-based approach for the analysis of large-scale RNAi screens. *Nature methods*, 4(10), pp.847–9.

Kovalenko, A. & Chable-bessia, C., 2003. The tumour suppressor CYLD negatively regulates NF- k B signalling by deubiquitination. *Nature.*, 424, pp.801–805.

Krejbich-Trotot, P., Gay, B., et al., 2011. Chikungunya triggers an autophagic process which promotes viral replication. *Virology journal*, 8(432), pp.1–10.

Krejbich-Trotot, P., Denizot, M., et al., 2011. Chikungunya virus mobilizes the apoptotic machinery to invade host cell defenses. *The FASEB journal*, 25(1), pp.314–325.

Kulathu, Y. & Komander, D., 2012. Atypical ubiquitylation — the unexplored world of polyubiquitin beyond Lys48 and Lys63 linkages. *Nature Reviews Molecular Cell Biology*, 13(8), pp.508–523.

Kumar, H., Kawai, T. & Akira, S., 2011. Pathogen Recognition by the Innate Immune. *Int. Rev. Immunol*, 30, pp.16–34.

Kumar, H., Kawai, T. & Akira, S., 2009. Pathogen recognition in the innate immune response. *Biochem journal*, 420, pp.1–16.

Labadie, K. et al., 2010. Chikungunya disease in nonhuman primates leads to long-term viral persistence in macrophages. *J Clin Invest*, 120(3), pp.894–906.

Landis, H. et al., 1998. Human MxA Protein Confers Resistance to Semliki Forest Virus and Inhibits the Amplification of a Semliki Forest Virus-Based Replicon in the Absence of Viral Structural Proteins. *Journal of virology*, 72(2), pp.1516–1522.

LaStarza, M.W., Lemm, J.A. & Rice, C.M., 1994. Genetic analysis of the nsP3 region of Sindbis virus: evidence for roles in minus-strand and subgenomic RNA synthesis. *Journal of virology*, 68(9), pp.5781–91.

Lavergne, A. et al., 2006. Mayaro virus: Complete nucleotide sequence and phylogenetic relationships with other alphaviruses. *Virus Research*, 117(2), pp.283–290.

Lee, R.C.H. et al., 2013. Mosquito Cellular Factors and Functions in Mediating the Infectious entry of Chikungunya Virus. *PLoS Neglected Tropical Diseases*, 7(2), p.e2050 (1-17).

Lehner, P.J. et al., 2005. Downregulation of cell surface receptors by the K3 family of viral and cellular ubiquitin E3 ligases. *Immunological Reviews*, 207, pp.112–125.

Lenschow, D.J. et al., 2007. IFN-stimulated gene 15 functions as a critical antiviral molecule against influenza , herpes , and Sindbis viruses. *Proc. Natl. Acad. Sci. USA.*, 104(4), pp.1371–1376.

Lescar, J. et al., 2001. The Fusion Glycoprotein Shell of Semliki Forest Virus : An Icosahedral Assembly Primed for Fusogenic Activation at Endosomal pH. , 105, pp.137–148.

Levitt, N.H. et al., 1986. Development of an attenuated strain of chikungunya virus for use in vaccine production. *Vaccine*, 4(3), pp.157–162.

Li, G.P. & Rice, C.M., 1989. Mutagenesis of the in-frame opal termination codon preceding nsP4 of Sindbis virus: studies of translational readthrough and its effect on virus replication. *Journal of virology*, 63(3), pp.1326–37.

Li, L. et al., 2015. Interferon-stimulated genes — essential antiviral effectors implicated in resistance to Theiler ' s virus-induced demyelinating disease. *Journal of Neuroinflammation*, 12(242), pp.1–14.

Li, S. et al., 2010. Regulation of Virus-triggered Signaling by OTUB1- and OTUB2-mediated Deubiquitination of TRAF3 and TRAF6 *. *Journal of Biological Chemistry*, 285(7), pp.4291–4297.

Liljestrom, P. & Garoff, H., 1991. Internally Located Cleavable Signal Sequences Direct the Formation of Semliki Forest Virus Membrane Proteins from a Polyprotein Precursor. *Journal of Virology*, 65(1), pp.147–154.

Lin, D. et al., 2015. Induction of USP25 by viral infection promotes innate antiviral responses by mediating the stabilization of TRAF3 and TRAF6. *Proceedings of the National Academy of Sciences*, 112(43), pp.11324–29.

Lin, R. et al., 2006. Negative Regulation of the Retinoic Acid-inducible Gene I-induced Antiviral State by the Ubiquitin-editing Protein A20. *The Journal of biological chemistry*, 281(4), pp.2095–2103.

Lindner, H.A. et al., 2005. The Papain-Like Protease from the Severe Acute Respiratory Syndrome Coronavirus Is a Deubiquitinating Enzyme. *Biotechnology*, 79(24), pp.15199–15208.

La Linn, M. et al., 2005. An arthritogenic alphavirus uses the alpha1 beta1 integrin collagen receptor. *Virology*, 336, pp.229–239.

La Linn, M. et al., 2001. Arbovirus of marine mammals: a new alphavirus isolated from the elephant seal louse, Lepidophthirus macrorhini. *Journal of virology*, 75(9), pp.4103–9.

Liu, H. et al., 2009. Regulation of ErbB2 Receptor Status by the Proteasomal DUB POH1. *PLoS ONE*, 4(5), pp.1–10.

Liu, X. et al., 2013. Dynamic regulation of innate immunity by ubiquitin and ubiquitin-like proteins. *Cytokine and Growth Factor Reviews*, 24(6), pp.559–570.

Liu, Y., Penninger, J. & Karin, M., 2005. Immunity by ubiquitylation: a reversible process of modification. *Nature Rev. Immunol.*, 5, pp.941–952.

Loewy, A. et al., 1995. The 6-Kilodalton Membrane Protein of Semliki Forest Virus Is Involved in the Budding Process. *Journal of Virology*, 69(1), pp.469–475.

Lowe, S.W. & Ruley, H.E., 1993. Stabilization of the p53 tumor suppressor is induced by adenovirus-5 E1A and accompanies apoptosis. *Genes & Dev*, 7, pp.535–545.

Ludwig, G. V, Kondig, J.P. & Smith, J.F., 1996. A Putative Receptor for Venezuelan Equine Encephalitis Virus from Mosquito Cells. , 70(8), pp.5592–5599.

Lundberg, E. et al., 2010. Defining the transcriptome and proteome in three functionally different human cell lines. *Molecular systems biology*, 6(450), pp.1–10.

Lundstrom, K. et al., 1999. Semliki Forest virus vectors for in vitro and in vivo applications. *Gene therapy and Molecular Biology*, 4, pp.23–31.

MacDonald, G.H. & Johnston, R.E., 2000. Role of Dendritic Cell Targeting in Venezuelan Equine Encephalitis Virus Pathogenesis. *Journal of Virology*, 74(2), pp.914–922.

Madariaga, M., Ticona, E. & Resurrecion, C., 2016. Chikungunya: Bending over the Americas and the rest of the world. *Brazilian Journal of Infectious Diseases*, 20(1), pp.91–98.

Mann, M. & Jensen, O.N., 2003. Proteomic analysis of post-translational modifications. *Nat Biotech*, 21, pp.255–261.

Mansur, D.S. et al., 2013. Poxvirus Targeting of E3 Ligase Beta-TrCP by Molecular Mimicry: A Mechanism to Inhibit NF-kB Activation and Promote Immune Evasion and Virulence. *PLoS Pathogens*, 9(2), pp.1–14.

Marsh, M., Kielian, M.C. & Helenius, A., 1984. Semliki forest virus entry and the endocytic pathway. *Biochem Soc Trans*, 12(6), pp.981–983.

Mathiot, C.C., Herve, V.M. & Georges, A.J., 1990. Antibodies to haemorrhagic fever viruses and to selected arboviruses in monkeys from the Central African Republic. *Transactions of the Royal Society of Tropical Medicine and Hygiene*, 84(5), pp.732–733.

Matsumiya, T. & Stafforini, D.M., 2010. Function and regulation of retinoic acid-inducible gene-I. *Critical reviews in immunology*, 30(6), pp.489–513.

Mayer, S. V., Tesh, R.B. & Vasilakis, N., 2017. The emergence of arthropod-borne viral diseases: A global prospective on dengue, chikungunya and zika fevers. *Acta Tropica*, 166, pp.155–163.

Medzhitov, R., 2007. Recognition of microorganisms and activation of the immune response. *Nature*, 449, pp.819–826.

Merits, A. et al., 2001. Proteolytic processing of Semliki Forest virus-specific non-structural polyprotein by nsP2 protease. *Journal of General Virology*, 82(4), pp.765–773.

Metz, S.W. et al., 2013. Chikungunya virus-like particles are more immunogenic in a lethal AG129 mouse model compared to glycoprotein E1 or E2 subunits. *Vaccine*, 31(51), pp.6092–6096.

Meyer, H. & Rape, M., 2014. Enhanced Protein Degradation by Branched Ubiquitin Chains. *Cell*, 157(4), pp.910–921.

Mielech, A.M. et al., 2014. MERS-CoV papain-like protease has deISGylating and deubiquitinating activities. *Virology*, 450(451), pp.64–70.

Moffat, J. & Sabatini, D.M., 2006. Building mammalian signalling pathways with RNAi screens. *Nat. Rev. Mol. Cell Biol.*, 7, pp.177–187.

Mohr, S., Bakal, C. & Perrimon, N., 2010. Genomic Screening with RNAi : Results and Challenges. *Annu. Rev. Biochem.*, 79, pp.37–64.

Morales, D.J. & Lenschow, D.J., 2013. The antiviral activities of ISG15. *Journal of Molecular Biology*, 425(24), pp.4995–5008.

Morreale, F.E. et al., 2016. Types of Ubiquitin Ligases. *Cell*, 165(1), p.248–248.e1.

Morrison, T.E. et al., 2011. A mouse model of chikungunya virus-induced musculoskeletal inflammatory disease: Evidence of arthritis, tenosynovitis, myositis, and persistence. *American Journal of Pathology*, 178(1), pp.32–40.

Moser, L.A., Pollard, A.M. & Knoll, L.J., 2013. A Genome-Wide siRNA Screen

to Identify Host Factors Necessary for Growth of the Parasite Toxoplasma gondii. *PLoS ONE*, 8(6), pp.1–9.

Moser, T.S. et al., 2010. A Kinome RNAi Screen Identified AMPK as Promoting Poxvirus Entry through the Control of Actin Dynamics. *PLoS Pathogens*, 6(6), p.6:e1000954 (1-15).

Nandakumar, V. et al., 2013. Epigenetic control of natural killer cell maturation by histone H2A deubiquitinase, MYSM1. *Proceedings of the National Academy of Sciences*, 110(41), pp.E3927–E3936.

Nasar, F. et al., 2012. Eilat virus, a unique alphavirus with host range restricted to insects by RNA replication. *Proceedings of the National Academy of Sciences*, 109(36), pp.14622–14627.

Nasar, F. et al., 2014. Eilat virus displays a narrow mosquito vector range. *Parasites & vectors*, 7(595), pp.1–10.

Nijman, S.M.B. et al., 2005. A Genomic and Functional Inventory of Deubiquitinating Enzymes. *Cell*, 123, pp.773–786.

Nijnik, A. et al., 2012. The critical role of histone H2A-deubiquitinase Mysm1 in hematopoiesis and lymphocyte differentiation. *Blood*, 119(6), pp.1370–1379.

Njenga, M.K. et al., 2008. Tracking epidemic Chikungunya virus into the Indian Ocean from East Africa. *Journal of General Virology*, 89, pp.2754–2760.

Novak, U. et al., 2009. The NF- kB negative regulator TNFAIP3 (A20) is inactivated by somatic mutations and genomic deletions in marginal zone lymphomas. *Blood*, 113(20), pp.4918–4922.

Oeckinghaus, A. & Ghosh, S., 2009. The NF- k B Family of Transcription Factors and Its Regulation. *Cold Spring Harb Perspect Biol.*, 1, pp.1–14.

Omar, A. & Koblet, H., 1988. Semliki Forest virus particles containing only the E1 envelope glycoprotein are infectious and can induce cell-cell fusion. *Virology*, 166(1), pp.17–23.

Ooi, Y.S. et al., 2013. Genome-Wide RNAi Screen Identifies Novel Host Proteins Required for Alphavirus Entry. *PLoS Pathogens*, 9(12), pp.1–10.

Ou, J. et al., 1982. Sequence studies of several alphavirus genomic RNAs in the region containing the start of the subgenomic RNA. *Proc. Nat. Acad. Sci. USA*, 79, pp.5235–5239.

Ozden, S. et al., 2007. Human Muscle Satellite Cells as Targets of Chikungunya Virus Infection. *PLoS ONE*, 2(6), pp.1–7.

Panda, D. & Cherry, S., 2012. Cell-based genomic screening: Elucidating virus-host interactions. *Current Opinion in Virology*, 2(6), pp.778–786.

Panda, S., Nilsson, J.A. & Gekara, N.O., 2015. Deubiquitinase MYSM1 Regulates Innate Immunity through Inactivation of TRAF3 and TRAF6 Complexes. *Immunity*, 43(4), pp.647–659.

Paredes, A.M. et al., 1993. Three-dimensional structure of a membrane-

containing virus. *Proc. Nat. Acad. Sci. USA*, 90(19), pp.9095–9.

Parkinson, J. & Everett, R.D., 2000. Alphaherpesvirus Proteins Related to Herpes Simplex Virus Type 1 ICP0 Affect Cellular Structures and Proteins. *Journal of Virology*, 74(21), pp.10006–10017.

Parrott, M.M. et al., 2009. Role of Conserved Cysteines in the Alphavirus E3 Protein. *Journal of Virology*, 83(6), pp.2584–2591.

Partidos, C.D. et al., 2012. Cross-protective immunity against o'nyong-nyong virus afforded by a novel recombinant chikungunya vaccine. *Vaccine*, 30(31), pp.4638–4643.

Peleg, 1969. Inapparent Persistent Virus Infection in Continuously Grown AFdes aegypti Mosquito Cells. *J. gen. Virol*, 5, pp.463–471.

Peng, X. et al., 2010. Unique signatures of long noncoding RNA expression in response to virus infection and altered innate immune signaling. *MBio*, 1(5), pp.1–9.

Pialoux G, Gaüzère BA, Jauréguiberry S, S.M. et al., 2007. Chikungunya, an epidemic arbovirosis. *Lancet Infect Dis*, 7(5), pp.319–327.

Pindel, A. & Sadler, A., 2011. The Role of Protein Kinase R in the Interferon Response. *journal of Interferon & Cytokine Research*, 31(1), pp.59–70.

Plante, K. et al., 2011. Novel chikungunya vaccine candidate with an ires-based attenuation and host range alteration mechanism. *PLoS Pathogens*, 7(7), pp.1–11.

Pohjala, L. et al., 2008. A luciferase-based screening method for inhibitors of alphavirus replication applied to nucleoside analogues. *Antiviral Research*, 78(3), pp.215–222.

Powers, A.M. et al., 2006. Genetic relationships among Mayaro and Una viruses suggest distinct patterns of transmission. *American Journal of Tropical Medicine and Hygiene*, 75(3), pp.461–469.

Powers, A.M. et al., 2000. Re-emergence of chikungunya and o ' nyong-nyong viruses : evidence for distinct geographical lineages and distant evolutionary relationships. *Journal of General Virology*, 81, pp.471–479.

Lo Presti, A. et al., 2016. Molecular epidemiology, evolution and phylogeny of Chikungunya virus: An updating review. *Infection, Genetics and Evolution*, 41, pp.270–278.

Pruneda, JonathanLittlefield, P.J. et al., 2012. StructureofanE3:E2~Ub Complex Reveals an Allosteric Mechanism Shared among RING/U-box Ligases. *MOLCEL*, 47(6), pp.933–942.

Pruneda, J.N. et al., 2011. Ubiquitin in Motion : Structural studies of the E2 ~ Ub conjugate. *Biochem*, 50(10), pp.1624–1633.

Puiprom, O. et al., 2013. Characterization of chikungunya virus infection of a human keratinocyte cell line: Role of mosquito salivary gland protein in suppressing the host immune response. *Infection, Genetics and Evolution*, 17, pp.210–215.

Qian, C. et al., 2005. Structure and chromosomal DNA binding of the SWIRM domain. *Nature Structural & Molecular Biology*, 12(12), pp.1078–1085.

Qin, J. et al., 2015. BAP1 promotes breast cancer cell proliferation and metastasis by deubiquitinating KLF5. *Nature Communications*, 6, p.8471.

Qin, J. et al., 2006. TLR8-mediated NF- kB and JNK Activation Are TAK1-independent and MEKK3-dependent. *The Journal of biological chemistry*, 281(30), pp.21013–21021.

Querido, E. et al., 2001. Degradation of p53 by adenovirus E4orf6 and E1B55K proteins occurs via a novel mechanism involving a Cullin-containing complex. *Genes and Development*, 15(23), pp.3104–3117.

Radoshitzky, S.R. et al., 2016. siRNA Screen Identifies Trafficking Host Factors that Modulate Alphavirus Infection. *PLoS Pathogens*, 31, pp.1–30.

Ramage, H. & Cherry, S., 2015. Virus-Host Interactions: From Unbiased Genetic Screens to Function. *Annual Review of Virology*, 2(1), pp.497–524.

Ramsauer, K. et al., 2015. Immunogenicity, safety, and tolerability of a recombinant measles-virus-based chikungunya vaccine: A randomised, double-blind, placebo-controlled, active-comparator, first-in-man trial. *The Lancet Infectious Diseases*, 15(5), pp.519–527.

Ratia, K. et al., 2006. Severe acute respiratory syndrome coronavirus papain-like protease: structure of a viral deubiquitinating enzyme. *Proc. Nat. Acad. Sci. USA*, 103(15), pp.5717–22.

Rausalu, K. et al., 2016. Chikungunya virus infectivity , RNA replication and non-structural polyprotein processing depend on the nsP2 protease ' s active site cysteine residue. *Scientific Reports*, 6(37124), pp.1–17.

Ravichandran, R. & Manian, M., 2008. Ribavirin therapy for Chikungunya arthritis. *Journal of infection in developing countries*, 2(2), pp.140–142.

Reyes-turcu, F.E., Ventii, K.H. & Wilkinson, K.D., 2009. Regulation and Cellular Roles of Ubiquitin-Specific Deubiquitinating Enzymes. *Annu Rev Biochem*, 78, p.363–397.

Reynaud, J.M. et al., 2015. IFIT1 Differentially Interferes with Translation and Replication of Alphavirus Genomes and Promotes Induction of Type I Interferon. *PLoS Pathogens*, 11(4), pp.1–31.

Rezza, G. et al., 2007. Infection with chikungunya virus in Italy: an outbreak in a temperate region. *Lancet*, 370, pp.1840–1846.

Rikkonen, M., 1996. Functional significance of the nuclear-targeting and NTP-binding motifs of Semliki Forest virus nonstructural protein nsP2. *Virology*, 218(2), pp.352–361.

Rikkonen, M., Peranen, J. & Kaariainen, L., 1994. ATPase and GTPase activities associated with Semliki Forest virus nonstructural protein nsP2. *Journal of virology*, 68(9), pp.5804–5810.

Robinson, M.C., 1955. An epidemic of virus disease in Southern Province, Tanganyika Territory, in 1952–53. *transactions of the royal society of tropical medicine and hygien*, 49(1), pp.28–32.

Rupp, J.C. et al., 2015. Alphavirus RNA synthesis and non-structural protein functions. *Journal of General Virology*, 96(9), pp.2483–2500.

Ryman, K.D. et al., 2000. Alpha / Beta Interferon Protects Adult Mice from Fatal Sindbis Virus Infection and Is an Important Determinant of Cell and Tissue Tropism. *J Virology*, 74(7), pp.3366–3378.

Ryman, K.D. et al., 2005. Sindbis Virus Translation Is Inhibited by a PKR / RNase L-Independent Effector Induced by Alpha / Beta Interferon Priming of Dendritic Cells. *Journal of virology*, 79(3), pp.1487–1499.

Ryman, K.D. & Klimstra, W.B., 2008. Host responses to alphavirus infection. *Immunological Reviews*, 225, pp.27–45.

Sabbah, A., Chang, T. H., Harnack, R., Frohlich, V., Tominaga, K., et al, 2009. Activation of innate immune antiviral response by NOD2 Ahmed. *Nature immunology*, 10(10), pp.1073–1080.

Salonen, A., Ahola, T. & Kaariainen, L., 2004. Viral RNA replication in association with cellular membranes. *Curr Top Microbiol Immunol*, 285, pp.139–173.

Sanz, M.A. et al., 2003. Interfacial domains in sindbis virus 6K protein: Detection and functional characterization. *Journal of Biological Chemistry*, 278(3), pp.2051–2057.

Saridakis, V. et al., 2005. Structure of the p53 binding domain of HAUSP/USP7 bound to epstein-barr nuclear antigen 1: Implications for EBV-mediated immortalization. *Molecular Cell*, 18(1), pp.25–36.

Sarvestani, S.T., Williams, B.R.G. & Gantier, M.P., 2012. Human Toll-Like Receptor 8 Can Be Cool Too : Implications for Foreign RNA Sensing. *journal of interferon & cytokine research*, 32(8), pp.350–361.

Sato, M. et al., 2000. Distinct and Essential Roles of Transcription Factors IRF-3 and IRF-7 in Response to Viruses for IFN-α/β Gene Induction. *Immunity*, 13(4), pp.539–548.

Sato, Y. et al., 2008. Structural basis for specific cleavage of Lys 63-linked polyubiquitin chains. *Nature*, 455, p.358-362.

Scheffner, M., Huibregtse, J.M. & Howley, P.M., 1994. Identification of a human ubiquitin-conjugating enzyme that mediates the E6-AP-dependent ubiquitination of p53. *Proc. Nat. Acad. Sci. USA*, 91(19), pp.8797–801.

Schilte, C. et al., 2012. Cutting Edge: Independent Roles for IRF-3 and IRF-7 in Hematopoietic and Nonhematopoietic Cells during Host Response to Chikungunya Infection. *The Journal of Immunology*, 188(7), pp.2967–2971.

Schilte, C. et al., 2010. Type I IFN controls chikungunya virus via its action on nonhematopoietic cells. *The Journal of Experimental Medicine*, 207(2),

pp.429–442.

Schlee, M., 2013. Master sensors of pathogenic RNA – RIG-I like receptors. *Immunobiology*, 218(11), pp.1322–1335.

Schlieker, C. et al., 2005. A Deubiquitinating Activity Is Conserved in the Large Tegument Protein of the Herpesviridae. *Journal of Virology*, 79(24), pp.15582–15585.

Schulz, O. et al., 2005. Toll-like receptor 3 promotes cross- priming to virus-infected cells. *Nature*, 433, pp.887–892.

Schwanhausser, B. et al., 2011. Correction: Global quantification of mammalian gene expression control. *Nature*, 473(7347), pp.337–342.

Schwartz, O. & Albert, M.L., 2010. Biology and pathogenesis of chikungunya virus. *Nature reviews. Microbiology*, 8(7), pp.491–500.

Schweitzer, K. et al., 2007. CSN controls NF- j B by deubiquitinylation of I j B a. *The EMBO Journal*, 26(6), pp.1532–1541.

Selvarajah, S. et al., 2013. A Neutralizing Monoclonal Antibody Targeting the Acid-Sensitive Region in Chikungunya Virus E2 Protects from Disease. *PLoS Neglected Tropical Diseases*, 7(9), pp.1–11.

Sen, G.C. & Peters, G.A., 2007. Viral Stress-Inducible Genes. *Advances in Virus Research*, 70, pp.233–263.

Sergon, K. et al., 2008. Seroprevalence of Chikungunya Virus (CHIKV) Infection on Lamu Island , Kenya , October 2004. *Am. J. Trop. Med. Hyg*, 78(2), pp.333–337.

Shabman, R.S. et al., 2007. Differential Induction of Type I Interferon Responses in Myeloid Dendritic Cells by Mosquito and Mammalian-Cell-Derived Alphaviruses. *Journal of virology*, 81(1), pp.237–247.

Shackelford, J., Maier, C. & Pagano, J.S., 2003. Epstein–Barr virus activates β-catenin in type III latently infected B lymphocyte lines: Association with deubiquitinating enzymes. *Proc. Nat. Acad. Sci. USA*, 100(26), pp.15572–15576.

Sheehy, A.M. et al., 2002. Isolation of a human gene that inhibits HIV-1 infection and is suppressed by the viral Vif protein. *Nature*, 418(6898), pp.646–650.

Shilatifard, A., 2006. Chromatin Modifications by Methylation and Ubiquitination : Implications in the Regulation of Gene Expression. *Annu Rev Biochem*, 75, pp.243–272.

Shirako, Y., Strauss, E.G. & Strauss, J.H., 2000. Suppressor mutations that allow Sindbis virus RNA polymerase to function with nonaromatic amino acids at the N-terminus: evidence for interaction between nsP1 and nsP4 in minus-strand RNA synthesis. *Virology*, 276, pp.148–160.

Shirako, Y. & Strauss, J.H., 1990. Cleavage between nsP1 and nsP2 initiates the processing pathway of Sindbis virus nonstructural polyprotein P123. *Virology*, 177(1), pp.54–64.

Shirako, Y. & Strauss, J.H., 1994. Regulation of Sindbis Virus RNA Replication : Uncleaved P123 and nsP4 Function in Minus-Strand RNA Synthesis , whereas Cleaved Products from P123 Are Required for Efficient Plus-Strand RNA Synthesis. *Journal of Virology*, 68(3), pp.1874–1885.

Simizu, B. et al., 1984. Structural proteins of Chikungunya virus. *J Virol*, 51(1), pp.254–258.

Singh, I.L.A. & Helenius, A.R.I., 1992. Role of Ribosomes in Semliki Forest Virus Nucleocapsid Uncoating. *Journal of Virology*, 66(12), pp.7049–7058.

Smith, A.L. & Tignor, G.H., 1980. Host cell receptors for two strains of Sindbis virus. *Arch Virol*, 66(1), pp.11–26.

Smith, T.J. et al., 1995. Putative receptor binding sites on alphaviruses as visualized by cryoelectron microscopy. *Proc. Nat. Acad. Sci. USA*, 92(23), pp.10648–52.

Smithburn, K. C.; Haddow, A.J., 1944. Semliki Forest Virus. I. Isolation and Pathogenic Properties. *Journal of immunology*, 49(3), pp.141–157.

Sohn, J. & Hur, S., 2016. Filament assemblies in foreign nucleic acid sensors. *Current Opinion in Structural Biology*, 37, pp.134–144.

Song, E.J. et al., 2010. Deubiquitinating Enzyme Control Reversible Ubiquitination at the Spliceosome. *Genes and Development*, 24, pp.1434–1447.

Sourisseau, M. et al., 2007. Characterization of Reemerging Chikungunya Virus. *PLoS Pathogens*, 3(6), pp.0804–0817.

Spuul, P. et al., 2007. Role of the Amphipathic Peptide of Semliki Forest Virus Replicase Protein nsP1 in Membrane Association and Virus Replication. *Journal of Virology*, 81(2), pp.872–883.

Stapleford, K.A. et al., 2015. Viral Polymerase-Helicase Complexes Regulate Replication Fidelity To Overcome Intracellular Nucleotide Depletion. *Journal of Virology*, 89(22), pp.11233–11244.

Stewart, M.D. et al., 2016. E2 enzymes : more than just middle men. *Nature Publishing Group*, 26(4), pp.423–440.

Strauss, E.G., Rice, C.M. & Strauss, J.H., 1984. Complete nucleotide sequence of the genomic RNA of Sindbis virus. *Virology*, 133(1), pp.92–110.

Strauss, E.G., Rice, C.M. & Strauss, J.H., 1983. Sequence coding for the alphavirus nonstructural proteins is interrupted by an opal termination codon. *Proc. Nat. Acad. Sci. USA*, 80, pp.5271–5275.

Strauss, J.H. & Strauss, E.G., 1994. The alphaviruses: gene expression, replication, and evolution. *Microbiological reviews*, 58(3), pp.491–562.

Suhrbier, A. et al., 2012. Arthritogenic alphaviruses—an overview. *Nature Reviews Rheumatology*, 8(7), pp.420–29.

Sun, S., 2008. Deubiquitylation and regulation of the immune response. *Nat. Rev. Immunol.*, 8, pp.501–511.

Suopanki, J. et al., 1998. Regulation of alphavirus 26S mRNA transcription by replicase component nsP2. *Journal of General Virology*, 79(2), pp.309–319.

T. Hase, P. L. Summers, and W.H.C., 1989. A comparative study of entry modes into C 6]36 cells by Semliki Forest and Japanese encephalitis viruses. *Archives of virology*, 108, pp.101–114.

Takeuchi, O. & Akira, S., 2010. Pattern Recognition Receptors and Inflammation. *Cell*, 140(6), pp.805–820.

Takkinen, K., 1986. Complete nucleotide sequence of the nonstructural protein genes of Semliki Forest virus. *Nucleic acids research*, 14(14), pp.5667–5682.

Takkinen, K. et al., 1990. The Semliki-Forest-virus-specific nonstructural protein nsP4 is an autoproteinase. *European Journal of Biochemistry*, 189(1), pp.33–38.

Takkinen, K., Peranen, J. & Kaariainen, L., 1991. Proteolytic processing of semliki forest virus-specif non-structural polyprotein. *Journal of General Virology*, 72(1991), pp.1627–1633.

Tauriello, D.V.F. et al., 2010. Loss of the Tumor Suppressor CYLD Enhances Wnt/??-Catenin Signaling through K63-Linked Ubiquitination of Dvl. *Molecular Cell*, 37(5), pp.607–619.

Teng, T.S. et al., 2012. Viperin restricts chikungunya virus replication and pathology. *Journal of Clinical Investigation*, 122(12), pp.4447–4460.

Thiberville, S.D. et al., 2013. Chikungunya fever: Epidemiology, clinical syndrome, pathogenesis and therapy. *Antiviral Research*, 99(3), pp.345–370.

Thomas, S. et al., 2010. Functional dissection of the alphavirus capsid protease : sequence requirements for activity. *Virology Journal*, 7(1), p.327.

Thon-Hon, V.G. et al., 2012. Deciphering the differential response of two human fibroblast cell lines following Chikungunya virus infection. *Virology journal*, 9(213), pp.1–10.

Tian, X. et al., 2011. Characterization of selective ubiquitin and ubiquitin-like protease inhibitors using a fluorescence-based multiplex assay format. *Assay and drug development technologies*, 9(2), pp.165–73.

Torre, S. et al., 2016. USP15 regulates type I interferon response and is required for pathogenesis of neuroinflammation. *Nature Immunology*, 18(1), pp.54–63.

Trobaugh, D.W. & Klimstra, W.B., 2017. Alphaviruses suppress host immunity by preventing myeloid cell replication and antagonizing innate immune responses. *Current Opinion in Virology*, 23, pp.30–34.

Trompouki, E., Hatzivassiliou, E. & Tsichritzis, T., 2003. CYLD is a deubiquitinating enzyme that negatively regulates NF- k B activation by TNFR family members. *Nature*, 107, pp.793–796.

Tsetsarkin, K.A. et al., 2007. A Single Mutation in Chikungunya Virus Affects Vector Specificity and Epidemic Potential. *PLoS Pathogens*, 3(12), pp.1895–1905.

Urbe, S. et al., 2012. Systematic survey of deubiquitinase localization identifies USP21 as a regulator of centrosome- and microtubule-associated functions. *Molecular Biology of the Cell*, 23(6), pp.1095–1103.

Vabret, N. & Blander, J.M., 2013. Sensing microbial RNA in the cytosol. *Front. Immunol.*, 4, pp.1–9.

Varghese, F.S. et al., 2016. The Antiviral Alkaloid Berberine Reduces Chikungunya Virus-Induced Mitogen-Activated Protein Kinase Signaling. *Journal of Virology*, 90(21), pp.9743–9757.

Vasiljeva, L. et al., 2000. Identification of a novel function of the Alphavirus capping apparatus. RNA 5'-triphosphatase activity of Nsp2. *Journal of Biological Chemistry*, 275(23), pp.17281–17287.

Vazeille, M. et al., 2007. Two Chikungunya Isolates from the Outbreak of La Reunion (Indian Ocean) Exhibit Different Patterns of Infection in the Mosquito , Aedes albopictus. *PLoS ONE*, 2(11), pp.1–9.

Vega-Rúa, A. et al., 2015. Chikungunya Virus Replication in Salivary Glands of the Mosquito Aedes albopictus. *Viruses*, 7(11), pp.5902–5907.

Vega-Rúa, A. et al., 2014. High level of vector competence of Aedes aegypti and Aedes albopictus from ten American countries as a crucial factor in the spread of Chikungunya virus. *Journal of virology*, 88(11), pp.6294–306.

Vogel, C. et al., 2010. Sequence signatures and mRNA concentration can explain two-thirds of protein abundance variation in a human cell line. *Molecular systems biology*, 6(400), pp.1–9.

Wahlberg, J.M. et al., 1992. Membrane fusion of Semliki Forest virus involves homotrimers of the fusion protein. *Journal of virology*, 66(12), pp.7309–7318.

Wang, J. et al., 2006. High-Molecular-Weight Protein (pUL48) of Human Cytomegalovirus Is a Competent Deubiquitinating Protease: Mutant Viruses Altered in Its Active-Site Cysteine or Histidine Are Viable. *Journal of Virology*, 80(12), pp.6003–6012.

Wang, L. et al., 2013. USP4 Positively Regulates RIG-I-Mediated Antiviral Response through Deubiquitination and Stabilization of RIG-I. *JVI*, 87(8), pp.4507–4515.

Wang, T. et al., 2013. The control of hematopoietic stem cell maintenance , self-renewal , and differentiation by Mysm1-mediated epigenetic regulation. *Blood*, 122(16), pp.2812–2822.

Wang, X., Herr, R.A. & Hansen, T., 2008. Viral and cellular MARCH ubiquitin ligases and cancer. *Seminars in Cancer Biology*, 18(6), pp.441–450.

Wang, Y. et al., 2004. A20 is a potent inhibitor of TLR3- and Sendai virus-induced activation of NF-k B and ISRE and IFN- b promoter. *FEBS J.*, 576, pp.86–90.

Wang, Y.F., Sawicki, S.G. & Sawicki, D.L., 1994. Alphavirus nsP3 functions to form replication complexes transcribing negative-strand RNA. *Journal of virology*, 68(10), pp.6466–75.

Weaver, S.C., 2014. Arrival of Chikungunya Virus in the New World: Prospects for Spread and Impact on Public Health. *PLoS Neglected Tropical Diseases*, 8(6), pp.1–5.

Weaver, S.C., 2016. Urbanization and geographic expansion of zoonotic arboviral diseases: mechanisms and potential strategies for prevention. *Trends Microbiol*, 21(8), pp.360–363.

Weaver, S.C. & Barrett, A.D.T., 2004. Transmission cycles, host range, evolution and emergence of arboviral disease. *Nat Rev Micro*, 2(10), pp.789–801.

Weaver, S.C. & Lecuit, M., 2015. Chikungunya Virus and the Global Spread of a Mosquito-Borne Disease. *New England Journal of Medicine*, 372(13), pp.1231–1239.

Weaver, S.C. & Reisen, W.K., 2010. Present and Future Arboviral Threaths. *Antiviral Research*, 85(2), pp.1–36.

Wengler, G. et al., 2003. Entry of alphaviruses at the plasma membrane converts the viral surface proteins into an ion- permeable pore that can be detected by electrophysiological analyses of whole-cell membrane currents. *general virology*, 84, pp.173–181.

Wengler, G., Wurkner, D. & Wengler, G., 1992. Identification of a Sequence Element in the Alphavirus Core Protein Which Mediates Interaction of Cores with Ribosomes and the Disassembly of Cores. *Virology*, 191, pp.880–888.

Wengler, G.G. & Wengler, G.G., 1984. Identification of a transfer of viral core protein to cellular ribosomes during the early stages of alphavirus infection. *Virology*, 134(2), pp.435–442.

Wengler, G.G. & Wengler, G.G., 2002. In vitro analysis of factors involved in the disassembly of Sindbis virus cores by 60S ribosomal subunits identifies a possible role of low pH. *Journal of General Virology*, 83(10), pp.2417–2426.

Wenzel, D.M. et al., 2011. UbcH7 reactivity profile reveals Parkin and HHARI to be RING/ HECT hybrids. *Nature*, 474(7349), pp.105–108.

Wertz, I.E. et al., 2004. De-ubiquitination and ubiquitin ligase domains of A20 downregulate NF- k B signalling. *Nature*, 430, p.694-699.

Weston, J.H. et al., 1999. Salmon Pancreas Disease Virus, an Alphavirus

Infecting Farmed Atlantic Salmon, Salmo salar L. *Virology Journal*, 256, pp.188–195.

White, J., Kartenbeck, J. & Helenius, A., 1980. Fusion of Semliki forest virus with the plasma membrane can be induced by low pH. *The Journal of Cell Biology*, 87(1), pp.264–272.

White, L.J. et al., 2001. Role of Alpha / Beta Interferon in Venezuelan Equine Encephalitis Virus Pathogenesis : Effect of an Attenuating Mutation in the 5 J Untranslated Region. *J Virology*, 75(8), pp.3706–3718.

Wilkineon, K.D. & Urban, M.K., 1980. Ubiquitin Is the ATP-dependent Proteolysis Factor I of Rabbit. *J Biol Chem*, 1(7), pp.7529–7532.

Wilkins, C. & Jr, M.G., 2010. Recognition of viruses by cytoplasmic sensors. *Current Opinion in Immunology*, 22, pp.41–47.

Willems, W.R. et al., 1979. Semliki Forest Virus: Cause of a Fatal Case of Human Encephalitis. *Science*, 203(4385), pp.1127–1129.

Wimmer, P. & Schreiner, S., 2015. Viral mimicry to usurp ubiquitin and sumo host pathways. *Viruses*, 7(9), pp.4854–4877.

Wintachai, P. et al., 2012. Identification of Prohibitin as a Chikungunya Virus Receptor Protein. *Journal of Medical Virology*, 84, pp.1757–1770.

Won, H. et al., 2016. Epigenetic control of dendritic cell development and fate determination of common myeloid progenitor by Mysm1. *Blood*, 124(17), pp.2647–2657.

Wu, B. & Hur, S., 2016. How RIG-I like receptors activate MAVS. *Curr. Opin. Virol.*, 12, pp.91–98.

Xu, G. et al., 2010. Ubiquitin-specific Peptidase 21 Inhibits Tumor Necrosis Factor alpha-induced Nuclear Factor kB Activation via Binding to and Deubiquitinating Receptor-interacting Protein 1. *The Journal of biological chemistry*, 285(2), pp.969–978.

Yoneyama, M. et al., 2007. Structural and Functional Differences of SWIRM Domain Subtypes. *Journal of Molecular Biology*, 369(1), pp.222–238.

Yoneyama, M. et al., 2004. The RNA helicase RIG-I has an essential function in double-stranded RNA-induced innate antiviral responses. *Nature immunology*, 5(7), pp.730–737.

Yoneyama, M. & Fujita, T., 2009. RNA recognition and signal transduction by RIG-I-like receptors. *Immunol Rev*, 227, pp.54–65.

Yu, X., 2003. Induction of APOBEC3G Ubiquitination and Degradation by an HIV-1 Vif-Cul5-SCF Complex. *Science*, 302(5647), pp.1056–1060.

Yu, Y., Wang, S.E. & Hayward, G.S., 2005. The KSHV immediate-early transcription factor RTA encodes ubiquitin E3 ligase activity that targets IRF7 for proteosome-mediated degradation. *Immunity*, 22(1), pp.59–70.

Zhang, M. et al., 2008. Regulation of IkB Kinase-related Kinases and Antiviral Responses by Tumor Suppressor CYLD. *The Journal of biological*

chemistry, 283(27), pp.18621–18626.

Zhang, W. et al., 2002. Placement of the Structural Proteins in Sindbis Virus Placement of the Structural Proteins in Sindbis Virus. *Journal of virology*, 76(22), pp.11645–11658.

Zhou, F. et al., 2012. Ubiquitin-specific protease 4 mitigates toll-like/interleukin-1 receptor signaling and regulates innate immune activation. *Journal of Biological Chemistry*, 287(14), pp.11002–11010.

Zhou, H. et al., 2008. Genome-Scale RNAi Screen for Host Factors Required for HIV Replication. *Cell Host and Microbe*, 4(5), pp.495–504. Available at: http://dx.doi.org/10.1016/j.chom.2008.10.004.

Zhou, W., Wang, X. & Rosenfeld, M.G., 2009. Histone H2A ubiquitination in transcriptional regulation and DNA damage repair. *The International Journal of Biochemistry & Cell Biology*, 41, pp.12–15.

Zhu, P. et al., 2007. A Histone H2A Deubiquitinase Complex Coordinating Histone Acetylation and H1 Dissociation in Transcriptional Regulation. *Molecular Cell*, 27(4), pp.609–621.

Appendices

Appendix A Countries and territories in which autochthonous cases of chikungunya disease have been reported as of April 22nd 2016. Countries in which cases were reported after the 2004 re-emergence, but had a history of earlier outbreaks are indicated with bold lettering.

Countries and territories where chikungunya outbreaks have been recorded:		
Africa	**Asia**	**Elsewhere**
Tanzania	**Thailand**	
Uganda	**Cambodia**	
Democratic Republic of Congo	**India**	
Zimbabwe	**Vietnam**	
Senegal	**Malaysia**	
Nigeria	**Myanmar (Burma)**	
South Africa	**Indonesia**	
Kenya	**Pakistan**	
Burundi	**Philippines**	
Gabon	**Timor**	
Malawi		
Guinea		
Central African Republic		
Countries in which the first recorded chikungunya outbreak occurred after its re-emergence in 2004:		
Africa	**Asia**	**Americas**
Benin	Bangladesh	Anguilla
Burundi	Bhutan	Antigua and Barbuda
Cameroon	Cambodia	Argentina
Central African Republic	China	Aruba
Comoros	India	Bahamas
Democratic Republic of the Congo	Indonesia	Barbados
Equatorial Guinea	Laos	Belize
Gabon	Malaysia	Bolivia
Guinea	Maldives	Brazil
Kenya	Myanmar (Burma)	British Virgin Islands
Madagascar	Pakistan	Cayman Islands
Malawi	Philippines	Colombia
Mauritius	Saudi Arabia	Costa Rica
Mayotte	Singapore	Curacao
Nigeria	Sri Lanka	Dominica
Republic of Congo	Taiwan	Dominic Republic
Reunion	Thailand	Ecuador
Senegal	Timor	El Salvador
Seychelles	Vietnam	French Guiana
Sierra Leone	Yemen	Grenada
South Africa	**Oceania/Pacific Islands**	Guadeloupe
Sudan	American Samoa	Guatemala
Tanzania	Cook Islands	Guyana
Uganda	Federal States of Micronesia	Haiti
Zimbabwe	French Polynesia	Honduras
Europe	Kiribati	Jamaica
Italy	New Caledonia	Martinique
France	Papua New Guinea	Mexico
	Samoa	Montserrat
	Tokelau	Nicaragua
	Tonga	Panama
		Paraguay
		Peru
		Puerto Rico
		Saint Barthelmy
		Saint Kitts and Nevis
		Saint Martin
		Saint Maarten
		Saint Lucia
		Saint Vincent and the Grenadines
		Suriname
		Trinidad and Tobago
		Turks and Caicos Islands
		Venezuela

Appendix B Details of PCR Primers used in this Study.

Target gene	Annealing temperature and number of cycles		Amplicon bp*
	Endpoint PCR conditions	QPCR conditions	
DUBs PCR primers			
BRCC3	55°C; 30 cycles	94°C/3min; [94°C/15s, 55°C/30s] x40	150
MYSM1	55°C; 30 cycles	94°C/3min; [94°C/15s, 55°C/30s] x40	316
mMYSM1	55°C; 35 cycles	94°C/3min; [94°C/15s, 60°C/30s] x40	139
UCHL1	55°C; 30 cycles	94°C/3min; [94°C/15s, 55°C/30s] x40	134
JOSD2	55°C; 40 cycles	94°C/3min; [94°C/15s, 55°C/30s] x40	148
USP1	55°C; 30 cycles	94°C/3min; [94°C/15s, 55°C/30s] x40	192
USP4	55°C; 30 cycles	94°C/3min; [94°C/15s, 55°C/30s] x40	92
USP5	55°C; 30 cycles	94°C/3min; [94°C/15s, 55°C/30s] x40	83
USP34	55°C; 30 cycles	94°C/3min; [94°C/15s, 55°C/30s] x40	130
USP45	55°C; 30 cycles	94°C/3min; [94°C/15s, 55°C/30s] x40	174
USP46	55°C; 30 cycles	94°C/3min; [94°C/15s, 55°C/30s] x40	106
USP53	55°C; 30 cycles	94°C/3min; [94°C/15s, 55°C/30s] x40	85
Housekeeping gene PCR primers			
Beta-actin	55°C; 30 cycles	94°C/3min; [94°C/15s, 55°C/30s] x40	158
Mouse 18S	55°C; 30 cycles	94°C/3min; [94°C/15s, 55°C/30s] x40	115
SFV and CHIKV PCR primers			
SFV	55°C; 30 cycles	94°C/3min; [94°C/15s, 55°C/30s] x40	173
CHIKV	55°C; 30 cycles	94°C/3min; [94°C/15s, 55°C/30s] x40	127
Human type 1 IFNs and pro-inflammatory cytokines primers			
IFN-α	55°C; 40 cycles	94°C/3min; [94°C/15s, 60°C/30s] x40	100
IFN-β	60°C; 40 cycles	94°C/3min; [94°C/15s, 60°C/30s] x40	328

TNF-α	60°C; 40 cycles	94°C/3min; [94°C/15s, 60°C/30s] x40	220
IL1-β	55°C; 40 cycles	94°C/3min; [94°C/15s, 60°C/30s] x40	174
Mouse type 1 IFNs and pro-inflammatory cytokines primers			
IFN-α	60°C; 40 cycles	94°C/3min; [94°C/15s, 60°C/30s] x40	213
IFN-β	55°C; 40 cycles	94°C/3min; [94°C/15s, 60°C/30s] x40	139
Mx1	55°C; 40 cycles	94°C/3min; [94°C/15s, 60°C/30s] x40	81
TNF-α	55°C; 40 cycles	94°C/3min; [94°C/15s, 60°C/30s] x40	148
IL1-β	55°C; 40 cycles	94°C/3min; [94°C/15s, 55°C/30s] x40	116

**bp base-pairs*

Appendix C End-point data. Note, these cDNA samples are derived from the experiment described in chapter 4

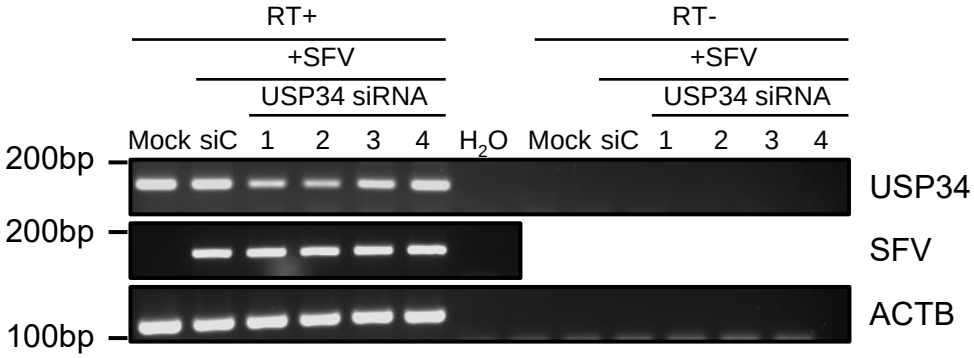

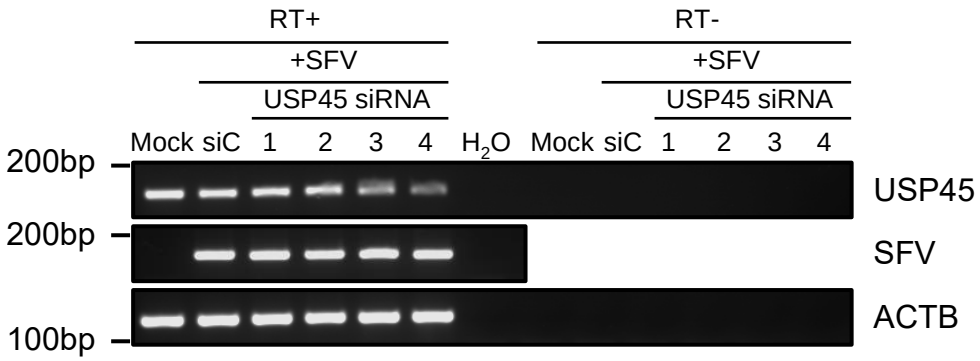
RT+
RT-
+SFV
+SFV
USP45 siRNA
USP45 siRNA
Mock siC 1 2 3 4 H2O Mock siC 1 2 3 4
200bp
200bp
100bp
USP45
SFV
ACTB

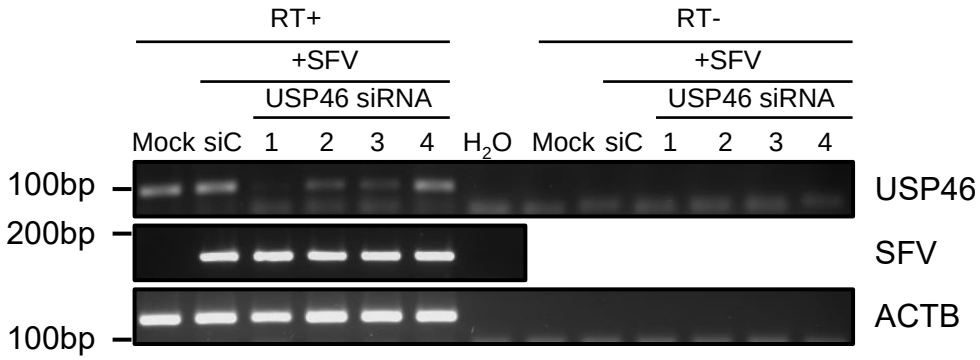
RT+
RT-
+SFV
+SFV
USP46 siRNA
USP46 siRNA
Mock siC 1 2 3 4 H2O Mock siC 1 2 3 4
100bp
200bp
100bp
USP46
SFV
ACTB

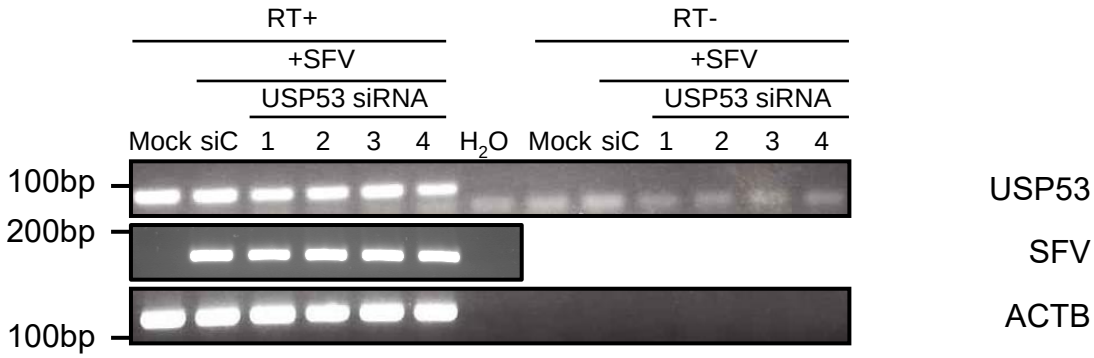
RT+
RT-
+SFV
+SFV
USP53 siRNA
USP53 siRNA
Mock siC 1 2 3 4 H2O Mock siC 1 2 3 4
100bp
200bp
100bp
USP53
SFV
ACTB

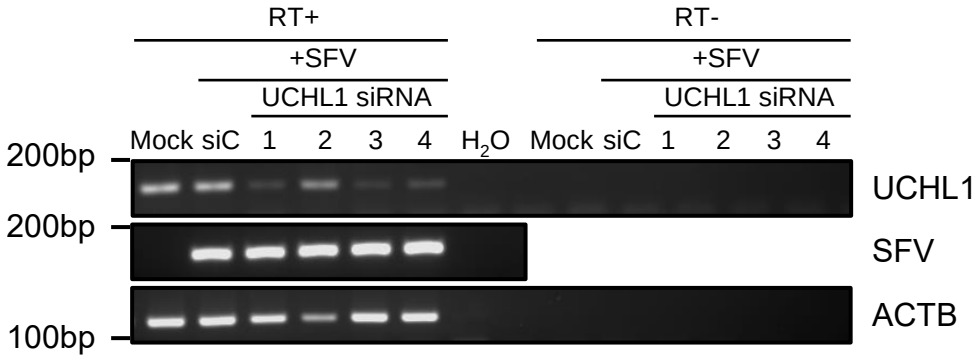
RT+
RT-
+SFV
+SFV
UCHL1 siRNA
UCHL1 siRNA
Mock siC 1 2 3 4 H2O Mock siC 1 2 3 4
200bp
200bp
100bp
UCHL1
SFV
ACTB

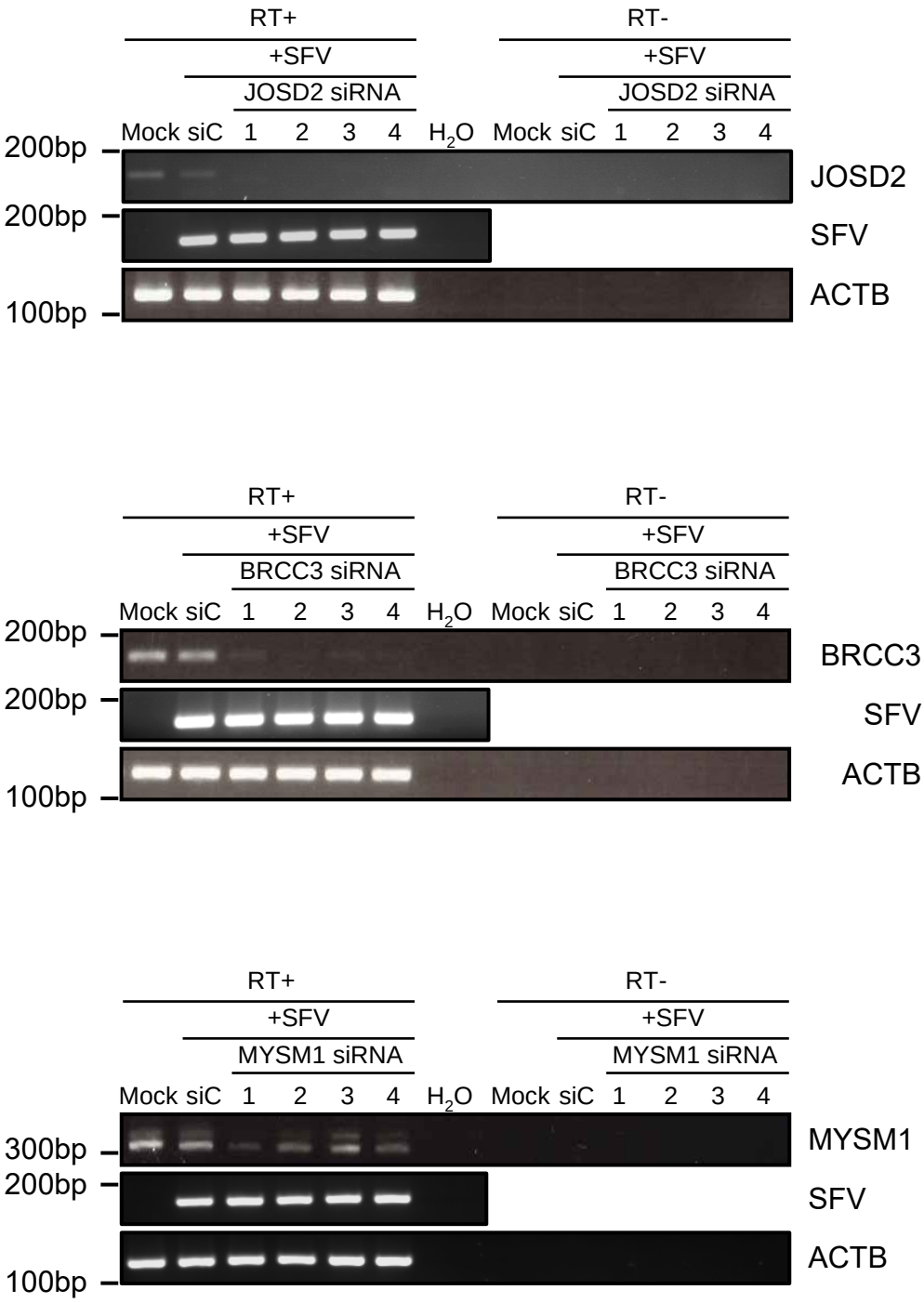
RT+
RT-
+SFV
+SFV
JOSD2 siRNA
JOSD2 siRNA
Mock siC 1 2 3 4 H2O Mock siC 1 2 3 4
200bp
200bp
100bp
JOSD2
SFV
ACTB
RT+
RT-
+SFV
+SFV
BRCC3 siRNA
BRCC3 siRNA
Mock siC 1 2 3 4 H2O Mock siC 1 2 3 4
200bp
200bp
100bp
BRCC3
SFV
ACTB
RT+
RT-
+SFV
+SFV
MYSM1 siRNA
MYSM1 siRNA
Mock siC 1 2 3 4 H2O Mock siC 1 2 3 4
300bp
200bp
100bp
MYSM1
SFV
ACTB